AGARD-R-600

AGARD

ADVISORY GROUP FOR AEROSPACE RESEARCH & DEVELOPMENT

7 RUE ANCELLE 92200 NEUILLY SUR SEINE FRANCE

AGARD REPORT No. 600

on

Problems of Wind Tunnel Design and Testing

NORTH ATLANTIC TREATY ORGANIZATION

DISTRIBUTION AND AVAILABILITY
ON BACK COVER

UNCLASSIFIED

AGARD-R-600

NORTH ATLANTIC TREATY ORGANIZATION

ADVISORY GROUP FOR AEROSPACE RESEARCH AND DEVELOPMENT

(ORGANISATION DU TRAITE DE L'ATLANTIQUE NORD)

AGARD Report No.600

PROBLEMS OF WIND TUNNEL DESIGN AND TESTING

12, 1973

This Report is sponsored by the Fluid Dynamics Panel of AGARD as a complementary paper to AGARD Advisory Report No.60 of the Large Wind Tunnels Working Group.

The AGARD Fluid Dynamics Panel wishes to thank Dr. R. Göthert, M. Ph. Poisson-Quinton, M.M. de Maistre and Mr. J.P. Hartzuiker for their contribution in editing papers included in this Report.

THE MISSION OF AGARD

The mission of AGARD is to bring together the leading personalities of the NATO nations in the fields of science and technology relating to aerospace for the following purposes:

- Exchanging of scientific and technical information;
- Continuously stimulating advances in the aerospace sciences relevant to strengthening the common defence posture;
- Improving the co-operation among member nations in aerospace research and development;
- Providing scientific and technical advice and assistance to the North Atlantic Military Committee in the field of aerospace research and development;
- Rendering scientific and technical assistance, as requested, to other NATO bodies and to member nations in connection with research and development problems in the aerospace field;
- Providing assistance to member nations for the purpose of increasing their scientific and technical potential;
- Recommending effective ways for the member nations to use their research and development capabilities for the common benefit of the NATO community.

The highest authority within AGARD is the National Delegates Board consisting of officially appointed senior representatives from each member nation. The mission of AGARD is carried out through the Panels which are composed of experts appointed by the National Delegates, the Consultant and Exchange Program and the Aerospace Applications Studies Program. The results of AGARD work are reported to the member nations and the NATO Authorities through the AGARD series of publications of which this is one.

Participation in AGARD activities is by invitation only and is normally limited to citizens of the NATO nations.

Published December 1973

533.6.071

Printed by Technical Editing and Reproduction Ltd
Harford House, 7–9 Charlotte St. London. W1P 1HD

PREFACE

The Large Wind Tunnels Working Group (LaWs) of the Fluid Dynamics Panel of AGARD has been helped considerably in its deliberations by a large number of non-member scientists and engineers from the participating countries, who investigated particular problems, provided specially-written papers, or took part in the discussions. This help was very much appreciated by the members of the Group, and the information contained in the LaWs Papers, in particular, has proved to be very valuable. However, the number of LaWs Papers is so large (over 130) that it was not possible to publish them all or to include them in full in the Report of the Group (AGARD Advisory Report 60 entitled "The Need for Large Wind Tunnels in Europe"). On the other hand, some of the LaWs Papers present substantial surveys of particular fields and others describe possible options for future wind tunnels in detail. These papers supplement the Report of the Group in essential respects. The Group decided, therefore, to publish a selection of the LaWs Papers in AGARD Reports, so that they are generally available and can be read in conjunction with the Report of the Group.

As a result, four AGARD Reports are being published, collecting a number of papers together on subjects related to the design and operation of low-speed and transonic wind tunnels, with particular reference to possible future large wind tunnels in Europe. There are thus three further Reports in addition to the present Report. Their contents are listed in Appendix I at the end of this Report.

Wherever appropriate, the individual papers have been edited by a member of the LaWs Working Group. On behalf of the members of the LaWs Group, the undersigned wishes to thank all those who helped the Group and especially the authors of the papers published here.

D.Küchemann
Chairman, LaWs Working Group

November 1972

CONTENTS

Note:

Another paper, "Testing at Supersonic Speeds", was intended for inclusion in this Report and is referenced in AR60 and in the complementary documents. It is regretted that it has not been possible to include this paper.

SOME CONSIDERATIONS OF FUTURE LOW-SPEED TUNNELS FOR EUROPE

by

A.Spence – RAE Farnborough
and
B.M.Spee – NLR Amsterdam

SUMMARY

At the request of the AGARD LaWs Working Group, two series of possible future low-speed windtunnels have been studied. The first series are high-Reynolds-number tunnels having a product of working section width in metres and maximum pressure in atmospheres kept constant at a value of 45, but including in addition a 60m atmospheric tunnel. The second series comprises atmospheric tunnels of widths ranging from 8m to 25m, and these are of more modest cost and generally lower capability than the first series. Very broad estimates of possible capital and running costs are given as an indication of the scale of expenditure which might be involved; no precise quotations have been obtained. Brief statements are made of the capabilities of the tunnels considered.

Each series in turn appears to offer attractive possibilities for future provision of low-speed tunnels in Europe.

1. INTRODUCTION

During the discussions of the AGARD LaWs Working Group, attention was given to Europe's needs for future low-speed tunnels. In order to provide a basis for these discussions, the present authors were asked to study two series of tunnels, to summarise their capabilities and to make cost estimates.

The first series studied consists of tunnels which could give high maximum Reynolds number, the value being the same for each tunnel at any chosen Mach number up to 0.2. The product of the working section width in metres and the maximum pressure in atmospheres is kept constant at a value of 45. But since there is a case for requiring the maximum Reynolds number to increase as the maximum pressure decreases because one then has a smaller range of Reynolds number (at constant Mach number) from which to extrapolate, a 60m atmospheric tunnel was added to the series.

In view of the very high capital costs of this first series, some thought has been given to several possible ways of reducing the cost, including

(a) shortening the air circuit

(b) using unconventional drives

(c) using reinforced concrete instead of steel for pressure shells

(d) using Eiffel type tunnels.

Also, a second series of tunnels has been studied, comprising atmospheric tunnels having working section widths from 8m to 25m, which could meet some of the requirements at more modest costs.

The authors each made completely independent estimates of the capital costs. Their totals agreed to better than 15 per cent, though it is not expected that the absolute values are as accurate as that might suggest. Mean values of the two estimates are given and it is believed that the orders of cost are correctly indicated. The figures given are all based on 1971 price levels. Estimates have also been made of the running costs of each facility.

2. THE FIRST SERIES; HIGH-REYNOLDS-NUMBER TUNNELS

2.1 Tunnels considered and their capabilities

Conventional return-circuit tunnels have been studied covering a range of working size and pressure from 11.25m wide at 4 atmospheres to 45m and 60m wide at atmospheric pressure. In all cases the ratio of working section width to height is 4:3.

In respect of four aircraft categories used by the LaWs Working Group in its studies, the capabilities of this series of tunnels may be summarised as follows:–

1 *For CTOL/RTOL aircraft with maximum lift coefficient* $\leqslant 4$. These tunnels could give three times the Reynolds number of tunnels currently proposed or under construction, for those cases which justify the extra cost of utilising this extra capability or of needing the use of a larger model.

2 *For RTOL/STOL aircraft with maximum lift coefficient between 4 and 8.* The tunnels could give maximum Reynolds numbers for this category of aircraft similar to those which can be reached in tunnels currently being built or planned for Category 1 above. For example, an STOL model at $C_L = 8$, sized to limit the tunnel constraint effect on the angle of incidence to 2°, could be tested at a Reynolds number of about 6 millions at a representative approach speed of 30 m/s.

3 *For powered-lift aircraft with effective lift coefficients greater than 8.* This series of tunnels can offer a greatly enhanced capability (by a factor of about 6 on Reynolds number and of 2 to 6 on scale of model) over what is currently available.

4 *For rotary-winged aircraft.* This category defines the power of each tunnel in the series as that required to give a maximum speed of 130 m/s at atmospheric pressure. Rotors of diameter two-thirds of the working section width could be tested at speeds from 130 m/s down to about 30 m/s. Lower speeds would require either a larger tandem working section or the use of a smaller model.

The Reynolds numbers, available in these tunnels (based on a length of 0.1 times the square root of the working section area) are shown as a function of Mach number in Figures 1 and 2, and are compared with those of existing and currently-planned tunnels.

2.2 Assumptions and Methods of Estimation

It has been assumed that the desirable standard of flow is similar to that intended in the RAE 5m tunnel or the NLR 8m x 6m tunnel. Accordingly, tunnel shell surface areas are those for return-circuit tunnels with a contraction ratio of about 8:1. Tunnel power factors have been taken from those of the above-mentioned tunnels with reductions for the increased Reynolds numbers and for the smaller models in relation to working section size.

For the pressurised tunnels it is assumed that the pressure shells would be made of steel. Since hoop stress largely determines the thickness required and this is proportional to the size and the pressure difference, the weight of steel is thus proportional to the cube of the scale and to the pressure difference. The cost is taken to be proportional to the weight, and therefore, based on the cost of the shell of the RAE 5m tunnel,

$$\text{Shell cost (£M)} = 20(P-1)\,(W/15)^3$$

where P is the maximum pressure in atmospheres and W is the working section width in metres.

For the atmospheric tunnels, it is assumed that the shells would be made of reinforced concrete. One of the authors (AS) made the drastic assumption that such a shell would cost $\frac{1}{8}$ of the price of a steel shell designed for 1 atmosphere differential pressure. The other (BMS) extrapolated from the value estimated for the NLR LST 8m x 6m, and since the two sets of estimates were in fair agreement if screens, corner vanes and motor housing were included, one can express the cost approximately by

$$\text{Shell cost (£M)} = 2.5\,(W/15)^3$$

but this is considered to be applicable only to tunnels larger than about 20m.

As stated earlier, each tunnel is powered to give a top speed of 130 m/s at atmospheric pressure because of the requirements of rotor testing. The maximum speed at other pressures varies as follows, depending on whether or not the fan blade angle can be varied

Pressure (atm)	2	3	4
Fixed fan V(m/s)	92	75	65
Variable fan V(m/s)	103	90	82

Either set of speeds is considered adequate since it would be acceptable to reduce the pressure when needing higher speeds for V/STOL transition work etc.

The costs of the main drive were estimated from a rough rule of £32K per megawatt. For the cooling and temperature control system of pressurised tunnels, a figure of £21K per megawatt has been used; in the case of atmospheric tunnels, however, an air interchange system would suffice and a lower cost has been taken for this of about £10K per megawatt.

Provision of pressurised air supplies becomes of major and increasing importance as the tunnel size increases, both for pumping up the pressurised tunnels and for use in engine representation in models in all tunnels. It is clear that pumping up the tunnels considered here would require impossibly large pumping capacity unless a large store of air is provided. For the pressurised tunnels the costs for the air system correspond to assuming pumps sufficient to fill the tunnel to maximum pressure in 6 hours and storage of enough air for one fill. For the atmospheric tunnels, a simple figure of about 4 to 5 per cent of the capital cost of the facility is taken for a model blowing air system.

Additional costs other than those mentioned above are estimated to vary from about 20 per cent of the total cost for an 11.25m, 4 atmosphere tunnel, to about 10 per cent for 45m and 60m atmospheric tunnels. This final addition completes the estimate and leads to capital costs which are set out in the next section.

2.3 Main Characteristics and Capital Costs of High-Reynolds-Number Tunnels

Item	*Tunnel A*	*B*	*C*	*D*	*E*	*F*
Max pressure (atm)	4	3	2½	2	1	1
Working section (m)	11.25 x 8.5	15 x 11.25	18 x 13.5	22.5 x 17	45 x 34	60 x 45
Power factor at 130 m/s, 1 atm	0.315	0.30	0.295	0.285	0.26	0.25
Power for 130 m/s (MW)	40	69	96	147	530	900
Power for 200 m/s (MW)	134	233	324	496	1800	3040
Air mass to fill (Mkg)	0.84	1.32	1.73	2.23	–	–
Reynolds number* for RTOL/STOL ÷ 10^6	1.5 – 6.0	2.0 – 6.0	2.4 – 6.0	3.0 – 6.0	6.0	8.0
Cost of shell (% of total)	67	69	71	73	65	75
Estimated total cost (£M)	35	55	70	90	110	225

* The Reynolds numbers quoted are those for a model with a maximum lift coefficient of about 8, sized to limit the tunnel constraint effect on the angle of incidence to 2°, and tested at a representative approach speed of 30 m/s. For an aspect ratio of 8, such a model would have a mean chord 0.08 times the square root of the cross-sectional area of the working section.

All the costs are estimated for continuous running at a maximum speed of 130 m/s at atmospheric pressure; the cost of the shells of the atmospheric tunnels as well as the cost of the drives of all the tunnels would increase if the maximum speed were higher.

In these estimates, the costs of compressed air systems were based on the known cost of providing pumps for the RAE 5m tunnel, together with a rough rule for storage vessels of £1 per pound of stored air. For tunnels A to D, the amount of air stored and the rate of pumping appear sufficient for model blowing requirements and engine simulation. Further study may well suggest that part of the flow should be compressed to a higher pressure than the 22 bars to which half the flow for the RAE 5m tunnel can be pumped; it may also be desirable to store some air at higher pressure. No allowance for this has been made in the cost estimates, but it seems unlikely that it would have a major effect since, as shown in the Table below, the costs of the pumps and air storage is estimated at only about 8% of the total capital cost of the whole facility.

For the atmospheric tunnels E and F, the tunnel itself has no pumping requirement, and a simple crude assumption of about 4 to 5 per cent of the total capital cost has been made for a model blowing system.

Costs of Air Pumping for High-Reynolds-Number Tunnels

Item	*Tunnel A*	*B*	*C*	*D*	*E*	*F*
Pumping rate (kg/s)	39	61	80	105	–	–
Cost of pumps (£M)	1.1	1.7	2.3	2.9	–	–
Air stored (Mkg)	0.84	1.32	1.73	2.23	–	–
Cost of storage (£M)	1.8	2.9	3.8	4.9	–	–
Estimate of rate of flow required for model with internal jet flap (kg/s)	120	160	200	250	490	870
Estimated total cost of air system (£M)	2.9	4.6	6.1	7.8	5	9

The cost estimates agree fairly well with NASA estimates given in LaWs Group Paper No. 19. There the cost of a 150 ft x 75 ft atmospheric tunnel is about £60M. The working section area of this is the same as that of a 37½m x 28m tunnel, for which the methods of the present report would give £70M, but the latter tunnel would have a longer circuit and a larger contraction ratio.

2.4 Running Costs of High-Reynolds-Number Tunnels

Estimates of running costs have been made, broadly on the lines used by Hills in LaWs Group Paper No. 49 and in Section 8.6 of the LaWs Group Report. The main assumptions are as follows:–

1 Each tunnel is powered for continuous running at 130 m/s at atmospheric pressure.

2 Tunnel usage is divided 40 per cent to rotary wing aircraft and 60 per cent to fixed-wing aircraft of the other three categories listed in Section 2.1. Since the latter are tested at lower tunnel speeds, the power used for them is reduced more in atmospheric tunnels than in pressurised tunnels in which the pressure would be raised for such tests. The ratio of mean power to maximum power has been taken to fall from 0.75 in a 4 atmosphere tunnel to 0.375 in the atmospheric tunnels.

3 The maximum power has been taken to be the sum of the main drive power and the pumping power.

4 Since testing of rotary wing aircraft will not usually demand compressed air, but for other types of work the pumps will require to run about twice the tunnel running hours for pressurised tunnels, the mean power consumption of these tunnels has been taken to be the sum of the mean power of the main drive and the maximum power of the pumps. For the atmospheric tunnels, a guess has been made that the average pumping power will be about a quarter of the maximum.

5 The same electricity charges have been used as in LaWs Group Paper No. 49, ie a maximum demand charge of £2500 per megawatt and a power consumption charge of £4.3 per megawatthour.

6 Again as in LaWs Group Paper No. 49 the costs of labour, materials and equipment are assumed to be £350K for 1000 hr/yr of running, and £410K for 2000 hr/yr.

7 It has been assumed that the average rate of data recording is 5 polars/hr for all types of work.

These running cost estimates are set out in the following table, both for 1000 hr/yr and 2000 hr/yr of running time and both including and excluding amortisation and interest on capital taken as a total of 10 per cent of the estimated capital cost.

Running Costs of High-Reynolds-Number Tunnels

Item	*Tunnel A*	*B*	*C*	*D*	*E*	*F*
Max drive power (MW)	40	69	96	147	530	900
Factor to mean power	0.75	0.625	0.56	0.50	0.375	0.375
Mean drive power (MW)	30	43	54	73	200	340
Max pumping power (MW)	19	30	41	56	37	67
Power for max demand (MW)	59	99	137	203	567	967
Mean power used (MW)	49	73	95	129	209	357
Max demand cost £2500/MW	£ 147K	£ 247K	£ 342K	£ 510K	£ 1410K	£ 2420K
10 per cent of capital cost	£3500K	£5500K	£7000K	£ 9000K	£11000K	£22500K
I For 1000 hr/yr						
Power charge, £4.3/MW hr	£ 210K	£ 314K	£ 408K	£ 555K	£ 900K	£ 1530K
Labour etc.	£ 350K	£ 350K	£ 350K	£ 350K	£ 350K	£ 350K
Total (without interest etc)	£ 707K	£ 911K	£1100K	£ 1415K	£ 2660K	£ 4300K
Total (with interest etc)	£4200K	£6400K	£8100K	£10400K	£13700K	£26800K
Cost/polar (without interest)	£ 141	£ 182	£ 220	£ 283	£ 532	£ 860
Cost/polar (with interest)	£ 840	£1280	£1620	£ 2080	£ 2740	£ 5360
II For 2000 hr/yr						
Power charge, £4.3/MW hr	£ 420K	£ 628K	£ 816K	£ 1110K	£ 1800K	£ 3060K
Labour etc.	£ 410K	£ 410K	£ 410K	£ 410K	£ 410K	£ 410K
Total (without interest, etc)	£ 977K	£1285K	£1568K	£ 2030K	£ 3620K	£ 5890K
Total (with interest, etc)	£4500K	£6800K	£8600K	£11000K	£14600K	£28400K
Cost/polar (without interest)	£ 98	£ 128	£ 157	£ 203	£ 362	£ 589
Cost/polar (with interest)	£ 450	£ 680	£ 860	£ 1100	£ 1460	£ 2840

2.5 Possibilities for Reducing the Costs

Because of the very high costs of all the tunnels in this series, some consideration has been given to various ways of reducing the costs of the tunnel shells and also of reducing the power requirements.

One possibility is to use reinforced concrete instead of steel in the construction of the shells of pressurised tunnels. Very brief discussions with UK experts in the use of concrete have suggested that the construction of a tunnel such as Tunnel B above is feasible and that the cost of the shell in reinforced concrete might be of the order of three-quarters of that for a steel shell. This suggestion was based on 2 man-days of work and for a better estimate a design study lasting about 3 months would be needed.

Another possibility is illustrated in Figure 3. This is based on two main ideas, first that the pressurised tunnels might well spend three-quarters of their usage at atmospheric pressure and therefore perhaps could do without the kind of access arrangements to the working section which are being provided in the RAE 5m tunnel; second that the compressed air supplies envisaged could be used for boundary layer control in rapid diffusers. A rather extreme circuit is shown in Figure 3 which keeps all its corners the same sizes as in the conventional circuit, but has its first and second diffusers shortened by a factor of 4, and the rapid expansion after the third corner by a factor of 2. If such a circuit could be made to work acceptably, the shell cost for a 15m, 3atm tunnel could be reduced by about £15M, though this would be offset to some extent by greater development costs and by the costs of the b.l.c. system. It is not clear how big the nett saving could be.

The high power requirements of the tunnels considered arise from the need to provide high speeds for rotor testing. Some thought has been given to the possibility of reducing the power level. The authors believe that, for a long time to come, it will be necessary to provide continuous running for V/STOL work, even more so than for CTOL/RTOL work, and discussions about testing of rotary-wing aircraft suggest that, as a minimum, a slow, controlled run-up and run-down are needed, leading to a total run time measured in minutes rather than seconds. Brief consideration has therefore been given to a scheme in which an electric drive is sized to drive the tunnel at a modest speed by means of a fan and the higher speeds are reached by use of stored compressed air applied to the fan in the form of a jet flap. In the case of the pressurised tunnels, the cost estimates included an allowance for storing sufficient air to fill the tunnel to maximum pressure. First results suggest that this method could be used to drive a 15m, 3atm tunnel for 3 minutes every hour at 130 m/s at atmospheric pressure, provided there was an electric drive sufficient to drive the tunnel at half speed at three atmospheres and this required 26 MW instead of 69 MW. For atmospheric tunnels, the savings in drive power could lead to greater percentage reductions in the overall capital costs than for pressurised tunnels, but this would be offset by the need for a large increase in compressed air supply.

It is sometimes suggested that for atmospheric tunnels, the Eiffel type would be considerably cheaper than a return-circuit tunnel. The authors' experience suggests that for the same, good quality of flow and the same drive power, the costs would be much the same even if the Eiffel tunnel has its diffuser divided so that it could be shortened. It may be that the cost could be reduced by having less diffusion and a larger power requirement, but we would not expect the cost reduction to be large.

2.6 Relative Merits of the Pressurised and the Atmospheric Tunnels

Although it is not possible to make any definite recommendations it seems desirable at this point to set out some of the main differences between the pressurised and the atmospheric tunnels.

1 For a given maximum Reynolds number, the pressurised tunnel will be considerably cheaper both in capital cost and in running cost.

2 The use of pressurisation gives a range of Reynolds number at constant Mach number, from which to extrapolate towards full scale and the required maximum Reynolds number may therefore be lower. However, it may not be safe to rely on this in all cases because of our limited ability to define Reynolds numbers above which scale effect will be regular and understandable.

3 It is expected that the smaller models for the pressurised tunnels will generally be quicker and cheaper to make in spite of the higher loading.

4 The large atmospheric tunnels offer the advantage of testing a larger range of full-scale hardware including real engines and real aircraft, but such tests will usually have to wait until a later stage in the development of a project.

2.7 Concluding Remarks on the Series of High-Reynolds-Number Tunnels

1 It is clear that both the capital costs and the running costs of these tunnels are extremely high and that they rise rapidly with increasing size.

2 In the opinion of the authors, tunnel A (11.25m, 4atm) is too small and that its high maximum pressure would make for serious difficulties arising from model distortion.

3 Tunnel B (15m, 3atm) is the smallest and cheapest facility of this series which deserves serious consideration if the high Reynolds numbers aimed at in this series are to be achieved.

4 Tunnel B is limited in its size and would not suffice to do much of the full-scale hardware testing discussed in Section 2.6.

5 The use of reinforced concrete pressure shells and of unconventional circuits and drives should be studied further as means of reducing the costs of these facilities.

3 THE SECOND SERIES: ATMOSPHERIC TUNNELS OF MORE MODEST COST

3.1 Cost Estimates

In view of the very high capital and running costs of the high-Reynolds-number tunnels discussed in Section 2, some thought has been given to atmospheric tunnels of more modest size and cost and to the question of whether these offer particular attractions in their capabilities. In this second series of windtunnels, the sizes of tunnel considered range from 8m to 25m, with a height which is three quarters of the width. The assumptions are consistent with those of Section 2:

1 Conventional return circuits with contraction ratio of 8:1.

2 Maximum speed 130m/sec, to satisfy conventional helicopter needs.

3 Tunnel shell constructed in reinforced concrete.

The main characteristics and costs of this series of windtunnels are given in the Table on page 1-7.

In the size range above 25m, it could be assumed that the mean thickness of concrete is proportional to the linear scale and, therefore, the weight of concrete and the cost of the shell are proportional to the cube of the scale. Below 25m, however, the mean thickness of concrete required is thought to be fairly constant and, therefore, the shell cost varies with the square of the scale. At the same time the ratio of shell cost to total cost falls from 0.46 for a 25m tunnel to about 0.24 for an 8m tunnel.

On these bases, a consistent set of estimates was made, which is given in the Table below.

Main Characteristics and Capital Costs of Atmospheric Tunnels

Item	*Tunnel 1*	*2*	*3*	*4*	*5*	*6*	*7*	*8*
Working section (m)	8 x 6	10 x 7.5	12 x 9	14 x 10.5	16 x 12	18 x 13.5	20 x 15	25 x 18.75
Power factor (130m/s, 1 bar)	0.33	0.325	0.32	0.31	0.30	0.295	0.29	0.28
Power for 130m/s (MW)	22	33	47	61	78	96	117	177
Power for 200m/s (MW)	75	112	159	207	264	325	380	600
Reynolds number for RTOL/ STOL tests ($\div 10^6$)	1.05	1.3	1.6	1.85	2.1	2.4	2.6	3.3
Cost of shell (% of total)	24	28	32	34	37	40	42	46
Estimated total cost (£M)	5	6½	8½	11	13	15	18	25

It is worth noting that the total cost of the main drive motors and cooling system for the RAE 5m tunnel is about £53K per MW. Taking half the cost for the cooling system, the drive and cooling costs for the above atmospheric tunnels are about two-thirds of the costs of the tunnel shell when the top speed is 130 m/sec. If the speed requirement were raised to 200 m/sec, the drive cost would be more than trebled and this would increase the capital cost of any of the above tunnels by about 60% without allowing for the extra costs of the thicker tunnel shell which would be needed.

Estimates of running costs have also been made, using the same assumptions as for the series of high-Reynolds-number tunnels. These are given in the Table below.

Running Costs of Atmospheric Tunnels

Item	*Tunnel 1*	*2*	*3*	*4*	*5*	*6*	*7*	*8*
Max drive power (MW)	22	33	47	61	78	96	117	177
Factor to mean power	0.375	0.375	0.375	0.375	0.375	0.375	0.375	0.375
Mean drive power (MW)	8	12	18	23	29	36	44	66
Max pumping power (MW)	1	2	3	4	5	6	7	11
Power for max demand (MW)	23	35	50	65	83	102	124	188
Mean power used (MW)	8	12½	19	24	30	38	46	69
Max demand cost, £2500/MW	£ 58K	£ 87K	£ 125K	£ 162K	£ 207K	£ 255K	£ 310K	£ 470K
10 per cent of capital cost	£ 500K	£ 650K	£ 850K	£1100K	£1300K	£1500K	£1800K	£2500K
I For 1000 hr/yr								
Power charge, £4.3/MW hr	£ 35K	£ 54K	£ 82K	£ 103K	£ 129K	£ 163K	£ 198K	£ 296K
Labour etc	£ 350K	£ 350K	£ 350K	£ 350K	£ 350K	£ 350K	£ 350K	£ 350K
Total (without interest etc)	£ 443K	£ 491K	£ 557K	£ 615K	£ 686K	£ 768K	£ 858K	£1120K
Total (with interest etc)	£ 943K	£1140K	£1410K	£1715K	£1990K	£2270K	£2660K	£3620K
Cost/polar (without interest)	£ 89	£ 98	£ 111	£ 123	£ 137	£ 154	£ 172	£ 224
Cost/polar (with interest)	£ 189	£ 228	£ 282	£ 343	£ 398	£ 454	£ 532	£ 724
II For 2000 hr/yr								
Power charge	£ 70K	£ 108K	£ 164K	£ 206K	£ 258K	£ 326K	£ 396K	£ 592K
Labour charge	£ 410K	£ 410K	£ 410K	£ 410K	£ 410K	£ 410K	£ 410K	£ 410K
Total (without interest etc)	£ 538K	£ 605K	£ 699K	£ 778K	£ 875K	£ 991K	£1116K	£1472K
Total (with interest)	£1040K	£1260K	£1550K	£1880K	£2180K	£2490K	£2920K	£3970K
Cost/polar (without interest)	£ 54	£ 60	£ 70	£ 78	£ 88	£ 99	£ 112	£ 147
Cost/polar (with interest)	£ 104	£ 126	£ 155	£ 188	£ 218	£ 249	£ 292	£ 397

3.2 Capabilities of the Series of Atmospheric Tunnels

Tunnels 1 to 4 of the above series were included mainly in order to connect the series back to existing and planned tunnels. They do not offer very significant advances over the latter.

Tunnels 6 to 8 (5 being a borderline case) are considered to offer very real advantages. Tunnel 6 (18m wide) could provide for testing rotors of a size (11m diameter) sufficient for use on a demonstrator aircraft. All three tunnels, to an increasing extent as size increases, could permit:–

1 tests on experimental aircraft and other small aircraft,

2 tests on full-scale engines,

3 noise measurements covering a considerably larger field surrounding a model than are currently possible in Europe.

Indeed, tunnels in this range are broadly equivalent to the NASA 40ft x 80ft tunnel, and the continuing usefulness and pressure of work of this tunnel argue strongly in favour of the provision of a tunnel of at least similar capability in Europe.

However, it must be noted that:–

1 the Reynolds numbers achieved in tunnels of this range are low compared with those of the first series discussed in Section 2,

2 even in Tunnel 8 (25m), the largest RTOL/STOL model or aircraft which could be tested at a lift coefficient of 8 say, would be only about 13 or 14m span.

4 CONCLUDING REMARKS

In order to help in the deliberations of the AGARD LaWs Working Group, two series of low-speed tunnels have been studied, their capabilities briefly surveyed, and estimates of both their capital costs and running costs given. The cost data shown are based on the authors' own estimates and it should be appreciated that a more detailed assessment would be needed to establish reliable cost information. In effect the conclusions are to be found in the report of the LaWs Group.

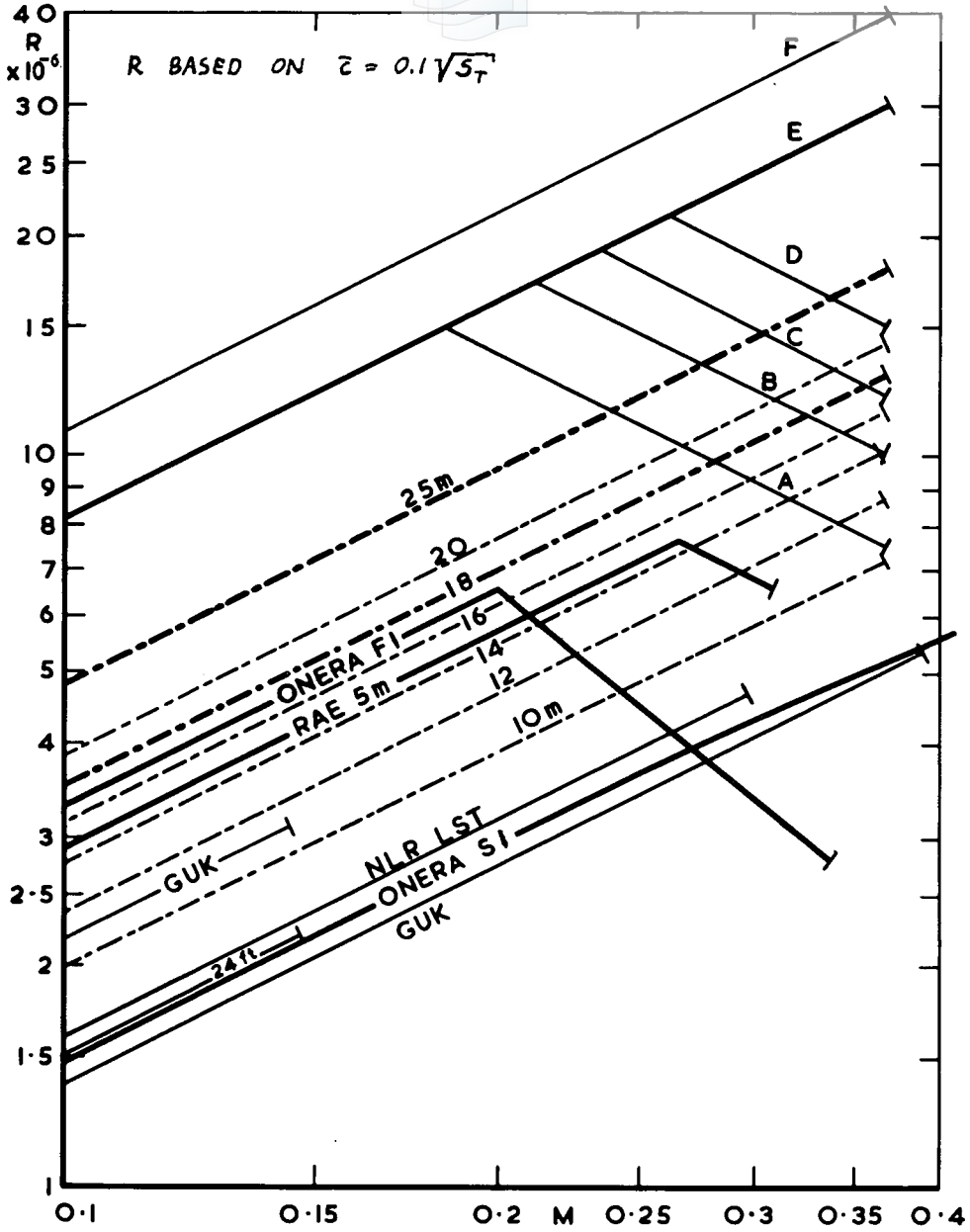

Fig.1 Maximum Reynolds numbers of low-speed windtunnels

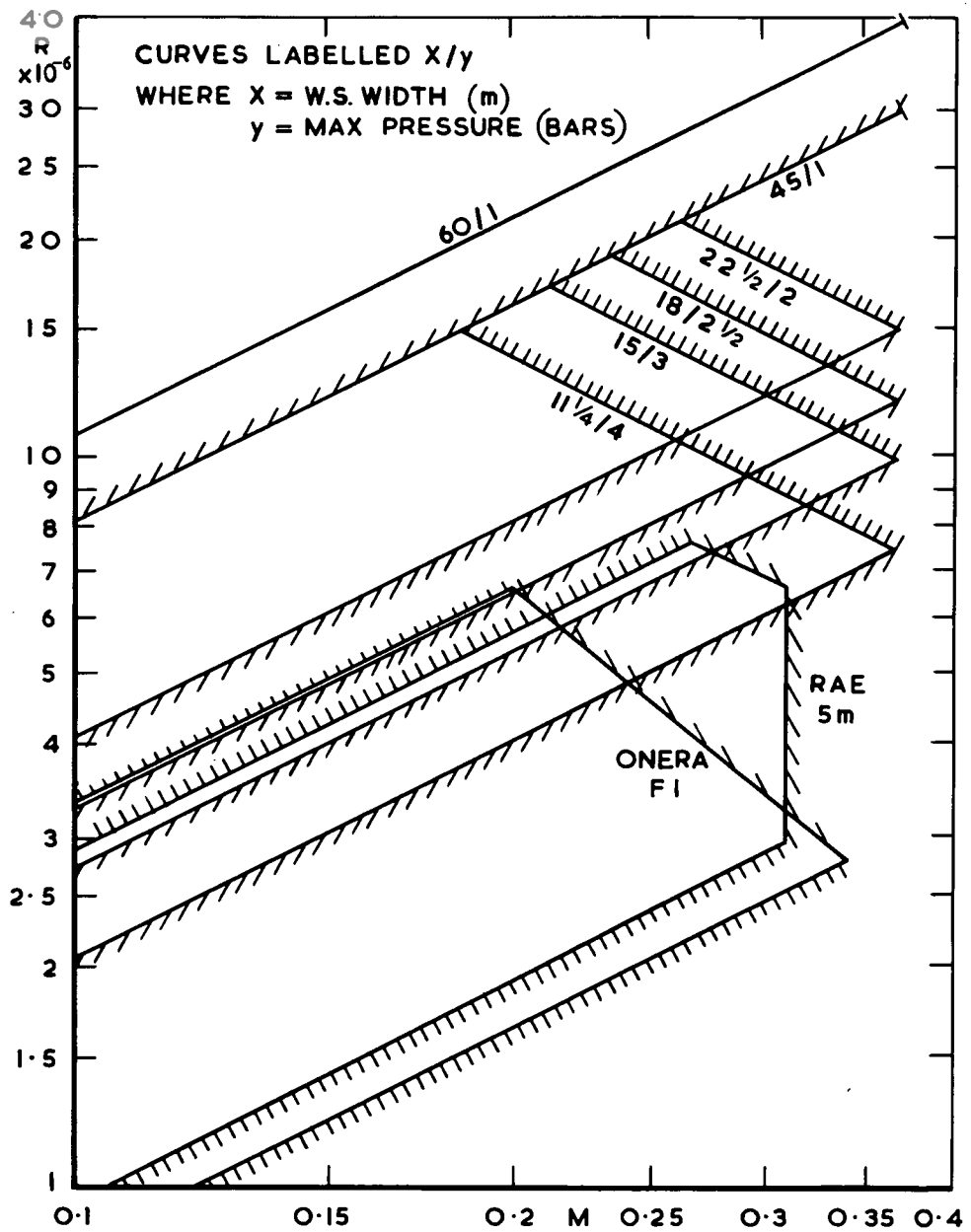

Fig.2 Operating envelopes of various low-speed windtunnels

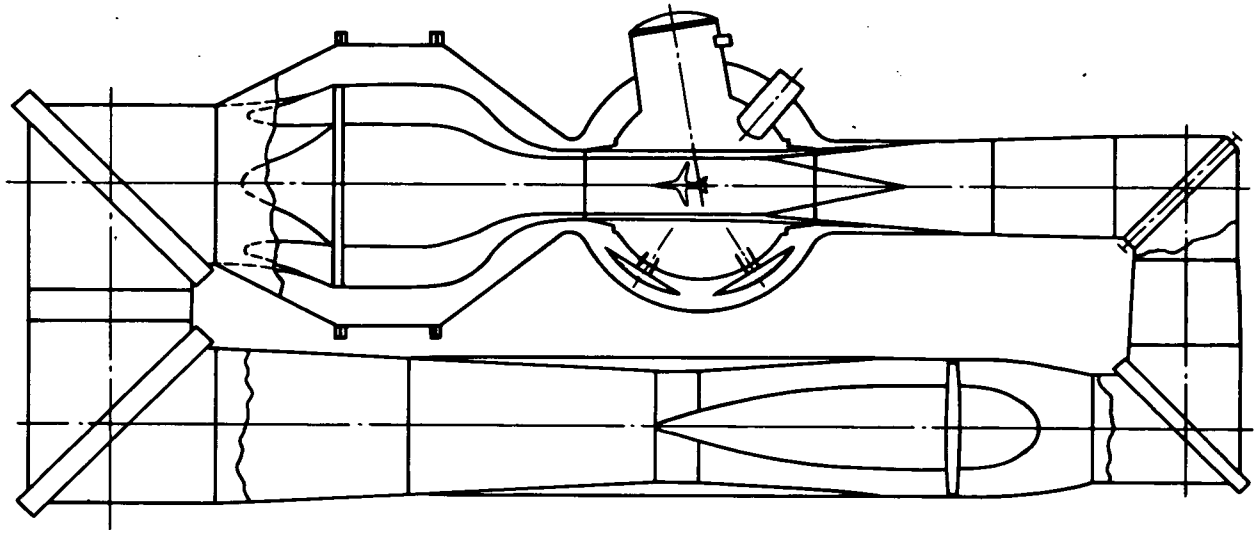

CONVENTIONAL CIRCUIT WITH ACCESS ARRANGEMENT

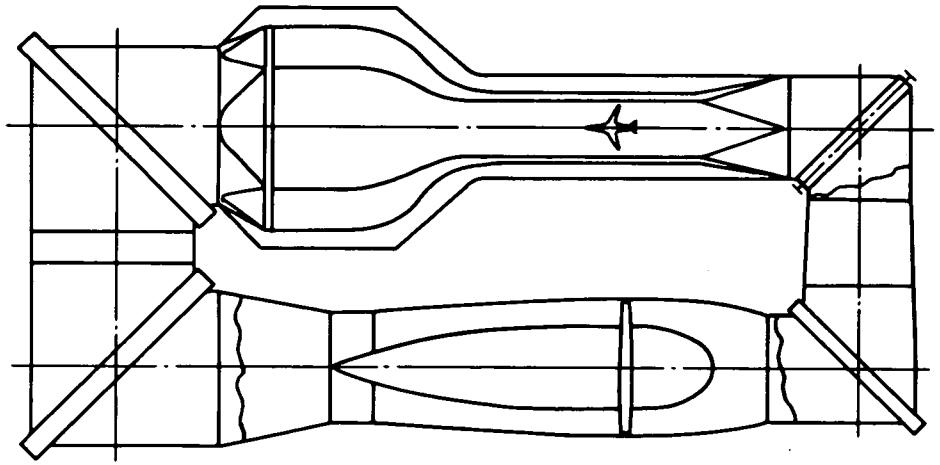

MINIMUM CIRCUIT WITH B.L.C. DIFFUSERS

Fig.3 Layouts for low-speed windtunnels

PROJECT STUDY OF A LARGE EUROPEAN TRANSONIC LUDWIEG TUBE WINDTUNNEL

by H. Ludwieg *), H. Grauer-Carstensen **), W. Lorenz-Meyer ***)

Deutsche Forschungs- und Versuchsanstalt für Luft- und Raumfahrt e.V.

- Aerodynamische Versuchsanstalt Göttingen -
Institut für Strömungsmechanik

SUMMARY

A Study of a transonic Ludwieg Tube windtunnel is presented. For a reliable extrapolation of windtunnel measurements to full-scale flight conditions of modern aircraft, a realistic simulation of flight Reynolds Numbers at transonic speeds becomes increasingly important. It is shown, how the need for a high Reynolds Number experimental facility can be satisfied by a Ludwieg Tube tunnel. The Ludwieg Tube is characterized by its unsurpassed simplicity which guarantees a high degree of reliability. Design data, dimensions, and cost estimates for the described tube windtunnel are presented. The basic facility characteristics are given in PART A and in a supplementary PART B , which adapts the tunnel characteristics to the LaWs-Specifications.

NOTATION

$a = \sqrt{\gamma \cdot R \cdot T}$	Speed of sound	τ	Tunnel run time
D_{tube}	Diameter of the charge tube	$\tilde{\tau} = \frac{U \cdot \tau}{\sqrt{F}}$	Non-dimensional run time
E	Energy	γ	Ratio of specific heats
F	Test section area	η	Efficiency
F_{tube}	Cross section of charge tube	μ	Viscosity
L	Length of tube	Subscripts	
$M = \frac{U}{a}$	Mach Number	$0'$	Charge tube (tube 1)
m	Mass	$0''$	Recovery tube (tube 2)
$\dot{m}$	Mass rate	1	Free-stream conditions in tube 1 behind expansion wave
N	Power	2	Free-stream conditions in tube 2 behind diffusor
p	Pressure		
$q = \frac{1}{\rho} \rho U^2$	Dynamic pressure	3	Free-stream conditions between contact surface and shock
$Re = \frac{U \cdot \rho \cdot 0.1 \cdot \sqrt{F}}{\mu}$	Reynolds Number		
$Re_m = \frac{U \cdot \rho}{\mu}$	Unit Reynolds Number	01	Stagnation conditions in tube 1 behind expansion wave
R	Gas constant (= 287.1 Joule/kg grd)	02	Stagnation conditions in tube 2 downstream of the diffusor
T	Temperature	03	Stagnation conditions between contact surface and shock
U	Velocity		
V	Volume	∞	Free-stream conditions in the test section
ρ	Density	ad	Adiabatic

*) Chief, Fluid Dynamics Department

**) Senior Scientist Fluid Dynamics Department

***) Deputy Chief, Fluid Dynamics Department

at	Atmospheric	comp	Compressor
test	Test section	term	Terminal conditions in the charge tube

PART A

1. INTRODUCTION

In recent years, the need for transonic test facilities at very high Reynolds Numbers was recognized after it has been demonstrated, that data obtained from existing windtunnels can not be extrapolated to full-scale flight conditions with sufficient reliability (see Ref. [2], [3]). Because of the extremely high power requirements, a continuously running windtunnel does not appear to be feasible and one depends on intermittently working tunnels with energy storage. Among other possibilities, a tube windtunnel, as described first by Ludwieg [1], is a suitable facility. Although all known windtunnel facilities of the Ludwieg -Tube-type have very short run times, it will be shown in this study, that also the LaWs-requirements with a run time of about $\tau = 10$ seconds clean flow can be satisfied perfectly by a tube windtunnel. A corresponding project proposal is outlined in the following.

2. GENERAL FACILITY REQUIREMENTS FOR A EUROPEAN TRANSONIC WINDTUNNEL

Projecting a transonic intermittent windtunnel, certain design data - such as Mach Number range, maximum Reynolds Number, stagnation pressure, tunnel run time and utilization (number of tests per hour) - are determined by the requirements of the prospective users. Principally, the stagnation temperature can be chosen independently, in practice, however, its value is bound by the operating principle of the tunnel if one wants to avoid expensive refrigeration. In order to determine the design data mentioned above, the following requirements should be satisfied in the authors' opinion.

2.1 Mach Number Range

The Mach Number range should cover the entire transonic and the compressible subsonic range, i.e. the Mach Number should range from about $M_\infty = 0.3$ to $M_\infty = 1.4$. But as Mach Numbers higher than 1.3 make it necessary to provide a flexible nozzle upstream of the transonic test section, it seems better to us, to restrict the Mach Number range to $M_\infty = 1.3$ at the maximum.

2.2 Reynolds Number Range

It should be possible to achieve a maximum Reynolds Number (based on mean wing chord) of 30 to 40 Million at a reference Mach Number of $M_\infty = 1.0$. This means a Reynolds Number of 4 to 5×10^8 based on $\sqrt{F}$ (F = area of test section). In addition, the Reynolds Number should be largely variable by variation of the total pressure (see also SECTION 2.3).

2.3 Stagnation Pressure

Admissible forces on models and model-supports put a restraint on the total pressures at maximum Reynolds Number [Ref. 6]. With regard to the fact that the projected windtunnel will be used mainly for measurements on airplane models, it appears to be reasonable to limit the stagnation pressure to values between 5 and 8 bar (1 bar = 10^5 N/m^2), or else to risk that the tunnel capability can not be utilized fully. It should be possible, however, to run the tunnel at largely reduced stagnation pressure with good flow quality. On the other hand the structure of the tunnel should be designed so that stagnation pressures of 11 bars are feasible to achieve much higher Reynolds Numbers on special models.

2.4 Tunnel Run Time

Rather than the actual running time τ a relevant parameter is a scaled nondimensional run time $\tilde{\tau}$ which is defined (in the form of a reciprocal Strouhal Number) by

$$\tilde{\tau} = \tau \cdot U_\infty / \sqrt{F} \qquad (1)$$

Comparing windtunnels of different sizes (especially at equal stagnation pressures) the frequency of disturbances (unsteadiness of the flow, model oscillations) is about inversely proportional to the tunnel size. Thus, in order to eliminate the disturbances by a time averaging procedure, the test job requires a certain value of $\tilde{\tau}$ (and not τ).

The run time should be sufficiently long, so that at least a complete six-component polar or a complete pressure distribution at fixed angle of attack can be measured with high accuracy during a single tunnel run. It should also be possible to a certain extent to investigate unsteady aerodynamic phenomena.

In order to meet these requirements we feel that a value of 400 to 700 for $\tilde{\tau}$ is appropriate. For a 4.5 x 4.5 m^2 tunnel this corresponds to an actual run time from 6 to 10 seconds.

From an economic point of view it is advantageous, if the tunnel can be operated with reduced run time. Thus, times for starting and stopping the tunnel should be as short as possible in order to save storage energy.

2.5 Run Frequency

The run frequency, which will satisfy future needs for high Reynolds Number transonic testing, can hardly be predicted. As a tentative estimate, we feel, that a run frequency of 20 to 40 tunnel runs per 8 hour shift at maximum Reynolds Number and transonic Mach Numbers is entirely sufficient. It should be mentioned that the run frequency can considerably be increased when tests are performed at lower Reynolds Numbers, low Mach Numbers or reduced run time.

2.6 Stagnation Temperature

For the tunnel under consideration one should aim at a low stagnation temperature T_{01}. For fixed Reynolds Number, stagnation pressure, and scaled run time a simple calculation yields, that total mass per tunnel run (m), total volume per tunnel run (V) and linear scale of the tunnel ($\sqrt{F}$) depend in the following way on T_{01}:

$$m \sim T_{01}^{2.78}; \qquad V \sim T_{01}^{3.78}; \quad \sqrt{F} \sim T_{01}^{1.26}$$

assuming that $\mu \sim T_{01}^{0.76}$.

Thus, construction costs ($\sim V$) and operational costs ($\sim m$) decrease more than proportional with the stagnation temperature T_{01}.

2.7 Flow Quality

Beside the LaWs-Fequirement, that the new tunnel should be substantially better than existing tunnels - with the cleanest and quietest possible airstream - there are for an intermittent tunnel special requirements regarding the flow uniformity in time. Expecially the presence of velocity fluctuations with medium frequencies (order 1 Hertz) would reduce the accuracy of force measurements if the test duration is of the order 1 sec.

2.8 Economic Requirements

Apart from technical needs it is important for a tunnel of this size, to keep construction costs and operation costs low. Also, the facility should be dependable in order to avoid deadlocks and easy to handle. A simple construction is favourable if construction time shall be saved.

3. FULFILMENT OF THE REQUIREMENTS BY A TUBE WINDTUNNEL

The requirements with regard to Mach Number range, maximum Reynolds Number, stagnation pressure and test duration (Sections 2.1 to 2.4) can be satisfied by a tube windtunnel if test section area, storage pressure, diffusor cross section and tube length are chosen appropriately.

The simultaneous fulfilment of the two requirements regarding test duration (2.4) and good flow quality (2.7) has to be discussed in some more detail. The operating principle of the tube tunnel, viz. the way of accelerating the gas flow, yields initially a highly uniform flow. However, after starting the flow in the tube, a time dependent boundary layer is formed on the wall of the tube, whose thickness increases with time. The rate of growth of this boundary layer depends on the flow velocity, the Mach Number, the Reynolds Number and the roughness of the tube wall. A certain time τ_1 after starting the tunnel, the outer edge of this boundary layer will reach the axis of the tube near the nozzle entrance, where reaching the tube axis means that time at which the first velocity fluctuations of the boundary layer reach the axis. This time τ_1 slightly differs from a time τ_2, marking that moment, at which the turbulent boundary layer profile has been fully established at the nozzle entrance. Experimental investigations of E. Piltz [7] show that τ_2 exceeds τ_1 by approximately 30 %. Cautious estimates of the boundary layer growth assuming a hydraulically smooth wall show, according to theoretical and experimental studies of

Piltz, that for a design tube Mach Number of $M_1 = 0.3$ the chosen running time (10 s observation time plus 1 s starting time) is well within τ_2. All this considerations, however, are related to the velocity distribution within the charge tube upstream of the nozzle. It has to be discussed now which is the influence of this velocity distribution on the velocity profile within the test section. If one assumes for this purpose, that, at the end of the run time, the turbulent pipe flow following an 1/11 power law has been fully established, one can compute the velocity distribution within the test section (for a test section Mach Number of $M_\infty = 0.9$) by assuming constant total pressure along each stream line during the expansion through the nozzle. This assumption is certainly valid except for a very thin region close to the wall, where a new boundary layer is formed, which exists in all types of tunnels and which has nothing to do with the Ludwieg tube principle.

The resulting velocity profile in the test section computed for the end of the observation time is presented in Fig 3 in a normalized form and compared to the profile ahead of the nozzle, assuming, for simplicity, a circular test section. The analysis shows, that the velocity distribution of a 63 % core remains within $\pm$ 0.5 % and that of a 90 % core within $\pm$ 1.0 % of the mean velocity.

The real distribution will be even better since, first the fully developed turbulent profile of a flow through a tube is fuller at high Reynolds Numbers than described by the 1/11 power law and second, as cited above already, the fully developed profile ahead of the nozzle has not been established at the end of the run time.

Another consequence of the continuous growth of the boundary layer is a slight change - linear with time - of the stagnation pressure. In Ref. [7] , however, it is shown that for tube Mach Numbers in the region of $M_1 = 0.2$ to $M_1 = 0.3$ the time variation of the stagnation pressure becomes very small, apparently due to compensation of opposing effects. More detailed estimates of the behaviour of the tube wall boundary layer are given by E. Becker [8, 9].

The radiation of noise from the charge tube into the test section is - due to the low flow velocity in the charge tube - insignificant and far below the unavoidable noise radiated from the boundary layer on nozzle and test-section walls.

There are two more arguments in favour of a tube windtunnel. The unsteady expansion wave reduces the stagnation temperature T_{01} below its value in the charge tube. The advantage of a low stagnation temperature was outlined in section (2.6).

The requirements of dependability, little service, and simple construction (2.8) are met in a perfect way by the principle of the tube tunnel, as there are no moving parts except for the opening valve.

With regard to the requirement of low costs, two different systems must be distinguished. If construction costs shall be saved, the first system is preferable. In this case, the tunnel blows into the open air. In order to recharge the tunnel, the air must be compressed from atmospheric to charge pressure. The second system, which keeps operating costs low, can be achieved by joining a pressure container at the downstream end of the diffusor. This container can be a normal pressure vessel or a secondary tube as it was used by A. Weise for his shock windtunnel. Both kinds of containers have advantages and disadvantages. We decided for a secondary tube. This tube is charged to a pressure just as high that the tunnel can still be started. During the test, a shockwave travels from the diffusor exit to the end of the tube and back, increasing thereby the pressure in the "recovery tube". To recharge the tunnel, the air is pumped back from the "recovery tube" into the charge tube. The energy savings that can be achieved in this way amount to 75 % - 80 % when the tunnel is operated at maximum stagnation pressure. The savings on compressor and air dryer systems make up for part of the additional costs of the "recovery tube". Another argument in favour of the "recovery tube" is that it reduces the emission of noise into the environment. Figure 1 gives an overall view of the proposed facility with an indication of the construction groups.

4. EVALUATION AND SPECIFICATION OF THE REGIME OF OPERATION OF THE TUNNEL

In the preceding sections, crucial reasons for selecting the Ludwieg-Tube concept to meet the data requirements were outlined. The most important aerodynamic design data which were selected in close agreement with LaWs-Specifications are summarized below. They are valid for a test section Mach Number of $M_\infty = 1.0$. The data are followed by an example of the computational procedures utilized in deriving the geometric tunnel parameters.

4.1 Project Data

Reynolds Number (based on $0.1\sqrt{F}$)	Re_{max}	$= 46 \cdot 10^6$
Stagnation pressure	p_{01}	= 7.0 bar
Dimensionless run time	$\tilde{\tau}$	= 700
Mach Number range	M_∞	= 0.3 to 1.3

The determination of the tunnel geometry requires further the knowledge of the tube Mach Number M_1 and the air temperature in the charge tube prior to the start of the tunnel

Tube Mach Number	M_1	= 0.3
Temperature in the charge tube	T_0'	= 308 K

The notation used in the following sections is shown in Figure 2. The slight deviation from the terminology commonly used, results from the Ludwieg - Tube concept.

4.2 Tube Mach Number

The ratio of test section area F to tube cross section F_{tube} can be obtained for a given tube Mach Number and a test-section Mach Number of $M_\infty = 1.0$ from standard gasdynamic flow tables. Here

$$F/F_{tube} = \frac{\rho_1 U_1}{\rho_{01} a_{01}} \quad (M_1 = 0.3) \; / \; \frac{\rho_\infty U_\infty}{\rho_{01} a_{01}} \quad (M_\infty = 1) = 0.4914$$

The area ratio allows the computation of the tube Mach Number for a given test section Mach Number with the aid of the following equation

$$0.4914 \cdot \frac{\rho_\infty \cdot U_\infty}{\rho_{01} \cdot a_{01}} \quad (M_\infty) = \frac{\rho_1 \cdot U_1}{\rho_{01} \cdot a_{01}} = f\,(M_1\,(M_\infty)) \qquad (2)$$

Figure 4 shows the variation of the tube Mach Number with M_∞.

4.3 Stagnation Temperature

The specified storage temperature of $T_0' = 308$ K is somewhat arbitrary, however, this temperature represents an upper limit, which is reached under unfavourable weather conditions which affect the cooling and drying processes.

The ratio of stagnation temperature T_{01} to storage temperature T_0' is for the Ludwieg-Tube tunnel a function of the tube Mach Number M_1

$$\frac{T_{01}}{T_0'} = \frac{1 + \frac{\gamma - 1}{2} M_1^2}{(1 + \frac{\gamma - 1}{2} M_1)^2} \qquad (3)$$

Figure 4 shows the variation of stagnation temperature T_{01} (in Centigrades) with M_∞.

4.4 Pressure Range

The maximum stagnation pressure was, selected to be $p_{01} = 7.0$ bar. The relation between charge and stagnation pressure for a Ludwieg -Tube tunnel is

$$\frac{p_{01}}{p_0'} = \left\{ \frac{1 + \frac{\gamma - 1}{2} M_1^2}{(1 + \frac{\gamma - 1}{2} M_1)^2} \right\}^{\frac{\gamma}{\gamma - 1}} \qquad (4)$$

Equation (4) allows the calculation of the charge pressure corresponding to $(p_{01})_{max.}$ at $M_\infty = 1.0$: $p_0' = 10$ bar.

The stagnation pressure that can be achieved with this charge pressure is plotted in Figure 5 as function of M_∞. The lower limit in stagnation pressure results from the requirement of being able to start the tunnel. The minimum stagnation pressure at $M_\infty = 1.0$ is, assuming atmospheric exhaust (Case 1) and a well designed diffusor, $p_{01\,min} = 1.5$ bar. The corresponding charge pressure ist $p_0' = 2.12$ bar. The latter determines the lower boundary of the stagnation pressure range. Also plotted in Fig. 5 ist the range of dynamic pressure q_∞.

4.5 Reynolds Number, Test Section Area and Tube Diameter

With the aid of the design Reynolds Number of $Re_{max} = 46 \cdot 10^6$ one can now easily determine the test section area F. At a Mach Number of $M_\infty = 1.0$ ($T_{01} = 279$ K, $p_{01} = 7.0$ bar), the unit Reynolds Number is $Re_m = 109.5 \cdot 10^6$ m^{-1}.

This results in a test section area of

$$\sqrt{F} = \frac{10 \cdot Re}{Re_m} = 4.2 \text{ m} \tag{5}$$

The Reynolds Number range of the tunnel is shown in Figure 6. The characteristic length here is $1/10.\sqrt{F}$. At higher Mach Numbers, $1/12.\sqrt{F}$ is sometimes used. The Reynolds Number range corresponding to the latter is indicated by the dashed line.

Tube cross section area and tube diameter can now be derived from the known test section area F and the ratio F/F_{tube}.

$$F_{tube} = F / 0.49139 = 35.898 \text{ m}^2 \longrightarrow D_{tube} = 6.76 \text{ m}$$

4.6 Run Time, Charge Tube Length

The actual run time τ can be determined from the given dimensionless run time $\tilde{\tau}$.

$$\tau = \tilde{\tau} \cdot \sqrt{F} / U_\infty = 9.61 \text{ s}$$

The length of the charge tube L_1 corresponding to a given τ may be obtained with the aid of

$$L_1 = \tau \cdot a_0' \cdot \frac{5 + 5 M_1}{10 + 6 M_1} \tag{6}$$

For a tube Mach Number of $M_1 = 0.3$, $a_0' = 351.8$ m/s and $\tau = 9.61$ s, the charge tube length becomes: $L_1 = 1862$ m.

Fig. 7 shows the actual run time τ versus test section Mach Number M_∞.

5. ENERGY - AND POWER - REQUIREMENTS

In considering the energy requirement of the tunnel, which is essentially given by the necessity to generate compressed air and move it into the charge tube, one must destinguish between two cases (see SECTION 3)

Case 1 The tunnel discharges downstream of the diffusor into the atmosphere, thereby wasting the energy still present in the air. The air consumption is identical to the amount going through the test section. The compressor recharges the charge tube by taking in air from the atmosphere.

Case 2 The air is discharged downstream of the diffusor into a second tube (recovery tube). During this process, a shock wave travels into the tube whose length L_2 is dependent on the desired run time τ. Here, one has a closed system with energy losses essentially restricted to the total pressure losses occuring in the test section and diffusor. The compressor has to pump a certain amount of air from the recovery tube back to the charge tube.

The determination of energy and power requirements makes it necessary to consider mass flow and pressure ratios for both cases.

Case 1 The mass flow through the test section during a run is

$$m_{test} = \rho_\infty U_\infty F \cdot \tau. \tag{7}$$

Figure 8 gives an indication of the rate of mass flow through the tunnel. If one assumes 3 runs per hour, the air corresponding to m_{test} must be replaced within 20 minutes. This requires a compressor mass flow rate of

$$\dot{m}_{comp} = m_{test}/1200 \ [kg/s] \tag{8}$$

During a run, the charge pressure drops theoretically to $0.5\, p_0'$ (Eqn. (4)). However, considering unavoidable losses due to leaks, the pressure will, under maximum conditions, drop further to about $p_{term} = 4.5$ bar. The compressor must increase the pressure during the recharging process from p_{term} to p_0'. The amount of energy per second required during the recharging period is, assuming single intercooling during compression,

$$dE_{ad}/dt = \frac{2\gamma}{\gamma - 1} T_{at} \cdot R \cdot \dot{m}_{comp} \left\{ \left(\frac{p(t)}{p_{at}} \right)^{\frac{\gamma - 1}{2\gamma}} - 1 \right\} \tag{9}$$

Assuming now a linear increase of charge pressure with time, one obtains by integration

$$E = \frac{1}{\eta} \frac{2\gamma}{\gamma - 1} T_{at} \cdot R \cdot m_{test} \left\{ \frac{p_{at}}{p_0' - p_{term}} \cdot \frac{2\gamma}{3\gamma - 1} \left(\left(\frac{p_0'}{p_{at}} \right)^{\frac{3\gamma - 1}{2\gamma}} - \left(\frac{p_{term}}{p_{at}} \right)^{\frac{3\gamma - 1}{2\gamma}} \right) - 1 \right\} \tag{10}$$

The power, N, to be installed depends on the final pressure ratio p_0'/p_{at} and the rate of mass flow

$$N = \frac{1}{\eta} \frac{2\gamma}{\gamma - 1} T_{at} \cdot R \cdot \dot{m}_{comp} \left\{ \left(\frac{p_0'}{p_{at}} \right)^{\frac{\gamma - 1}{2\gamma}} - 1 \right\} \tag{11}$$

The following table lists the performance data (efficiency of compression $\eta = 0.8$) for Case 1 at $M_\infty = 0.8$ and $M_\infty = 1.0$

M_∞	m_{test}	m_{comp}	E	N
	kg	kg/s	kWh	kW
0.8	277 500	231.0	18 200	65 800
1.0	284 500	237.0	18 700	67 500

Case 2 The addition of the second tube does not affect the test section flow. It serves only to reduce the energy consumption. Its treatment was, therefore, postponed up till now. Nevertheless, the determination of the pressure ratio and the mass flow makes it necessary, to consider briefly the conditions in the recovery tube.

Subsequent to the start of the tunnel (opening of the quick opening valve), three distinct areas exist in the second tube (Fig. 2):

a) Upstream of the shockwave: The air is at rest under the conditions (p_0'', T_0'') set prior to the start of the tunnel.

b) Immediately downstream of the shockwave: The shock has caused an increase in total pressure and total temperature. The following equations allow a determination of the stagnation conditions in this regime.

$$\frac{T_{03}}{T_0''} = \frac{1 + \frac{\gamma - 1}{2} M_3^2}{\left(1 - \frac{\gamma - 1}{2} M_3\right)^2} \tag{12}$$

$$\frac{p_{03}}{p_0''} = \left\{ \frac{1 + \frac{\gamma - 1}{2} M_3^2}{\left(1 - \frac{\gamma - 1}{2} M_3\right)^2} \right\}^{\frac{\gamma}{\gamma - 1}} \tag{13}$$

c) Immediately downstream of the diffusor: The flow through the test section of a windtunnel does not effect its total enthalpy. Accordingly, one may write for stagnation temperature and speed of sound $T_{02} = T_{01}$ and $a_{02} = a_{01}$ respectively.

The tube Mach Number M_2 can be derived from standard gasdynamic tables with the stream density $\rho_2 U_2 / \rho_{02} a_{02}$ as input, where $\rho_2 U_2$ follows directly from the mass flow m_{test} and the chosen area of the secondary tube while ρ_{02} can be computed by means of the total pressure losses in the test section using the simple relation

$$\rho_{02} = \rho_{01} \cdot \frac{p_{02}}{p_{01}} \tag{15}$$

A jump in temperature separates this area c) from area b). Velocity and static pressure remain unchanged in going from b) to c). Tube Mach Number and total pressure change at the contact surface according to the following relations

$$M_3 = \frac{M_2}{\sqrt{\frac{T_0''}{T_{02}} \left(1 + \frac{\gamma - 1}{2} M_2^2\right)} + \frac{\gamma - 1}{2} M_2} \tag{16}$$

$$\frac{p_{03}}{p_{02}} = \left\{ \frac{1 + \frac{\gamma - 1}{2} M_3^2}{1 + \frac{\gamma - 1}{2} M_2^2} \right\}^{\frac{\gamma}{\gamma - 1}} \tag{17}$$

Thus, all changes in conditions at the two boundaries are known. The tube length L_2 may now be derived from

$$L_2 = a_0'' \cdot \tau \cdot \frac{25 - 4 M_3^2}{10 (5 - M_3)} \tag{18}$$

The known run time τ ensures the correspondence of L_1 and L_2.

Now the calculation of energy consumption and power requirement is given for a test section Mach Number of $M_\infty = 0.8$.

Pressure loss in the test section: $\frac{p_{02}}{p_{01}} = 0.819 \longrightarrow p_{02} = 5.76$ bar

from Eqn.	(15)	$M_2 = 0.361$
"	(16)	$M_3 = 0.318$
"	(17)	$p_{03} = 5.64$ bar
"	(13)	$p_0'' = 3.32$ bar
"	(18)	$L_2 = 1781$ m

Thus, both the pressure in the recovery tube prior to the start of the tunnel (which is equal to the minimum starting pressure) p_0'', and the tube length L_2 are known.

During a run, the pressure in the recovery tube increases according to Eqn. (13) while the pressure in tube 1 decreases according to Eqn. (4). After the run, the pressure in tube 2 is, in the present example, higher than in the charge tube. It is possible, therefore, that, during a pressure equalization process, a part of the air m_{test} flows back into the charge tube. The system pressure after equalization is

$$p_m = 6.64 \text{ bar}$$

The amount of air, remaining to be transfered back to the charge tube, is

$$\Delta m = 239\,900 \text{ kg}$$

The compressor must now pump this amount from 2 to 1; the pressure in 1 increases during this process while the pressure in 2 drops. The pump energy can be determined from

$$E = \frac{1}{\eta} \cdot \frac{2\gamma}{\gamma - 1} \cdot R \cdot T \int_0^{t_1} \left\{ \left(\frac{p_0'(t)}{p_0''(t)} \right)^{\frac{\gamma - 1}{2\gamma}} - 1 \right\} \dot{m}_{comp} \cdot dt \qquad (19)$$

The pressure ratio is comprised of two time-dependent pressures. Assuming a linear variation of the pressures (t_1 = 20 min), one obtains by means of graphic integration for the pump energy required at M_∞ = 0.8 (η = 0.8).

$$E = 3980 \text{ kWh}$$

The corresponding calculation for M_∞ = 1.0 yields

$$E = 4440 \text{ kWh}$$

The power, N, to be installed is determined by the maximum pressure ratio

$$N = \frac{1}{\eta} \frac{2\gamma}{\gamma - 1} \cdot R \cdot T \cdot \dot{m}_{comp} \cdot \left\{ \left(\frac{p_o'}{p_0''} \right)_{max}^{\frac{\gamma - 1}{2\gamma}} - 1 \right\} \qquad (20)$$

This pressure ratio will occur at M_∞ = 1.0 and the calculation for these conditions yields

$$N = 29\,100 \text{ kW}$$

The following table lists the performance data (efficiency of compression η = 0.8) for Case 2 at M_∞ = 0.8 and 1.0. The data in parenthesis are for Case 1.

M_∞	$\dot{m}_{comp}$ kg/s	E kWh	N kW
0.8	200	3 980	-
	(231)	(18 200)	
1.0	208	4 440	29 100
	(237)	(18 700)	(67 500)

The results of the preceding computations are summarized in APPENDIX 1.

6. DESCRIPTION OF THE PROPOSED PLANT

6.1 Survey of the Plant

Characteristic of a Ludwieg Tube (Fig. 1) is the longcharge tube (1). After opening a valve, a flow is established from the charge tube through the nozzle into the test section (2) and further into the open air (or into a second tube). For a Ludwieg Tube, no moving parts or regulating devices are required to maintain constant flow conditions after starting.

For Ludwieg Tubes operating at subsonic and transonic speeds the outlet valve is suitably located downstream of the test section in order not to impair the flow uniformity by any disturbing devices.

With this arrangement of the outlet valve, the pressure within the test section is - between runs - the same as in the pressure tube. In order to enter the test section, the pressure must be released. If frequent access to the test section is necessary a test section isolation valve should be provided upstream of the test section, so that only the test section has to be discharged while the remaining energy in the pressure tube is saved.

The high pressure air supply is provided by a compressor plant (3). The air enters the tube at the end opposite of the test section. For large facilities, the whole compressor plant will be located at this place.

The buildings (4) with installations for signal handling, data acquisition and processing and operation control are close to the test section.

In the following sections it will be outlined, how a Ludwieg Tube with the dimensions given in APPENDIX 1 can be realized.

6.2 Proposed Construction Elements

In order not to depend on mere estimations concerning the technical realization of the plant, a number of manufactures with special practice in the field have been asked to issue specified proposals to solve the different problems. In view of the restrictions under which the present study had to be accomplished only rough schemes could be established. Previous experience with the consulting companies let expect, that only proposals were made which render possible the solution of remaining detail problems.

6.2.1 Charge Tube and Test Section

The charge tube is 1862 m long and 6.76 m in diameter. There are no special requirements on the tube, except that its inner suface should be hydraulically smooth, which can be achieved by coating the otherwise untreated surface.

Furthermore, the tube should be protected against sunlight by a light roofing in order to avoid non uniform heating of the tube and a resulting temperature gradient within the stored air. For details see APPENDIX 2.

The test section unit consists of the following elements:

Nozzle and test section isolation valve,
Transonic test section,
Model mount,
Quick opening outlet valve,
Choke.

A view of this unit is given in Fig. 9. Its length in 68.9 m. The nozzle entrance is directly attached to the end of the charge tube.

A predominant facility requirement is, to comply with static requirements as well as with aerodynamic needs (as simulation range and transonic properties) and operational demands (as quick achievement of steady flow conditions). The entire unit between storage tube and outlet valve downstream of the model mount is normally at operating pressure of max. 10 bars.

Consequently the structure is subject to axial forces of more than $3 \cdot 10^7$ N. To avoid expensive force transmitting constructious, the structure had to be designed in a way that the stress flux is not disrupted. All elements of the unit are therefore placed inside of a continuous tube to guarantee a simple stress flux.

A fixed nozzle connects pressure tube and transonic test section. Supersonic test Mach Number up to $M_\infty = 1.3$ can be achieved by wall suction and variation of wall angles.

The test section isolation valve at the end of the nozzle allows access to the test section with high pressure in the charge tube and makes it possible to conserve large amounts of energy. The isolation valve is designed in a way that the flow is not impaired when the valve is in its open position.

The test section is not quadratic but a dodecagon (ref. to Fig. 10). By this means the dead volume between test section walls and surrounding pressure tube can be minimized. This is important to keep the tunnel starting time as short as possible. Also, pressure loads on the test section walls are easier to handle. The single wall elements are smaller and can be manufactured more easily and at less expense. The inclination angle of the twelve wall elements is adjustable and the permeability of the perforated walls can be varied.

The entire wall structure is self supporting. It can be moved 5.5 m upstream and the mounted model becomes accessible from a working platform which is shifted under the model through a door in the surrounding pressure tube (Fig. 10).

The model mount has to withstand forces up to $3 \cdot 10^5$ N. It is supported by a separate foundation, which is independent on the rest of the tunnel structure. An hydraulic cylinder carries the dead weight of the model mount; the angle of attack of the model is varied by means of a second cylinder. The position of the centre of motion of the model can be varied, too.

The independent foundation of the model mount minimizes the transmission of vibrations from the tunnel structure onto the model.

The fixpoint of the facility is located at the housing of the outlet valve. This outlet valve is driven by the pressure difference between charge and atmospheric pressure. Opening times of less than one second can thus be obtained easily. The test Mach Number can be preselected by setting the limit plug position. Suction rate at the test section walls may be adjusted by means of a group of special throttle valves.

The outlet valve is integrated into the central body of the choke. The choke allows to run the tunnel at low stagnation pressure and therefore extends the range of Reynolds Number of the facility.

The outblow of the tunnel is axisymmetric. Thus there is no objection to the attachment of another storage tube downstream of the diffuser, a "recovery tube". The operating principle of the recovery tube is the same as that of the Ludwieg Tube.

All units were designed under consideration of present day technologies in spite of the extreme facility dimensions.

6.2.2 Compressed Air Supply

Pumping power requirements for a facility with only one tube are very high. Nevertheless, pumping power requirements can be matched by approved standard compressors, which meet the requirement of high reliability of the plant.

It is suggested to utilize sets of two or three independently driven motorpump units. The units can be connected in series or parallel in order to obtain partial load operation with good effeciency. The use of separate compressor units favour multi stage air cooling for high thermic efficiency. The use of separate motors facilitates operation of the plant.

Utilization of electric power has been assumed although under certain conditions other kinds of driving power may be advantageous. The pressure ratios of the single compressor units are chosen so that identical motors may be used. Details are listed in APPENDIX 2.

Before the pressurized air is filled into the charge tube, it must be cooled and desiccated. Coolers have been offered together with the compressor plants (see APPENDIX 2). A quotation for a desiccating plant is given in APPENDIX 2.

6.3 Estimate of Costs

6.3.1 Construction Costs

In order to estimate the construction costs of the suggested facility, two different groups of construction elements must be distinguished.

First, there are those elements of the plant whose design data, dimensions, and characteristics are determined solely by aerodynamic and operational requirements. Only for these elements definite offers can be obtained. Examples are the charge tube, the test section and the compressor plant.

On the other hand there are elements whose design depends to a high extent on climatic and geologic conditions of the construction site. For this group of elements only tentative cost estimates can be given. Here we have the costs for cooling water supply, for land acquisition, foundations and buildings. The signal handling equipment depends very much on individual needs and conceptions and can, therefore, only poorly be estimated, too.

For the first category, the following offers have been submitted (APPENDIX 2).

1. Charge tube	26.0 Mio. DM
2. Test section	25.0 Mio. DM
3. Compressor plant	11.5 Mio. DM
	62.5 Mio. DM

These costs are valid for a facility with one tube only. For a facility with charge tube and recovery tube the costs for the recovery tube must be added, i.e. an amount about equal to the costs of the charge tube. The costs for the compressor plant, on the otherhand, will be reduced in this case, so that a total increase of about 20.0 Mio. DM will result.

Regarding the costs of the elements of the second category the following figures are considered to give the correct magnitude:

1. Buildings and foundations	11 Mio. DM
2. Land acquisition	3 Mio. DM
3. Cooling water supply	1 Mio. DM
4. Data acquisition equipment	5 Mio. DM
	20 Mio. DM

The following analysis of the expected standing charges are therefore based on total costs of 80 Mi. DM for a one tube facility or 100 Mio. DM respectively for a facility with two tubes.

6.3.2 Standing Charges

After a detailed estimate of the construction costs we will now briefly consider the standing charges.

From a business point of view, both, operating expenses and capital costs, are part of the standing charges.

Frequently only operating costs are considered at installations funded by the government. Since this gives important distortions of the calculation, both kind of costs are taken into account in the present study.

Operating costs: The operating costs of a windtunnel facility consist in essence of three parts

- labour costs
- power charges
- materials (new equipment, repairs, replacements etc.)

The expenses depend strongly on the frequency and mode of operation. In a paper by R. Hills [10], e.g., it is suggested to take a productivity of 5000 polars per year at maximum Reynolds Number (six-component force measurements, pressure distribution measurements and miscellaneous tasks). It should be possible to achieve this productivity with a staff of 100 people of different qualification in a single shift plus some overtime (about 2000 h occupation time of the tunnel) [10].

Based on the German labour conditions, one must consider an average salary of about DM 25.000,-- p.a. for every employee.

Concerning electricity costs, it is common practice of the German power companies to make a maximum demand charge based on the maximum power taken during any quarter of an hour during the year (DM/MW and year) and a mega-watt-hour charge for the actual power consumed (DM/MWh).

But a well balanced relation between the maximum demand charge and the actual power charge, which is normally subject to an individual contract with the power company, leads to an average power charge of DM 120,- /MWh (including maximum demand charge) based on present day prices.

The material costs under the operating conditions considered can amount to as much as DM 1.5 Mio. (according to Hills [10]).

Capital costs: The capital costs are determined by the amount of investment and consist of depreciation and running interest. The capital costs are independent of the operating conditions.

The depreciations are established so, that after ten years the tunnel will be written off (i.e. 10 % p.a.), and the rate of interest is fixed at a value of 8 % p.a.

All costs are based on a productivity of 5000 polars per year and related to a single polar.

The two cases of tunnel design. which were described in detail in the previous sections, are regarded in the following tables.

For Case 1 the construction costs amount to DM 80. Mio. ; for Case 2 the construction costs amount to DM 100. Mio. ; however, the higher amount of investment yields, compared to Case 1 an essential reduction in power charges.

The comparison of costs shows that, at the specified operating conditions (5000 polars per year at maximum Reynolds Number) Case 2 is to be preferred in spite of the higher initial investment. (APPENDIX 3).

Changes in operating conditions, however, (e.g., only a small part of the total productivity is done under maximum conditions or the number of polars is substantially decreased) can change the superiority of Case 2.

7. CONCLUSIONS

This paper presents a review of the basic requirements that are to be satisfied by a common European transonic windtunnel. It is shown in turn that all the requirements can be satisfied perfectly by a Ludwieg Tube tunnel. Subsequently, a project proposal is given for a Ludwieg Tube, that can be operated in the Mach Number range from $M_\infty = 0.3$ to $M_\infty = 1.3$ at a maximum Reynolds Number (based on mean wing chord) of 40 Million, with a stagnation pressure of 7 bar. The tunnel run time is 10 sec. The tunnel has a test section area of $4.2 \times 4.2\ m^2$, a charge tube of 1860 m length and 6.76 m diameter. The tunnel blows either into the open air (Case 1) or into a recovery tube of about the same size as the charge tube (Case 2). In Case 2, the recovery tube is charged just so much, that the tunnel can still be started. The pressure at the diffusor exit remains constant during the full run time, when a shock wave travels along the recovery tube and back according to the principle of the tube tunnel.

The alternative Case 1 has the advantage of lower construction costs while Case 2 provides essential savings in operating costs. The energy costs, which are, for a tunnel of this size, the main portion of the operating costs, can be reduced by about 75 % to 80 % when Case 2 is utilized. Part of the additional construction costs for the recovery tube are made up for by savings in the compressor and air dryer system. Another advantage of Case 2 is, that noise emitted into the environment is effectively damped without additional expenses for an exhaust silencer.

A Ludwieg Tube of the described type is characterized by its simple construction which guarantees high reliability and a flow free of low frequency oscillations. Except for a simple quick opening valve - for which there are no special demands concerning the time law of the opening process - there are no moving parts that could cause failure. Stagnation pressure and temperature are kept constant without regulation merely by utilizing the principle of the Ludwieg Tube. None of the tunnel components goes beyond present day technology or require special developing effort. There is no need for a demonstrator tunnel because every desired information can be delivered by existing Ludwieg Tubes.

Finally, an estimate of construction and operating costs, based on specified bids of leading companies, is given.

PART B

8. PRELIMINARY REMARKS

During the course of the discussion on LaWs Paper No. 98 (PART A) at Rome, the authors were asked by the LaWs-Group to reinvestigate the development of instationary boundary layer in the charge tube behind the expansion wave and, as there is a claim for a very clean flow within the test section, to reduce the tube Mach Number if necessary.

Furthermore, the design data should be adapted to the final specifications stated by the Group, in order to facilitate comparisons between different options.

9. ADAPTION OF DESIGN DATA TO BASIC LAWS-SPECIFICATIONS AND INFLUENCE OF REDUCTION OF TUBE MACH NUMBER

Independent of the driving mechanism of a tunnel, the run time and the utilization, for a proper tunnel design it is necessary to fix at least three parameters of which only two are independent. These parameters are the Reynolds Number, the stagnation pressure, and the test section area.

During several LaWs-Meetings (Farnborough, Jan. 6 - 7, and Porz-Wahn, Mai 9 - 10, 1972) specifications were discussed but not stated. The proposal for a Ludwieg Tube windtunnel as outlined in PART A was based on these first estimates, and the derived performance data are summarized in APPENDIX 1.

Specifications were stated at the Rome Meeting of the Group (July, 5 - 7, 1972):

Reynolds Number (based on $0.1\sqrt{F}$ at $M_\infty = 0.9$)	$Re = 40 \cdot 10^6$
Stagnation pressure (normal)	$p_{01} = 7$ bars
Stagnation pressure (maximum)	$p_{01} = 11$ bars
Mach Number capability	$M_\infty \leq 1.3$
Number of runs per hour	$n = 5\ h^{-1}$
Run time (clean flow)	$\tau = 10$ s
Test section : rectangular, aspect ratio	4.2 : 5

At the end of September, 1972, data were communicated by R. Hills, which were claimed to be the final specifications of the Group, and which state

Stagnation pressure	$p_{01} = 6$ bars
Test section area	$F = 4.2\ m \times 5\ m$

In the following, we refer to these data as the final specification.

Further, to obtain very small influences of the tube wall boundary layer on the test section flow, the tube Mach Number is reduced from $M_1 = 0.3$ to $M_1 = 0.2$.

Although the flow quality which can be achieved with a tube Mach Number of $M_1 = 0.3$ seems fully sufficient in our opinion (see PART A; Fig. 3) we would like to give some estimates on the improvements obtainable by decreasing the tube Mach Number to $M_1 = 0.2$. A computation as given in PART A, SECTION 3, based on the same assumptions, yields a velocity profile in the test section with relative velocity variations of less than $\pm 0.25\,\%$ within 67 % and less than $\pm 0.5\,\%$ within 92 % of the test section diameter (Fig. 11). These deviations, however, do not occur until towards the end of the run time.

The above considerations show that a decrease of the tube Mach Number yields a considerable improvement of the spatial uniformity of the velocity within the test section. The tube Mach Number has thus been assumed to be

Tube Mach Number	$M_1 = 0.2$

All these informations now form the basis for a new computation. The results for $p_{01} = 6$ bar as well as for $p_{01} = 7$ bar are summarized in APPENDIX 1.

Regarding the costs quoted in PART A, the following should be noted.

The claim for a rectangular test section gives an increase of the costs of this part of the tunnel. But a realistic estimate of the costs can be made only after a new engineering study, which is not available at present time.

The compressor plant will change essentially, according to new requirements caused by the recovery tube. Since the total power decreases, the price will decrease, too.

The price for the charge tube depends on the steel consumption only. Taking the original prices quoted in the report, it is possible to get a new price estimate by means of the factor f

$$f = \frac{L}{L_1} \frac{p_0'}{p_{01}'} \left(\frac{D}{D_1}\right)^2 ,$$

where L is the tube length, p_0' the charge pressure, D the tube diameter and the subscript 1 means the characteristics of the already quoted tube.

The following table gives the factor f for the cases considered.

p_{01}	6 bar	7 bar
f	1.50	1.26

The diameter of the recovery tube can be chosen independently of the Mach Number within the charge tube and therefore gives no increase in price.

10. REFERENCES

[1] Ludwieg, H. — Der Rohrwindkanal. Z.f. Flugwiss. Vol. 3 (1955), p. 206 - 216

[2] Whitfield, J.D., Schueler, C.J., Starr, R.F. — High Reynolds Number Transonic Wind Tunnels-Blowdown or Ludwieg Tube? AGARD Conf. Proc. No. 83 (1971), p. 29 - 1 to 17

[3] Dietz, R.O. et. al. — AGARD Study of High Reynolds Number Wind Tunnel Requirements for the North Atlantic Treaty Organisation Nations. AGARD Conf. Proc. No. 83 (1971), p. 32-1 to 9

[4] Evans, J.Y.G. — A Scheme for a Quiet Transonic Flow Suitable for Model Testing at High Reynolds Numbers
AGARD Conf. Proc. No. 83 (1971), p. 35-1 to 5

[5] Poisson-Quinton, Ph. — Note sur la conception d'un grand centre aerodynamique pour essais en sub-transonique et en supersonique
LaWs-Paper No. 31 (1972)

[6] Evans, J.Y.G. Taylor, C.R. — Some Factors Relevant to the Simulation of Full-Scale Flows in Model Tests and to the Specification of New High-Reynolds-Number Transonic Tunnels
AGARD Conf. Proc. No. 83 (1971), p. 31-1 to 13

[7] Piltz, E. — Druckänderung als Grenzschichteffekt im Rohrwindkanal
Thesis Abstract D 17, Darmstadt 1971

[8] Becker, E. — Das Anwachsen der Grenzschicht in und hinter einer Expansionswelle
Ing.-Arch. Vol. 25 (1957), p. 155 - 163

[9] Becker, E. — Reibungswirkungen im Rohrwindkanal
Mitt. Max-Planck-Inst. /Aerodynamische Versuchsanstalt No. 20 Göttingen 1958

[10] Hills, R. — Comparison of Tunning Costs of Transonic Tunnels (Revised version)
ARA MEMO No. 126
LaWs Paper No. 49 (1972)

LIST OF FIGURES

APPENDIX 1 Results of the Gasdynamic Calculation for the Ludwieg Tube with Recovery Tube

		Design concept given in PART A	Design concept according to LaWs-Specifications (PART B)		
a) Design Parameters	at M_∞ =	1.0	0.9		-
Reynolds Number (based on $0.1\sqrt{F}$	Re	$46 \cdot 10^6$	$40 \cdot 10^6$		
Dimensionless run time	ϑ	700	-		-
Total run time	τ	-	11		s
Storage temperature	T'_0	308	308		K
Mach Number range	M_∞	0.3 - 1.3	0.3 - 1.3		
Number of test per hour	n	3	5		h^{-1}
Tube Mach Number	M_1	0.3	0.2		-
Stagnation pressure	p_{01}	7.0	6.0	7.0	bar
b) Derived Parameters					
Test section area	F	17.64	20.5	14.9	m^2
Charge pressure	p'_0	10	7.7	8.9	bar
Run time	τ	9.61	-	-	s
Diameter, tube 1	D_1	6.76	8.76	7.46	m
Diameter, tube 2	D_2	6.76	8.00	7.00	m
Length, tube 1	L_1	1.862	2.073	2.073	m
Length, tube 2	L_2	1.781	2 023	2 020	m
Energy consumption each test	E	4 440	4 600	3 800	kWh
Power requirement	N	29 100	55 100	45 500	kW

APPENDIX 2 Quotations for Charge Tube, Test Section, and High Pressure Air Supply

I. Charge Tube

(Turbo Lufttechnik GmbH., Zweibrücken, Quotation No. 65 168)

Design Data:

Length of cylindrical tube	1 780	m
Inner diameter	6.76	m
Thickness of wall	24.5	mm
Distance of supports	49	m
Max. operating pressure	10	bar

Extent of Quotation: Tube, propping belts, supports, protection roof over total length, freight and assembling costs, conservation..

Estimated Costs: ca. 26.000.000,-- DM

II. Test Section

(Hausammann + Isler, Consulting Engineers, Zürich, Quotation of May 31, 1972)

Design Data:

Area of test section	17.6	m^2
Diameter of test section (Dodecagon)	4.7	m
Total length (nozzle entrance to choke exit)	68.9	m
Max. operating pressure	10	bar
Weight	ca. 1 6000	Mp

Extent of Quotation: Corresponding to Fig. 9 and 10

Estimated Costs: ca. 25.000.000,-- DM

III. High Pressure Air Supply

(Assuming tunnel without recovery tube)

III. A Version 1 (2 Units)

(DEMAG AG., Duisburg, Quotation No. 9181/5786

		Low Pressure	High Pressure	
Design Data:	Compressors	1 x Ax 600 - 8V8	1 x Ax 250 - 8V8	
	Intake mass rate	240	240	kg/s
	Intake volume	716 700	236 500	m^3/h
	Intake pressure	1.0	3.2	bar
	Outlet pressure	3.3	9.9	bar
	Outlet temperature	146	161	^oC
	Revolutions	3 000	4 700	rpm
	Power requirements	32 600	32 700	kW
	Cooling water requirements	5 400		m^3/h
	Cooling water temperature	20		^oC

Extent of Quotation: 2 compressors plus accessories, 2 electric motors of 36 MW each, 2 transmissions, lubricating oil supply, air filter, coolers, connecting pipers.

Estimated costs: ca. 10.000.000,-- DM

III. B Version 2 (3 Units)

(GUTEHOFFNUNGSHÜTTE AG., Sterkrade, Quotation m 72/10 181a)

		Low Pressure	High Pressure	
Design Data:	Compressors	2 x Agr 12/12L (in parallel)	1 x Agr 11/7L	
	Intake mass	350 000 each	700 000	Nm^3/h
	Intake pressure	0.98		bar
	Outlet pressure		9.8	bar
	Outlet temperature (cooled)		ca. 30	^oC
	Revolutions	3 000	3 000	rpm
	Power requirements	67 800		kW
	Power of motors	27 000	27 000	kW

Extent of Quotation: 3 compressors plus accessories, 3 electric motors of 27 MW each, coolers, connecting piper, transformer.

Estimated Costs: ca. 13.500.000,-- DM

IV. Air Desiccation Unit

(SILICA GEL GES., Berlin, Quotation No. 8012)

Design Data:	Mass rate	230	kg/s
	Operating pressure	4.5 - 10	bar
	Max. intake temperature	30	^oC
	Intake humidity	saturated	
	Outlet humidity (dew-point at 1 bar)	-40	^oC
	Operating capacity	5	h
	Regeneration time	10	h
	Construction	5 adsorbers in parallel	
	Length	14	m
	Diameter	2.8	m

Extent of Quotation: 5 adsorbers incl. regeneration units, filling with Silica Gel KC-desiccating pebbles, assembling costs, thermic isolation, motors.

Estimated Costs: 1.400.000,-- DM

APPENDIX 3 Standing Charges (Operating Costs and Capital Costs) of the Ludwieg Tube Facility Proposed in PART A

Kind of Charge		unit charge	Case 1		Case 2	
			expense per polar	costs per polar	expense per polar	costs per polar
Operating costs:	Labour costs	DM 25.000,-- / man and year	0.02 man, year	500,--	0.02 man, year	500,--
	Power charge	DM 120,--/MWh	18.7 MWh	2.240,--	4.5 MWh	540,--
	Materials	DM 1.5 Mio. p.a.	-	300,--	--	300,--
Total operating costs:				3.040,--		1.340,--
Capital costs:	Depreciation	10 % p.a.	-	1.600,--	-	2.000,--
	Interest	8 % p.a.	-	1.280,--	-	1.600,--
Total capital costs			-	2.880,--	-	3.600,--
Total standing charges			-	5.920,--	-	4.940,--

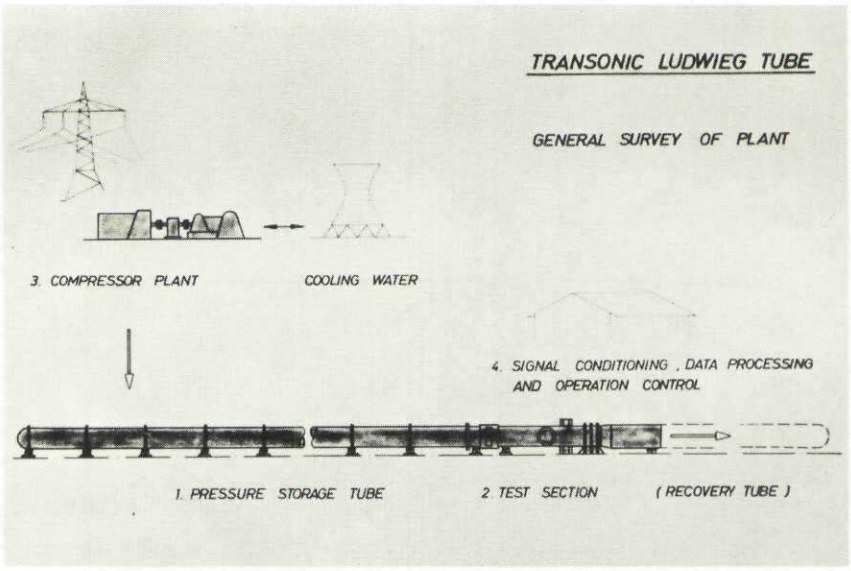

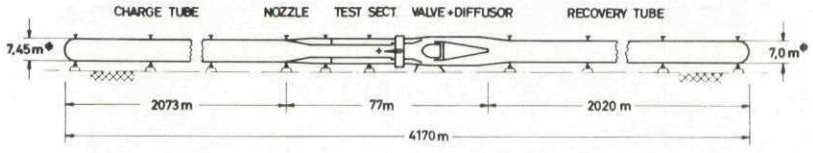

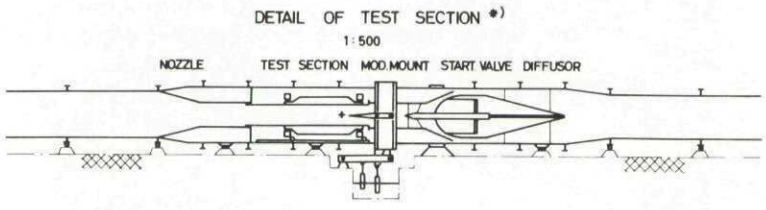

Fig. 1: Transonic Ludwieg Tube

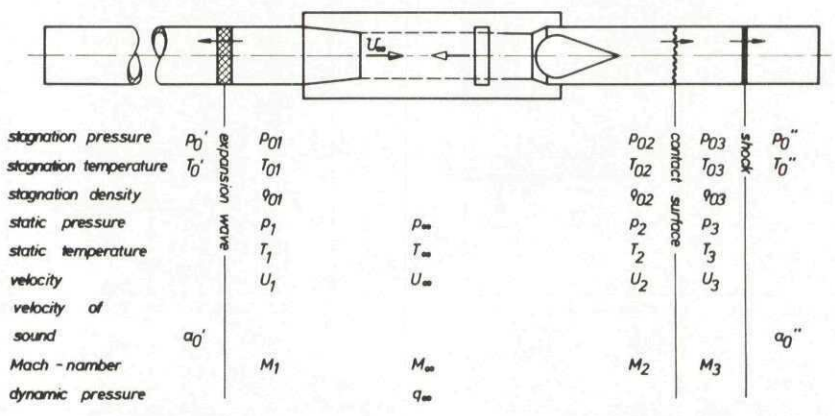

Fig. 2: Scheme of Flow Cycle

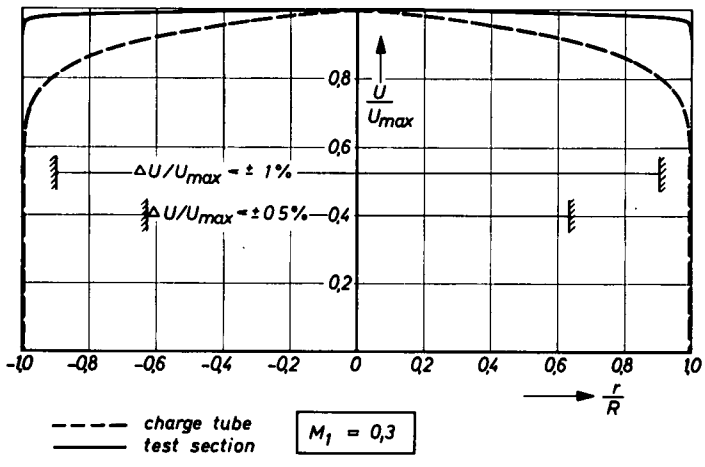

Fig. 3: Normalized Velocity Distribution in the Charge Tube (dotted line) and in the Test Section (drawn line) at the End of the Observation Time. $M_1 = 0.3$ ($M_\infty = 0.9$)

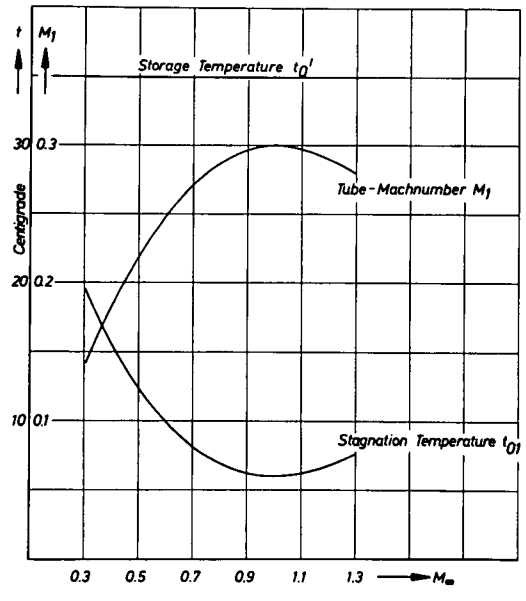

Fig. 4: Variation of Tube Mach Number and Stagnation Temperature with Mach Number

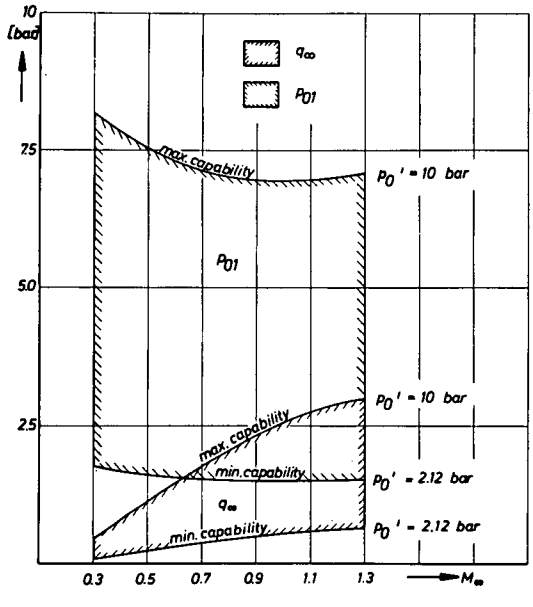

Fig. 5: Variation of Stagnation Pressure and Kinetic Pressure with Mach Number

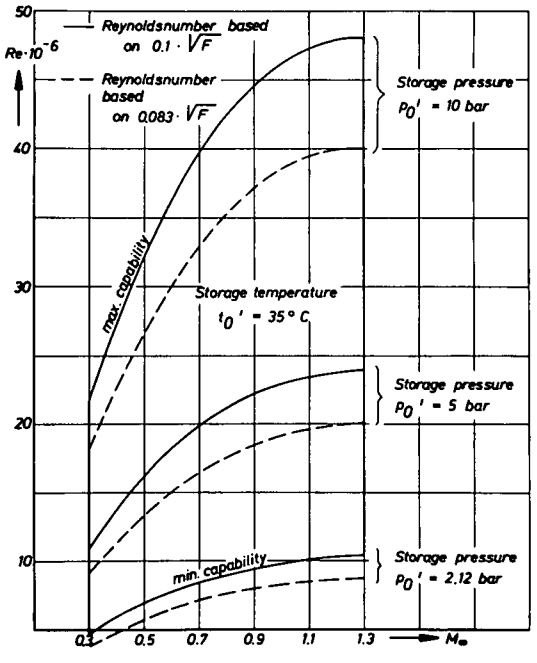

Fig. 6: Reynolds Number Capability of the Ludwieg Tube Project

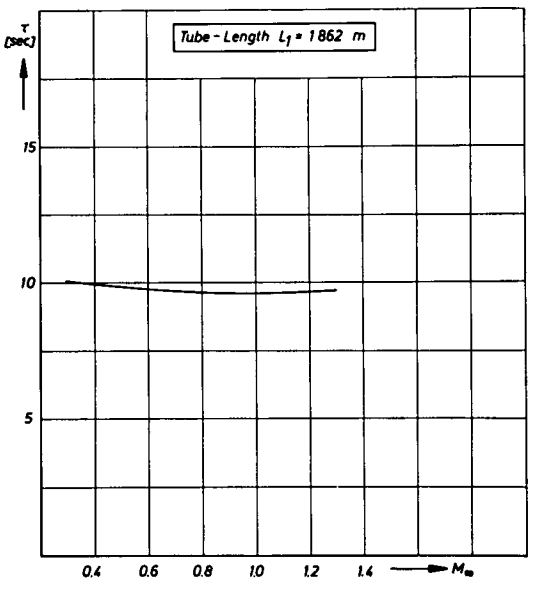

Fig. 7: Run Time of Ludwieg Tube Versus Mach Number

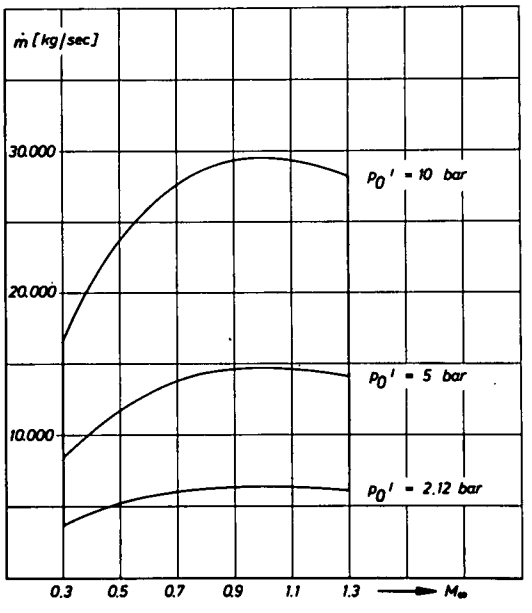

Fig. 8: Rate of Mass-Flow Through Nozzle Versus Mach Number

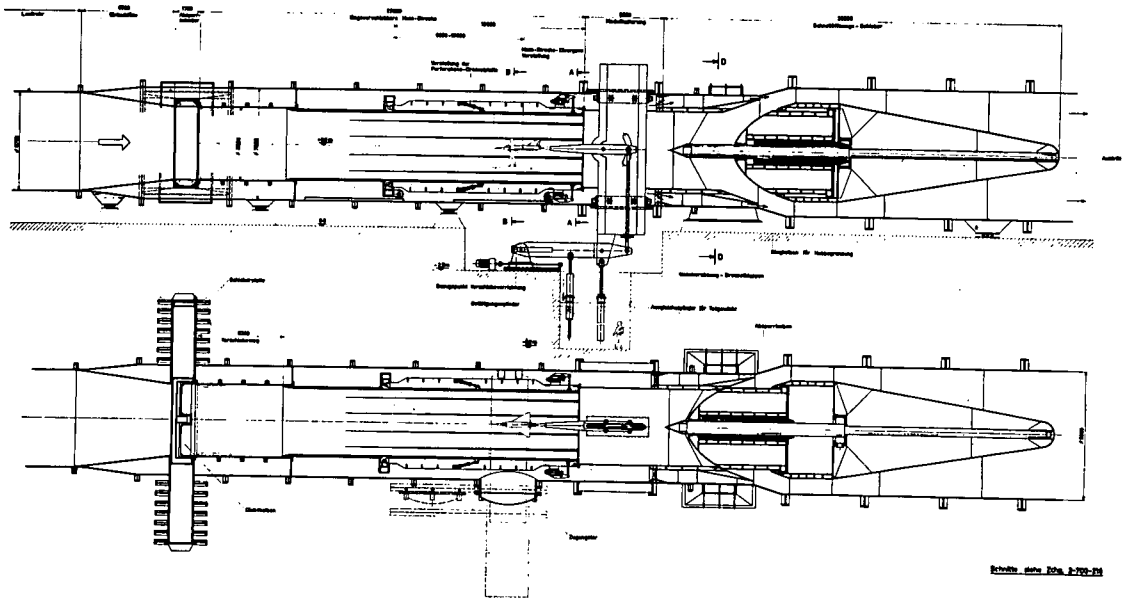

Fig. 9: Project: Test-Section of Ludwieg Tube

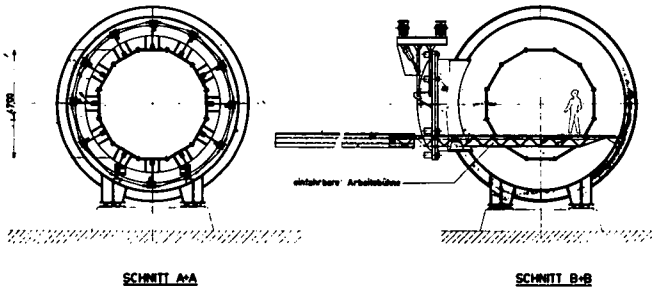

Fig. 10: Project: Test-Section of Ludwieg Tube, Profiles

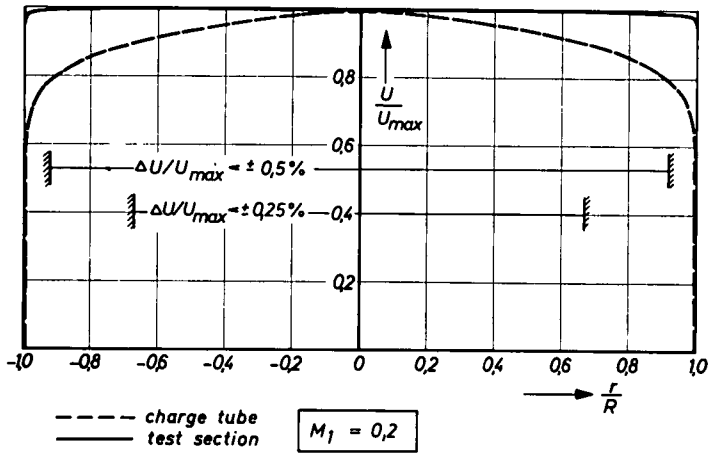

Fig. 11: Normalized Velocity Distribution in the Charge Tube (dotted line) and in the Test-Section (drawn line) at the End of the Observation Time. $M_1 = 0.2$ ($M_\infty = 0.9$)

THE DEVELOPMENT OF AN EFFICIENT AND ECONOMICAL SYSTEM FOR THE GENERATION OF QUIET TRANSONIC FLOWS SUITABLE FOR MODEL TESTING AT HIGH REYNOLDS NUMBER

by

P. G. Pugh

Royal Aircraft Establishment, Bedford, England

SUMMARY

Current work on the development of the ECT drive system is reviewed. It is shown that this is a particularly economical and effective means of providing a radical improvement in the Reynolds numbers at which transonic, wind-tunnel tests can be performed. Experimental trials which confirmed the practicability of the essential features of this system are described, and the problems of optimising the design of a particular wind-tunnel are discussed.

NOTATION

(see also Fig 10)

a_o^1	initial acoustic speed in air in charge tube
$\tilde{C}_p$	pressure coefficient based on rms value of fluctuating component of the test-section static pressure and the dynamic pressure of the flow through the test-section
F_1	cross-sectional area of charge tube
L_1	length of charge tube
M_1	Mach number of flow in charge tube
M_∞	Mach number of flow through test-section
p_{o1}	stagnation pressure of flow through the test-section
Δp_e	pressure change effected by part of expansion wave
Δp_f	total pressure change due to either the expansion or the compression wave
Δp_p	pressure change effected by part of compression wave
$\Delta\hat{p}_{r_1}$, $\Delta\hat{p}_{r_2}$ etc	peak to peak amplitude of disturbances of stagnation pressure due to imperfect wave cancellation
$\hat{R}$	maximum usable Reynolds number (see section 5)
T_o^1	initial temperature of air in the charge tube
t	time elapsed since start of run
t_e	time at which the head of the expansion wave passes a station in the tube
t_d	time at which the piston is released
η_e	energy efficiency as defined in section 1
η_m	mass efficiency, as defined in section 1
τ	duration of steady flow through the test-section
τ_o	time taken, at start of the run, to establish steady flow in the test-section

1 INTRODUCTION

The need for transonic wind-tunnels giving much higher Reynolds numbers than can be attained in existing facilities is now firmly established[1]. There can be little doubt that such new tunnels will be built during the next decade, providing that efficient and economical drive systems are used.

The extent of the improved performance that is required has been extensively debated[1,2]. It clearly depends upon the anticipated nature of the workload of the facility. This report concentrates upon the

specification prepared by the LaWs group, although it should be noted that the general considerations are equally applicable to the design of less ambitious facilities - such as might be built as demonstrator facilities or to serve some forms of research and development. The LaWs group specification calls for a Reynolds number, based on 0.1 $\sqrt{\text{test-section area}}$, of 40 x 10^6 at a test Mach number (M_∞) of 0.9 and a rectangular test-section whose dimensions are 5m x 4.2m. For a stagnation temperature of 25°C, this corresponds to a stagnation pressure of 6 atm. The maximum Mach number is 1.35 and runs of 10s duration are required at M_∞ = 0.9.

Unhappily, straightforward increases in the size of existing conventional continuously running wind-tunnels yields solutions which are quite unacceptable both as regards capital cost and peak power demand. For example a wind-tunnel with atmospheric stagnation pressure of the size required to meet the LaWs group specification would cost around £5400M and need a power supply of about 6000MW. These astronomical figures can be reduced by increasing pressure rather than size as a means of attaining higher Reynolds numbers. However, there are limits to the pressures which can be used and the most economical design of continuously running wind tunnel of this performance may cost around £150M and may require a power supply of around 1000MW.

Thus, the design of large wind tunnels has reached the end of one stage of its development. One road is blocked by exorbitant running and capital costs. Some form of stored energy system (intermittent operation), in which energy is put into store at a modest rate and suddenly released over a short period, is necessary if the peak power demands (and, hence, running costs) are to be kept within tolerable limits. Fortunately, the last decade, or so, has seen dramatic advances in experimental techniques. In particular, the rate at which aerodynamic data can be acquired has greatly increased. Thus, despite the tendency towards more complex and demanding experiments, the utilisation and amount of testing in one year could be about the same in an intermittent tunnel as in existing continuous wind tunnels[1,3].

While intermittent operation is a necessary condition of the achievement of acceptable costs it is not, in itself, sufficient. Stored energy systems are less efficient than continuously operating systems performing the same function. They suffer from conversion losses ie energy can be dissipated, but never created, during its input to storage and its subsequent release and use. Accordingly, low efficiencies can largely offset the benefits of energy storage (in the reduction of peak power demand) which then cease to be commensurate with the reductions in useful testing time. Also, the capital cost of a wind tunnel is strongly influenced by the amount of steel-work required for construction. This is, in turn, closely related to the quantity of air that can be stored within the circuit. Indeed, for a given standard and type of pressure vessel design, the weight of steel used is approximately proportional to the maximum mass of air that can be stored. Thus, if the capital cost is to be minimised, the wind tunnel design must be such that a large proportion of the air that can be stored within its circuit is passed through the test-section within the useful run-time. It must be noted that the relevant quantity of stored air is <u>not</u> the mass actually stored within the wind tunnel, but is the mass of air that could be stored if each section of the wind tunnel was simultaneously charged with air at the maximum pressure which is attained in that section at any time during the operating cycle, ie the maximum working pressure of that section. It is the maximum working pressures that determines the structural strengths and, hence, the weights of steel used. Thus, two efficiencies can be defined, each of which must be high if the design is to be economical. Firstly, an energy (or drive) efficiency (η_e) can be defined as the ratio of the minimum energy needed to drive the air through the test-section and the total energy actually expended in performing a run. This will be related to the running costs of the tunnel. It should be noted that the minimum energy required is only the energy associated with driving the air through the test-section during the time for which the flow through the test-section is steady (ie the period during which aerodynamic data can be acquired); energy expended while starting and stopping the flow is energy wasted. Secondly, a mass efficiency (η_m) can be used. This is the ratio of the mass of air that flows through the test-section during the steady part of a run to the total mass of air contained in the wind tunnel when each section is charged to its maximum working pressure. This efficiency will be related to the capital cost of the tunnel. Thus, a satisfactory design must have high values of η_m and η_e, give an adequate run duration (τ) and must not generate aerodynamic noise within the test-section.

Initial studies[4], concentrated upon two forms of short-duration wind tunnel namely the blowdown wind tunnel, which is a well established device for smaller scale testing, and the Ludwieg tube[7], which has been used successfully for supersonic testing (Fig 1). Unfortunately, in their original, and simplest, forms both of these types of wind tunnel have poor energy efficiencies. For example, in designs to the LaWs specification, air must be pumped through a pressure ratio of at least 6 from atmosphere into the high pressure storage vessel (the charge tube or the storage bottles); whereas a pressure ratio of, typically, 1.1 is all that is required to maintain flow through the test-section during a run. Thus, η_e cannot exceed about 0.06.

Additional disadvantages of these forms of short-duration facilities emerged as further study identified various desirable features of new high-Reynolds-number wind tunnels. In particular, it became clear that it is essential to have low levels of aerodynamic noise in the test-sections of these wind tunnels and also to have a flow which is uniform and of constant speed and pressure during a running time of 10s (these requirements being an integral part of the LaWs specification). The blowdown type of wind tunnel suffers from a high level of aerodynamic noise in the test-section which can only be reduced to acceptable levels through the use of high-loss devices in the settling chamber (thus further degrading the drive efficiency). Additionally, the temperature variations induced by sudden changes in pressure in both the air storage and, at the start of a run, in the settling chamber[5] cause difficulties in maintaining an acceptably constant Reynolds number. It is unlikely that a satisfactory design could be developed on these lines. Thus, another road is blocked by inadequate technical performance.

In response to this situation, a novel design of wind tunnel drive system has been proposed. This is the Evans Clean-flow Tunnel (ECT)[6], shown schematically in Fig 2. Also, it has been proposed[7] that a "recovery tube" should be added to the exhaust of a Ludwieg tube (LT) because the combination of the Ludwieg tube and recovery tube (LT and RT) has a higher energy efficiency than that of the plain LT system.

The following sections of this paper first outline the operating principles of an ECT. A design to

the LaWs specification is then described; followed by a resume of recent experimental work which has confirmed both the practicability of the mutual wave cancellation that is a basic feature of the ECT and also the absence of noise generated by the drive system. The performances of the ECT, LT and LT and RT systems are then compared. Finally, some comments are made on the development of optimum designs of wind tunnels.

2 THE ECT DRIVE SYSTEM

2.1 Principles of operation

In the ECT, the settling chamber of a conventional wind tunnel is extended as a long tube. Air is allowed to settle quietly in this tube before the start of a run, during which it is pushed through the test-section by moving a piston along the tube. Downstream of the test-section, the air is decelerated in a conventional, high-efficiency, diffuser and returned under pressure to the upstream side of the piston, thus giving a drive efficiency similar to that of a continuously running tunnel. If the flow were started by merely accelerating the piston, a compression wave would travel down the tube and be reflected from the contraction section only to be reflected again from the piston, continuing in this manner until the pressure had attained the steady-state condition. During this period, much of the piston travel time would be wasted. This is avoided by a controlled opening of a valve at the end of the diffuser, which allows air to escape into the return circuit and thereby starts an expansion wave travelling towards the piston. By suitable timing, this expansion wave reaches the piston when the piston is started. The expansion and compression waves then mutually cancel so that uniform flow is maintained throughout the travel of the piston along the tube. Virtually all the air originally contained in the tube is exhausted through the test-section and provides usable testing time thus ensuring a high mass efficiency. This process is illustrated by the wave diagram included in Fig (2).

A convenient way of moving the piston is to make use of the pressurised air within the circuit to operate a group of counterbalancing (or "driving") pistons which are mechanically connected to the main piston. If these pistons draw air from suitable points in the main tube, they also function as a boundary layer bleed system which obviates the temporal and spatial variations in the flow into the nozzle that often limits the performance of Ludwieg tubes. The avoidance of troubles due to the growth of the boundary layer within the main (or charge) tube is greatly helped also by the fact that the run time is governed by the volume of the main tube rather than, as in a Ludwieg tube, by its length. Thus, it is practicable for the main tube of an ECT to be short and of a comparatively large diameter, as compared to the charge tube of a Ludwieg tube. Thus, not only does the boundary layer occupy a smaller fraction of the diameter of the tube but also the larger contraction ratios, consequent upon the larger diameters, are more effective in thinning down this boundary layer prior to the entry to the test-section. Accordingly, the ECT is well adapted to providing flows of the required duration and quality at an acceptable cost and with a tolerable peak power demand.

2.2 A design to the LaWs specification

A design to meet the LaWs group functional requirements is illustrated in Fig (3). In this, the contraction ratio between the charge tube and the test-section is 8:1. The charge tube has a diameter of 14.5m and is 270m long. The maximum speed of the piston is 25.5m/sec, which corresponds to sonic speed at the test-section. At a test-section Mach number (M_∞) of 0.9, the piston traverses the tube at a maximum speed of 25.2m/sec.

As noted in the preceeding section, the attainment of steady flow requires that each run is initiated by a controlled opening of the valve downstream of the test-section, whereby an expansion wave is generated. This travels towards the piston and establishes the flow in the working section and in the tube. Mutual cancellation of the expansion and compression waves is possible through the matching of the valve opening and piston motion by suitable time-laws. Then, by starting the piston at the moment when the head of the expansion wave arrives at the piston, the two waves cancel each other out. During the subsequent travel of the piston along the charge tube uniform flows are maintained in the tube and in the test-section.

The expansion wave reduces the pressure and the temperature of the air in the main tube. To have a stagnation pressure (p_{01}) of 6 atm in the test-section at $M_\infty = 0.9$, the initial pressure ($p_o{}^1$) of the air in the charge tube must be 6.6 atm. The reduction in temperature (of about 8°C) increases the unit Reynolds number of the flow in the test-section. The required Reynolds number (R_d) of 40×10^6 can then be achieved in a test-section of the size 4.86m x 4.00m.

The cyclic changes in pressure and temperature (once per run) are small enough in this scheme not to cause any significant structural fatigue problems as might be the case if a smaller contraction ratio were used.

Downstream of the test-section, the air passes through a second throat. The flow through this is choked (at sonic speed) during a run so that repeatability and constancy of the Mach number M_∞ is assured, and so that aerodynamic noise, which may be generated in the diffuser or in the exhaust valve, cannot be transmitted to the test-section. The second throat is followed by a conventional diffuser in which the air is decelerated with the minimum loss of energy. The air then passes the exhaust valve and enters the return circuit which leads to the upstream side of the piston. The difference in pressure across the piston, which is needed to sustain the flow, will be somewhat less than in a conventional wind tunnel circuit because of the absence of coolers, screens, etc. On the basis of experience with large conventional wind tunnels, including some specially-devised, large-scale experiments in the RAE 3ft x 3ft wind tunnel[9], the stagnation pressure ratio (β) is estimated as 1.10 for $M_\infty = 0.9$ and as 1.15 for $M_\infty = 1.35$. Thus, the maximum pressure difference across the piston will be 1.65 atm for a Mach number of 0.9 and $p_{01} = 6.0$ atm. During the starting process this will fall to 0.55 atm. Corresponding values for $M_\infty = 1.35$ and the same stagnation pressure are 1.88 atm and 0.80 atm.

The driving pistons, used to counterbalance the load on the main piston, are connected to the latter by cables and pulleys. These driving pistons have a near-vacuum on the opposite face, so that the force produced is proportional to the stagnation pressure. In this way, the pressure ratio across the main

piston is determined by the geometry of the system and is independent of the stagnation pressure.

The force needed to balance the pressure load on the main piston is higher at the start than during the steady run. The drive tubes can be sized so that the piston is in balance prior to a run. Restrictions in the form of conventional throttles are built into the upstream ends of the drive tubes so that, as the main piston and the drive pistons accelerate and air is drawn into the drive tubes, the pressure acting on the drive pistons falls progressively. By suitable sizing of the restrictors, this fall in pressure can be made just sufficient to bring the main piston into balance during the run also.

A design, which is of ECT type and in which the air for the drive pistons is drawn from the charge tube, uses 9 drive tubes, each having a diameter of 1.88m. These are equally spaced around the periphery of the main tube. A merit of this arrangement is that the combined cross-sectional area of the drive tubes, and hence the pressure ratio, can be matched to the minimum ratio needed to sustain flow at the chosen value of M_∞. In this design, all 9 pistons are operative for $M_\infty = 1.35$; but for $M_\infty = 0.9$, 3 of the tubes are rendered inoperative (these tubes will be spaced at 120° to each other). Fine adjustments to the pressure ratio can be made by small changes to the flow restrictors on the active tubes. By drawing air for the drive cylinders from the charge tube, the drive tubes are kept small and an effective boundary-layer bleed system is provided.

In order to meet the LaWs requirement that the airstream should be quiet and steady throughout the run, it is essential that the boundary layer on the walls of the test-section should be thin and should not grow significantly during a run. Similar requirements are also necessary to obtain sensibly constant wall interference effects throughout a run. The ECT scheme is well suited to fulfil these requirements, mainly because the airspeed in the charge tube is low (and the contraction ratio is high) and partly because an effective boundary-layer bleed is incorporated. In the proposed design, the maximum thickness of the boundary-layer at the beginning of the contraction (at the end of the run) is estimated to be 0.8m and the maximum displacement thickness 0.1m. The innermost 60% of the total boundary layer is removed by the bleed action of the drive tubes. The remaining boundary layer is greatly thinned down when the air passes through the contraction. In the working section, opposite to the model, the displacement thickness of the boundary layer is estimated to grow from 0.012m to 0.0124m during a run without bleed, and to 0.0122m with bleed. The variation during a run of this boundary-layer thickness is thus kept below 2%.

Precautions are taken to avoid secondary flows and to prevent air from the boundary layer in the charge tube being swept up by the piston and pushed ahead of it in the middle of the charge tube. A gap is left between the outer edge of the piston and the walls of the charge tube (during a run). It is estimated that a gap of between 0.04m and 0.06m will suffice for this purpose.

The main piston can be comparatively light, and a feasible target for the weight of the piston is considered to be about 20000Kg. The achievement of a light piston is aided by the fact that the highest pressure difference across the piston is only a small fraction of the stagnation pressure and also by the long wavelength of the expansion wave, which allows the use of a domed piston. The piston is supported by wheels running on rails which are mounted on the inner surface of the charge tube.

Three important consequences stem from the smallness of the weight of the piston compared to the aerodynamic forces acting upon it.

Firstly, the frictional forces, tending to retard the piston, are very small compared with the airloads. Thus, the pressure of the air in the charge tube is very insensitive to variations in these frictional forces.

Secondly, this feature eases the task of arranging for the mutual cancellation of the expansion and compression waves at the beginning of the run. The responsiveness of the piston to changes in airloads is such that there is a favourable interaction between the expansion wave and the motion of the piston. Any deviation of the piston acceleration from the correct time-law calls into play large pressure forces tending to restore the piston motion to the correct form.

Thirdly, this feature obviates any tendency for the piston to oscillate during its travel along the tube. The variation of the pressure loads with piston motion provides essentially damping forces and, since the weight is small compared with these airloads, the product of the stiffness and inertia constants is relatively small and oscillatory motion is prevented.

Both the compression and the expansion waves are weak so that the highest precision in matching the two waveforms is not necessary in order to achieve satisfactory constancy of the stagnation pressure during a run. It is, therefore, not necessary to provide for very high rates of opening of the valve or extreme accelerations of the piston. The minimum time required to establish a steady flow in the test-section will limit useful reductions of the time taken to open the valve to little less than the 2 sec proposed in this design. This implies an average piston acceleration of, at most, 13m/sec^2 ie 1.3g, which is relatively modest. Similar accelerations of a plug exhaust valve are needed. Control of the acceleration of the piston is facilitated by an actuator which operates during the first 20m of travel. The maximum force required from the accelerator will not exceed twice the weight of the piston.

Uniformity of the flow in the return circuit is not important so that this component can be routed with economy and engineering convenience as primary considerations. It can be smaller and of a simpler and cheaper construction than in conventional wind tunnels. For large wind tunnels like the proposed design, reduction of its length, compatability with suitable designs of exhaust valves, and land costs will favour either annular or multiple return circuit designs. (For smaller wind tunnels the availability of standard components and the possibility of shop fabrication will favour a single, separate return circuit[10]). In the annular design of the proposed wind tunnel the overall diameter of the complete pressure vessel is 19.9m and its total length is 350m. The pressure loads on the walls of the charge tube are relatively small, unidirectional, and favourable to the use of relatively lightweight construction. Initial design studies show that the dimensional tolerances required in normal codes of practise for pressure vessels are adequate both for the charge tube and for the remainder of the circuit.

Several different designs are possible for the valve. A plug valve has the merit that, during the opening at the start of a run, inertia loads are opposed by the pressure loads. This facilitates accurate control of the valve opening. Alternatively, a design could be based on the "digital" valves which have recently found favour for computer controlled systems[11]. These comprise an array of small valves of various sizes, chosen so that any flow area, within the range of the device, may be obtained by opening a selection of the small valves. By choosing the sizes to be some variant of a binary series, quantisation errors can be kept small. For the present application less than 10 small valves would provide adequate resolution. Control of such a device involves only the timing of the rapid opening and closure of small valves of low inertia and not the precise control of the time law of each opening or closure.

When the main piston approaches the downstream end of the charge tube, the drive pistons pass a porting arrangement in the drive tubes, which allows high pressure air to by-pass the drive pistons, thus unbalancing the load on the main piston and causing it to decelerate quickly. Some further deceleration may also be accomplished by mechanical systems which must be provided for emergency use also. The mass of air in the circuit is much larger than that of the piston and its inertia tends to reaccelerate the piston. This is prevented by closing the exhaust valve and by the provision of non-return valves in the main piston itself, which open under any reversal of the pressure difference across the piston and allow air to flow through it. These valves also ensure the unidirectionality of the pressure difference on the charge tube.

To prepare for a subsequent run, air is pumped from the return circuit into the charge tube at a point downstream of the main piston. This first raises the pressure there until the pressure ratio across the piston is equal to that needed during the run. The forces on the main piston are then balanced and continued pumping causes the piston to move back along the main tube to its starting position. Further pumping raises the pressure in the charge tube and reduces that in the return circuit until the tunnel is ready for another run. The pressure ratios through which the air has to be pumped are low (a maximum of 1.34 for operation at $M_\infty = 0.9$). A conventional wind tunnel fan, and cooler, can be used for this duty. The required fan diameter is about 1.2m. The fan should be designed to operate with high efficiency over a wide range of flow rates and pressures, eg by using variable pitch blades. By such means a relatively high isothermal efficiency (90% say) can be achieved. With motor and transmission efficiencies each of 80% (ie 58% overall), an installed motor input power of 8.3MW will be required in order to recharge the wind tunnel in 10 min, after a run at a stagnation pressure of 6 atm and $M_\infty = 0.9$, and for an identical subsequent run. The power input to an ideal isothermal compressor would be 4.75MW, and the energy efficiency $\eta_e = 0.82$. For runs at a stagnation pressure of 6 atm and $M_\infty = 1.35$, the minimum time between runs, including 2 min settling time, is about 15 min.

The complete wind tunnel circuit contains 6.24×10^5 Kg of air when charged to 6atm. To fill the system up from 1atm to 6atm in 8 hours requires a compressor of about 3.3MW power, assuming typical efficiencies: compressor (isothermal) 60%, motor 80%, gearbox 80%. However, this air will need to be dried and it may be more economical to do this at a higher pressure of 10atm, say. Then, the input power of the revised compressor is about 6.6MW.

The working section is contained within a separate pressure sphere so that access to the model does not require depressurising of the whole circuit.

If the maximum stagnation pressure were raised to 11atm, the recharge times, pressures and pressure differences must be increased pro-rata. The dynamics of the piston motion, the ease of wave cancellation etc are unaffected because the inertia and pressure loads increase in proportion.

3 EXPERIMENTAL TRIALS

3.1 Purpose

The experiments that have been conducted to date were aimed at confirming the feasibility of implementing the basic aerodynamic ideas and establishing that the potential merits of the ECT system can be realised in practice. To this end a simple test rig was constructed. It was not a complete scale model of an ECT - from which it differed primarily in having an unrepresentative form of drive for the main piston. Based on the results thus obtained, and on design studies of large, complete, ECT systems, a new, fully-representative, small pilot wind tunnel has been designed and is now nearing completion.

3.2 Experimental apparatus and techniques

The rig used is illustrated schematically in Fig (4), and comprised a barrel of 0.305m diameter connected at one end via a valve and flow restrictor to a large reservoir of compressed air (in fact, the RAE Vertical Spinning Tunnel (VST)). At its other end, the barrel was connected to an axisymmetric contraction and a parallel "test-Section", 61mm in diameter and 152mm long. Air flow through the test-section exhausted to atmosphere via a conical diffuser of $5\frac{1}{2}^o$ half-angle which had an exit diameter of 229mm. The downstream end of the diffuser could be closed by the exhaust valve. Running in the barrel was a lightweight piston constructed of foamed plastic with a glass-cloth and araldite outer skin. Leakage of air past the piston was prevented by a peripheral sliding leather seal carried on the rear of the piston. Weights could be added to the rear face of the piston to increase its mass from the normal 2.63Kg to the "heavy piston" value of 3.45Kg. The distance from the front face of the piston to the upstream end of the throat, when the former was in its most upstream position, was either 12.65m or 21.8m, this change being effected by varying the length of the barrel.

Steady pressures were measured using self-balancing, weighbeam manometers to an accuracy of $\pm$ 35N/m^2. Transient static pressures in the test-section were measured using variable-capacitance differential transducers[12] referenced to atmospheric pressure.

Preparations for a run began with the piston at the upstream end of the barrel and hooked-up to a bomb release. The barrel was charged to a pressure of typically 1.23atm (using valve 10) and the pressure in the VST adjusted to the desired value (typically 1.44atm). The upstream side of the barrel was then connected to the VST (by opening valve 9), thus applying a higher pressure to the rear of the piston. The

piston remained stationary, being restrained by the bomb release.

The run was started by closing a switch on the control unit (14), which thereafter controlled the run. The first action of the control unit was to send a signal to the valve bomb release (4) which opened and allowed the weight (18) to fall. After falling a distance of up to 0.91m (this distance being varied to alter the opening time of the exhaust valve), the weight snatched the cam plate. The action of pulling the cam plate down opened the exhaust valve, thus establishing flow through the test-section and causing an expansion wave to travel upstream towards the piston. The commencement of opening of the exhaust valve broke a pair of electrical contacts. This caused the control unit, after a pre-programmed delay, to send a signal to the piston bomb release unit (5). On receipt of this signal, the piston was released and accelerated rapidly, under the action of the pressure difference across it, thus producing a compression wave which interacted with the expansion wave. The motion of the piston also caused air to flow from the VST into the upstream end of the barrel. The pressure of this air fell on passing through the flow restriction (17), the pressure loss being the greater the larger the flow rate, ie the pressure acting on the upstream face of the piston fell as the piston velocity increased. The pressure in the VST had been set before the run so that the pressure difference across the piston fell from an initial value of $18KN/m^2$ to the $0.7KN/m^2$ required to balance mechanical friction when the piston was travelling at the speed corresponding to a steady stagnation pressure of the flow through the test-section (7.74m/s for $M_\infty = 1.0$).

The run terminated when the piston reached the end of the barrel, after which the barrel was shut off from the VST (using valve 9) and vented to atmosphere (through valve 11).

As noted above, variable capacitance transducers were used to measure transient pressures, operating at an excitation frequency of 400kHz. The output signal from each transducer was demodulated to obtain an analogue dc voltage (proportional to the pressure applied to the transducer) which was recorded on a multi-channel ultra-violet oscillograph, running at a paper speed of 330mm/s. The recorder traces, typical examples of which are given in Figs (5 and 6), display histories of the following quantities:-

TABLE 1

Recorder traces

Trace number	Quantity	Pressure change to produce 25.4mm (1.0 in) deflection of recorder trace
1	Pressure in barrel at most upstream transducer station	$8.6kN/m^2$
2	Pressure in barrel at intermediate transducer station	$8.6kN/m^2$
3	Pressure in barrel at most downstream transducer station (stagnation pressure)	$6.2kN/m^2$
4	Pressure on wall of test-section	$15.2kN/m^2$
5 & 6	Traces used for event marking	-

(The recorder deflections mentioned above refer to the original traces and not to the reproductions given in this report which are considerably reduced in size. The interval between the horizontal lines superimposed on the traces was 2.54mm (0.1 in) on the original records, and the interval between the vertical lines corresponds to a time interval of 10 ms).

All components of the pressure measuring system were suitable for use with dc and low-frequency signals. The bandwidth of the system was thus determined by the combined effect of the upper frequency limits of the various components. Significant factors in determining this were:-

a) the natural frequency of the diaphragm of the pressure transducers (27.7kHz)

b) acoustical resonance of the short inlet pipe to the transducers. The lowest frequency at which such resonances could occur was estimated to be 27kHz

c) the upper frequency limit of the demodulator (20kHz)

d) the frequency response of the galvanometers in the ultra-violet oscillograph. These had undamped natural frequencies of 833Hz and were less than critically damped giving a frequency response which was flat (to within ± 5%) up to approximately 700Hz.

Thus, the frequency response of the complete pressure recording system was flat to within ± 5% from 0 to 700Hz, within ± 3dB to 1kHz (at which it was about 3dB down), and rolled off at approximately - 6dB per octave thereafter ie broadly the characteristics of a low-pass filter of bandwidth 0 to 1kHz. Accordingly, the aerodynamic noise levels infered from the recorder traces correspond to the range of frequency parameter n of $0 \leq n \leq 0.2$. They cover the range of n in which troublesome, low-frequency, flow unsteadiness is often found for conventional wind tunnels[13].

3.3 Typical pressure histories

The start of a run is shown in Fig (5). The passage of the expansion wave, due to the opening of the exhaust valve (the start of which is indicated by the discontinuity in trace 6), across each transducer caused the initial fall in pressure which can readily be seen on each of the traces 1, 2, 3 and 4. Trace 4 indicates the establishment of sonic flow through the test-section approximately 50ms after the start of the opening of the exhaust valve. For a short time thereafter, the stagnation pressure was constant. During

this period, which was identical to the useful run time of the rig when run as a Ludwieg tube, the piston was released (as indicated by the discontinuity in trace 5). This period ended with the return of the reflected expansion wave and the superimposed compression wave. Since the stagnation pressure transducer (trace 3) was situated close to the end of the barrel, the distance between the transducer and the end of the barrel was short compared to the length of either wave. Thus, the compression wave (or the reflected expansion wave) as seen by the stagnation pressure transducer was, in fact, composed of each wave superimposed on an identical wave delayed by the time required for the return trip from the transducer station to the end of the barrel. Accordingly, the stagnation pressure transducer sensed a pressure change whose amplitude was twice that of the incident wave and which was slightly different in shape from the latter.

In the absence of the compression wave, the stagnation pressure would fall by a total pressure difference Δp_f in a manner described by $\Delta p_e/\Delta p_f = (f_1\ (t - t_c)$ where t_e is the time at which the head of the reflected expansion wave first passes the transducer. In the absence of the reflected expansion wave, the stagnation pressure would rise by a total amount Δp_f in a manner described by $\Delta p_p/\Delta p_f = f_2\ (t - t_d)$, where t_d is the time at which the piston was released.

If the two waves were perfectly matched in shape and time, the stagnation pressure would remain constant. If the matching were imperfect, the algebraic addition of the contributions from the expansion and compression waves resulted in a ripple of peak to peak amplitude $\Delta\hat{p}_{r1}$. Subsequent reflections at the contraction and at the piston resulted in subsequent ripples of peak to peak amplitude $\Delta\hat{p}_{r2}$, $\Delta\hat{p}_{r3}$,..., $\Delta\hat{p}_{rn}$. These successive ripples were of diminishing amplitude. They can be seen on Fig 5 and their oscillatory motion in the tube can be followed by observing the relative times at which ripples occur on traces 1, 2 and 3.

The shape of the expansion wave could be obtained directly from the recorder traces, while the shape of the compression wave was obtained algebraically differencing the measured pressure histories and the influence of a reflected expansion wave (computed from the measured shape of the expansion wave).

3.4 Discussion of results

In this section, the salient experimental results are described. Space does not permit inclusion of details of all the data nor of the theoretical methods which were developed in order to explain and predict the observed phenomena. Reference should be made to earlier and more complete accounts[14,15] for such details.

The first of the essential features to be substantiated by experiment was the ability to vary the shape of the expansion wave so as to match that of the compression wave. This was done by varying the shape of the cam which controlled the opening of the exhaust valve and by adjusting its speed of operation. The making of these changes was guided by a simple theory[14], and typical comparisons between theory and experiment are provided in Fig 7. It will be seen that the theory is generally in good agreement with experiment as regards the shape of the expansion wave although there is a small discrepancy in the times at which a given value of Δp_e is reached. The experimental data show a period of between 4ms and 6ms at the start of the wave during which Δp_e changes very little. This behaviour and length of time is consistent with the expected behaviour of the compliant seal between the exhaust valve and its seating at the end of the diffuser. At the start of the valve opening, the compression of this seal is released so that the seal expands, reducing the mass flow from the diffuser below that assumed by the theory.

The comparison shown for "cam F at slow speed" is of especial interest since it demonstrates the successful use of the theory to design a cam profile to obtain a specified expansion wave. This cam was designed with the aim of obtaining a match with a target variation, provided by a measured compression wave, over the period $0 \leq (t - t_e) \leq 38$ms. A most satisfactory match was obtained. This diagram also illustrates an overshoot of the final pressure (ie $\Delta p_e > \Delta p_f$) in the target wave. This corresponds to an overshoot in the measured compression wave ($\Delta p_p > \Delta p_f$), which arose from the type of drive system used for the piston. This drive system, while convenient and suitable for the purposes of these tests, was not representative of that proposed for a full scale wind tunnel (see section 2) for which this overshoot can easily be avoided. The overshoot on the compression wave set a limit to the extent to which the expansion and compression waves could be matched and, thus, in the absence of any interaction between the expansion wave and the motion of the piston, to the quality of the wave cancellation ie to the minimum value of $\Delta\hat{p}_{r1}$.

In Fig 8, predicted and measured values of $\Delta\hat{p}_{r1}$ are compared as a function of t_d for two combinations of cam shape and speed. Data for both barrel lengths (L_f = 12.65m and L_f = 21.8m) are plotted in this figure. The main causes of scatter in the experimental data were errors in the measurement of t_d and variations in the time taken by the piston release mechanism. These were estimated to have a combined effect on the measured times equivalent to a standard deviation of about 1ms. The theory used a compression wave shape which was calculated theoretically[14]. This was algebraically combined with the calculated shapes of the expansion waves, neglecting any interaction between the piston motion and the expansion wave, with appropriate relative timings of the two waves.

It will be seen from Fig (8) that an optimum value of t_d exists in the sense that $\Delta\hat{p}_{r1}$ is a minimum for $t_d \simeq L_f/a_0$[1]. The theory appeared to predict both this optimum value of t_d and the penalty, in terms of increased $\Delta\hat{p}_{r1}$, for deviations from this value. The absolute values of $\Delta\hat{p}_{r1}$ tended to be lower than the theory predicted. Also, it was possible, with the cam ("F") designed to closely match the compression wave, to obtain values of $\Delta\hat{p}_{r1}$ which were consistently lower than the overshoot in the compression wave (indicated as "piston overshoot" on Fig 8). Both these effects were attributed to the favourable interaction between the expansion wave and the motion of the piston. Detailed analysis of the recorder traces confirmed that the two waves tended, by such means, to "lock together".

This interaction was also manifest in the diminishing amplitude of the ripples in the stagnation pressure records due to successive passages of the small amplitude wave left following deliberately imperfect cancellation of the compression and expansion waves. Each time that this wave was reflected from the piston it induced small variations in the motion of the piston which acted so as to partially cancel the wave.

Experimental values of this decay were difficult to measure because of the smallness of $\Delta\hat{p}_{r1}$. Some data, albeit scattered, was obtained from those runs during which t_d was deliberately made widely different from its optimum value. Those data are presented in Fig 9 and compared with theoretical estimates[14]. Within the admittedly limited accuracy of the experimental data, the theory was in reasonable accord with experiment and, hence, confirmed the nature of the favourable interaction between the piston and the waves.

The quality of the wave cancellation achieved demonstrated the practicability of achieving a sufficiently small level of fluctuations in the stagnation pressure to give the required stability of stagnation pressure in a full-scale tunnel. It was clear that yet further reductions in Δp_{r1} could be obtained if the overshoot in the compression wave were eliminated. This was difficult to achieve with the unrepresentative piston drive used in these experiments because the damping forces acting on the piston were closely coupled to the stiffness forces and the final velocity of the piston. In the full-scale drive system the stiffness and damping can be more easily controlled and the damping can be uncoupled from the final piston velocity. In this way Δp_{r1} can be considerably improved.

Preliminary measurements of the aerodynamic noise levels were also made[15]. Comparison of the recordings of test-section static pressure after flow establishment (trace 4) either with the same signal prior to opening of the exhaust valve or with the (dc) signals on traces 5 and 6 enabled the level of aerodynamic noise in the test-section to be estimated. As can be seen from Figs 5 and 6, this was extremely small. The unsteady pressure coefficient $\tilde{C}_p$ was found to be no greater than 0.002. This is less than half that which it is reasonable to assume would be permissible even for most dynamic tests[13]. Some noise was observed on the stagnation pressure (trace 3) of rms amplitude of about 0.07% of the stagnation pressure and with a predominant frequency of about 300Hz. This is extremely small and was due[15] to noise generation in a component of the piston drive which was not representative of a complete ECT facility. Thus, a full-scale tunnel would be expected to have an even quieter flow.

In order to obtain such quiet flows it is essential, of course, to prevent the aerodynamic transmission to the test-section of noise originating in the diffuser. This requires that flow be at sonic speed either in the test-section or in a second-throat located immediately downstream of the test-section. This has been demonstrated both for the rig described above[14], and for ventilated test-sections[9].

4 GENERALISED PERFORMANCE ANALYSIS

Having experimentally confirmed that the proposed drive system was aerodynamically feasible, it was appropriate to analyse its performance in a generalised manner. This analysis served both to indicate desirable values for the main design parameters and also to compare the ECT with other drive systems. By adopting a fundamental and generalised approach to the making of such a comparison it was possible to distinguish any important differences between the various drive systems without the need to develop detailed specific designs. This was advantageous because the time and effort involved in developing specific designs would preclude the provision of enough examples for systematic analysis. Further, comparisons between a limited number of specific designs can easily be obscured by the effects of differences in structural design codes, engineering implementations of various components, etc which are not germane to the study of the fundamental characteristics of various drive systems.

Three systems were considered. These were the Ludwieg tube (LT), the Ludwieg tube with the addition of a recovery tube (LT and RT), and the ECT. Their performances were compared in terms of the mass and energy efficiencies (η_m and η_e) defined in section 1. In all three systems, the air is initially accelerated by an expansion wave which travels along the charge tube. In principle, the same mass of air can be processed and used during the test, and the same quality of flow and the same run time can be achieved, whether the expansion wave is reflected from an end wall or cancelled by the motion of a piston. More generally, all three types of tunnel can be represented by a single diagram, Fig 10, where for convenience the wind tunnel circuit has been laid out along a straight line. In the LT and LT + RT systems, the extreme ends of the charge and recovery tubes are closed, whereas, in the ECT, the tunnel forms a closed loop so that the pistons shown in the diagram at the extreme ends are, in fact, one and the same. Also, the counterbalancing pistons used in the ECT are not shown although their influence on the performance was accounted for. The test medium was assumed to be air with a ratio of specific heats of 1.4 and the Mach number of the flow through the test-section during a run was taken to be unity. However, the relative merits of the drive systems considered are insensitive to M_{∞} providing that this remains within the transonic speed range.

When calculating the energy requirements of the pumping processes involved in the different drive systems (and in the calculation of the theoretical minimum energy requirements), it was assumed that isothermal compressors were employed. This means that the calculated energy efficiencies (η_e) are correct if all the compressors used have the same isothermal efficiencies. This is a reasonable assumption, but may have the effect of being somewhat optimistic for cases where η_e is low because the isothermal efficiencies of compressors pumping air through high pressure ratios are usually lower than the isothermal efficiencies of low-pressure-ratio compressors.

Figure 10 shows the flow processes occurring within the tunnel at a time shortly after the flow through the test-section has been established. During a run, the air flow rates are high and the run duration is short. Thus, the aerodynamic processes are essentially adiabatic. After the run has been completed equilibrium is established between the air in the charge tube and in the recovery tube (or return circuit). The run, taken together with the subsequent establishment of equilibrium, then constitutes a gigantic version of Joule's classic experiment. Thus, the temperature of the air returns to be everywhere equal to its initial value T_o[1]. All the drive systems are prepared for a subsequent run by returning air to the charge tube. In a LT facility, this involves pumping air from atmosphere into the charge tube. In a LT + RT wind tunnel, the air is transferred from the recovery tube to the charge tube. Similarly, in an ECT, air is pumped from the return circuit into the volume between the main piston and the contraction. These processes are relatively slow, taking typically 50 to 150 times the duration of a run, and the aerodynamic processes within the wind tunnel are then essentially isothermal. Although there are inputs of heat (due to degredation of mechanical energy by irreversible thermodynamic processes), this heat must be lost to the atmosphere, if necessary via active cooling devices, if repeatability of test conditions and the absence of large scale convection currents is to be ensured.

In order to calculate the mass and energy efficiencies corresponding to specified values of the independent variables (run time, Reynolds number, test-section size etc), it is necessary to calculate the pressures that must be set up prior to the commencement of a run. To do this, the stagnation pressure of the flow through the test-section (during the run) must be determined. This can be found from the Reynolds number requirements and the specified area of the test-section. In the calculations that have been made, the Reynolds number was taken, in accordance with the LaWs group specification, to be 40×10^6 when based on test-section "free-stream" conditions and the mean chord of the model. The latter was assumed to be $0.1 \sqrt{F_\infty}$ (F_∞ being the cross-sectional area of the test-section), Allowance was made for the reduction in stagnation temperature due to the passage of the expansion wave through the charge tube, and the stagnation pressure was adjusted to keep the Reynolds number constant. While this is a normal procedure, recent evidence suggests that it may not be entirely valid. The reduction in stagnation temperature implies that there will be heat-transfer from the model to the airstream during a run. Preliminary calculations[18] suggest that this heat-transfer has a significant effect on the boundary-layer over the model. A net increase in stagnation pressure may be required in order to obtain similar boundary-layers to those occurring at the desired Reynolds number and zero-heat transfer. This effect is small, but, if substantiated by further work, may require a small reduction in the values of η_m and η_e at high values of charge tube Mach number.

The remaining independent variable is the Mach number of the flow, downstream of the expansion wave, in the charge tube (M_1). This is determined by the contraction ratio F_1/F_∞. This Mach number characterises the design of the wind tunnel in the sense that it is the only primary variable whose value may be selected by the designer once the performance required of the wind tunnel has been fixed. Hence the broad outlines, and many of the details, of the design of the wind tunnel are fixed by the choice of M_1. Also, the combination of M_1, the running time τ, the test-section area F_∞ and the stagnation pressure p_{01} determine the growth of the boundary layer within the charge tube.

Space permits neither an account of the details of the thermodynamic calculations[16] nor a full account of all the results. Instead, some typical results are shown as Fig (11). This illustrates both the general trends found in all the data and also the influence of variations in the time required to establish steady flow (τ_o). The latter effect is small (as are the influences of likely variations in other variables) when compared with the differences between the efficiencies of the various drive systems and the effect of changes in M_1.

The Ludwieg tube drive system has an inherently poor drive efficiency, but this can be greatly improved by the addition of a recovery tube. However, this gain is obtained at the expense of a serious loss in mass efficiency. A further difficulty arises from the fact that high energy efficiencies are attained at low values of the charge tube Mach number, when the mass efficiency is low; whereas the best mass efficiencies are obtained at high charge tube Mach numbers, when the energy efficiency is low.

The ECT drive system, when operated at low charge-tube Mach numbers, attains high values of both mass and energy efficiencies. It is a more balanced and superior design since the virtues of high mass efficiency and high energy efficiency can be realised in a single wind tunnel. The ECT drive system can provide the highest energy efficiencies of any of the systems considered. The mass efficiencies that can be obtained using an ECT system are at least as good as those which can be realised using a LT drive. The superiority of the ECT drive system in terms of high mass and energy efficiencies will be strongly reflected in economy of both capital and running costs.

Further effects become apparent when the effects of boundary-layer growth in the charge tube are considered. This causes a variation with time of the uniformity of the flow entering the contraction, and of the thickness of the boundary-layer on the walls of the test-section (and, hence, of wall interference effects). These effects must be kept small throughout the run. Unfortunately, not only are uncertainties introduced into the calculation of the growth of the boundary-layer in the charge tube by the virtually unprecedently high Reynolds numbers involved, but also it is difficult to quantify the influence of this boundary-layer on the quality of the flow in the test-section. However, approximate calculations have been made[16]. Also, it seems to be clear that it is possible to obtain satisfactory flow quality in the test-section using all three schemes when the run time is short, ie of the order of 2s or 3s, even when the charge-tube Mach number is as high as 0.4 or 0.5. Accordingly, it is prudent to require that conditions in the charge tube be varied in such a way as to preserve a similar flow quality when the run time is increased to 10s. A simple, order of magnitude, argument makes this point clear. At the end of a run, the boundary-layer in the charge tube has developed over a length of approximately $u_1\tau$ (where u_1 is the velocity of the air entering the contraction). Since, for $M_1 < 0.5$, the unit Reynolds number and u_1 are both approximately proportional to M_1, the thickness of this boundary-layer is proportional to $(M_1\tau)/(M_1^2\tau)^{1/7}$ ie $M_1^{5/7}\tau^{6/7}$. For $M_1 < 0.5$, and a constant value of F_∞, the area F_1 is approximately proportional to $1/M_1$. Hence, the diameter of the charge tube is proportional to M_1^{-2} and the fraction of the diameter of the charge tube that is occupied by the boundary layer is proportional to $M_1^{17/14}\tau^{6/7}$. Thus, if the uniformity of the stagnation pressure of the flow entering the contraction is to be kept constant, then M_1 must vary as $\tau^{-12/17}$. Accordingly, if satisfactory flow is obtained for τ = 2s and M_1 = 0.5, the same quality will not be obtained for τ = 10s unless $M_1 \leq 0.16$.

More refined calculations[16], including estimates of the temporal variation of the thickness of the boundary layer in the test-section, support this conclusion. It was found that the growth of the boundary layer in the charge tube imposed a severe limitation, which is common to all three types of drive system, and constrains their operation, for run times of the order of 10s, to low charge tube Mach numbers, near 0.1 or 0.2 at the most. This limit is above the values at which the ECT achieves its best performance, but it precludes the attainment of high mass efficiencies by the other two systems. Thus, the ECT has added merit when run times of the order of 10s are required, as in the LaWs specification.

5 OPTIMISATION OF THE DESIGN

The functional performance of a wind tunnel is defined primarily in terms of the run time, the Mach number range, and the Reynolds numbers that must be achieved. Before embarking on detailed designs, it remains to decide the most economic and effective manner in which this performance can be achieved.

In common with any engineering construction, the wind tunnel is an assembly of mutually compatible

components. The total cost of the tunnel comprises the sum of the costs of the individual components, due allowance being made in each cost for their assembly and erection to make the completed wind tunnel. If a specific, near optimum, design is prepared and costed it will be possible to break it down into sub-assemblies whose individual functions are relatively simple. Accordingly, from fundamental physical relationships, supplemented as necessary by additional design studies, it will be possible to set up a series of equations. Each equation will represent the variation of a cost element with the primary design parameters, ie linear scale, operating pressure, and run-time. In a study of the costs of a particular wind tunnel[17], a set of 23 such equations were used in a computer based optimisation procedure. This degree of complexity is essential when performing detailed optimisation studies for specific designs. However, some general rules emerge which are neither complex nor specific to particular designs.

The most important of these general rules concerns the means by which a desired Reynolds number is achieved. Reynolds number can be increased either by increasing the pressure or by increasing the size of the test-section. Almost invariably, the most economical way is by increasing the pressure. However, in practice, the pressure cannot be increased advantageously beyond some limit even when to do so results in a more economic tunnel structure. The limits on the pressure which it is practicable to use are at their most severe when testing models with swept wings. They arise because Reynolds number is not the sole arbiter of the utility of a transonic wind tunnel and increasing pressure aggravates other problems of simulation such as model strength, aeroelastic distortion, and errors in shape due to model supports. Unfortunately, current knowledge does not permit of the combining of all these effects into a single measure of the utility of a given combination of model size and static pressure. However, providing that the Reynolds number is high enough to ensure that the flow patterns about the model have no gross differences from full-scale, it can be shown[2] that increases in test-section static pressure above about 3.5 atm or 5 atm are disadvantageous because the benefits of increasing Reynolds number are more than balanced by the worsening of model stresses, aeroelastic distortions and sting interference effects. Having regard to the Mach number range and likely uses of the proposed wind tunnel which was the subject of detailed optimisation studies[17], it appeared that this upper limit to pressure would be at about a stagnation pressure of 10 atm. Accordingly, a measure of the utility of different designs could be defined as the "maximum usable Reynolds number", R. This was the Reynolds number, based on the mean chord of a typical wing, during tests at sonic speed and at a stagnation pressure, of either the maximum allowed by the strength of the tunnel structure or 10 atm (whichever was the less).

The implications of this on the design of high Reynolds number wind tunnels is illustrated by Fig 12 which shows the variation of maximum usable Reynolds number R as a function of stagnation pressure p_{01} for fixed capital cost. Two curves are shown in the figure, corresponding to two different capital costs. It is clear that the use of a high stagnation pressure enables higher Reynolds numbers to be obtained for a fixed capital cost. However, if the design p_{01} exceeds that which is usable in practice (in this example 10 atmospheres), the maximum usable Reynolds number is less than that which would result from designing for p_{01} equal to the maximum usable stagnation pressure. Funds are then being expended upon unnecessary strength in the structure. This can be seen by considering a design having a maximum p_{01} above 10 atm (ie a design corresponding to a point such as X on the dotted extension of the curve for $p_{01} < 10$ atm). If the maximum stagnation pressure cannot be used for a particular test, then p_{01} must be reduced. Since the tunnel size (and, hence, model size) is then fixed, the Reynolds number is proportional to p_{01} so that the operating conditions of a given tunnel lie on a straight line through the origin as indicated. It can be seen that this line lies below the curved locus of the design points of the family of designs having a fixed cost. Thus, operating a facility at less than its designed maximum p_{01} results in a lower Reynolds number than can be obtained from a second facility having the same cost but designed ab initio for a maximum p_{01} equal to the operating value.

In thus restricting the maximum stagnation pressure there is, of course, a loss in performance compared to a tunnel having a higher maximum pressure whenever the test is such as to permit larger than normal usable pressures ($p_{01} \geq 10.4$ atm in the example shown).

The tunnel design is strongly influenced, therefore, by the requirements of the most important tests for which it will be used. In general, the most economic design is obtained by designing the tunnel for p_{01} as high, but no higher, than the maximum at which the most important tests can be run. It also follows that the greater the extent to which the work load of the tunnel can be defined, prior to the design of the wind tunnel, the higher the performance of the tunnel. Uncertainties in the nature of the workload, especially in the maximum usable stagnation pressure, can easily lead to an incorrect choice of p_{01} and consequently either failure to achieve the maximum performance or unnecessary expenditure.

The lower curve, which is for a low cost facility, illustrates an additional effect. For $p_{01} \simeq 4$ atm, the maximum usable Reynolds number rises rapidly with increasing stagnation pressure. This reflects the fact that, for a fixed total cost, the size of the tunnel decreases with increasing p_{01}. Thus, at stages in this process, it becomes possible to fabricate some components at the manufacturers works rather than on site. This change from site to shop fabrication is accompanied by a decrease in the cost of a given design so that, if the total cost is fixed, a more potent design becomes possible. Similar departures from the general trend may be caused by variations in the extent to which existing equipment can be re-used etc.

6 CONCLUSIONS

The work described in this report is part of a continuing effort directed at the development of transonic wind tunnels giving radical improvements in the Reynolds numbers at which tests can be conducted. This has, so far, established the following points:-

1) neither conventional, continuously-running wind tunnels nor established forms of short duration facilities can give the required performance without exorbitant capital and/or running costs

2) use of an ECT drive system will enable the required performance to be obtained at capital and running costs which are comparable, with those of existing, lower performance, continuously running wind tunnels

3) the practicability of the mutual wave cancellation, which is a basic feature of the ECT, has been confirmed experimentally

4) experiments have also confirmed that an ECT driven wind tunnel will generate an exceptionally clean, quiet airflow

5) the ECT is a more efficient and balanced design than other, related, intermittent drive systems. It has especial advantages when run times of the order of 10s are required

6) the maximum benefit will be derived from a fixed capital cost if a new wind tunnel is designed for a maximum stagnation pressure equal to the maximum at which the most important tests can be conducted.

REFERENCES

1. LaWs Group report.

2. Evans, J.Y.G., and C.R.Taylor, "Some Factors relevant to the simulation of Full Scale Flows in Model Tests and to the Specification of New High Reynolds Number Transonic Tunnels", Paper 31 presented at AGARD Specialists' Meeting at Göttingen, April 1971, (AGARD Conference Proceedings No 83).

3. Hills, R., "Comparison of Running Costs of Transonic Tunnels", ARA Memo 126 (LaWs Paper 49),March 1972.

4. Whitfield, J.D., C.J. Schueler and R.F.Starr, "High Reynolds-Number Transonic Wind Tunnels - Blowdown or Ludwieg Tube?", Paper No 29 presented at AGARD Specialists' Meeting at Göttingen, April 1971, (AGARD Conference Proceedings No 83).

5. Leavey, L.E., "A Note on the Temperature Transients in a Supersonic Blowdown Wind Tunnel", J. Royal Aero Soc, August 1958.

6. Evans, J.Y.G., "A Scheme for a Quiet Transonic Flow suitable for Model Testing at High Reynolds Number", RAE Technical Report 71112, May 1971.

7. Ludwieg, H., N. Grauer-Carstensen and W.Lorenz-Meyer, "Project Study of a Large European Transonic Ludwieg Tube Wind Tunnel", DFVLR Report 062 72A, June 1972.

8. Ludwieg, H., "Tube Wind Tunnel - A Special Form of Blowdown Tunnel", AGARD Report 143, (1957).

9. Pugh, P.G., T.Gell and W.A. Beckett, "RAE Report in Preparation".

10. Evans, J.Y.G., and P.G. Pugh, "A Proposed High Reynolds-Number, ECT-Driven, Transonic Wind Tunnel at RAE Bedford", RAE Technical Report 72054, (March 1972).

11. Wingrove, A.A., Private Communication.

12. Macdonald, W.R., and P.W. Cole, "A Subminiature Differential Pressure Transducer for use in Wind Tunnel Models", RAE Tech Note, Instn 169, (1961).

13. Mabey, D.G., "Flow Unsteadiness and Model Vibration in Wind Tunnels at Subsonic and Transonic Speeds", ARC Current Paper 1155, (1970).

14. Pugh, P.G., "Experimental Trials of a Novel (ECT) Drive System for a Transonic Wind Tunnel", RAE Technical Report 71208, (1971).

15. Pugh, P.G., and G.R. Spavins, "Some Preliminary Measurements of the Quality of Flows Generated by an ECT", RAE Tech Memo, Aero 1389, (1972).

16. Pugh, P.G., and J.Y.G. Evans, "RAE Report to be Published, (LaWs 100).

17. Pugh, P.G., and J.Y.G. Evans, "Optimisation of the Design of a Transonic Wind Tunnel for Tests at High Reynolds Number", RAE Tech Memo, Aero 1427, (1972).

18. Green, J.E., D.J. Weeks and P.G. Pugh, "Some Observations upon the Influence of Charge-Tube Mach Number upon the Utility of Flows Generated by Expansion Waves", unpublished RAE work.

ACKNOWLEDGEMENT

This paper is British Crown Copyright reproduced by permission of the Controller of Her Brittanic Majesty's Stationery Office.

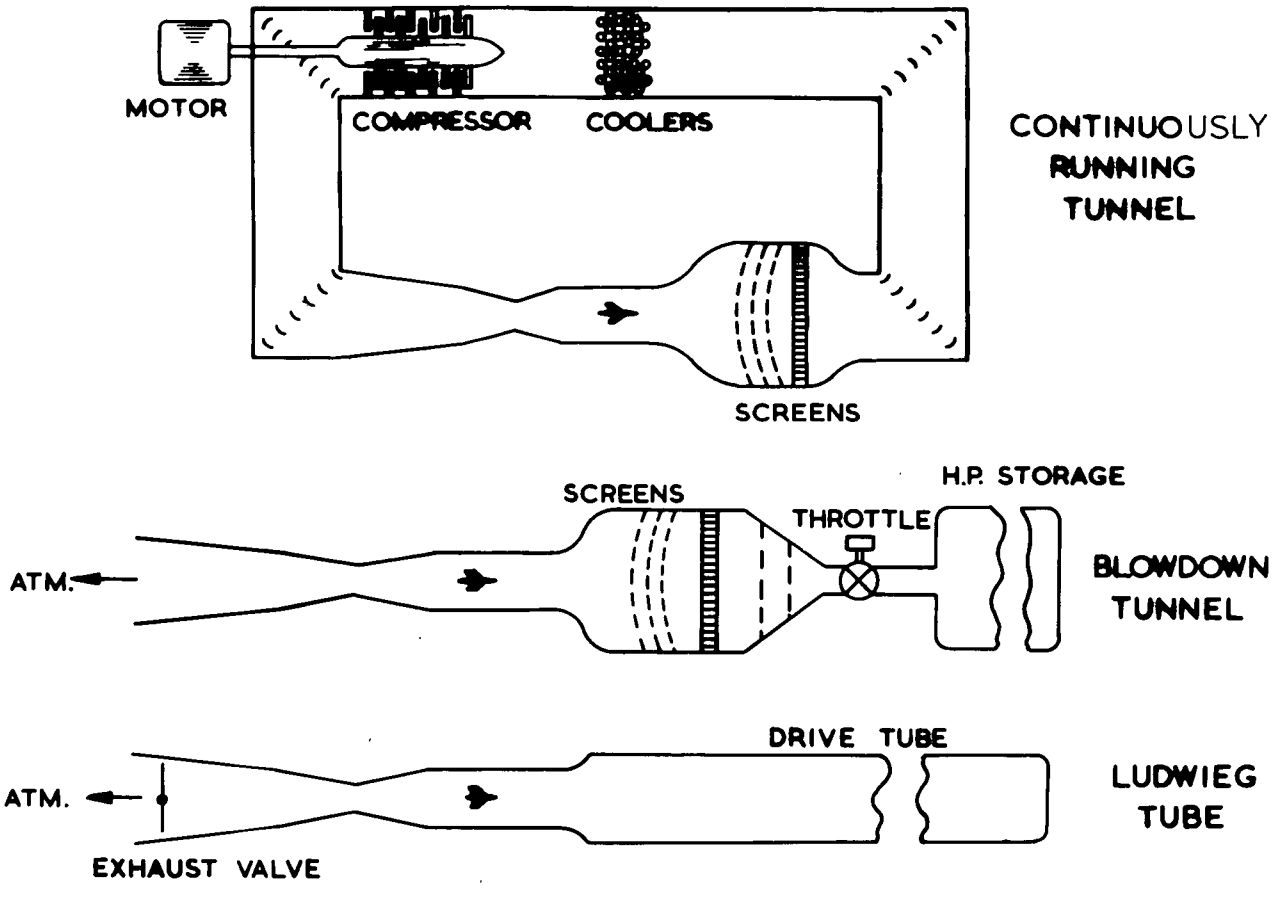

FIG. 1 CONVENTIONAL WIND TUNNELS

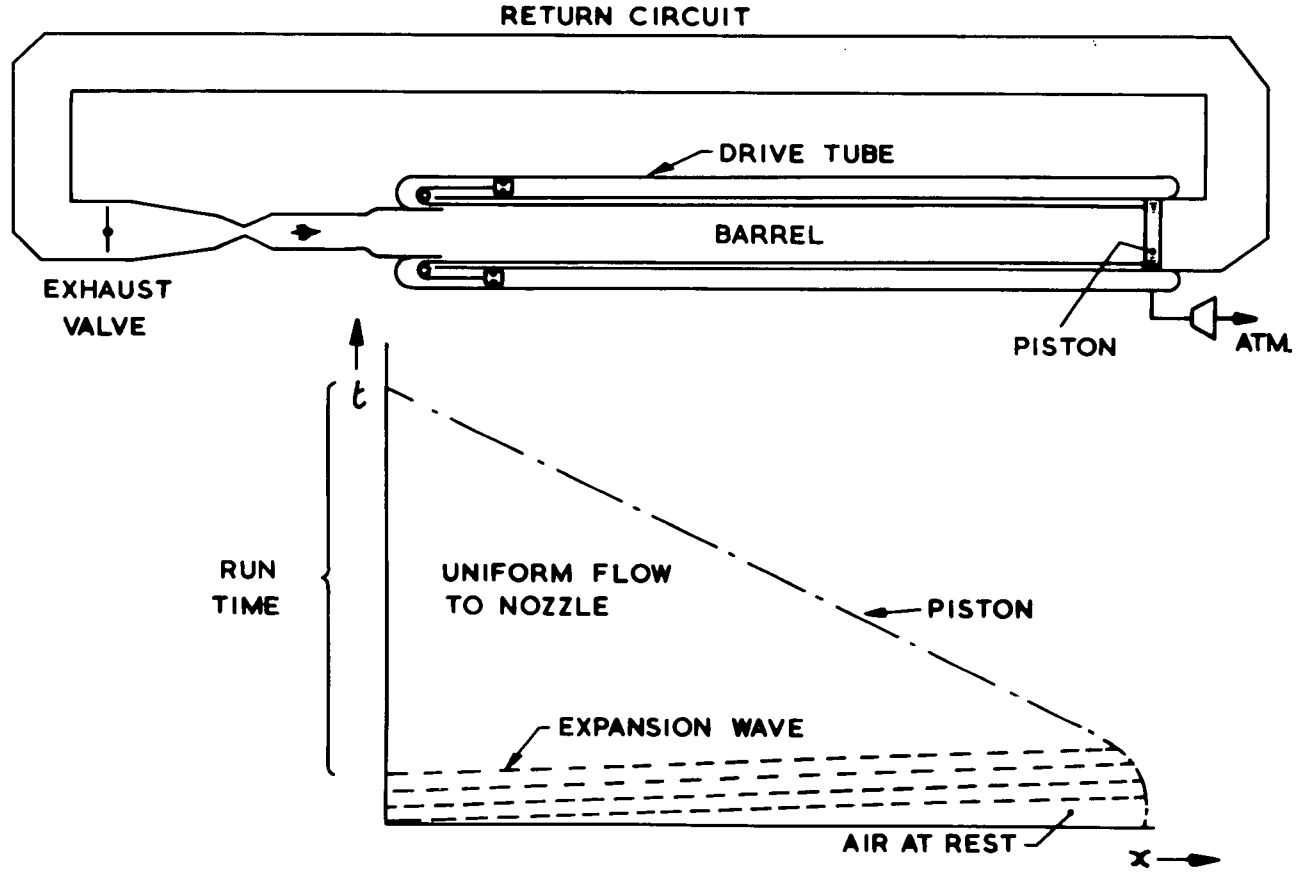

FIG. 2 ECT DRIVEN WIND TUNNEL

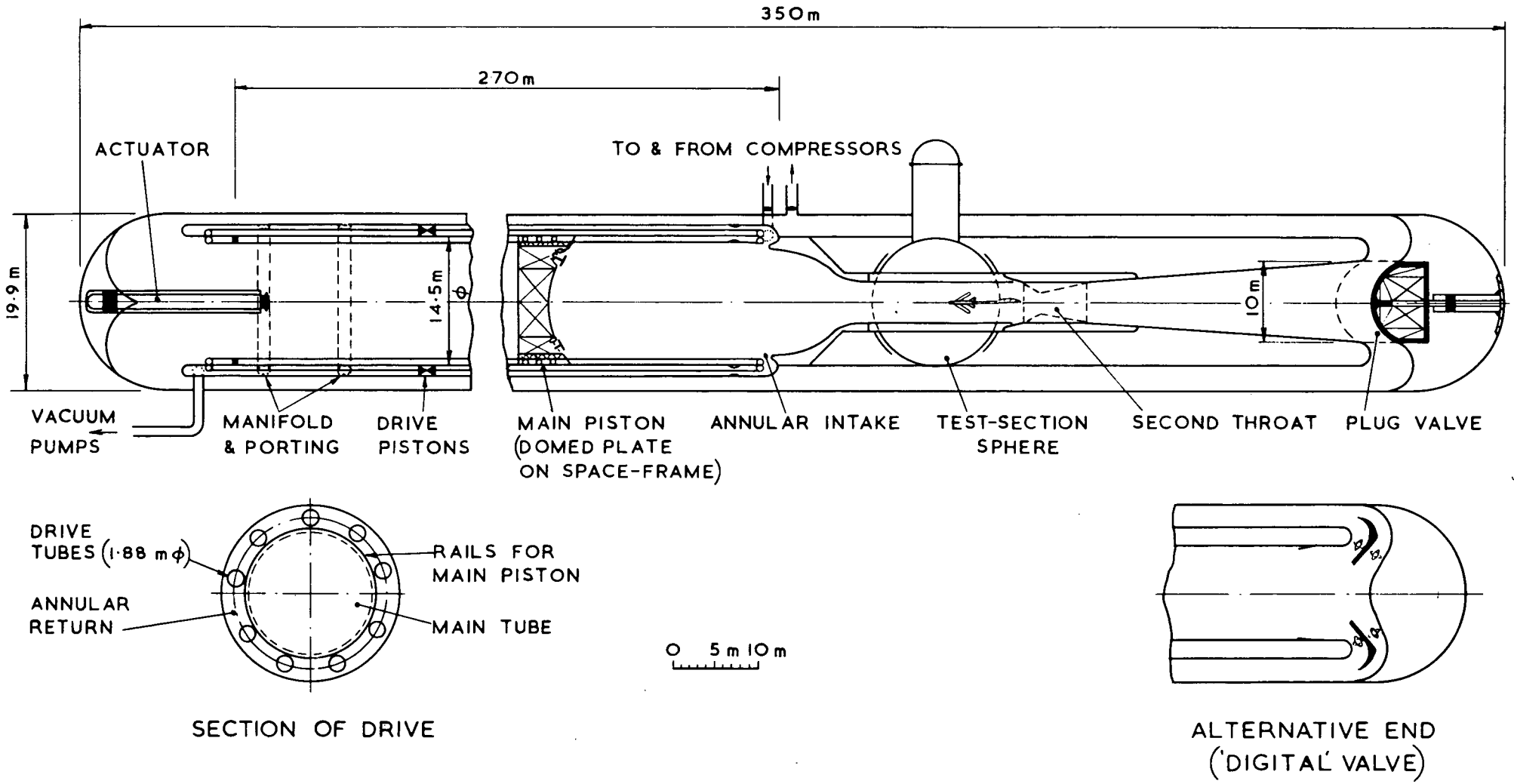

FIG. 3 GENERAL LAYOUT OF ECT TRANSONIC WINDTUNNEL

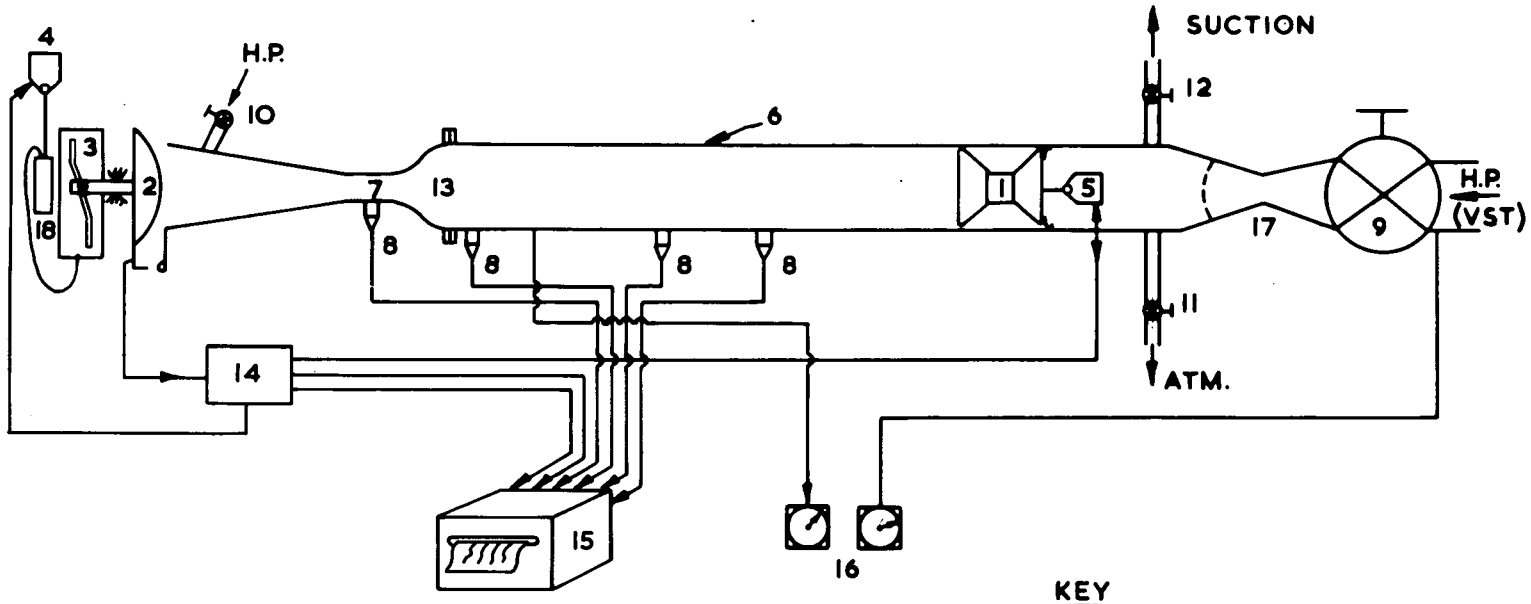

KEY

1	PISTON
2	EXHAUST VALVE
3	CAM PLATE
4,5	BOMB RELEASES
6	BARREL
7	TEST SECTION
8	TRANSDUCERS
9,10,11,12	VALVES
13	CONTRACTION
14	CONTROL UNIT
15	U.V. RECORDER
16	MIDWOOD MANOMETERS
17	FLOW RESTRICTOR
18	WEIGHT

FIG. 4 SCHEMATIC DIAGRAM OF TEST RIG

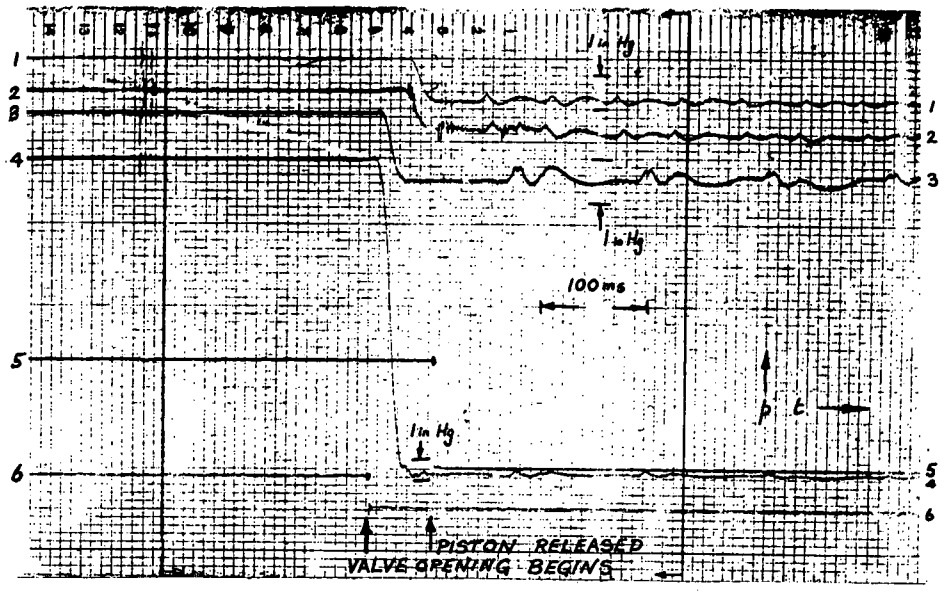

FIG. 5 START OF ECT RUN

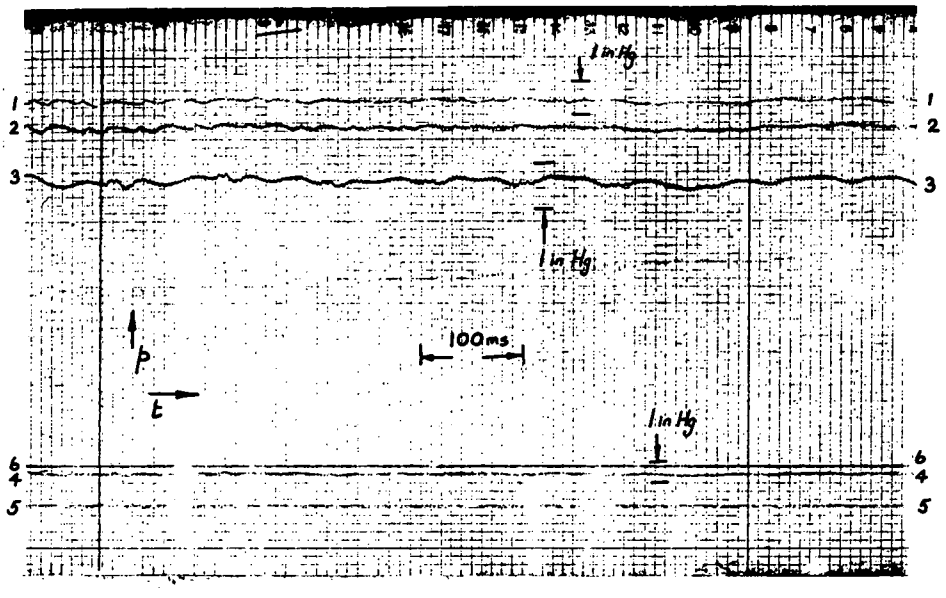

FIG. 6 ECT RUN (SONIC SPEED)

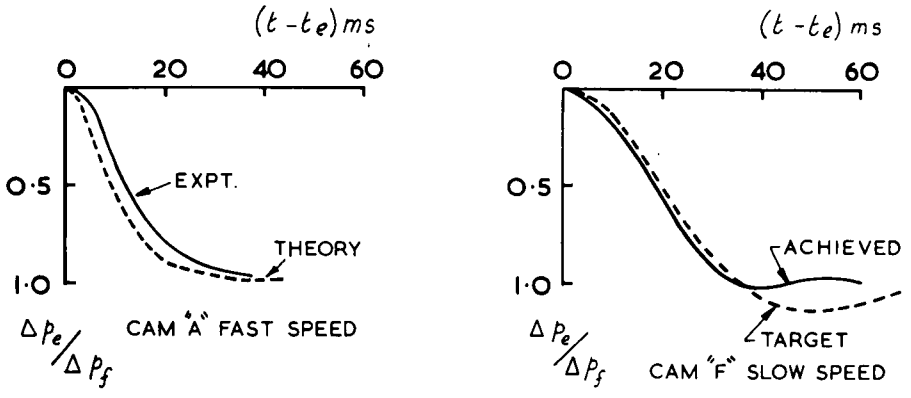

FIG. 7 EFFECT OF THE EXPANSION WAVE (CAMS. A & F)

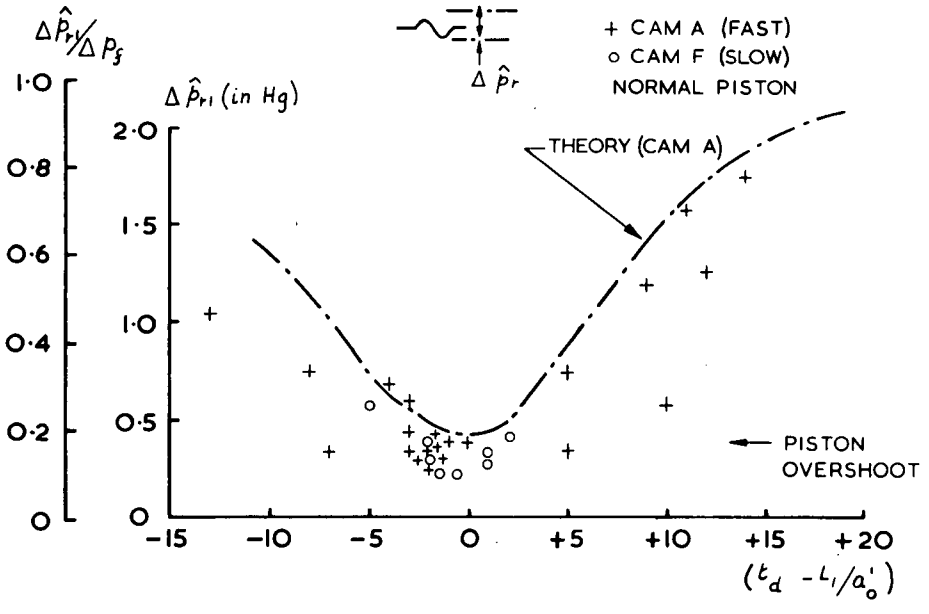

FIG. 8 MUTUAL CANCELLATION OF COMPRESSION AND EXPANSION WAVES

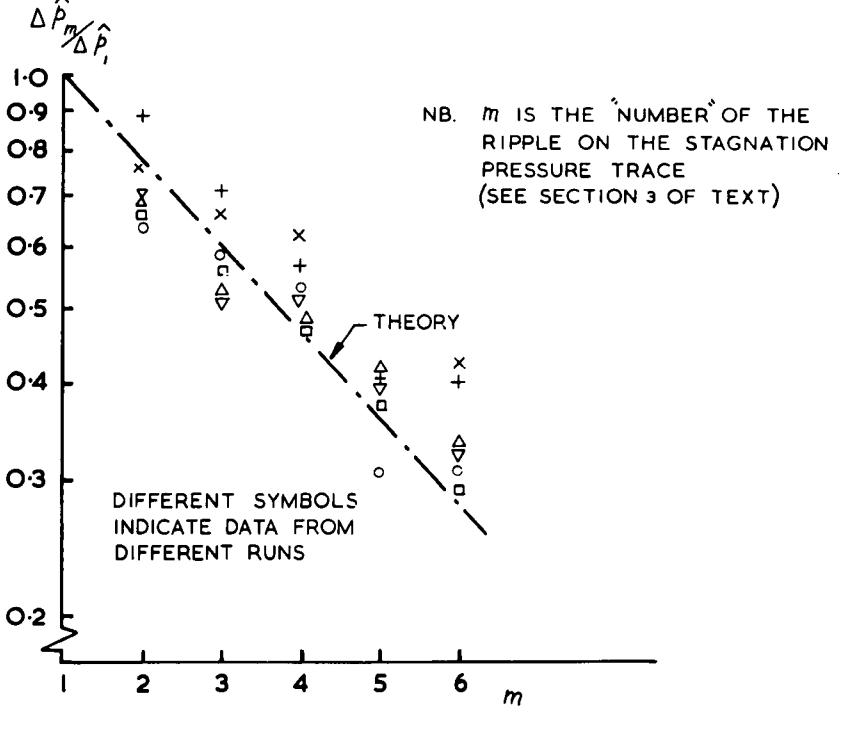

FIG. 9 ATTENUATION OF RESIDUAL DISTURBANCES IN STAGNATION PRESSURE

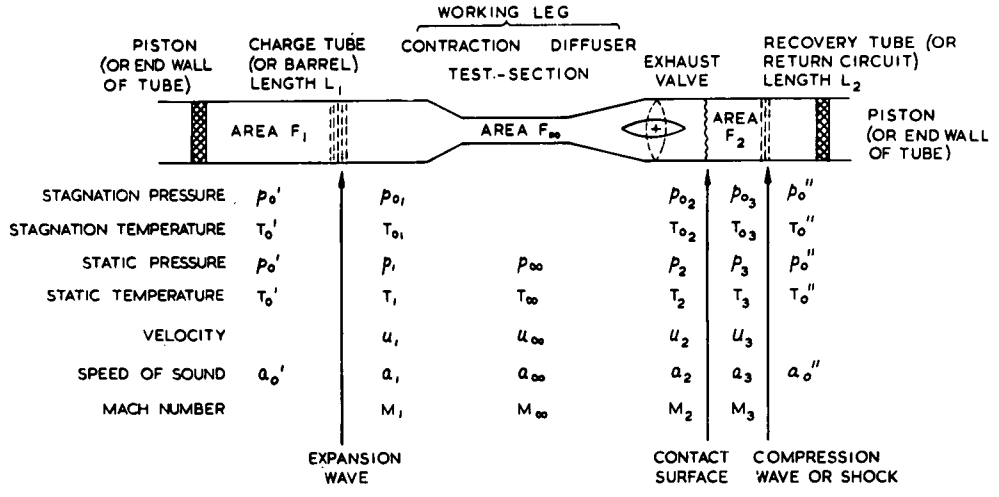

FIG. 10 NOMENCLATURE & FLOW CYCLES OF LT, LT+RT, & ECT DRIVE SYSTEMS

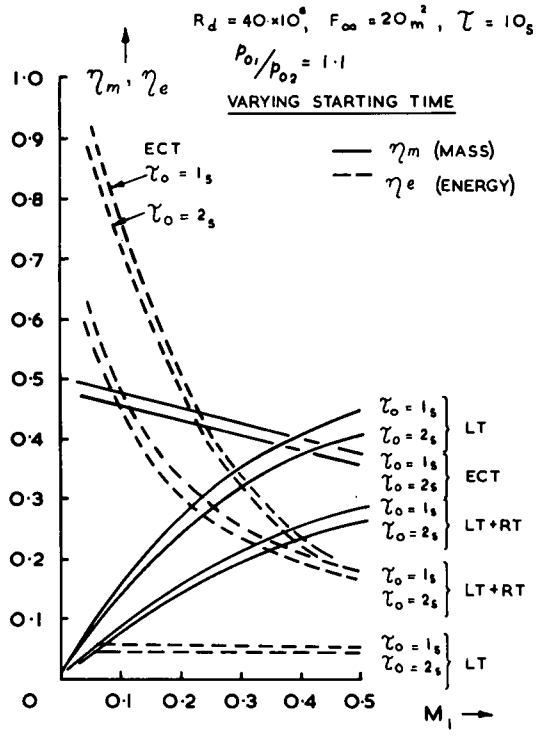

FIG. 11 INFLUENCE OF VARYING STARTING TIME ON MASS AND ENERGY EFFICIENCIES

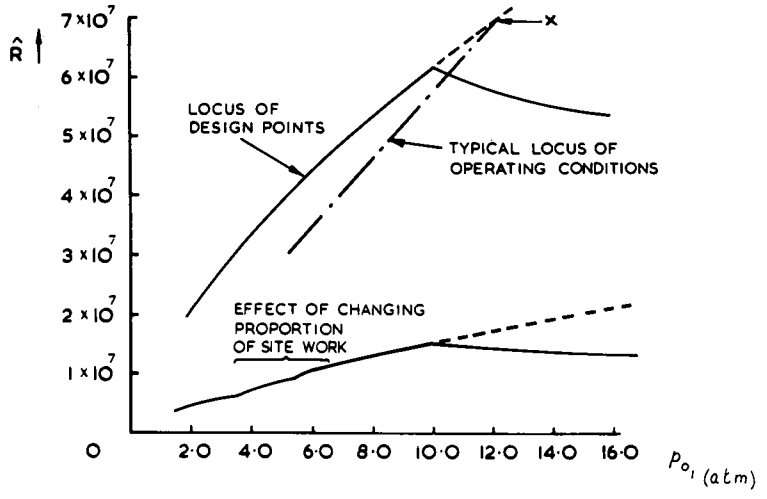

FIG. 12 INFLUENCE OF MAXIMUM USABLE PRESSURE AND SITE WORK ON PERFORMANCE ATTAINED FOR FIXED COST

THE INJECTOR DRIVEN TUNNEL

by

Pierre Carrière
Office National d'Etudes et de Recherches Aérospatiales (ONERA)
92320 Châtillon, France

Note: A brief description of the LaWs project of IDT can be found in AGARD Advisory Report AR60.

MAIN NOTATION

p		pressure
p_i		isentropic stagnation pressure
h		enthalpy
h_i		adiabatic stagnation enthalpy
s		entropy
ρ		density
a		velocity of sound
T		absolute temperature
M		Mach number
C_p, C_v		specific heat coefficients
γ	$= C_p/C_v$	
u		axial velocity
ω		sectional area
j	$= p + \rho u^2$	, dynalpy (in French: dynalpie)
m		mass flow, injected (>0) or extracted (<0) } per unit area
f		frictional force at the wall } per unit area
q		heat flow, injected (>0) or extracted (<0) } per unit area
m', j', f', q'	$= \frac{\partial}{\partial x}(m,j,f,q)$	
C_f		friction coefficient
x		abscissa
t		time
τ	$= \frac{\text{jet exit area}}{\text{mixing chamber area}} = \frac{\omega_j}{\omega_m}$	

q_{mj} injected mass flow $= m\omega$

q_{me} extracted mass flow

$\mu^{-1} = \dfrac{q_{mj}}{q_{m_1}} = \dfrac{\text{injected mass flow}}{\text{driven mass flow}}$

$X = \dfrac{p_{ij}}{p_{i_1}}$

$Y = \dfrac{p_{im}}{p_{i_1}}$

$\bar{\omega}(M) = \left(1 + \dfrac{\gamma - 1}{2} M^2\right)^{-\gamma/(\gamma-1)}$

$\Sigma(M) = \dfrac{1}{M}\left(\dfrac{2}{\gamma+1} + \dfrac{\gamma-1}{\gamma+1} M^2\right)^{-(\gamma+1)/[2(\gamma-1)]}$

$\phi(M) = (1 + \gamma M^2)\,\bar{\omega}(M)\,\Sigma(M)$

δ boundary layer thickness

$h\delta$ height of the boundary layer bleed system

$Q(h) = \dfrac{1}{h}\int_0^h \dfrac{\rho u}{\rho_1 u_1}\, d\left|\dfrac{y}{\delta}\right|$

$D(h) = \dfrac{1}{h}\int_0^h \dfrac{(p + \rho u^2)}{p_1 + \rho_1 u_1^2}\, d\left|\dfrac{y}{\delta}\right|$

} auxiliary functions for boundary layer losses computation

ϵ_q mass flow non-uniformity parameter $= 1 - Q(h)$

ϵ_d dynalpy non-uniformity parameter $= 1 - D(h)$

$\Pi(x) = \dfrac{p_{i_0} - p_i(x)}{p_{i_0}}$, stagnation pressure loss coefficient

$U = \dfrac{u}{a_0}$

$S = \dfrac{s}{C_p}$

$A = \dfrac{a}{a_0}$

$Z = \log \dfrac{p}{p_0}$

$\Omega = \log \dfrac{\omega}{\omega_0}$

$x^* = \dfrac{x}{L}$

$t^* = \dfrac{a_0 t}{L}$

Subscripts

o	reference state
j	inductor jet exit
1	main flow at the ejector exit section
m	mixing chamber exit, or mean flow
v	testing chamber

Superscripts

bar	particular value for adapted regime ($\bar{p}_j = p_1$)
*	non-dimensional quantity

INTRODUCTION

In this paper the specific problems attached to a project of an Injector Driven Tunnel are examined:

(a) methods for evaluating and optimizing its performance in steady continuous flow,

(b) analysis of unsteady phenomena during the wind tunnel start,

(c) problems of intense noise generated by the jets.

Some general indications will also be presented on the orders of magnitude of certain basic technological data.

Appendix I presents the main features of an IDT pilot wind tunnel, under construction at the Toulouse Centre of ONERA.

Appendix II presents some mathematical developments used in the paper.

Fig.1 BASIC CONSIDERATIONS ON THE INDUCTION TYPE WIND TUNNEL

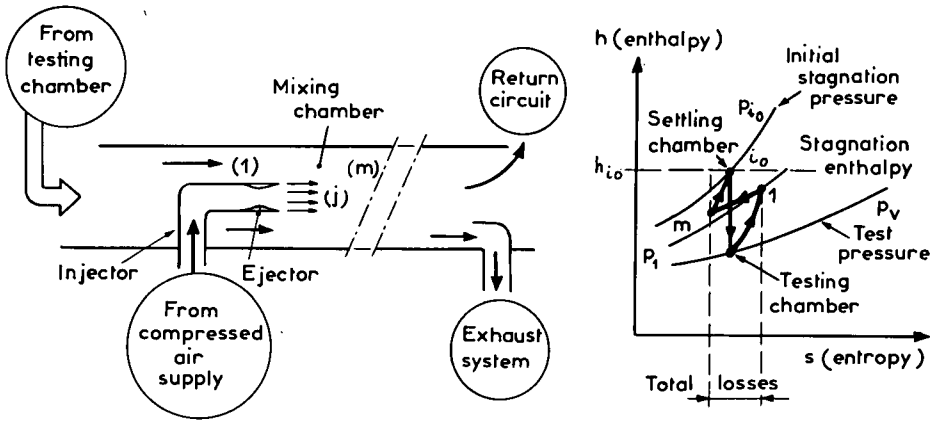

(a) PRINCIPLE (b) THERMODYNAMIC CYCLE (steady)

Figure 1a gives the operating sketch of the active part of an Induction Driven Tunnel (IDT).

It includes a supersonic ejector, supplied by a source of compressed air, and placed within the flow (1) at a convenient location downstream of the testing chamber. The jet (j) emitted by the ejector mixes with flow (1) in a mixing chamber, from where both flows emerge in a theoretically uniform state (m). The circuit, being closed, must include an extraction system so that a steady condition can establish itself and be sustained.

Figure 1b outlines the thermodynamic cycle on a Mollier diagram: the air, practically at rest in the settling chamber, state (i_0), expands almost isentropically up to the testing chamber, then recompresses up to pressure p_1 at the entrance of the mixing chamber, where losses (entropy rise) accumulated along the circuit are at their maximum. The induction system overcompensates these losses, so that at its return to the settling chamber the air is back in its initial state i_0.

Fig.2 SOME EXISTING INDUCTION DRIVEN WIND TUNNELS

		Test section size (m)	Mach number	Stagnation pressure (atm)
URSS	Central Aerodynamic and Hydrodynamic Institute (TSAGI), Joukovski URSS T (109) 1943	2,25 x 2,25	0,5 → 3,6	6
ISRAEL	Technion Israel Institute of Technology Haifa (1970)	0,6 x 0,8	1,1	2
	(1972)	1,5 x 1,5	1,2	5
U K	National Physical Laboratory N P L (1956)	0,63 x 0,51	0,3 → 1,8	1

Figure 2 shows, in a few examples, that the application of the operating principle to a wind tunnel is not new, even for large scale facilities such as the T109 wind tunnel of TSAGI, whose performance easily includes the transonic domain. This tunnel is some thirty years old and is pressurized at quite a high level for that time.

One of the most recent IDT facilities is the new Israëli wind tunnel at the Technion, whose performance, (pressure and Mach number) is near to that proposed by the LaWs Group, but at 1/3 length scale.

It should however be noted that all these facilities are based on concepts that now look somewhat obsolete, and that, in particular, no special precaution was taken against propagation of internal noise up to the testing chamber.

They include a technologically very simple injection system, made up either by a central ejector in a low speed leg of the circuit, or by a peripheral blowing slit, installed along the wall at the testing chamber outlet.

It will be shown that it is possible to apply to this concept very noticeable improvements in order to increase the quality and the cost-effectiveness of this type of wind tunnel.

Two projects including present-day technology are under study at the NASA (Langley Research Center and Ames): the test section and the corner vanes are acoustically treated. The test section dimensions will be 2 x 2 m, and the planned maximum stagnation pressure is about 13 bars. A pilot wind tunnel of this type, at 1/13 scale, has been built in 1972. The characteristics of the Ames project will be of the same order.

Fig.3 IDT MAIN SPECIFIC PROBLEMS

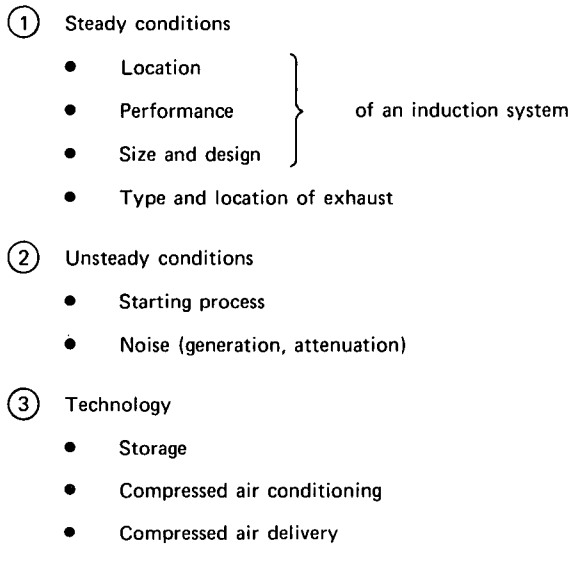

Figure 3 gives a list of the questions that will be considered and which constitute the principal specific problems of an IDT.

Fig.4 LOSSES EVALUATION

Assumptions, Definitions

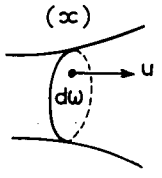

one directional flow

$p = p(x,t)$

$h + \frac{u^2}{2} = h_{i_0} = C^{te}$

(E_r): uniform reference flow

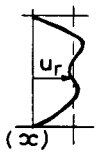

u_r = arbitrary, about main stream velocity

$p_r = p(x) \qquad h_{i_r} = h_{i_0}$

$(h_{i_0}, u_r, p_r) \Longrightarrow p_{i_r}, \rho_r, M_r$ ---

(E_m): mean uniform equivalent flow

$$\rho_m u_m \omega = \int \rho u d\omega = \rho_r u_r \omega (1 + \varepsilon_q)$$

$$(p_m + \rho_m u_m^2)\omega = \int (p + \rho u^2) d\omega = (p_r + \rho_r u_r^2)\omega(1 + \varepsilon_d)$$

$$h_{i_m} = h_{i_0}$$

$\varepsilon_q, \varepsilon_d$: non uniformity parameters of the actual flow (E)

Figure 4 presents the method that will be used to characterize the stagnation pressure losses suffered by the flow throughout the circuit.

In each cross-section, of area ω, it is assumed:

(i) that the flow is one-directional (velocity u),

(ii) that pressure is uniform within (ω) at any time, but it may vary with time,

(iii) that stagnation enthalpy (i.e. stagnation temperature) is invariant except, possibly, while crossing a heat exchanger.

We assume known the real flow (E), i.e. the velocity pertaining to every elementary area $d\omega$ within ω. Then we arbitrarily choose a uniform flow (E_r) as a reference, which approximately represents the central flow in section $\omega(x)$, e.g. the flow at the limit of the boundary layer, or the ideal flow that would result from an isentropic expansion up to section $\omega(x)$. Choosing u_r, p_r and h_{i_0} determines all the other parameters pertaining to (E_r), in particular its stagnation pressure p_{ir}.

This being done, we determine a uniform mean flow (E_m), *equivalent to the real flow*, i.e. having the same flow rates of mass, dynalpy and energy, and occupying the same section area ω, which defines it completely (u_m, p_m, ρ_m, etc.). Then, by comparing (E_r) and (E_m), we can define *two non-uniformity parameters* of the real flow (E), ϵ_q (concerning the flow rate) and ϵ_d (concerning the dynalpy) globally expressing the difference (E) − (E_r).

Fig.5 LOSSES EVALUATION

a) Main stream losses

$$\Pi_r = \frac{P_{i_0} - P_{i_r}}{P_{i_0}}$$

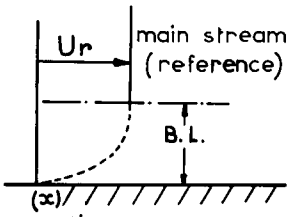

b) Non uniformity losses computation

① $\delta p = p_m - p_r = 0$

② $\delta(\rho u) = \rho_m u_m - \rho_r u_r = \varepsilon_q \rho_r u_r$

③ $\delta(p+\rho u^2) = (p+\rho u^2)_m - (p+\rho u^2)_r = \varepsilon_d (p_r + \rho_r u_r^2)$

④ $\delta h_{i_0} = 0 \qquad \delta s = s_m - s_r$

④ $\Longrightarrow T_r \, \delta s + \frac{\delta p}{\rho_r} + u_r \, \delta u = 0$

①②③ $\Longrightarrow \Pi_\delta = \frac{\delta s}{c_p - c_v} = -\frac{\delta p_i}{p_{i_r}} = \gamma M_r^2 \varepsilon_q - (1+\gamma M_r^2)\varepsilon_d$

$$\boxed{\Pi(x) = \Pi_r + \gamma M_r^2 \varepsilon_q - (1+\gamma M_r^2)\varepsilon_d}$$

This being done, we can first calculate the loss Π_r localized in the reference flow, i.e. in the central flow: this loss would be that which would be obtained if the real flow were perfectly uniform and identical to (E_r). [This loss would naturally be nil if (E_r) had been chosen as the perfectly isentropic flow up to $\omega(x)$.]

Then we have to calculate the complementary loss due to the non-uniformity of the real flow, as compared to flow (E_r).

Equations (1), (2), (3), (4) express this comparison and speak for themselves. It is assumed that the differences considered are small enough for the second order to be neglected.

In these conditions, the identity $dh = Tds + dp/\rho$ permits us to deduce the entropy difference δs, and hence, by considering the stagnation state ($\delta T_i = 0$), the complementary loss due to non-uniformity; we shall denote it as Π_δ to express that it is essentially due to the boundary layer, if (E_r) was properly chosen.

Naturally, the total loss is $\Pi_\delta + \Pi_r$ at abscissa (x). Thence the framed equation which underlines the influence of ϵ_d and ϵ_q.

Let me insist on the fact that the distinction between Π_r and Π_δ, though rather arbitrary, will be very convenient for discussing the choice of the extraction zone location, as it is clear that this extraction will be all the more beneficial if it is located in a zone where Π_δ is high.

Let us also note that, owing to the various causes of boundary layer diffusion, losses Π_δ are not necessarily increasing along (x): in certain zones they decrease, being transferred to Π_r. Only the total $\Pi_r + \Pi_\delta$ increases along the circuit but, obviously, at singular points, such as inductor, exhaust, etc. It is clear, in particular, that just behind the settling screen, if it is efficient, Π_δ must be nil, total losses being uniformly diffused in the stream.

Fig.6 NUMERICAL EXAMPLES

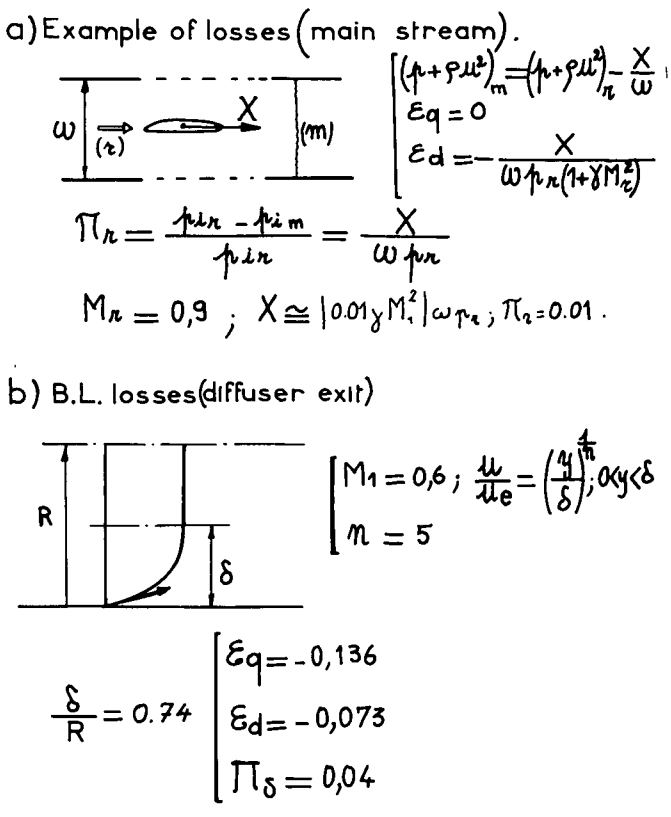

The calculation method of losses is illustrated by two examples.

Figure 6a – An obstacle with drag X placed in the flow creates a wake, and thence a dynalpy loss expressed by the parameter ϵ_d , from which there results, according to the preceding theory, at $M = 0.9$ and for $X = 0.02\omega p_r$ corresponding to an aircraft model at moderate angle of attack, a loss $\Pi_r = 0.01$ (this loss obviously diffuses within the main flow).

Figure 6b – At the first diffuser outlet the boundary layer profile can be expressed by a power law ($n = 1/5$).

One can immediately deduce

$$\Pi_\delta = \gamma M_1^2 \epsilon_q - (1 + \gamma M_1^2)\epsilon_d = \gamma M_1^2 \frac{2}{R} \int_0^\delta \frac{\rho u}{\rho_1 u_1} \left(1 - \frac{u}{u_1}\right) dy = \frac{2\gamma M_1^2}{R} \theta$$

where R is the hydraulic radius of the section being considered. With the δ/R values experimentally determined in the non-pressurized transonic wind tunnel S3 existing at Chalais-Meudon, one finds:

$$\Pi_\delta = 0.04 , \quad \text{for} \quad M_1 = 0.6 \quad \text{and} \quad \frac{\delta}{R} = 0.04 .$$

Fig.7 PRESSURE LOSSES IN THE CIRCUIT

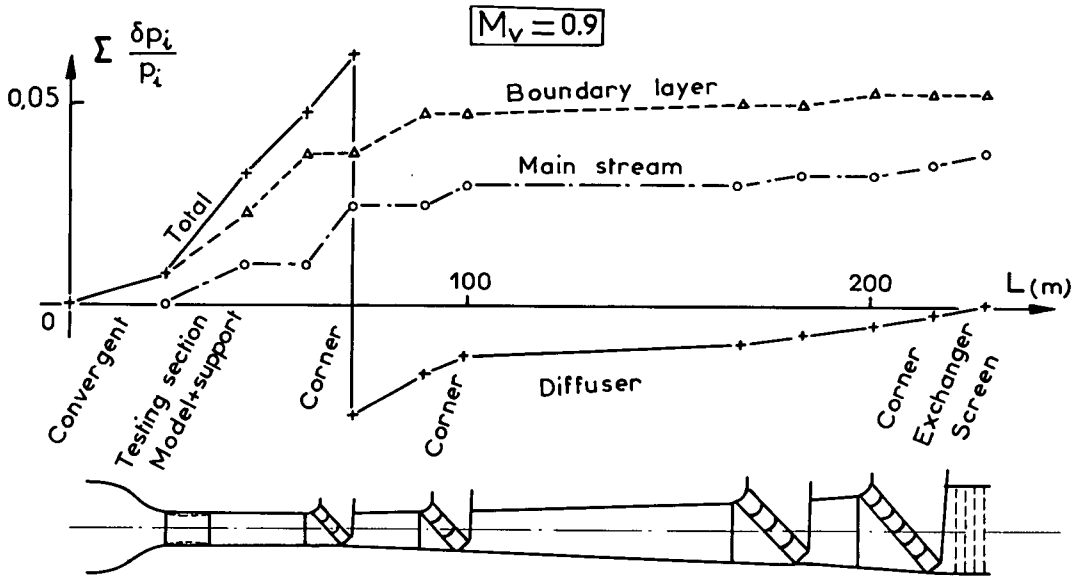

Figure 7 sums up the evaluation made by this method, based on experimental readings of boundary layer and stagnation pressure in the circuit of the S3 Chalais-Meudon wind tunnel (0.75 m^2 cross-section, atmospheric pressure) of the total losses Π for $M_1 = 0.9$, transposed to a 21 m^2 test section wind tunnel, without taking into account the reduction to be expected from a rise in Reynolds number in the ratio

$$\frac{6 \text{ atm.}}{1} \sqrt{\frac{21}{0.75}} \sim 30 .$$

This curve, very conservative, will be used as a basis in the following discussion.

Fig.8 TOTAL PRESSURE LOSSES

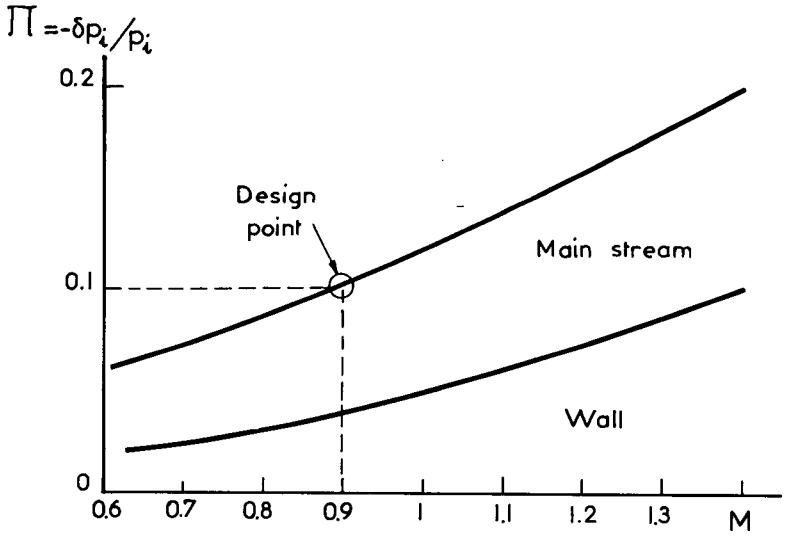

Figure 8 sums up the evolution of losses as a function of Mach number, and makes clear the distribution of these losses between main flow and boundary layer flow.

Applications made from now on will use the design point:

$$M_1 = 0.9 - \Pi_{total} = 0.1 ,$$

a value estimated as prudently cautious.

Fig.9 THEORY OF EJECTORS

(Steady conditions)

Basic equations

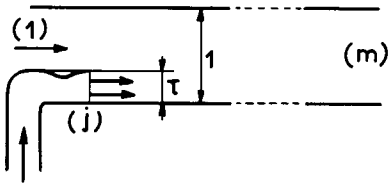

Assumptions : $\omega = C^{te}$

(1) : p_1 , M_1 , ρ_1 ....
(j) : p_j , M_j , ρ_j .... } uniform flows
(m) : p_m , M_m , ρ_m ....

no losses at the wall

$$h_{ij} = h_{i1}$$

Conservation laws :

Mass $\Longrightarrow (1-\tau)\,\rho_1 u_1 + \rho_j u_j \tau = \rho_m u_m$

Dynalpy $\Longrightarrow (1-\tau)(p+\rho u^2)_1 + \tau(p+\rho u^2)_j = (p+\rho u^2)_m$

Energy $\Longrightarrow h_{i1} = h_{ij} = h_{im}$

Definition $\boxed{\mu^{-1} = \dfrac{\rho_j u_j \tau}{\rho_1 u_1 (1-\tau)} = \dfrac{q_{mj}}{q_{m1}}}$

Figure 9 –

- For simplicity's sake, the constant section configuration has been chosen for the mixing chamber.
- Losses due to wall friction along the mixing chamber are included in the overall evaluation. They are discussed later.
- The classical *Fabri* et al. notation makes use of $\lambda = 1/\tau$. Parameter τ , which in our case is small, will be used; this will lead to a simplified theory.

Fig.10 THEORY OF EJECTORS

Numerical computation

Given : M_1 , M_j , μ^{-1} , τ .

$$\Phi(M_m) = \frac{\Phi(M_1) + \mu^{-1}\Phi(M_j)}{1 + \mu^{-1}} \longrightarrow M_m.$$

$$Y = \frac{p_{im}}{p_{i_1}} = (1+\mu^{-1})(1-\tau)\frac{\Sigma(M_m)}{\Sigma(M_1)}$$

$$X = \frac{p_{ij}}{p_{i_1}} = \mu^{-1}\cdot\frac{1-\tau}{\tau}\cdot\frac{\Sigma(M_j)}{\Sigma(M_1)}$$

$$\frac{p_m}{p_1} = \frac{\varpi(M_m)}{\varpi(M_1)}\cdot\frac{1}{X}$$

with : Tabulated functions

$$\Sigma(M) = \frac{1}{M}\left[\frac{1+\frac{\gamma-1}{2}M^2}{\frac{\gamma+1}{2}}\right]^{\frac{\gamma+1}{2(\gamma-1)}} = \frac{A}{A^*}$$

$$\varpi(M) = \left(1+\frac{\gamma-1}{2}M^2\right)^{-\frac{\gamma}{\gamma-1}} = \frac{p}{p_i}$$

$$\Phi(M) = \left(1+\gamma M^2\right)\cdot\frac{1}{M\sqrt{1+\frac{\gamma-1}{2}M^2}}$$

Figure 10 – Introducing the classical functions of isentropic expansion $\bar{\omega}(M)$, $\Sigma(M)$ permits us to write the conservation equations as:

$$(1-\tau)\frac{p_{i_1}}{\Sigma(M_1)} + \frac{\tau p_{ij}}{\Sigma(M_j)} = \frac{p_{im}}{\Sigma(M_m)}$$

$$(1-\tau)p_{i_1}\bar{\omega}(M_1)(1+\gamma M_i^2) + 2p_{ij}\bar{\omega}(M_j)(1+\gamma M_j^2) = p_{im}\bar{\omega}_m(1+\gamma M_m^2) .$$

Combination of these two equations introduces a function $\phi(M)$ and parameters X (determining the injection pressure) and Y (useful effect). Figure 10 gives the method for calculating

$$Y(M_1 , M_j , \mu^{-1} , \tau) \quad \text{and} \quad X(M_1 , M_j , \mu^{-1} , \tau) .$$

Fig.11 SIMPLIFIED FORMULAE FOR LARGE INDUCED MASS FLOW

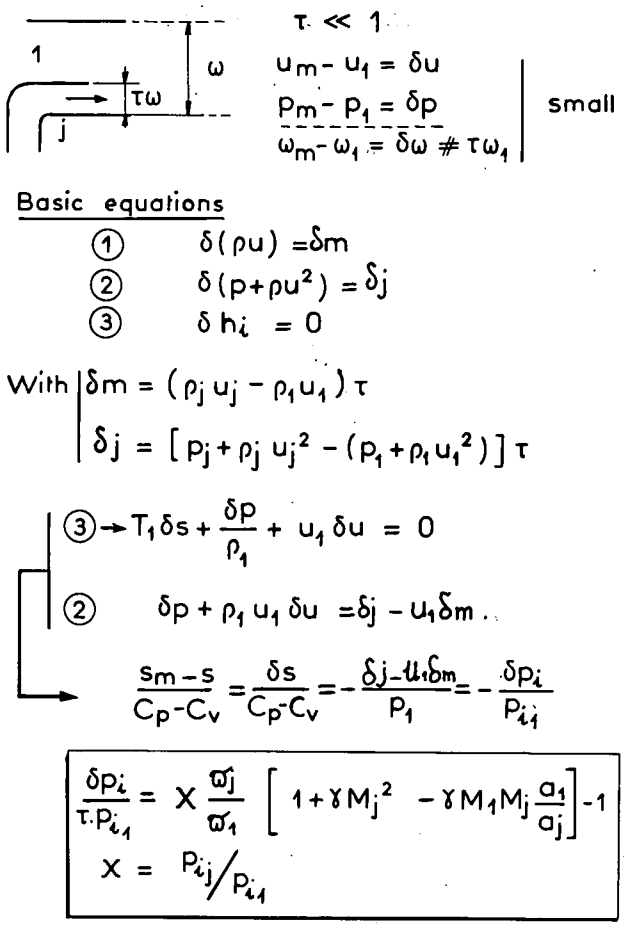

Figure 11 – The above calculations (Fig.10) permit us to establish exact numerical tables of μ^{-1}, τ, Y as functions of X, for given M_1 and M_j.

But in the case where μ^{-1} and τ are small with respect to unity it is interesting to write simplified formulae, valid up to the second order.

The basic equations are rigorously transformed into (1), (2), (3): δm and δj denote respectively the complements of mass and dynalpy flux brought up by the jet, per unit area of the mixing chamber *total cross-section.*

One can then write, up to the second order

$$\delta h_i = \delta\left(h + \frac{u^2}{2}\right) = \delta h_1 + u_1 \delta u$$

with $$\delta h_1 = T_1 \delta s + \frac{\delta p}{\rho_1} \ .$$

But in the local isentropic stagnation state:

$$\delta s = C_p \frac{\delta T_i}{T_i} - r \frac{\delta p_i}{p_i}$$

whence $$\frac{\delta s}{r} = -\frac{\delta p_i}{p_{i_1}}, \quad (\delta T_i = 0)$$

which justifies the framed formulae, where functions $\bar{\omega}_j = \bar{\omega}(M_j)$; $\Sigma_j = \Sigma(M_j)$ were introduced, as well as the definition of $X = p_{ij}/p_{i_1}$.

It is thus seen that for a given injector (τ, M_1, M_j) the useful effect $\delta p_i/p_i$ is a *linear function of injection pressure.* This effect is proportional to τ, i.e. to the jet emissive section.

Fig.12 EJECTOR PERFORMANCE

a) General case $p_j \neq p_1$

$$D = \frac{\varpi_j}{\varpi_1}\left(1 + \gamma M_j^2\right) - \gamma M_1^2 \frac{\Sigma_1}{\Sigma_j}$$

$$\frac{\delta p_i}{\tau \cdot p_i} = X D(M_j, M_1) - 1$$

$$X = \frac{p_{ij}}{p_{i1}}$$

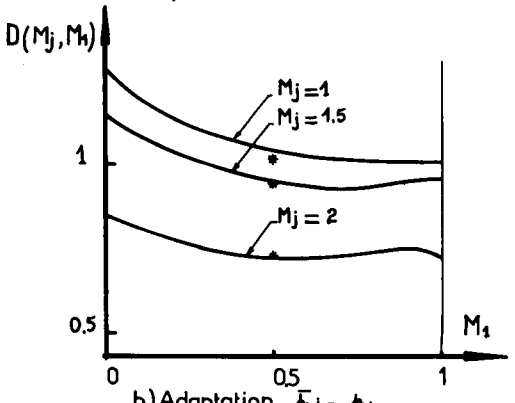

b) Adaptation $p_j = p_1$

$$\frac{\delta p_i}{\tau \cdot p_i} = \gamma M_j^2 - \gamma M_1^2 \frac{\varpi_1 \Sigma_1}{\varpi_j \Sigma_j} = \frac{\mu}{\tau} \bar{E}(M_1, M_j)\text{; see fig13}$$

$$\bar{X} = \frac{\varpi_1}{\varpi_j} \quad ; \quad \bar{\mu}^{-1} = \frac{\tau}{1-\tau} \cdot \frac{\varpi_1 \cdot \Sigma_1}{\varpi_j \cdot \Sigma_j} = \frac{\bar{\tau}}{1-\bar{\tau}} \frac{a_j}{a_1}$$

Figure 12 expresses the preceding relation in the form of a function $D(M_1, M_j)$ knowledge of which permits the immediate approximate calculation of $\delta p_i / p_i$, if X and τ are given.

On the figure the discrepancies of these results are underlined, exact to the first order, compared with some exact results for $\tau = 0.05$. It is seen that when τ is small enough the solution is satisfactory.

Fig.13 EJECTOR PERFORMANCE

(Simplified formulae)

Special case: $p_1 = \bar{p}_j$ (adaptation)

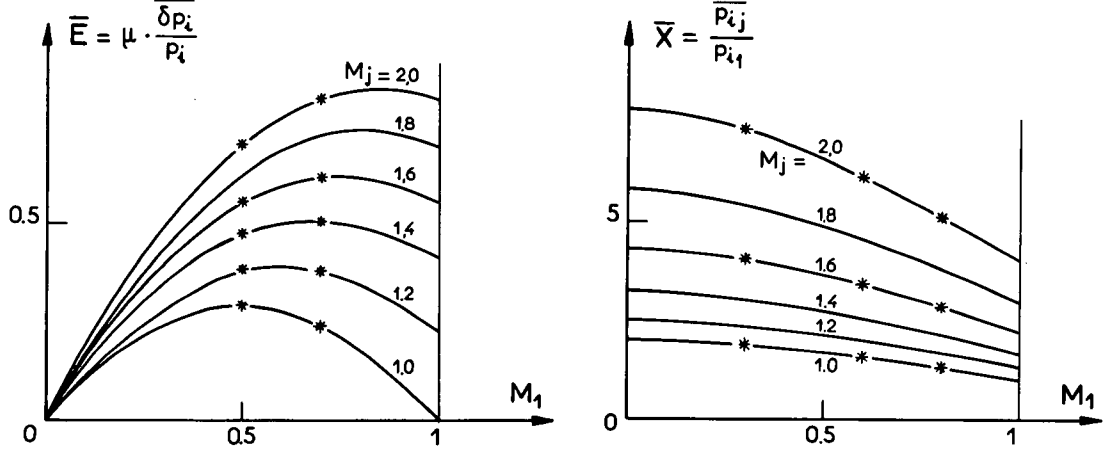

* exact computation

Figure 13 describes the particular case where the ejector functions at the *adapted regime*, i.e. when the jet is emitted at a pressure $\bar{p}_j$ equal to pressure p_1 of the main flow; in this case a free parameter disappears; $\bar{X} = \overline{p_{ij}}/p_{i_1}$ is fixed by the choice of M_1 and M_j, so that τ can be expressed as a function of μ^{-1} (see Fig.10) and, to the approximation degree chosen, $\delta\bar{p}_i/p_i$ is proportional to $1/\mu = \mu^{-1}$.

The correction curve allows us to estimate the error of this simplified formula or, if necessary, to calculate a more precise result for relatively large values of μ^{-1}.

The function $\bar{E}(M_1, M_j)$ expresses this proportionality and makes it clear that, *for each value of* M_j, *there exists an optimal value of* M_1. This is a very important result for design purposes.

Fig.14 EXAMPLE OF INJECTOR PERFORMANCE

$M_1 = 0.6$; $M_j = 1.6$

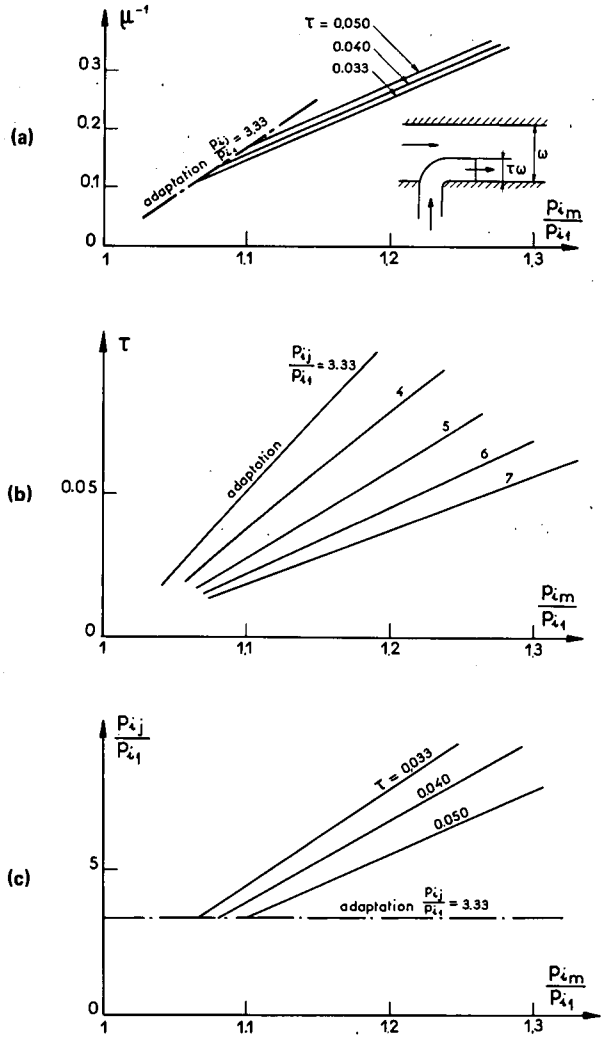

Figure 14 expresses the preceding results, as an example, in a typical particular case: $M_1 = 0.6$, $M_j = 1.6$, as a function of the compression ratio $Y = p_{im}/p_{i_1}$. It gives the values of

$$\mu^{-1} = \frac{q_{mj}}{q_{m_1}} = \frac{\text{injected air flow rate}}{\text{flow rate to be entrained}}$$

$$\tau = \frac{\text{emission area}}{\text{mixing chamber area}}$$

$$\frac{p_{ij}}{p_{i_1}} = \frac{\text{injection pressure}}{\text{local stagnation pressure}} .$$

It is clearly seen that for high values of Y , corresponding to high testing Mach numbers, it is mandatory to forgo the adapted regime in order to minimize the expenditure of compressed air. Using the adaptation regime is in fact suggested only in order to limit the intensity of the noise proceeding up to the test section from the mixing chamber; it is then obvious that this regime can be dispensed with in supersonic tests, provided that the return circuit is acoustically treated.

Fig.15 EXPENDED MASS FLOW

versus mixing chamber length

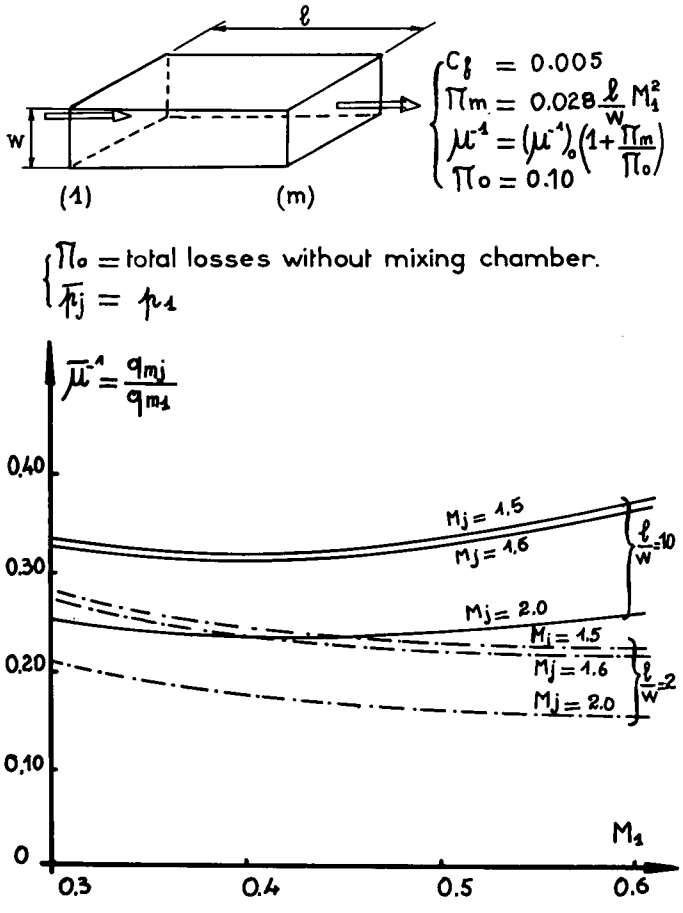

Figure 15 – The mixing chamber problem consists in a compromise between the mixing efficiency and the friction losses, which increase with length l.

If w is the crosswise characteristic dimension of the mixing chamber, it is generally assumed that in the case of a single central jet l/w should be in the order of 10 (at least).

The classical boundary layer theory gives for the losses the expression

$$\Pi_m = 4\gamma M_1^2 C_f \cdot \frac{l}{w} .$$

Fabri[2] recommends taking $C_f = 0.005$ (which is a conservative value); whence

$$\Pi_m = 0.028\, M_1^2 l/w .$$

If Π_0 represents the total losses in the circuit (apart from the mixing chamber), and q_{mj_0} the theoretical flow-rate necessary to compensate them, the actual flow-rate q_{mj} for a mixing chamber of non-zero length is then defined by

$$\frac{q_{mj}}{q_{mj_0}} = 1 + \frac{\Pi_m}{\Pi_0} .$$

q_{mj_0} and Π_m being functions of M_1, the figure represents the influence of M_1, and that of l/w, for three typical values of M_j, and $\Pi_0 = 0.10$ (nominal case), and an ejector *functioning at adaptation.*

One may notice the interest there is to choose, (i) M_j as high as possible and, (ii) for a given M_j, the value $l/w = 2$, which seems feasible with a multiple ejector, as will be seen later.

The optimum of M_1 happens to be around $M_1 = 0.6$, and is rather flat. In the following, we shall keep this value for the numerical examples, but the experiments which are in progress at ONERA could demonstrate that a slightly lower value would be better – for example $M_1 \sim 0.5$.

MIXING PROCESS OF A CASCADE OF FREE JETS

Fig.16 Velocity profiles

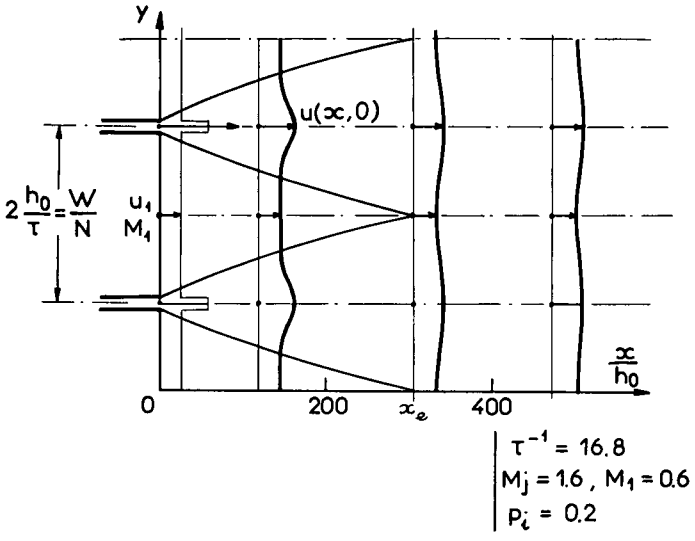

Fig.17 Efficiency of mixing

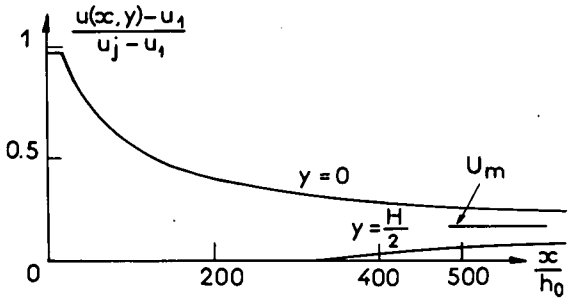

Figure 16 sums up recent results obtained at ONERA by *O.Leuchter*[4] in the study of isobaric, parallel, free jets by a finite difference method and the use of a turbulent friction model based on a recently improved mixing length concept.

The isobaric assumption can be maintained here for a mixing chamber of constant section, as the length-wise variations of p are small.

The figure shows the evolution of the mixing profiles as a function of x/h_0 (h_0 being the half-height of the slit).

It should be noted that if, in the width w of the mixing chamber, we set N equidistant injector vanes, we have, by definition,

$$\tau = \frac{2Nh_0}{w} .$$

The half spacing of the jets is given by

$$\frac{y_e}{h_0} = \frac{w}{2Nh_0} = \frac{1}{\tau} .$$

It is shown that, in the typical case $M_j = 1.6$, $M_1 = 0.6$, $\tau^{-1} = 16.8$, $N = 8$, the jets join up for $x_e = 300\, h_0$, i.e. $x_e = 1.25\, w$.

Figure 17 presents, in the same typical case as in Figure 16, the mixing efficiency as a function of length.

At the location where the jets join up ($l = 1.25\, w$), the difference Δu of axial and lateral velocities is in the order of 30% of the initial difference; at the location $500\, h_0$ ($l/w \sim 2$), the difference Δu is reduced to 15%; as a consequence, it is considered that this limit ($l/w = 1$) can be accepted for the mixing chamber length, as:

(i) the velocity increase near the wall will then have reached about half of its theoretical final value, at the diffuser entrance,

(ii) a partial evacuation of the boundary layer at this point is possible,

(iii) within the flow, mixing will continue to take place in the diffuser.

Experiments under way at ONERA verify this statement.

Other calculations are also undertaken to study the effect of mixing at increasing pressure, which should permit reduction of the length of the mixing chamber to almost zero (see Figure 43).

Fig.18 OPTIMIZATION OF EXHAUST

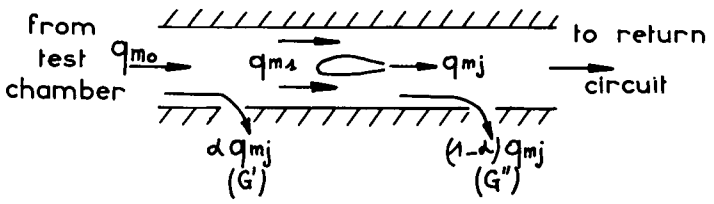

$q_{m_0} = f(M_{test}, p_{i_0}) = \text{Given}.$

$\Pi_0 = \text{Total losses without exhaust effect.}$

$G'.\Pi_0 = \text{Reduction of losses due to } \alpha q_{mj}.$

$G''.\Pi_0 = \text{Reduction of losses due to } (1-\alpha)q_{mj}.$

$q_{mj_0} = K.\Pi_0.q_{m_0}$ without exhaust.

$q_{mj} = K.\Pi_1.q_{m_1}.$ for $\alpha \neq 0$

$\Pi_1 = \Pi_0 (1 - G' - G'')$

$q_{m_1} = q_{m_0} - \alpha q_{mj}$

$$\boxed{\frac{q_{mj} - q_{mj_0}}{q_{mj_0}} = -G' - G'' - \alpha \frac{q_{mj_0}}{q_{m_0}}}$$

Example: $\alpha = 1$; $G' = G'' = 0$; $\frac{q_{mj_0}}{q_{m_0}} = 0.2$

$$q_{mj} = 0.8\, q_{mj_0}$$

Figure 18 – To maintain steady conditions it is obviously necessary to evacuate a flow rate q_{me} equal to the injected flow rate q_{mj}. In pressurized wind tunnels as considered here, this raises no problem of supplementary energy expenditure. This condition may be utilized to reduce air consumption.

If we evacuate q_{me} between the test section, where the total flow rate is q_{m_0}, and the injector, we reduce the entrained flow rate by the same quantity, as shown by the numerical example. If, moreover, we take advantage of this evacuation to eliminate part of the boundary layer, the losses to be compensated are reduced. In this respect, it may be advantageous to reserve a part $(1-\alpha)q_{mj}$ of the flow rate to be evacuated to improve the losses in the mixing chamber and in the second diffuser.

It should be noted that if a part of the mixing chamber boundary layer is evacuated before location x_e, where the action of the jets starts being felt along the wall, this flow rate should be included in the part αq_{mj}.

The formula sums up the discussion and can be used as a basis for optimizing the evacuation, provided G' and G'' are known as functions of α and of the position of exhaust.

Fig.19 REDUCTION OF LOSSES BY BOUNDARY LAYER BLEED

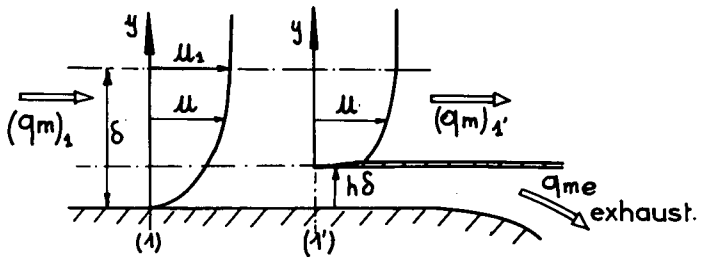

- Total capture area $\beta B.h\delta = \chi \omega_1$

$$\beta = \frac{\text{lateral extension of bleed } \beta B}{\text{sectional perimeter } B}$$

- Non uniformity functions.

$$Q(h) = \frac{1}{h}\int_0^h \frac{\rho u}{\rho_1 u_1} \cdot \frac{dy}{\delta} \; ; \; D(h) = \frac{1}{h}\int_0^h \frac{p_1 + \rho u^2}{p_1 + \rho_1 u_1^2}\, dy$$

- Bleed mass flow $q_{me} = \rho_1 u_1 \omega_1 \chi Q(h)$.

- $$q_{m_1'} = \rho_1 u_1 \omega_1 (1 + \varepsilon q_1) - \rho_1 u_1 \omega_1 \chi Q(h).$$
$$= \rho_1 u_1 \omega_1 (1 - \chi)(1 + \varepsilon q_{1'}).$$

- Variation of non uniformity coefficient due to bleed :

$$\begin{cases} \Delta\varepsilon_q = \varepsilon_{q_{1'}} - \varepsilon_{q_1} = \chi\left(1 - Q(h) + \varepsilon_{q_1}\right) \\ \Delta\varepsilon_d = \varepsilon_{d_{1'}} - \varepsilon_{d_1} = \chi\left(1 - D(h) + \varepsilon_{d_1}\right) \end{cases}$$

Figure 19 sums up the method applicable for calculating the reduction of losses by boundary layer bleed, as a function of the assumed shapes as well as the velocity profile.

We assume a bleed of height $h\delta$, extending over a fraction β of the perimeter B of the section considered, of total area ω_1.

The calculation takes account of the functions $Q(h) = 1 + \epsilon_q$ and $D(h) = 1 + \epsilon_d$ given in Appendix II, which express respectively the non-uniformity in flow rate and in dynalpy of the bled flow, relative to the main flow taken as a reference.

This way, we determine by a very simple calculation the variations $\Delta\epsilon_q$ and $\Delta\epsilon_d$ of the non-uniformity parameters of the whole flow between the sections upstream and downstream of the bleed, the values of which determine the loss reduction factor G.

Fig.20 LOSS DUE TO NON-UNIFORMITY

$$\Pi_\delta = \gamma M_1^2 \varepsilon_q - (1+\gamma M_1^2)\varepsilon_d .$$

$$\Delta\Pi = \Pi_{1'} - \Pi_1 = \gamma M_1^2 \Delta\varepsilon_q - (1+\gamma M_1^2)\Delta\varepsilon_d .$$

$$G_\delta = -\frac{\Delta\Pi}{\Pi_\delta} = G(\chi, h) \qquad G = G_\delta \cdot \frac{\pi_\delta}{\pi_0}$$

$$q_{me} = \rho_1 . u_1 \omega_1 . \chi . Q(h) \Longrightarrow \alpha = \frac{q_{me}}{q_{mj}} .$$

Example :

$$\begin{cases} M_1 = 0.6 \\ \beta = 1 \\ \frac{B\delta}{\omega_1} = 0.2 \end{cases}$$

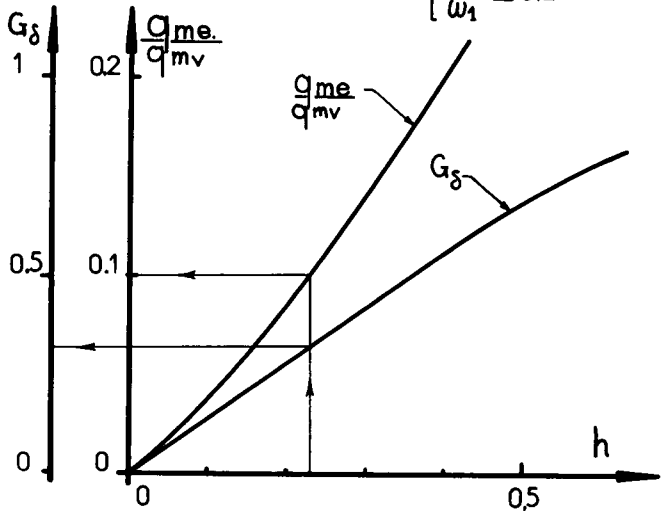

Figure 20 shows how, from the previous considerations, we can deduce the variation $\Delta\Pi$ of the losses and the corresponding evacuated flow q_{me}, as functions of relative height h and of the parameter β of transverse extension defined in Figure 19.

The numerical example illustrates in a typical case the application of this method, and shows that with $q_{me} \sim 0.10\ q_{mv}$, we evacuate 35% of the boundary layer losses; if $\Pi_\delta/\Pi_0 \sim 0.5$, $G = 0.17$.

Fig.21 VARIOUS TYPES OF BLEED

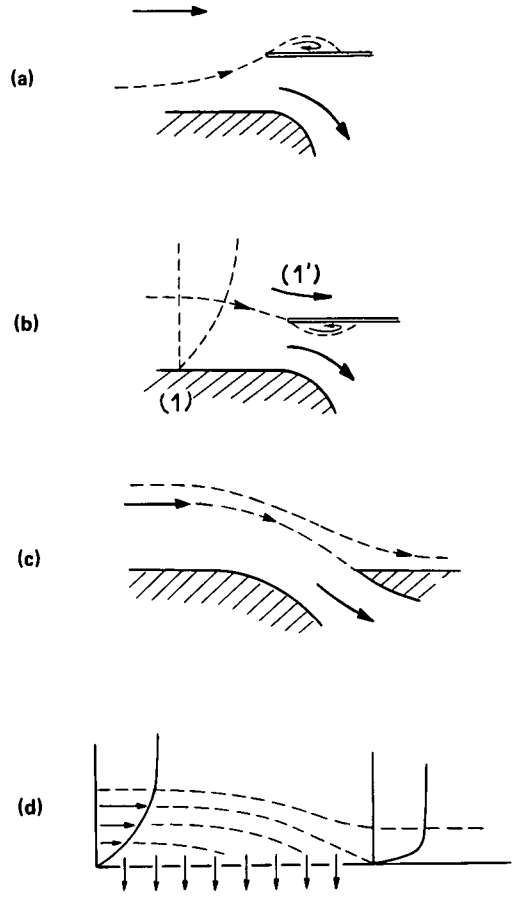

Figure 21 gives a few examples of cases which are less simple to calculate than the preceding one, in which we assumed that the bleed brought no perturbation to the flow.

The same bleed, badly adjusted in flow rate, may function according to models (a) or (b).

In case (a) the evacuated flow rate is insufficient, and there is a risk of separation at the entrance, on the external side, thence an evacuation efficiency loss.

In case (b) (too large evacuated flow) the supplementary loss is nil on the external side, but there is a risk of blockage of the bleed flow at the entrance.

In both cases, the main flow is subject to a positive or negative acceleration between sections (1) and (1′).

Case (c) represents another possibility, a limit of case (b) for $h \to 0$ (submerged air intake).

Case (d) represents a type of continuous bleed through porous walls.

The methods for calculating these various cases are rather complicated; they will not be discussed here; it is to be observed that these various bleed configurations could also be very different from the acoustic point of view.

Fig.22 INJECTOR DESIGN BASIS

Assumptions

- Losses given : fig 8

(Taking account of non-optimized boundary layer bleed)

- $M_v < 1 \Longrightarrow \overline{\pi_j} = \pi_1$

  (regulation of injected mass flow by varying $\overline{\lambda} = \overline{\tau}^{-1}$)

- $\pi_{ij} \leqslant 30$ bars $\qquad M_j = 1.6$ (for $\pi_{i1} \leq 11$ bars)

- $M_v > 1$ $\qquad \lambda = \tau^{-1}$ constant

  regulation by π_{ij}

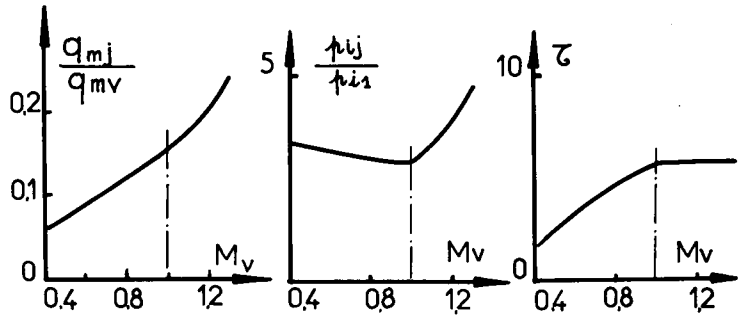

Figure 22 – Losses in the circuit that have been previously defined (Fig.7) are derived from data provided by existing non-pressurized wind tunnels. Moreover they do not take into account the gains made possible by boundary layer bleed optimization. Though these evaluations are pessimistic, they will be taken as a basis for conservative ejector dimensioning.

It is recalled that

- for $M_v < 1$, it is assumed that operation of adapted regime is used; jet piloting must therefore be done with τ variable;
- for $M_v > 1$, on the contrary, τ maximum is used, and piloting is done through injection pressure.

Lastly, we reckon that p_{ij} must not exceed 30 bars in order to avoid excessive storage pressure or capacity.

A simple calculation shows that if we want to reach exceptionally test stagnation pressures up to 10 bars, M_j should be taken at 1.6 to fulfil this condition.

It is then possible to trace the ejector functioning curves as a function of the test Mach number – see at bottom of figure.

Fig.23 INJECTOR DESIGN

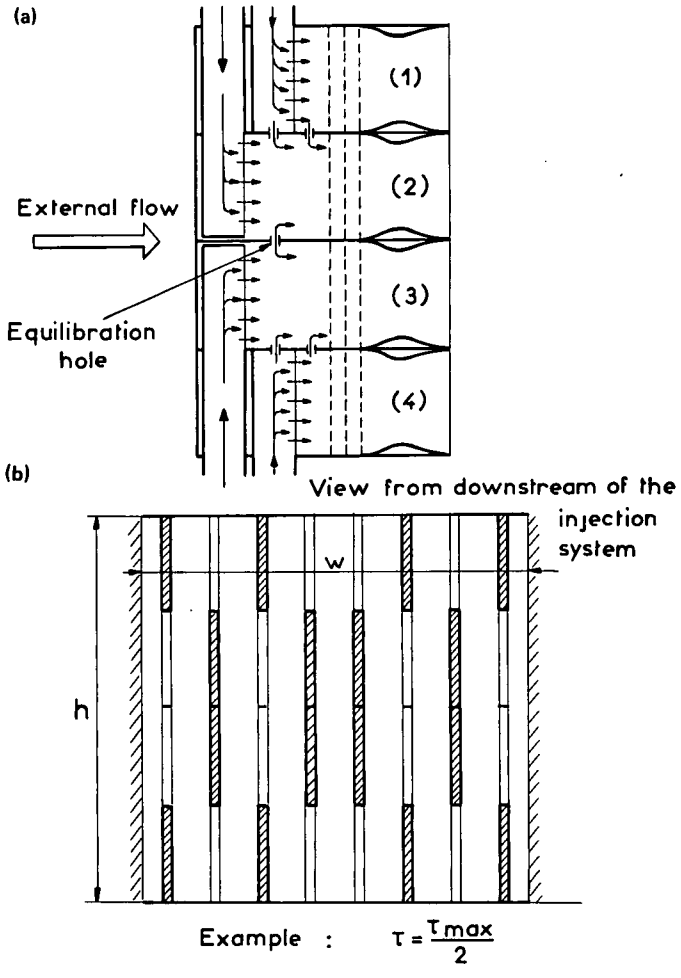

Fig.24 PERSPECTIVE OF AN INJECTOR VANE

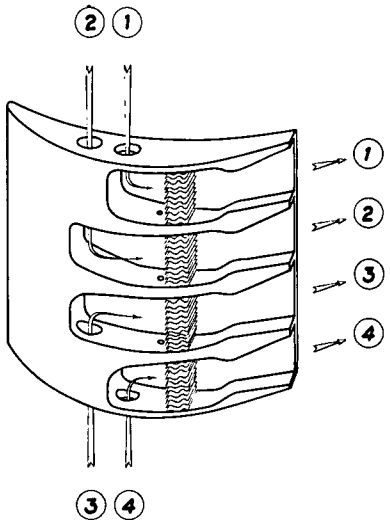

Figure 23a – Shows a possible sketch of the ejector located in one of the vanes of corner 1. It is planned to divide it into four equal compartments, individually supplied with air.

Air entering into a compartment is distributed as evenly as possible through orifices bored in the supply tubing.

In order to stabilize pressure p_{ij} and to avoid any pulsation, a system of pressure drops is inserted between the air plenum chamber and the $M_j = 1.6$ nozzle. A properly calibrated small orifice is bored in the wall separating two neighbouring compartments:

- to equalize the pressures p_{ij} if they are supplied simultaneously at full rate,
- to provide a moderate blowing flow reducing the base drag if the compartment is not in use.

Figure 23b – Shows, from downstream, the emission system with 8 vanes, i.e. 32 compartments.

In the subsonic regime, governed by the parameter τ, the number of operating compartments will determine this parameter. The grouping to be realized for obtaining the best functioning must be the subject of a special study, planned on the pilot wind tunnel T2 of ONERA (the grouping shown here is only given as an example).

Figure 24 – gives a perspective of the vane just described.

Fig.25 EJECTOR VANE DESIGN

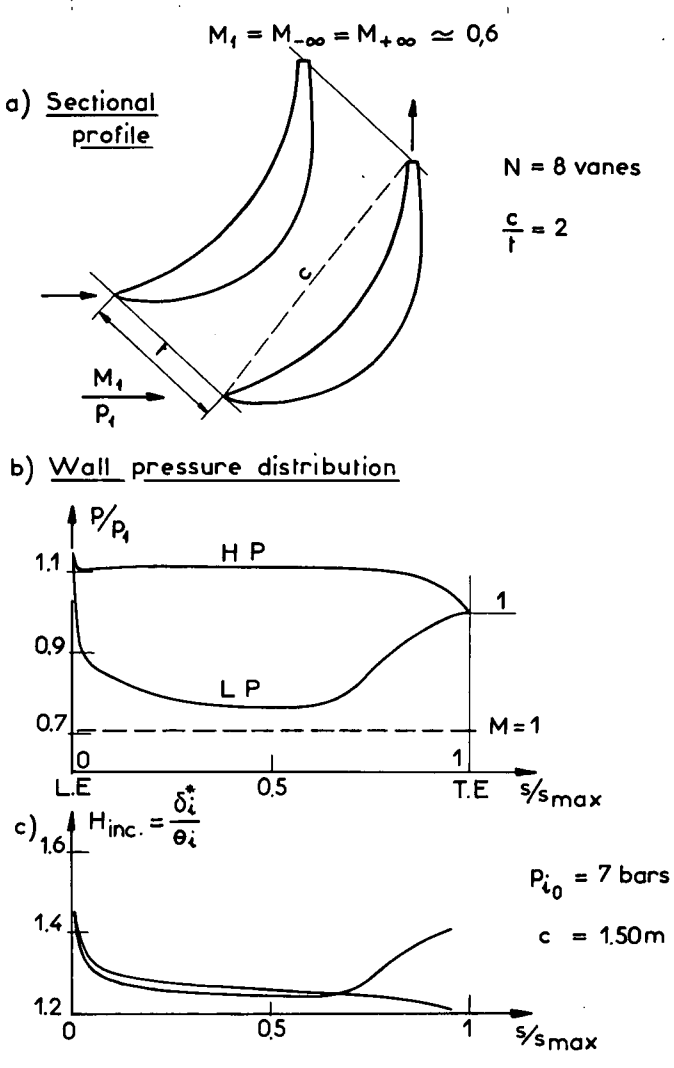

Figure 25 sums up the theoretical study of the external shroud profile of the ejector vane. Calculations are first made in ideal fluid by the hodograph method of R.Legendre; the $\pi/2$ deviation at infinity is imposed. The hodograph chosen depends on two free parameters which permit the velocity distribution to be varied within a broad range. A boundary layer calculation permits elimination of solutions which would involve flow separation and calculation of the profile losses of each acceptable solution.

The figure gives the result of these calculations. Naturally the computed profiles are not closed at the trailing edge and leave room for the nozzle exhaust.

Fig.26 SECONDARY FLOW NEAR THE SIDE WALL

(Without boundary layer bleed)

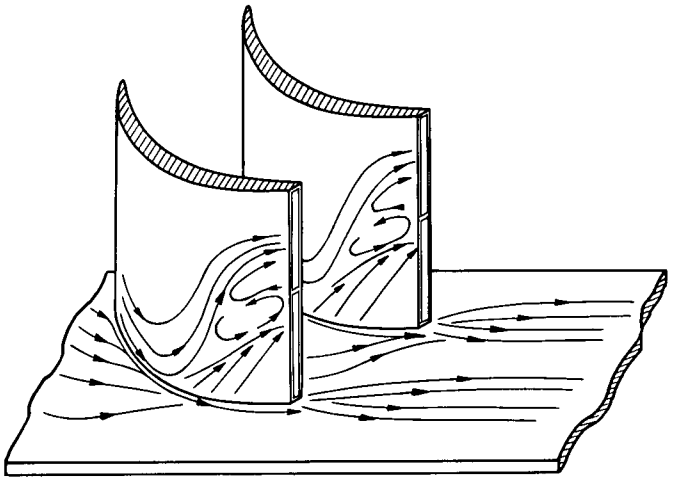

Figure 26 – Shows the three-dimensional behaviour of the boundary layer, observed on the lateral walls, between two successive vanes.

The vortex sheet which forms from the separation lines of the lateral boundary layer also creates a secondary flow entailing non-negligible losses.

An ONERA research on large deviation vane cascades showed that a boundary layer suction conveniently located on the lateral walls permits almost complete elimination of this effect provided the suction rate is sufficient; in the case considered, this rate would be of about 2% of that of the main flow, in nominal operating conditions ($M_1 = 0.6$).

Fig.27 LOSSES THROUGH CORNER No.1

Assumptions $\begin{cases} M_1 = 0{,}6 \; ; \; p_{i_1} = 6 \text{ bars.} \\ \frac{C}{t} = 2 \; ; w = 5 \text{ m.} \end{cases}$

- Sectional B.L. $= \frac{\delta p_i}{p_i} = 0.004$
- Secondary flow : 0.010

Total loss (without bleed) : 0.014

- With a bleed on the sidewalls,

$\left(\frac{q_{m_e}}{q_{m_1}} \sim 0.02\right)$, secondary flows disappears.

(from O.N.E.R.A.'s recent results)

Figure 27 sums up these results, and shows that the total losses in the corner may be brought down from 0.014 to 0.004 by suction which, at $M_v = 0.9$, represents a saving of 14% on compressed air expenditure ($q_{mj} = 0.15\, q_{m_0}$) and means an evacuation of 1.5% of the main mass flow q_{m_0}.

STARTING PROCESS ANALYSIS

INTRODUCTION

Starting the inductor initiates in the wind tunnel circuit a transient process whose duration is governed essentially by three characteristic times:

- Θ : time necessarily for the inductor to reach its maximum flow rate, an a priori arbitrary time.
- L/a_0 : time taken by an acoustic wave to travel the whole circuit length L. This time is in the order of one second in the case considered.
- L/u_{mean} : time taken by a fluid particle to travel the whole circuit length, in the order of 5 to 10 seconds.

To these characteristic times are associated two types of phenomena:

(i) The establishment of a steady pressure and velocity regime by action of the acoustic waves emitted by the inductor. This problem may be discussed rather simply by a one-dimensional, unsteady calculation method (x, t).

(ii) The formation and propagation of a main vortex at the start of the inductor, carried along by the flow and whose intensity depends on the starting law of the inductor.

We shall analyze these two types of phenomena one after the other.

Fig.28 STARTING PROCESS ONE-DIMENSIONAL ANALYSIS

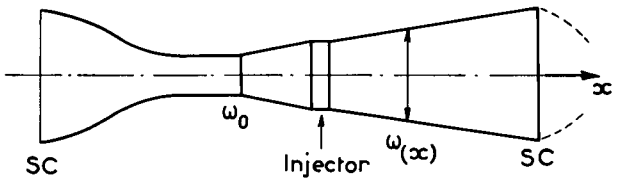

Schematic drawing of the circuit developped along $\vec{x}$

Basic equations

$$(1)\quad \mathrm{Log}\frac{\omega}{\omega_0} = \Omega(x) \qquad \text{(Given)}$$

$$(2)\quad \frac{\partial}{\partial t}(\rho\omega)+\frac{\partial}{\partial x}(\rho\omega u) = m'\omega$$

$$(3)\quad \frac{\partial}{\partial t}(\rho u\omega)+\frac{\partial}{\partial x}\left[(p+\rho u^2)\omega\right] = p_w\frac{\partial\omega}{\partial x}+(j'-f')\omega$$

$$(4)\quad \frac{\partial}{\partial t}(\rho\omega h_i)+\frac{\partial}{\partial x}(\rho u\omega h_i) = \frac{\partial}{\partial t}(p\omega)+q'\omega$$

With $h_i = h + \frac{u^2}{2}$

$\omega m'$ = injected (or extracted) mass flow
$\omega j'$ = " (") momentum flow
$\omega f'$ = drag force
$\omega q'$ = injected (or extracted) heat flow

} per unit length

p_w = effective pressure at the wall.

Figure 28 sums up the bases of the unsteady study of the establishment of the flow, by the one-dimensional method.

The circuit is supposed developed along the x axis, between abscissae O and L, the end point being arbitrarily placed. Naturally the conditions (p, u, s) acquired at time t at abscissae $x = L$ and $x = O$ are identical.

Evolution laws of the cross-section area ω are given in the form of Equation (1) where ω_0 represents a reference area, arbitrarily chosen, e.g. the test section area.

Equation (2) expresses mass conservation; the right-hand side $m'\omega$ represents the lengthwise derivative of the flow rate that may be introduced (>0) or extracted (<0) at section ω, and supposedly evenly distributed in this section ($m' = \partial m/\partial x$).

Equation (3) expresses the momentum theorem in conservative form; on the right-hand side there is first the term $p_w\,\partial\omega/\partial x$, which represents the axial impulse given to the flow by the wall pressure effect on diverging ($\partial\omega/\partial x > 0$) or converging ($\partial\omega/\partial x < 0$) walls; the term j' expresses the momentum flux per unit length ($j' = \partial j/\partial x$) and per unit sectional area, and permits us to account for the effects of inductor or boundary layer bleeds; the term f' corresponds to friction or drag forces per unit length, supposedly evenly distributed over ω ($f' = \partial f/\partial x$).

In Equation (4), which expresses energy conservation, we placed on the right-hand side a term $q' = \partial q/\partial x$ which corresponds to the effect of a possible heat exchanger, or to the introduction of a stagnation enthalpy flux attached to injection or extraction of a mass flow rate m. If, for example, we inject the rate m of a fluid whose specific stagnation enthalpy is h_i, we write: $q = mh_i$.

Fig.29 STARTING PROCESS ANALYSIS

Main dependent variables: $Z = \log p$, $U = \frac{u}{a_0}$, $S = s/C_p$

Characteristics equations [from (2), (3), (4)]

dimensionless variables

$$t^* = \frac{a_0 t}{L} \qquad x^* = \frac{x}{L}, \quad A = \frac{a}{a_0} \qquad \rho^* = \frac{\rho}{\rho_0}$$

$$(\eta)\quad \frac{\delta^+ x^*}{\delta^+ t^*} = U + A \longleftrightarrow \frac{A}{\gamma}\delta^+ Z + \delta^+ U = (Q' + AP')\delta^+ t^*$$

$$(\xi)\quad \frac{\delta^- x^*}{\delta^- t^*} = U - A \longleftrightarrow \frac{A}{\gamma}\delta^- Z - \delta^- U = (-Q' + AP')\delta^- t^*$$

$$(S)\quad \frac{dx^*}{dt^*} = U \qquad dS = R'\,dt^*$$

P', Q', R' } linear combinations of m', j', f', q', $\Omega' = \frac{d \log \omega}{dx^*}$

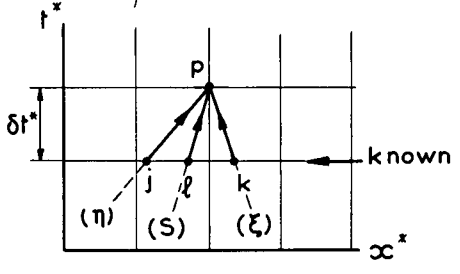

standard method of computation (fixed grid)

Standard algebraic derivations leading to the characteristic equations of the basic system are omitted here (see Appendix II). It is convenient to make use of non-dimensional parameters for computation:

$$t^* = \frac{a_0 t}{L} \qquad x^* = \frac{x}{L} \qquad U = \frac{u}{a_0} \qquad A = \frac{a}{a_0} \qquad \bar{\rho} = \frac{\rho}{\rho_0} \qquad S = \frac{s}{C_p} \qquad Z = \log p/p_0$$

Expressions m', f', j', q' of the right-hand side are also non-dimensionalized.

The three classical families of characteristics are naturally found:

- (η) acoustic waves propagating faster than the flow (velocity $U + A$),
- (ξ) acoustic waves travelling upstream (velocity $U - A$),
- (S) trajectories (x, t) of fluid particles (velocity U).

To any displacement, of duration δt, along each of these characteristics in the (x^*, t^*) plane, is associated a relation expressing the variations of Z, S, U (the three functions of state which determine the flow at every point). Functions P', Q', R' from the right-hand sides of the basic equations are simple linear combinations of m', j', f', q', $\Omega' = d \log \omega / dx^*$.

At the bottom of the figure is recalled the classical outline of the calculation method of Z, U, S at a point $p(t + \delta t)$ when their values are known at every point at time t. It is advantageous to carry out a calculation on a fixed network (x^*, t^*), appropriately chosen in each case.

Fig.30 UNSTATIONARY INJECTOR ANALYSIS

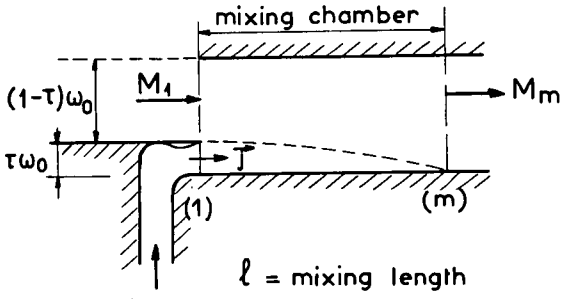

ℓ = mixing length

Injected mass flow m $\longrightarrow m' = \dfrac{\tau \rho_j u_j}{\ell}$

" dynalpy j $\longrightarrow j' = \dfrac{\tau}{\ell}\left[p_j(1+\gamma M_j^2) - p\right]$ } P', Q', R'

" total enthalpy q $\longrightarrow q' = m' h_{ij} = m' h_{i_1}$

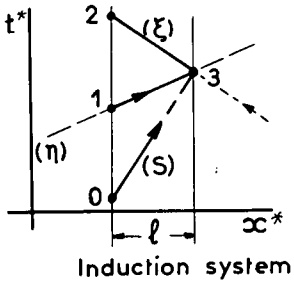

Induction system

Characteristics equation for induction system traverse

$$(\eta) \longrightarrow \frac{A}{\gamma}(Z_3 - Z_1) + U_3 - U_1 = \frac{1}{U+A}(Q'\ell + AP'\ell)$$

$$(\xi) \longrightarrow \frac{A}{\gamma}(Z_2 - Z_3) - U_2 + U_3 = \frac{1}{U-A}(AP'\ell - Q'\ell)$$

$$(S) \longrightarrow S_3 - S_0 = R'.\ell$$

Calculation along the mixing chamber, by the general method outlined in Figure 30, would require information on the evolution of mixing between end sections (1) and (m).

One may, for example, assume a linear evolution with x of $m\omega$ and $j\omega$ (jet mass and dynalpy contributions), as well as of cross-section ω. These assumptions determine m', j', Ω' and, consequently, the right-hand sides P', Q', R' of the characteristic equations (parameter q', expressing the total enthalpy contribution, eliminates itself, as $h_{ij} = h_{i_1}$ by hypothesis; if not, it should be taken into account).

The sketch in the centre of the figure shows for example how point 3 at the mixing chamber outlet would be calculated from the relations of the characteristics: $(\eta)_{\overline{13}}$ (acoustic wave), $(S)_{\overline{03}}$ (stream line) both expressing the inductor effect, and of the characteristic (ξ) coming from upstream at point 3. These three relations would determine Z_3, U_3, S_3. Then, point 2 would be calculated from point 3 [characteristic (ξ)] and from information brought from downstream by characteristics (η) and (S), intersecting at this new point.

The equations at the bottom of the page show the characteristic relations to be applied across the mixing chamber; they contain the global effect of the mixing chamber alone:

$$P = P'l$$

$$Q = Q'l$$

$$R = R'l\,.$$

Fig.31 INJECTOR MODELIZATION

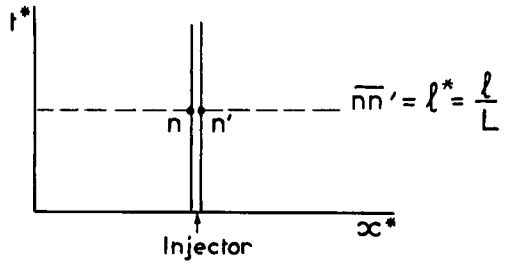

Integration of the basic equation through the injector
(t = constant)

$$\int_{x}^{x+\ell} \frac{\partial}{\partial t} \begin{Bmatrix} \rho\omega \\ \rho\omega u \\ \rho\omega h_i \end{Bmatrix} dx + \delta \begin{Bmatrix} \rho\omega u \\ (p+\rho u^2)\omega \\ \rho\omega u h_i \end{Bmatrix} = \begin{Bmatrix} \rho_j u_j \tau\omega \\ (p_j+\rho_j u_j^2)\tau\omega - f\omega \\ \rho_j u_j h_i \tau\omega \end{Bmatrix}$$

$\ell \longrightarrow 0$: steady conditions (fig 11)

$$\begin{cases} \delta(\rho u) = \delta m \\ \delta(p+\rho u^2) = \delta j \\ \delta h_i = 0 \end{cases} \quad \text{with} \quad \begin{cases} \dfrac{\delta m}{\tau} = \rho_j u_j - \rho_1 u_1 \\ \dfrac{\delta j}{\tau} = (p+\rho u^2)_j - (p+\rho u^2)_1 - \dfrac{f}{\tau} \end{cases}$$

$$\Longrightarrow \begin{Bmatrix} \Delta U \\ \Delta Z \\ \Delta S \end{Bmatrix} \text{ linear functions of } \delta m, \delta j$$

Fig.32 FIXED GRID METHOD OF CHARACTERISTICS

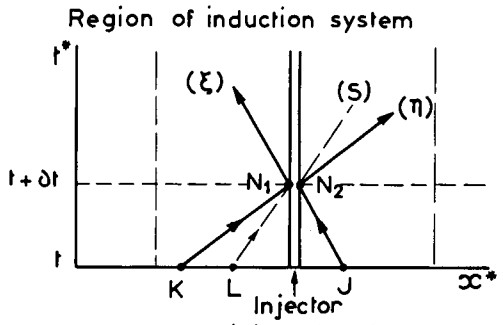

K, L, J : known at time t
N_1N_2 unknown

$$(\eta) \quad \frac{A}{\gamma}(Z_{N_1} - Z_K) + U_{N_1} - U_K = \frac{Q'+AP'}{U+A}\,\delta t^*$$

$$(\xi) \quad \frac{A}{\gamma}(Z_{N_2} - Z_J) - (U_{N_2} - U_J) = \frac{Q'-AP'}{U-A}\,\delta t^*$$

$$(S) \quad S_{N_1} - S_L = \frac{R'}{U}\,\delta t^*$$

Induction effect
$$\begin{cases} Z_{N_2} - Z_{N_1} = \Delta Z \\ U_{N_2} - U_{N_1} = \Delta U \\ S_{N_2} - S_{N_1} = \Delta S \end{cases}$$ functions of $\delta m, \delta j$

6 unknown quantities ($Z = \log p, U, S$) N_1N_2

6 relations

Study of the result of Figure 30 suggests the schematic representation proposed in **Figure 31**, in which the inductor unit is represented by a discontinuity. The three general equations of movement integrated *at time t* across the cut determine a system linear in ΔU, ΔZ, ΔS. The terms in $\partial/\partial t$ eliminate themselves when the mixing chamber length tends toward zero, and the indicated relations to determine the discontinuities at the considered time are obtained. In these expressions, P, Q, R, let us remember, are linear functions of flow rate m, of jet dynalpy j, of injector wall friction f — which is subtracted from j — and of the injector geometric parameter $\tau = 1/\lambda$.

It will then be sufficient in practice to place the corresponding cut between two successive lines x^* and $x^* + \Delta x^*$ of the network, and to proceed as indicated in **Figure 32** for calculating points N_1 and N_2.

Fig.33 INJECTOR START ANALYSIS

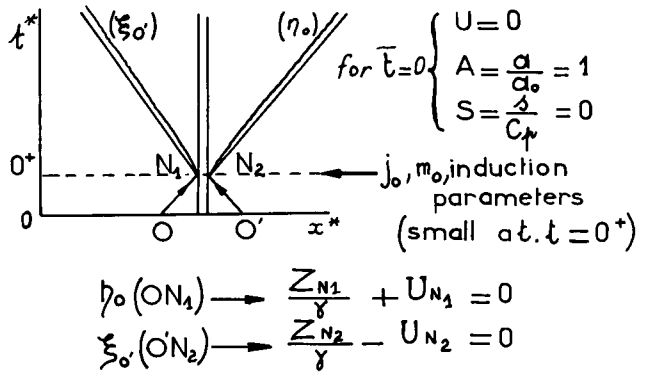

$$\eta_0(ON_1) \longrightarrow \frac{Z_{N1}}{\gamma} + U_{N_1} = 0$$

$$\xi_{0'}(O'N_2) \longrightarrow \frac{Z_{N_2}}{\gamma} - U_{N_2} = 0$$

Initial induction effect

$$j_0, m_0 \Longrightarrow \begin{cases} \Delta Z_0 = Z_{N_2} - Z_{N_1} > 0 \\ \Delta U_0 = U_{N_2} - U_{N_1} > 0 \end{cases}$$

$$\begin{cases} Z_{N_1} = -\frac{\gamma}{2}\left(\frac{\Delta Z_0}{\gamma} - \Delta U_0\right) \\ U_{N_1} = \frac{1}{2}\left(\frac{\Delta Z_0}{\gamma} - \Delta U_0\right) \\ Z_{N_2} = \frac{\gamma}{2}\left(\frac{\Delta Z_0}{\gamma} + \Delta U_0\right) \\ U_{N_2} = \frac{1}{2}\left(\frac{\Delta Z_0}{\gamma} + \Delta U_0\right) \end{cases}$$

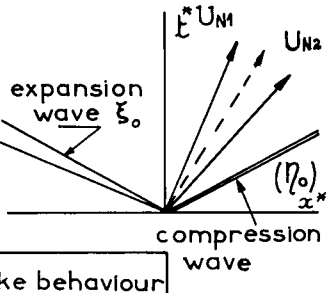

double-piston-like behaviour of starting process

The study of injector start, as shown in **Figure 33**, is quite instructive. At the initial time ($t^* = 0$) everything is at rest. A short moment later ($t^* = 0^+$), injector parameters j, m take finite but small values, j_0, m_0. Parameters Z, U, S at N_1, N_2 can be calculated by the method described in Figure 33.

The characteristic equations are then simplified, and give immediately the initial pressure and velocity jumps in N_1 and N_2, i.e. determine the intensities of the two waves (ξ_0) and (η_0) emitted respectively upwards and downwards at injector start. It is seen that wave (η_0) emitted downwards can be assimilated to a shock wave generated by a velocity jump δu_2 and proportional to:

$$\left.\frac{\delta u_2}{a_0}\right|_0 = \frac{j_0^* + m_0^*}{2} = \frac{\tau}{2\gamma p_0}\left[p_j - p + \rho_j u_j (u_j + a_0)\right]$$

while expansion wave (ξ) is expressed, at its origin, by:

$$\left.\frac{\delta u_1}{a_0}\right|_0 = \frac{j_0^* - m_0^*}{2} = \frac{\tau}{2\gamma p_0}\left[p_j - p + \rho_j u_j (u_j - a_0)\right] .$$

The initial effect of injection start may thus be represented as equivalent to that produced by an extensible piston whose rearward front would progress faster than its forward front. The velocity of the centre of gravity of this piston is defined by j_0 (the jet dynalpy), and the relative velocity of the two ends by m_0 (the jet mass flow). The distance between the two ends of the piston is then interpreted as the volume necessary to insert the fluid emitted by the jet between the two masses of fluid driven downstream and sucked from upstream.

SIMPLIFIED APPROACH TO THE STARTING PROCESS

Let us suppose that at each instant the flow regime is quasi-stationary in the circuit, which permits us to write the two following relations:

$$\rho u \omega = q_m(t) \tag{1}$$

$$p(x,t) = p_0(t)\, g[\omega(x)] \ . \tag{2}$$

The first equation expresses the fact that at each instant the flow is the same in all sections, and the second that the pressure distribution law in the circuit remains self-similar. Let us then integrate the momentum equation at instant t on the whole circuit.

$$\frac{\partial}{\partial t}\oint \rho u \omega dx + \oint \frac{\partial}{\partial x}(p + \rho u^2)\, dx = \oint p \frac{\partial \omega}{\partial x}\, dx + j(t) - \oint f' dx \ .$$

One verifies immediately that, taking account of (1) and (2), this equation is reduced to:

$$L \frac{dq_m}{dt} = j(t) - F(t) \tag{3}$$

where L = circuit length

$F(t)$ = sum of friction and drag losses.

When, at time Θ, the steady condition is reached $d(q_m j)/dt = 0$

$$j = J, \qquad F(\Theta) = J \ .$$

At any intermediary instant, one can write:

$$\frac{F(t)}{F(\Theta)} = \left(\frac{u}{u_{max}}\right)^2 \simeq \left(\frac{q_m}{q_{m\,max}}\right)^2$$

as losses are everywhere proportional to the square of velocity; on the other hand, the jet impulse j will be considered here as proportional to its mass rate, viz:

$$\frac{j(t)}{J} = \frac{q_{mj}}{q_{m\,max}} \ .$$

Equation (3) then becomes

$$\frac{L}{J}\frac{dq_m}{dt} = \frac{q_{mj}}{q_{m\,max}} - \left(\frac{q_m}{q_{m\,max}}\right)^2$$

from which, by integration from 0 to Θ, the total consumption for the starting phase becomes:

$$\int_0^\Theta \frac{q_{mj}}{q_{m\,max}}\, dt = \frac{L}{J}(q_{m\,max}) + \int_0^\Theta \left(\frac{q_m}{q_{m\,max}}\right)^2 dt \ .$$

Let us write:

$$\int_0^\Theta \frac{q_{mj}}{q_{m\,max}}\, dt = t_{eq.} \qquad \text{(loss of useful running time due to starting)}$$

and

$$\frac{q_m}{q_{m\,max}} = \delta(t) \ .$$

$\delta(t)$ represents the flow starting law in the circuit. We thus obtain:

$$t_{eq.} = \frac{L}{J}(q_m)_{max} + \int_0^{\Theta} \delta^2(t)\, dt \,. \qquad (4)$$

If we note that, by definition of μ

$$\mu q_{mj} = (q_m)_{max}$$

and that

$$\frac{q_{mj}}{J} = \frac{\rho_j u_j}{p_j(1 + \gamma M_j^2)}$$

it is easily found that the first term of (4) is equivalent to

$$\frac{L(q_m)_{max}}{J} = \frac{0.8}{\phi(M_j)} \frac{L}{a_0}$$

i.e., for $M_j = 1.6$,

$$t_{eq.} = 3.5 \frac{L}{a_0} + \int_0^{\Theta} \delta^2\, dt \,.$$

If we assume, for instance, a linear starting law $\delta = t/\Theta$ we then get:

$$t_{eq.} = 3.5 \frac{L}{a_0} + \frac{1}{3}\Theta \,.$$

It is finally seen that the equivalent starting time includes a fixed term corresponding to the momentum variation of the air mass contained in the circuit, and a second term depending on the law chosen to reach the steady condition.

In the particular case considered ($L \simeq 250$ m , $a_0 \simeq 330$ m/s), we have:

$$t_{eq.} = 2.6 + \frac{\Theta}{3} \,.$$

If, as an example, we assume $\Theta = 3$ seconds , the starting process will cost about 3.5 seconds of useful duration. It is also seen that there is no great interest in reducing Θ to a large extent, as the minimum loss is already 2.6 seconds.

REMARK

A calculation of the same type shows easily that if, the steady condition being established, injection is stopped, the velocity decrease law is:

$$\frac{u(t)}{u_{max}} = \frac{1}{1 + t^*/3.5} \qquad \left(t^* = \frac{a_0 t}{L}\right) \,.$$

It thus takes 2.6 seconds for the velocity to be reduced by half, in the particular case considered.

Figure 34a

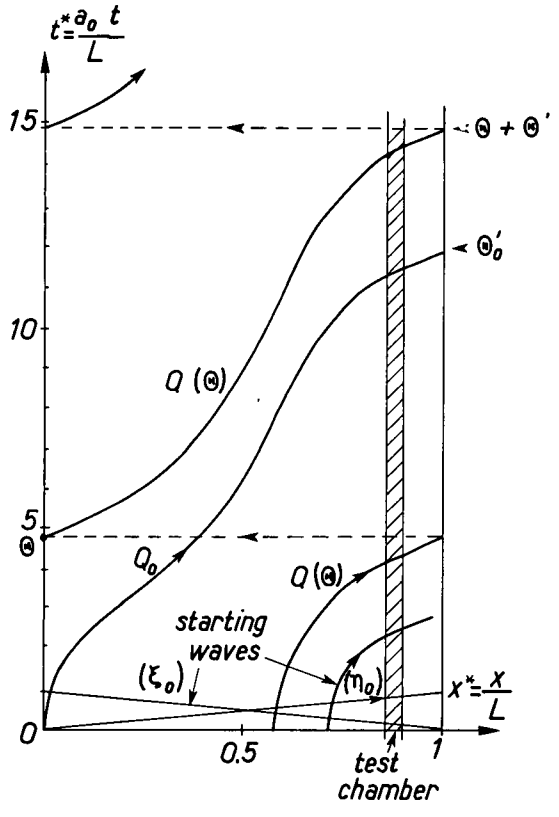

Figure 34b

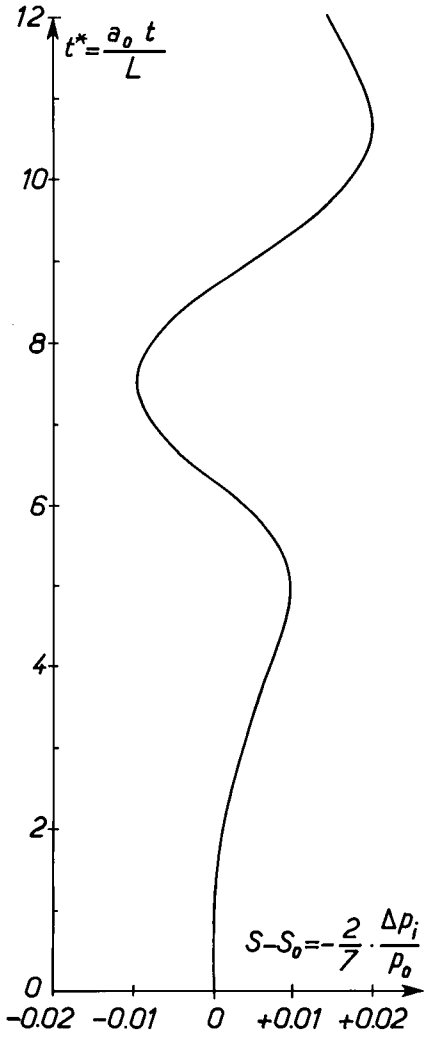

The preceding approximate method is obviously only a first approximation: it does not take into account the transient aspects of the problem, which can be characterized by the propagation duration L/a_0 (~ 0.75 sec) of an acoustic wave in the air at rest in the circuit, and by the duration $\Theta' = \oint dx/u$ of the run of a fluid particle round the circuit, in steady conditions.

Figure 34a represents the run diagrams of a few typical particles, during the initial phase: if we call Θ the instant from which the steady velocity regime is approximately established in the circuit, the particle crossing the exit section ($x = 0$) of the injector has the trajectory $Q(\Theta)$, and completes its first complete circuit at time $\Theta + \Theta'$; it is the first fluid particle subjected to losses Π foreseen in steady conditions. Any particle crossing $x = 0$ before instant $\Theta + \Theta'$ is affected by only part of losses Π: it is thus necessary to adjust accordingly the injection rate q_{mj} for $\Theta < t < \Theta + \Theta'$ in order to ensure a constant stagnation pressure at the test chamber entrance after instant $t = \Theta + \Theta'$.

Let Θ'_0 be the complete circuit time for the particle near $x = 0$ at $t = 0$ (trajectory Q_0). It is obvious that the particles crossing the test chamber between $t = \Theta$ and $t = \Theta'_0$ will have increasing entropies. If the initial jet opening has been very fast, there will be, moreover, a fast decrease of entropy at the crossing of (Q_0). We should thus expect in any case a stagnation pressure variation in the test section for a duration in the order of $\Theta + \Theta'$.

Figure 34b gives an example of this stagnation pressure variation, calculated step by step by the x, t non-stationary method, in a particular case: $\Theta = 3$ sec, $\Theta' = 7.5$ sec, corresponding to a 250-m long circuit and an $M_v = 0.9$.

On the other hand, the Mach number M_v in the test chamber can be established quickly ($\Theta^* \sim 4$), and maintained constant by a properly adjusted sonic throat at the diffuser entrance, as shown on Figure 35c.

It thus appears that, thanks to a proper adjustment of the injection law and a continuous measurement of the stagnation pressure, it is possible to limit the starting phase unusable for measurements to about $\Theta = 4.5\ L/a_0$, i.e. about 4 seconds in the case considered.

Figure 35a

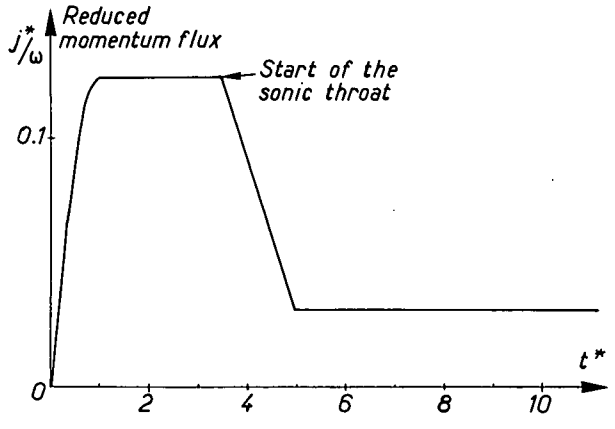

Figure 35b

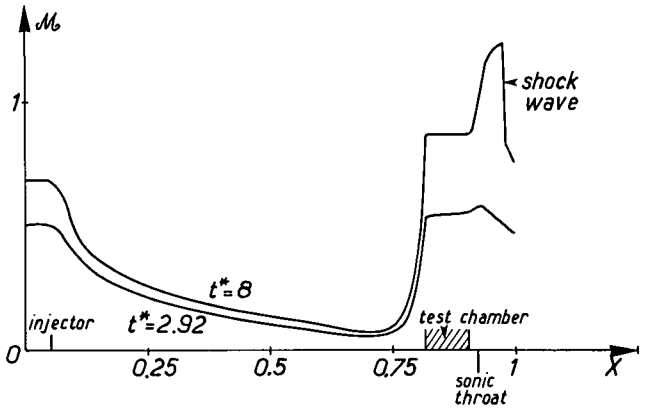

Figure 35c

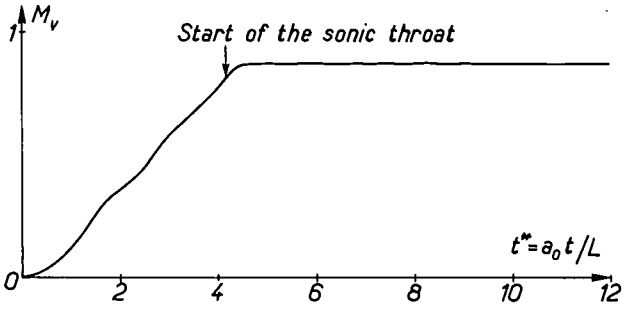

Figure 35d

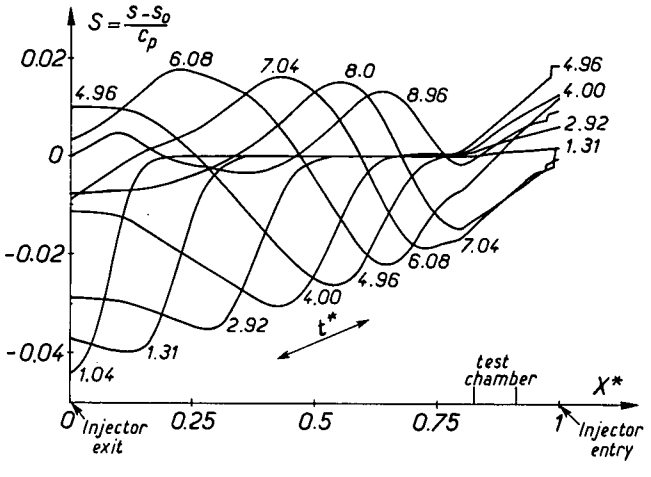

Figure 35a shows, to substantiate the previous considerations, a few interesting details of the results obtained by a step by step calculation with the x*t* numerical method in a particular case. The adopted injection law includes, in a first phase, a rapidly increasing flow rate, followed by a plateau up to the starting of a sonic throat at the first diffuser inlet. Immediately after that starting the flow rate is reduced so as to maintain the shock wave near the diffuser throat.

Figure 35b shows that the velocity distribution in the circuit remains, during the build-up phase, practically similar to the final distribution; this validates the assumption adopted in the previously described simplified theory.

Figure 35c presents the evolution of the Mach number in the chamber, which stabilizes quite well after time $t^* = 4.5$.

Figure 35d outlines the entropy distribution along the circuit at various moments during the initial phase. We can clearly see the evolution of the entropy pocket predicted by the considerations of Figure 34. The strong initial variations decrease gradually, but for $t^* = 8.96$ (i.e. 7 seconds), they are still in the order of $\delta S = 0.02$, corresponding to a 7% variation of stagnation pressure.

Though the initial injection law had not been optimized in this respect, we have little chance of totally suppressing this slow entropy drift unless we accept a considerable lengthening of the build-up phase: it will thus be necessary, for a correct interpretation of the results, to continuously measure the stagnation pressure in the test chamber.

Fig.36 STARTING VORTICES

(H.Werlé visualization)

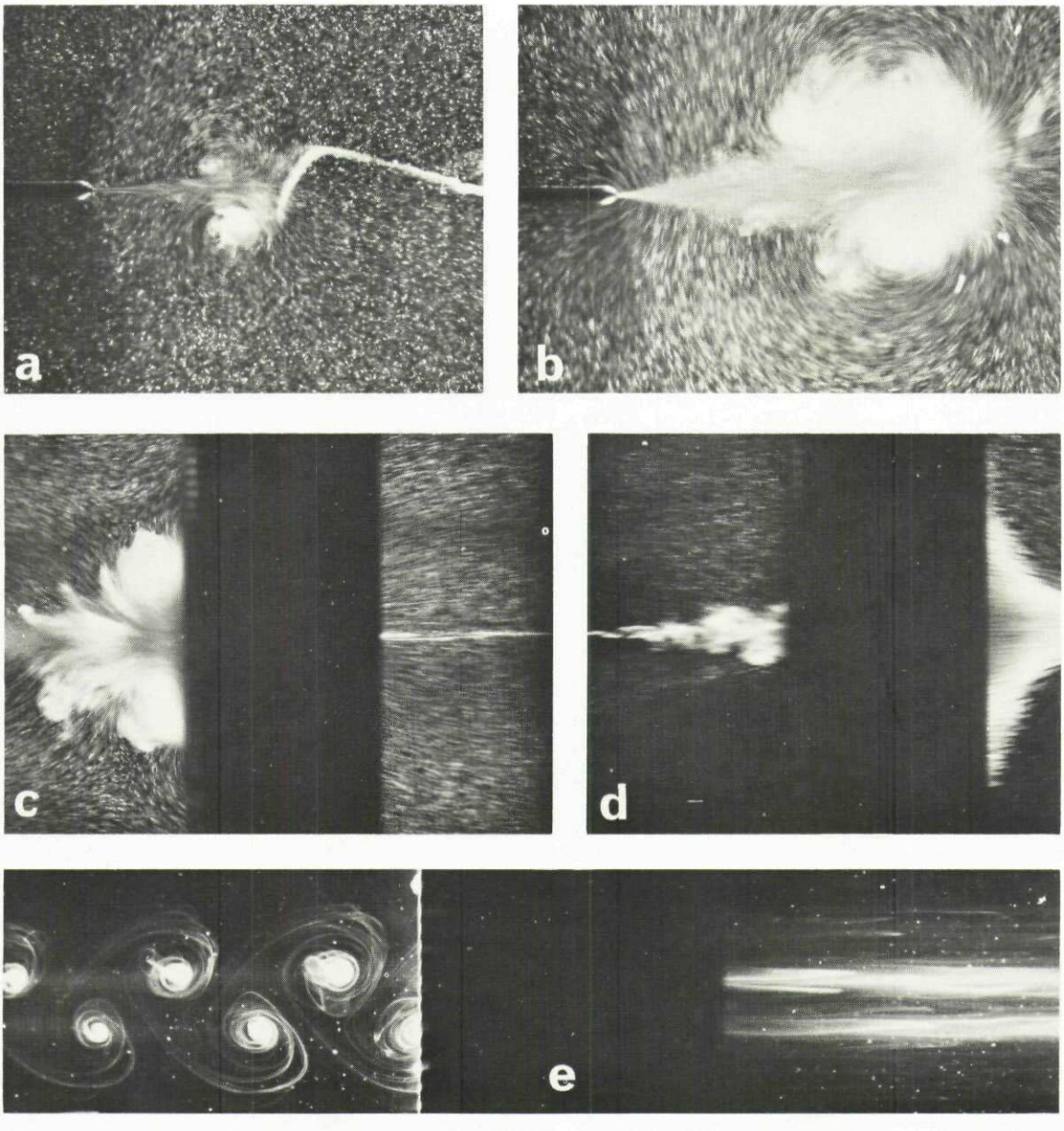

The velocity discontinuity occurring at injection start entails the formation, around each jet, of a vortex whose intensity increases with rate of jet pressure build-up (**Fig.36**).

This vortex will then travel along the circuit at the same velocity as the fluid: we have seen (Fig.35) that its passage through the testing chamber might occur during the useful part of the run, if its diffusion were not yet completed.

To facilitate this diffusion, various processes may be considered:

- slow build-up of each elementary jet (compare Figures 36a and 36b);
- successive opening of jets;
- it will also be noted that, in the proposed system of parallel jet planes, two neighbouring vortices are contra-rotative, with is favourable.

Moreover, the successive corners crossed, and the settling screen (Figs.36c, 36d, 36e) assist completion of the required diffusion.

Fig.37 PRELIMINARY PILOT IDT (T_2')

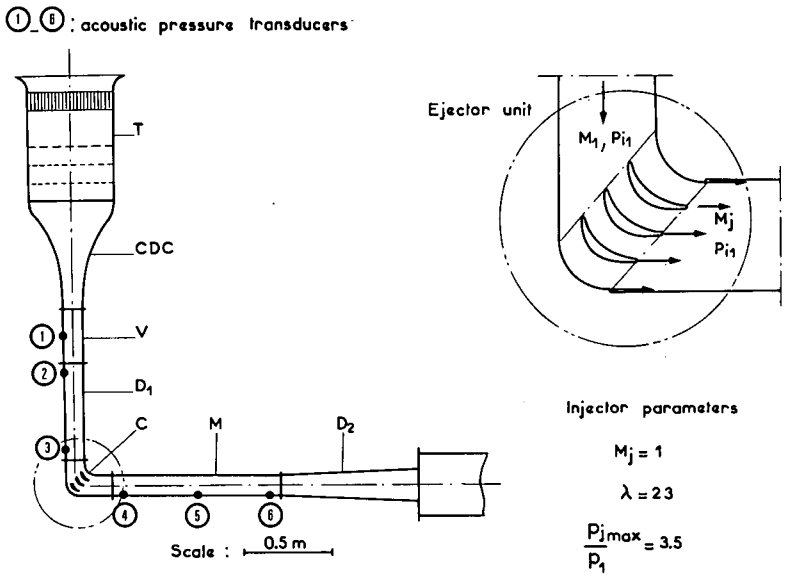

To study experimentally some of the difficulties which might be raised by the use of an IDT, a small scale installation (10-cm square test section) was operated at Chalais-Meudon. It functions in a circuit open to atmosphere, according to the layout of **Figure 37**. The constituent elements of this facility are interchangeable in order to allow the variation of a number of parameters.

Experiments already undertaken, at present in a developing stage, have already been the source of some very interesting observations, which will be briefly commented upon. They concern:

(a) noise problems,

(b) performance verification.

As regards *noise problems*, we installed acoustic sensors with very short response time (piezo-electric ceramics) in the wall, at various points of the circuit [elements (1), (2), (3), (4), etc.], and we recorded spectra by a classical method, for various conditions of installation and operation. We also recorded supply pressure spectra.

As regards *performance problems*, we record crosswise soundings, upstream and downstream of the ejectors.

This installation will soon be transferred to Toulouse, to be incorporated in a closed circuit where experiments will be carried out at various pressures above atmospheric.

The whole pilot operation, called T_2', aims at developing a research wind tunnel, called T_2, whose construction is under way, at a larger (fourfold) scale under the responsibility of Dr R. Michel, Chief of Aerothermodynamic Research Department (DERAT).

Fig.38 EXAMPLE OF NOISE SPECTRUM OBTAINED AT T_2'

(Station 1: testing chamber)

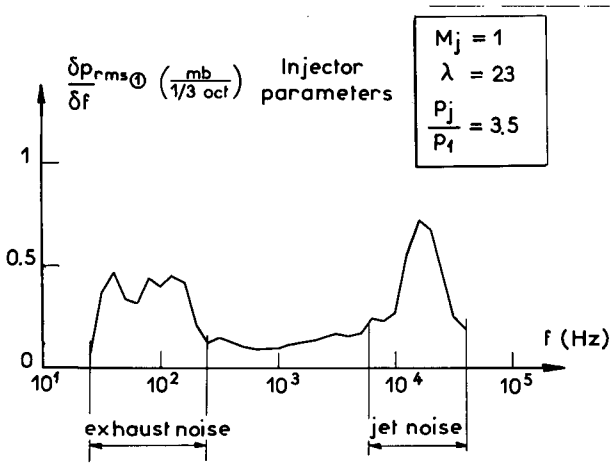

Noise measurements carried out up till now were performed at first without any special precautions. They led to interesting observations.

Figure 38 – The spectrum recorded in the testing chamber includes two zones of high intensity. The first one, in the low frequency range, is generated by the evacuation system, where flow separation takes place. The suppression of this separation made this first singularity disappear completely, so that it presents no further problem.

The second high intensity zone, appearing at the right end of the spectrum, is due to the jet itself, and to mechanical vibrations of the induction unit, whose natural frequencies happen to be in this range. The spectrum considered here corresponds to a very much under-expanded jet ($p_j/p_1 \sim 3.5$).

Fig.39 NOISE ATTENUATION BETWEEN MIXING CHAMBER AND TESTING CHAMBER

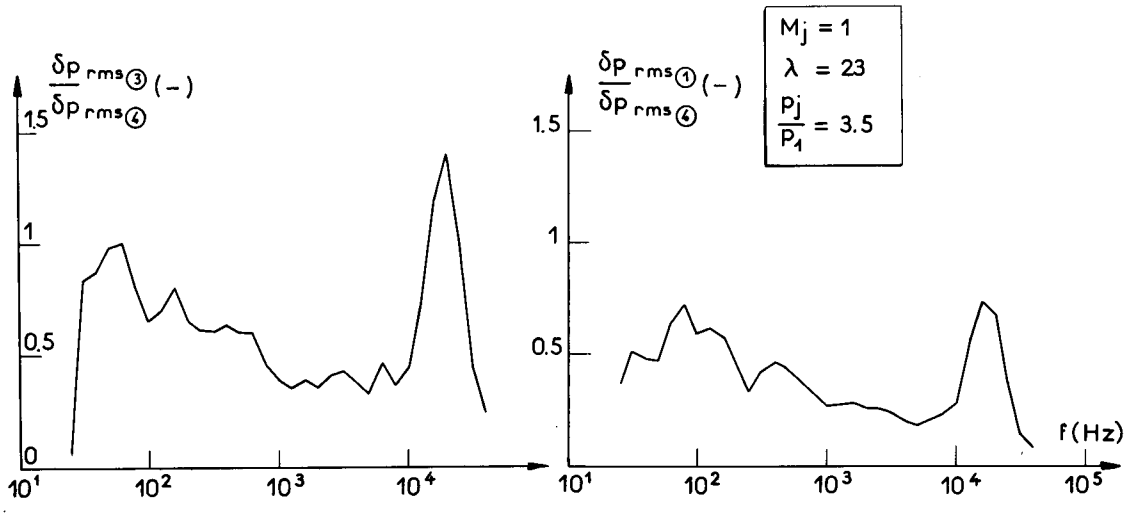

(a) EFFECT OF CORNER C_1

(b) COMBINED EFFECT OF CORNER C_1 AND DIFFUSER D_1

Figure 39 emphasizes the effect of acoustic attenuation to be observed upstream, between the noise source (mixing chamber) and various points of the circuit; we verify, in particular, the favourable effect of the corner, except at a very high frequency where, on the contrary, an intensity increase can be noted (Fig.39a). The explanation of this phenomenon is simple: the relevant frequency is the natural frequency of the vanes, and is excited by the underexpanded jet, radiating directly on the pick-up placed upstream of the corner. Let us note once more that no acoustical treatment of the walls has yet been applied.

Fig.40 ACOUSTIC NOISE IN THE TESTING CHAMBER WITH ADAPTED JET PRESSURE

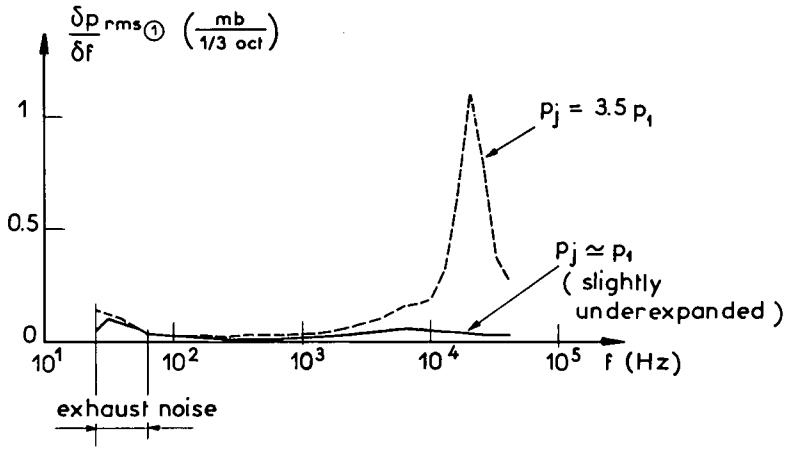

Figure 40 shows the considerable effect on acoustic intensity of the confluence of the jet with the main stream. We have traced on this figure the noise spectrum, for a pressure ratio where the adaptation condition ($p_j = p_1$) is fulfilled, and for a case where it is not.

The general pressure level being, in our present tests, fixed by ambient atmosphere, we had, to obtain the adaptation conditions, to act on the supply pressure p_{ij}. But as, in all cases, the jet is turbulent, it is reasonable to admit that, everything else being unchanged, the part of Δp_{rms} coming from the jet is proportional to p_{ij}.

This result confirms the validity of the choice we made to adjust the inductor to operate at adaptation ($p_j = p_1$), at least as long as there is no risk of direct travel of noise upstream to the testing chamber. This favourable effect of adaptation is clearly linked to the disappearance of shock wave disks forming in a non-adapted free jet, which constitute intense noise sources by their very instability.

Fig.41 FLUCTUATIONS OF JET STAGNATION PRESSURE

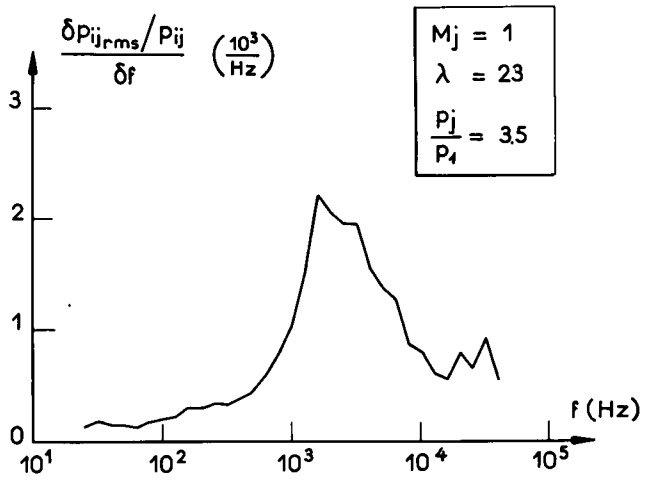

Figure 41 reveals another cause of noise initiation in jets, and concerns the pulsations of supply pressure p_{ij}.

In our present experimental set-up, no special steps have been taken to settle the supply air before its eventual expansion. The measured p_{ij} spectrum shows very large fluctuating amplitudes. It is quite obvious that discontinuities, in magnitude and in direction, that result in the jet outlet velocity constitute a very important acoustic excitation source.

That is why we proposed, in Figure 23, to insert between the vane plenum chamber and the nozzle of the ejector a pressure drop sufficient to dampen the inevitable pulsations of the supply air, at its entrance into each compartment.

Fig.42 ACOUSTIC DAMPING DUE TO ABSORBING MATERIALS

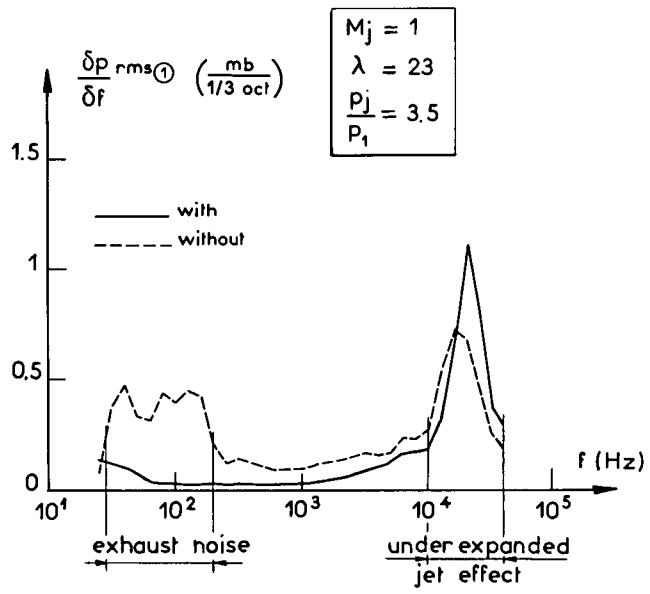

Figure 42 shows, by comparison with Figure 38, the attenuation effect obtained by acoustical treatment of the mixing chambers and upstream diffuser walls with a standard available material, in the case of an under-expanded jet; the experiment with adapted jet and absorbing material has not been made yet.

★ ★ ★

Following these various observations, a new, much more sophisticated experimental set-up has been designed and is in the course of fabrication. It will permit checking of the preceding conclusions; the acoustic spectrum which will characterize it will determine the choice of absorbing materials to be installed in order to attenuate the residual noise as much as possible.

Taking account of the acquired results, we can already estimate that the overall noise in the testing chamber* at nominal regime ($M_v = 0.9$), will reach the following values, expressed as $\nu = \Delta p_{rms}/0.7\ pM_v^2$.

	Acoustical treatment of the walls	
	NO	*YES*
Underexpanded jet ($p_j \simeq 3\ p_1$)	0.0067	0.0052
Jet near adaptation ($p_j \simeq 1.2\ p_1$)	0.0067	0.0014

* Without sonic throat at its exit.

Fig.43 ENTRAINMENT COEFFICIENT FOR TWO MIXING CHAMBER LENGTHS

(T_2' results)

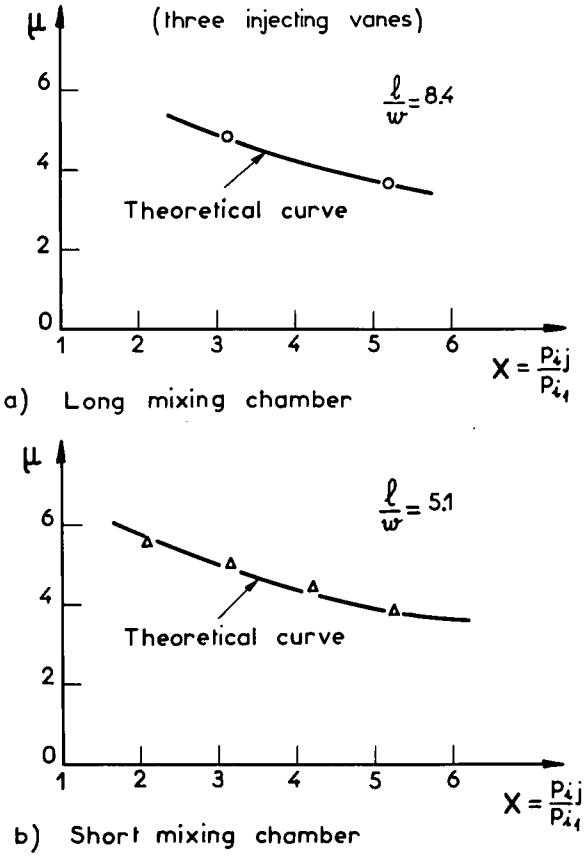

Figure 43 is intended to show that the entrainment coefficients of the injector system used in the pilot installation, equipped with three injecting vanes in the first corner of the circuit, are in agreement with the theoretical predictions, for two mixing chamber lengths respectively equivalent to $l/w = 8.4$ and $l/w = 5.1$.

Experimental points were calculated from flow rates q_{mv} measured in the test section (boundary layers being accounted for), flow rates q_{mj} measured at injector entrance, and injection pressures p_{ij} . Isentropic stagnation pressure p_{i_1} , taken as reference for X , was deduced from initial pressure p_{i_0} (atmospheric pressure) minus the losses observed at the corner entrance and the estimated losses through the vanes.

Theoretical curves were deduced, for each case, from the known parameters (X , μ , τ , $M_j = 1$) and from Mach number M_1 at inductor entrance, evaluated from the measured local pressure.

The two diagrams confirm that a mixing chamber with a length $l/w = 2.5$ gives satisfactory results with the design proposed (eight injecting vanes).

Fig.44 ADIABATIC TEMPERATURE LOSSES OF THE COMPRESSED AIR DURING THE RUN

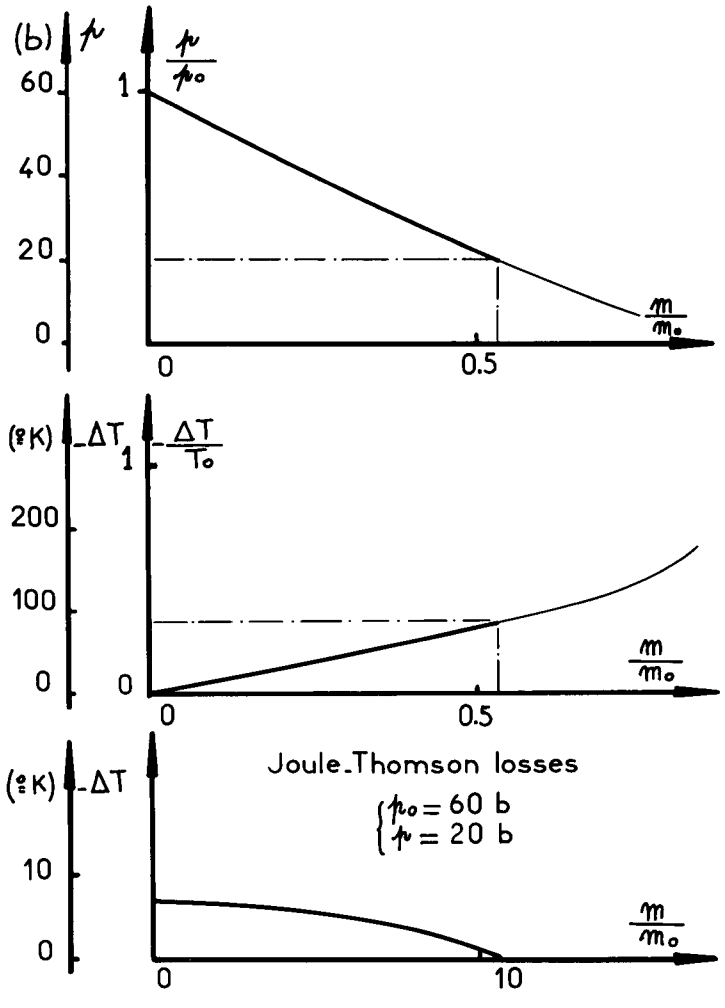

Figure 44 summarizes the essential data for the system of compressed air production and conditioning. As a basic reference, we assumed the storage pressure to be 60 bars.

In these conditions, the upper curve shows the pressure isentropic decrease in the tank, during the run, as a function of the fraction m/m_0 of the expended air mass. The nominal conditions of the project require a minimum pressure of 20 bars; the result is that we can use during a run at most 50% of the stored air.

The corresponding temperature decrease is shown on the middle curve, in degrees K; we see that it reached considerable values.

The virial effect in the adiabatic expansion which takes place in the pressure regulator (Joule-Thomson effect) is indicated in the bottom curve.

The sum of these two effects must be compensated by a heat exchanger. We propose to use to this end a heat accumulator of the hot water pool type, maintained at about 80°C, in which tubing of a sufficient length is immersed. A fraction $\alpha(t)$ of the cold air is diverted through the exchanger, then mixed with the rest $(1 - \alpha)$, upstream of the regulator, thus avoiding any icing in this device. A simple calculation shows that, to recover there the temperature of initial storage, supposed equal to the wind tunnel stagnation temperature, α varies regularly between $\alpha(0) = 0.10$ at start of operation and $\alpha = 0.50$ for $m/m_0 = 0.5$.

REMARKS

1. The installation of an IDT industrial wind tunnel should not be considered except at an important aerodynamic centre including other subsonic or supersonic tunnels, whose operation also requires large quantities of compressed air. Therefore the dimensioning of the storage capacity should not be determined for this facility alone: it is always possible to avoid using all facilities at maximum consumption at the same time.

In such a test centre, the production and storage facility should be planned so as to allow further extensions; it is not necessary to build ab initio the maximum imaginable potential (which, by the way, is unlimited).

2. To fulfil the LaWs specifications it would be absurd, with such an IDT installation, to limit the maximum run duration to 10 seconds; it would be much preferable to consider runs of the order of 30 seconds at the rate of two per hour, which would ensure a test rate much higher than with a system limited, by its very principle, to 10-sec runs every 12 minutes. The two systems are equivalent only if no work on the model is necessary between two consecutive runs; but it is almost impossible, in a pressurized tunnel of that size, to assume that any sort of work could be completed in less than a half-hour interval between runs. In this case, the IDT rate is not affected; in a 10-sec tunnel, any such intervention is equivalent to the loss of three runs. If it is assumed that work on the model is necessary every ten 10-sec runs, the efficiency loss of a 10-sec wind tunnel is thus 25%.

Furthermore, it is certain that 10-sec runs are not sufficient for all types of tests: the inconvenience could be accepted if the test can be separated in 10-sec fractions – e.g. very extended polars. But if not, the test is impossible: the solution suggested by the champions of 10-sec runs is to plan a test section of half size, which leads to the use of a special model, and above all which reduces the Reynolds number by 30%.

3. An IDT wind tunnel, having by nature a closed circuit, allows tests at continuously variable pressure or Mach number which is of great interest, especially in transonic flow for flutter and buffeting tests and, above all, for tests on motorized models.

CONCLUSIONS

I hope to have shown that the main problems pertaining to an IDT are now well understood. Research in progress on small pilot wind tunnels (T_2', T_2) at the DERAT (Appendix I), in Toulouse, under the direction of R. Michel, will soon permit us to ascertain some parameters, only briefly mentioned here, such as the regulation mode to be adopted for this type of wind tunnel. It could then be considered that the detailed design of a large industrial transonic wind tunnel of this type would not meet with any fundamental difficulty.

The main objection raised against the use of this solution concerns the injector-generated noise level in the testing chamber. Though the experimental programme undertaken at ONERA is not yet completed, the results already acquired are sufficient to define the essential precautions to be taken to eliminate this objection. In particular, the adjustment of the inductor jets at the adaptation regime is of paramount importance for subsonic testing. Some other design features such as the positioning of inducting jets at the trailing edges of the tunnel corner vanes, an efficient settling of air supply pressure and, obviously, acoustic treatment of the walls, still improve the system.

As regards noise in the testing chamber, it must be emphasized that the essential problem, not discussed here as it is not specific to IDT, remains that of the transonic treatment of the test section walls, the main noise source in present-day conventional solutions.

Another conclusion of this study is that the IDT solution is not very appropriate for very short runs, such as those proposed by the LaWs Group. An IDT solution fulfilling the general LaWs specifications (50 seconds of useful run time per hour) should be planned, for example, on the basis of 30-second runs followed by 30-minute rests: this would clearly permit to carry out in a single run a programme identical to that that would require three runs with the competitive solutions, with the advantage of an interruption time compatible with a relatively important intervention on the model without breaking the mean output rate of results. But above all, some tests in industrial wind tunnels such as unsteady flow measurements, flutter studies or work on motorized models, which would probably raise very severe, if not absolutely insolvable problems in a facility with ten-second runs, would undoubtedly be much easier to handle in an IDT.

If, after a first period of operation, it appeared necessary to increase the maximum duration or the repetition rate of the tests, a relatively modest expense would be sufficient to raise the compressed air storage or production capacity.

It should also be noted that the installation of an IDT would call only upon technological means and processes in current application in many industrial installations.

These advantages are not without counterparts: only through a thorough technological study will it be possible to characterize this solution as regards cost effectiveness, for a complete comparison with competitive solutions.

APPENDIX I

PILOT WIND TUNNEL, T2

The transonic, pressurized wind tunnel, called T2, is studied for two purposes:

(a) To provide a more precise knowledge of the possibilities of and to solve problems raised by the induction entrainment principle;

(b) to be used later for fundamental research.

With this in view, it was decided to build it at the ONERA Toulouse Centre (CERT).

1. MAIN CHARACTERISTICS

- Pressurized closed circuit with vertical return (see diagram A1).
- Square test section, 0.4 x 0.4 m. Contraction ratio: 20.
- Operation by discrete runs (mean nominal duration: 35 seconds).
- Stagnation conditions: room temperature; max. pressure: 5 bars.
- Entrainment by induction (max. induction flow rate: 35 kg/sec; jet stagnation pressure: 30 bars; stagnation temperature: 350°K).
- Air storage: 45 m^3 at 80 bars.

2. PARTICULAR POINTS OF THE PROJECT

- Injection is planned in the vanes of No.1 corner, by means of adapted nozzles (M_j = 1.6): 6 vanes with 14 nozzles each, supplied in groups of 3 or 4 permitting variation of τ in order to obtain induction appropriate to the tunnel regime.
- Constant pressure and temperature of injector supply will be ensured by a noise-limiting pressure reducer and by a hot-water pool heat exchanger.
- Evacuation of injected air is planned in several locations along the circuit: about 60% upstream of No.1 corner, 40% between No.1 and No.2 corners. An 8% flow rate could also be bled from a plenum chamber that would be part of the ventilated wall transonic equipment.

  No.2 corner is of diffusing type.

  The pressure loss calculation in a part of the circuit from collector to second diffuser for various distributions of ejected flow rates was carried out for: p_i = 1 bar ; T_i = 293°K ; M_v = 0.9 (Fig.A2). This example shows the importance of the gain obtained: more than 50% with an 11.3% bleed properly distributed among the diffusers.

3. PRESENT STATE

The design of the aerodynamic circuit and of its installation and its ancillary equipment is complete, apart from a few details. Financing and construction authorization have been obtained. Responses to bids for external supplies (compressors, tanks, etc.) have been received. On these bases, and taking account of expected construction delays, the planned date for starting operation is the first semester of 1974.

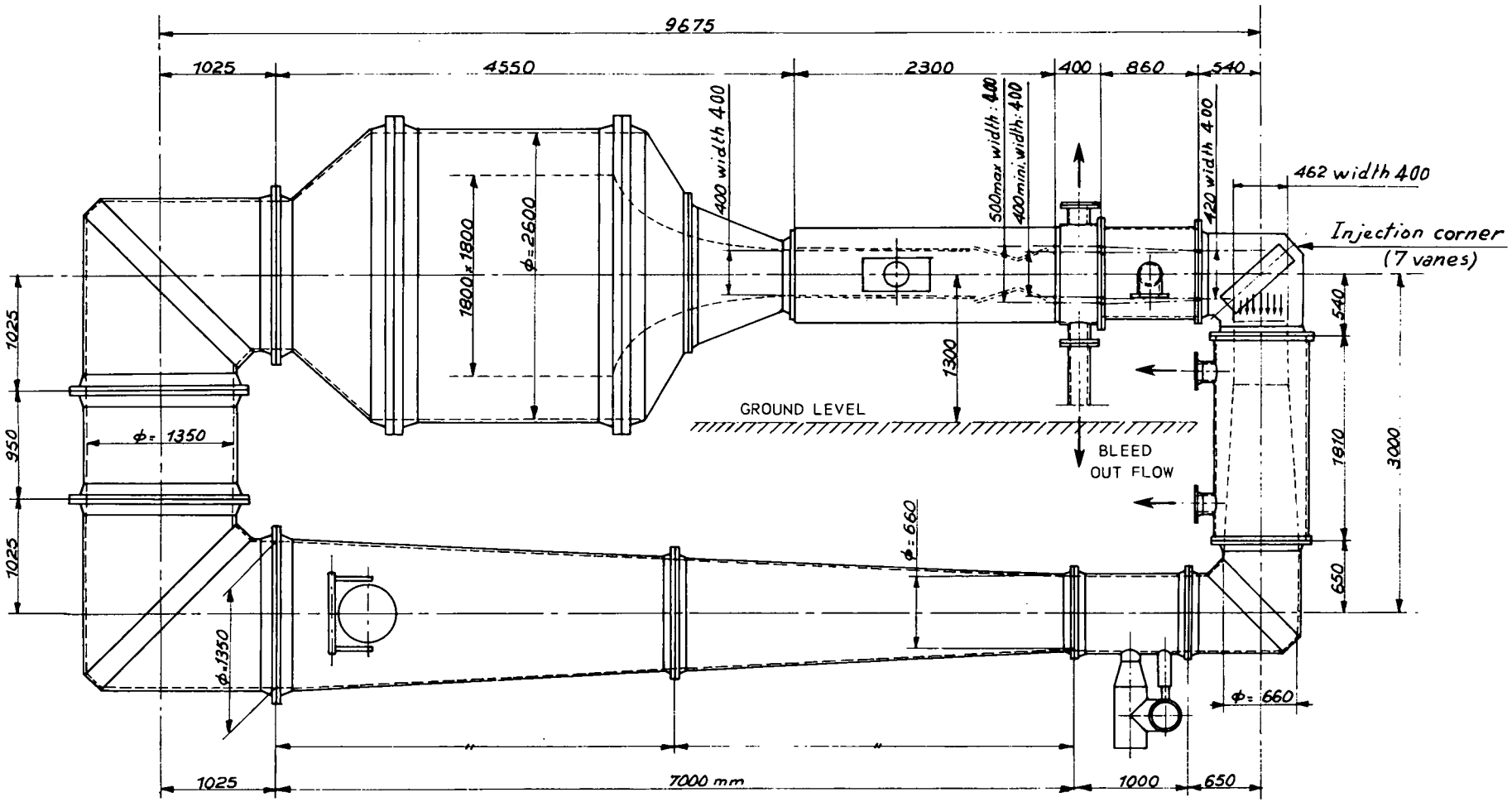

Fig.A1 T2 IDT PILOT WIND TUNNEL – INJECTION IN THE FIRST TURNING VANE

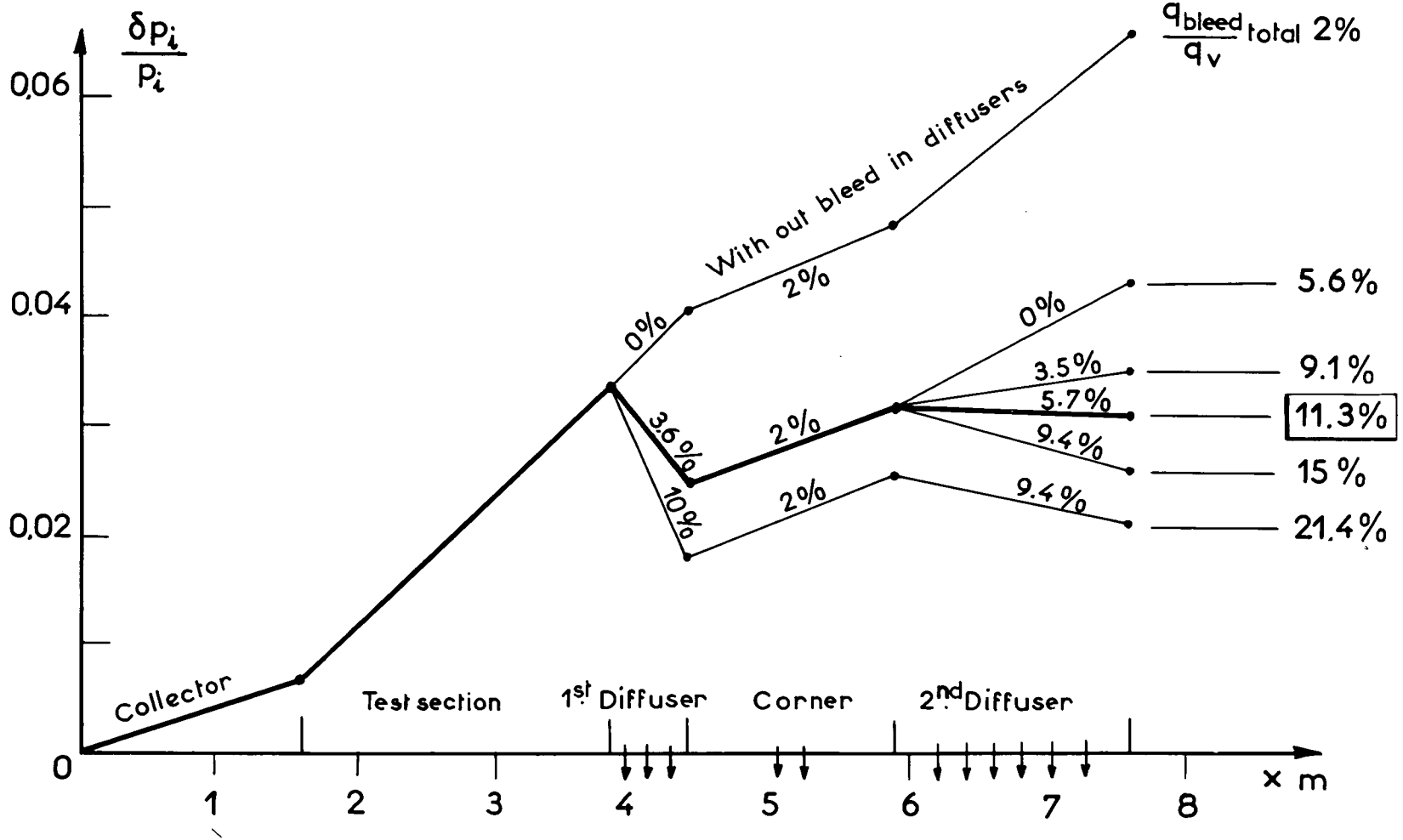

Fig.A2 EVOLUTION OF PRESSURE LOSSES AS A FUNCTION OF BLEED (T2)

APPENDIX II

SOME COMPLEMENTARY THEORETICAL EXPLANATIONS

1. SUMMARY OF EJECTOR THEORY

Assumptions and Notation

The case of constant section mixing chamber is considered a priori; it will be seen that, in the domain of application envisaged, the pressure total variation along such a mixing chamber is very low, so that the thermodynamic behaviour of the flow remains very close to that of an isobaric flow; even though this isobaric flow is theoretically better, the gain to be expected with it would not justify the complication that the corresponding shape would imply.

Fig.A3 NOTATION

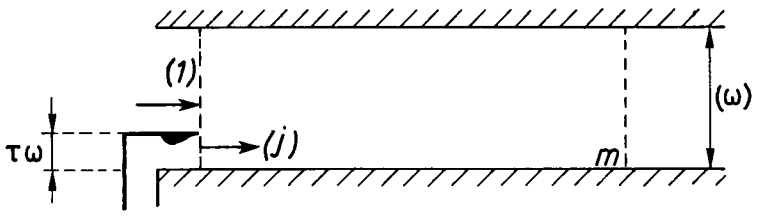

Figure A3 provides the notation:

(1) p_1 , p_{i_1} , h_{i_1} , M_1 , ρ_1 , u_1 : main flow,

(j) p_j , p_{ij} , h_{ij} , M_j , ρ_j , u_j : injector jet flow,

(m) p_m , p_{im} , ... : mixed flow,

ω : total mixing chamber area,

$\tau\omega$: jet emission area.

- Jet flow (j) will always be considered as supersonic ($M_j > 1$). But it will not be assumed a priori that the jet is adapted ($p_j \neq p_1$); this case will however be eventually retained in the applications.
- Only *mixed regimes* (M_1, $M_m < 1$) will be considered.
- The total enthalpies ($h_i = h + u^2/2$) are the same in (1), (j) and (m), thence:

$$T_{i_1} = T_{ij} = T_{im} \, . \tag{1}$$

As usual, the mass rate ratio is denoted by

$$\mu = \frac{q_{m_1}}{q_{mj}} \tag{2}$$

but the interesting parameter is really μ^{-1}, which characterizes the compressed air consumption.

Basic Equations and General Calculation Methods

They result from the conservation laws between (1) and (m).

(a) Mass Flow (q_m)

$$(q_m)_1 + (q_m)_j = (q_m)_m \, .$$

Each flow rate can be written:

$$q_m = K(\gamma, T_i)\, p_i\, \omega_c \, ,$$

ω_c being the critical area of the flow considered.

As γ and T_i are common to the three flows we may write:

$$p_{i_1}\omega_{c_1} + p_{ij}\omega_{ci} = p_{im}\omega_{cm} \cdot \tag{3}$$

If we introduce the function

$$\Sigma(M) = \frac{\omega}{\omega_c} = \frac{1}{M}\left(\frac{2}{\gamma+1} + \frac{\gamma-1}{\gamma+1}M^2\right)^{(\gamma+1)/[2(\gamma-1)]}$$

and if we note that

$$\mu^{-1} = \frac{q_{mj}}{q_{m_1}} = \frac{p_{ij}\omega_{cj}}{p_{i_1}\omega_{c_1}}$$

we find, from (3):

$$Y = \frac{p_{im}}{p_{i_1}} = (1+\mu^{-1})(1-\tau)\frac{\Sigma(M_m)}{\Sigma(M_1)} \cdot \tag{4}$$

(b) Dynalpy Conservation

The walls being parallel to the flow, their action on the movement is reduced to a friction force F. In these conditions we must have the relation

$$\omega p_m(1+\gamma M_m^2) = p_1(1+\gamma M_1^2)(1-\tau)\omega + p_j(1+\gamma M_j^2)\tau\omega - F \cdot$$

Introducing a function $\phi(M)$:

$$\phi(M) = \frac{p}{p_i}(M) \cdot \Sigma(M)(1+\gamma M^2)$$

permits us to write (5) in the form:

$$p_{im}\omega_{im}\phi(M_m) = p_{i_1}\omega_{c_1}\phi_1 + p_{ij}\omega_{cj}\phi_j - F \cdot$$

or, taking account of (3):

$$(p_{i_1}\omega_{c_1} + p_{ij}\omega_{cj})\phi_m = p_{i_1}\omega_{c_1}\phi_1 + p_{ij}\omega_{cj}\phi_j - F \cdot$$

viz., after dividing by $p_{i_1}\omega_{c_1}$ and introducing μ^{-1} :

$$\boxed{\phi(M_m) = \frac{\phi(M_1) + \mu^{-1}\phi(M_j) - \delta\phi_1}{1+\mu^{-1}}} \tag{5}$$

with:

$$\delta\phi_1 = \frac{F}{p_{i_1}\omega_{c_1}} = \frac{F\Sigma(M_1)}{p_{i_1}\omega} \cdot$$

The influence of this term will be neglected in the following calculation, as we shall include them, by convention, in the evaluation of the stagnation pressure losses throughout the circuit.

(c) Energy

Energy conservation is expressed by Equation (1).

SOLUTION:

M_1, M_j, τ, μ^{-1} are given; Equation (5), with $\delta\phi_1 = 0$, gives M_m which, carried into (4), gives the ejector compression ratio Y. Supply pressure p_{ij} remains to be determined. One has the obvious relation

$$X = \frac{p_{ij}}{p_{i_1}} = \frac{p_{ij}\omega_{cj}}{p_{i_1}\omega_{c_1}} \cdot \frac{\omega_{c_1}}{\omega_1} \cdot \frac{\omega_1}{\omega_j} \cdot \frac{\omega_j}{\omega_{ij}} = \mu^{-1}\frac{1-\tau}{\tau}\frac{\Sigma(M_j)}{\Sigma(M_1)},$$

and the last term gives X :

$$\boxed{X = \mu^{-1} \frac{1-\tau}{\tau} \frac{\Sigma_j}{\Sigma_1} .} \tag{6}$$

Particular Case of Adaptation: $p_j = \bar{p}_j = p_1$

It will be seen that this case presents a great practical interest for jet noise reduction.

The preceding equations remain valid, but we introduce the constraint

$$p_j = \bar{p}_j = p_1$$

(all quantities concerning the adapted regime will be overlined).

If we introduce the function

$$\varpi(M) = \frac{p}{p_i}(M) = \left(1 + \frac{\gamma-1}{2} M^2\right)^{-\gamma/(\gamma-1)}$$

we have

$$\bar{X} = \frac{\overline{p_{ij}}}{p_{i_1}} = \frac{\overline{p_{ij}}}{\bar{p}_j} \cdot \frac{\bar{p}_j}{p_1} \cdot \frac{p_1}{p_{i_1}} = \frac{\varpi(M_1)}{\varpi(M_j)} . \tag{6'}$$

Equation (6) then gives the relation

$$\overline{\mu^{-1}} = \frac{\bar{\tau}}{1-\bar{\tau}} \cdot \frac{\Sigma_1 \bar{\omega}_1}{\Sigma_j \bar{\omega}_j} ,$$

i.e., in developing:

$$\boxed{\overline{\mu^{-1}} = \frac{\bar{\tau}}{1-\bar{\tau}} \cdot \frac{M_j}{M_1} \sqrt{\frac{1 + \frac{\gamma-1}{2} M_j^2}{1 + \frac{\gamma-1}{2} M_1^2}} .} \tag{7}$$

There are only three independent parameters left, viz., M_1 , M_j , $\bar{\tau}$, Equation (7) giving μ^{-1} . From there, the solution is obtained as for the general case, and we finally obtain

$$\bar{X} = \frac{\overline{p_{ij}}}{p_{i_1}} , \qquad \bar{Y} = \frac{\overline{p_{im}}}{p_{i_1}} , \qquad \overline{\mu^{-1}}$$

as functions of M_1 , M_j , $\bar{\tau}$.

All these calculations are easily performed on a computer.

Simplified Formulae for Ejectors with Large Induced Flow

The formulation can be greatly simplified and the interesting properties can be emphasized when τ is small relative to unity – which is the case considered here.

$$u_m = u_1 + \delta u \qquad \frac{\delta u}{u_1} \ll 1 ,$$

$$p_m = p_1 + \delta p$$

. . . . . .

$$\omega_m = \omega_1 + \delta\omega , \qquad \text{with} \qquad \delta\omega = \tau\omega .$$

The conservation equations are then written

$$\delta(\rho u) = \delta m \,, \tag{8}$$

$$\delta(p + \rho u^2) = \delta j \,, \tag{9}$$

$$\delta h_i = 0 \,, \tag{10}$$

with

$$\left.\begin{aligned} \delta m &= \tau(\rho_j u_j - \rho_1 u_1) \,, \\ \delta j &= \tau[(p + \rho u^2)_j - (p + \rho u^2)_1] \,. \end{aligned}\right\} \tag{11}$$

A simple combination of Equations (8) and (9) gives

$$\delta p + \rho_1 u_1 \delta u = \delta j - u_1 \delta m \,. \tag{12}$$

Then, Equation (10) becomes

$$\delta\left(h + \frac{u^2}{2}\right) = T_1 \delta s + \frac{\delta p}{\rho_1} + u_1 \delta u = 0 \,, \tag{13}$$

whence, taking account of (12):

$$\frac{\delta s}{r} = -\frac{\delta j + u_1 \delta m}{r \rho_1 T_1} = -\frac{\delta j + u_1 \delta m}{p_1} \,.$$

As $T_{im} = T_{i_1}$, we may write, for the stagnation conditions:

$$\frac{\delta s}{r} = \frac{C_p}{r}\frac{\delta T_i}{T_{i_1}} - \frac{\delta p_i}{p_{i_1}} = -\frac{\delta p_i}{p_{i_1}} \,,$$

and the stagnation pressure increase due to the injector becomes:

$$\frac{\delta p_i}{p_{i_1}} = \frac{\delta j - u_1 \delta m}{p_1}$$

and, replacing j and m by their values (11):

$$\frac{1}{\tau}\frac{\delta p_i}{p_{i_1}} = \frac{p_j}{p_1}\left(1 + \gamma M_j^2 - \gamma M_j M_1 \frac{a_1}{a_j}\right) - 1 \tag{14}$$

which can be written, as a function of $X = p_{ij}/p_{i_1}$:

$$\boxed{\frac{1}{\tau}\frac{\delta p_i}{p_{i_1}} = X\frac{\bar{\omega}_j}{\bar{\omega}_1}\left[(1 + \gamma M_j^2) - \gamma M_1 M_j \sqrt{\frac{1 + \frac{\gamma - 1}{2} M_j^2}{1 + \frac{\gamma - 1}{2} M_1^2}}\right] - 1} \,. \tag{15}$$

Thus, the compression effect $\delta p_i/p_i$ is a linear function of $X = p_{ij}/p_{i_1}$, for a given M_1 and a supersonic injector of a given geometry (which fixes M_j and τ).

Figure 12 represents the function

$$D(M_1, M_j) = \frac{\bar{\omega}_j}{\bar{\omega}_1}\left[(1 + \gamma M_j^2) - \gamma M_1 M_j \sqrt{\frac{1 + \frac{\gamma - 1}{2} M_j^2}{1 + \frac{\gamma - 1}{2} M_1^2}}\right] \tag{16}$$

from which the calculation of $\delta p_i/p_i$ is immediate:

$$\frac{\delta p_i}{p_i} = \tau XD(M_1 M_j) - \tau \, .$$

At adaptation ($\overline{p_j}/p_1$), Equation (14) is simplified:

$$\frac{1}{\tau}\frac{\overline{\delta p_i}}{p_i} = \gamma M_j^2 - \gamma M_j M_1 \sqrt{\frac{1 + \frac{\gamma - 1}{2} M_j^2}{1 + \frac{\gamma - 1}{2} M_1^2}} \, .$$

Equation (7) gives

$$\bar{\tau} = \frac{\overline{\mu^{-1}} \frac{M_1 a_j}{M_j a_1}}{1 + \mu^{-1} \frac{M_1 a_j}{M_j a_1}} \, , \qquad (7')$$

and, as $\tau \ll 1$, we may as a first approximation write (14) in the form:

$$\boxed{\frac{\overline{\delta p_i}}{p_{i_1}} = \overline{\mu^{-1}} \left[\gamma M_1 M_j \sqrt{\frac{1 + \frac{\gamma - 1}{2} M_1^2}{1 + \frac{\gamma - 1}{2} M_j^2}} - \gamma M_1^2 \right]} \, , \qquad (17)$$

viz.:

$$\frac{\overline{\delta p_i}}{p_{i_1}} = \mu^{-1} E(M_1, M_j) \, .$$

$E(M_1, M_j)$, the expression between brackets in Equation (17), is represented in Figure 13. It becomes null for $M_1 = 0$ and $M_1 = M_j$ and, for a given M_j, passes through a maximum. This fundamental result shows that, for a given M_j, there is an optimal value for M_1.

For M_j values in the order of 1.5, this optimum is around $M_1 \sim 0.6$, and $\overline{E_{opt}}$ is then in the order of 0.5. As a consequence, μ^{-1} is in the order of $2\delta p_i/p_i$ for such values of M_j.

Figure 14 shows the functioning diagrams of an ejector for $M_j = 1.6$, established according to the preceding simplified equations. We traced on these diagrams an auxiliary curve showing the discrepancies between these results and those resulting from exact formulae. It can thus be verified that the simplified method is sufficient in this domain of application.

Study of Ejector Starting Conditions

The wind tunnel being at rest, we have

$$M_1 = 0 \, , \qquad p_1 = p_0 \, , \qquad \rho_1 = \rho_0 \, , \qquad a_1 = a_0 \, , \ldots \, .$$

The general formulae are then in error but Equation (14) gives directly, if we assume the injector immediately started at M_j and at outlet pressure p_j:

$$\left.\frac{\delta p_i}{p_i}\right|_0 = \tau \left[\frac{p_j}{p_0} (1 + \gamma M_j^2) - 1 \right] \, . \qquad (18)$$

In Equation (8) we may identify u_1 to zero and u_m to δu. We then find, assuming $\rho_m \neq \rho_0$:

$$\delta u_0 = \frac{\rho_j u_j \tau}{\rho_0} \, . \qquad (19)$$

If the adaptation regime is realized ($p_j = p_1 = p_0$) as soon as injector start, we find:

$$\frac{\delta p}{p_0} = \left.\frac{\overline{\delta p_i}}{p_i}\right|_0 = \gamma M_j^2 \tau \; ; \qquad \left.\frac{\delta u}{a_0}\right|_0 = \tau M_j \sqrt{1 + \frac{\gamma - 1}{2} M_j^2} \; .$$

EXAMPLE:

$$M_j = 1.6 \; ; \qquad \tau = 0.04 \; .$$

The global stagnation pressure jump realized at the instantaneous start in adaptation conditions gives:

$$\frac{\delta p}{p_0} = 0.143 \; ; \qquad \frac{\delta u}{a_0} = 0.08 \qquad (\sim 30 \text{ m/sec}) \; .$$

It has been seen that this discontinuity appears actually as two waves: a shock wave downstream and an expansion wave upstream; we then find:

- for the shock: $\delta p \sim 0.12\, p_0$; $\delta u \sim 24$ m/s ;
- for the expansion: $\delta p \sim -0.03\, p_0$; $\delta u \sim 6$ m/s .

2. ONE-DIMENSIONAL ANALYSIS OF THE STARTING PROCESS

The circuit, of length L, is supposed to be developed along the x axis, from an arbitrary section: the result is that at each instant the flow state is the same at $x = 0$ and $x = L$.

It is assumed that in every cross section (x) the flow is uniform, defined by the three variables u, p, s, considered as average values, i.e. respecting at the instant considered the conservation laws in the said cross section.

The area evolution law $\omega(x, t)$ is given in the form

$$\log \frac{\omega}{\omega_0} = \Omega(x, t) \; .$$

In certain parts of the circuit we may inject or extract a mass of fluid, or momentum, or energy. We shall call respectively $m'\omega dx$, $j'\omega dx$, $q'\omega dx$ the quantities *injected* in a continuous manner between x and $x + dx$ in the ω cross section.

In these conditions, the conservation equations can be written:

$$\begin{cases} \dfrac{\partial}{\partial t}(\rho\omega) + \dfrac{\partial}{\partial x}(\rho u \omega) = m'\omega \; , \\[2ex] \dfrac{\partial}{\partial t}(\rho u \omega) + \dfrac{\partial}{\partial x}(\rho u \omega h_i) + p\dfrac{\partial \omega}{\partial t} = p\dfrac{\partial \omega}{\partial x} + j'\omega \; , \\[2ex] \dfrac{\partial}{\partial t}\left[\rho\omega\left(e + \dfrac{u^2}{2}\right)\right] + \dfrac{\partial}{\partial x}(\rho u \omega h_i) + p\dfrac{\partial \omega}{\partial t} = q'\omega \end{cases}$$

with:

$$h_i = e + \frac{p}{\rho} + \frac{u^2}{e} \; .$$

After some calculations, these equations may also be written:

$$\begin{cases} \dfrac{dp}{\rho dt} + \dfrac{\partial u}{\partial x} = \dfrac{m'}{\rho} - \dot{\Omega} & \text{(A1)} \\[2ex] \dfrac{du}{dt} + \dfrac{1}{\rho}\dfrac{\partial p}{\partial x} = \dfrac{j' + m'u}{\rho} & \text{(A2)} \\[2ex] \dfrac{dh_i}{dt} = \dfrac{1}{\rho}\dfrac{\partial p}{\partial t} + \dfrac{q' - m'h_i}{\rho} & \text{(A3)} \end{cases}$$

with:

$$\frac{d}{dt} = \frac{\partial}{\partial t} + u\frac{\partial}{\partial x} \qquad \text{and} \qquad \dot{\Omega} = \frac{d}{dt}\log\left(\frac{\omega}{\omega_0}\right) .$$

REMARKS

- In a part of the circuit where there is no injection, we have: $m' = q' = 0$ and j' is reduced to the wall friction effect:

$$j' = -\frac{2}{D_h}\rho u^2 C_f = -f' \qquad (D_h : \text{hydraulic diameter}).$$

- In a part with boundary layer bleed, the extracted flow rate m' (<0) entrains with it an axial momentum: $j' = m'ku$, and an energy: $q' = m'h_i$ (assuming the total enthalpy is uniform in the whole boundary layer).

- In a part, of length Δx, where an obstacle imparts a drag X to the flow, we can write:

$$j' = -\frac{X}{\omega_{mean}\Delta x} = -\frac{X}{\mathcal{V}}$$

with $\mathcal{V}$ being the volume of the part of the circuit in which we assume that the drag effect diffusion takes place. To this effect is added that of the wall friction $-f'$.

- In the same manner, through a possible heat exchanger occupying a volume $\mathcal{V}$ of the circuit, we shall assume that the total heat H is continuously extracted, at the rate $q' = H/\mathcal{V}$ and that the drag X of the device appears as:

$$j' = -X/\mathcal{V} .$$

- Through the injection and mixing zone, if m_j is the injected mass flow rate through section ω_j, at velocity u_j and pressure p_j, and if we call $\mathcal{V}$ the volume of this zone, we shall have

$$m' = m/\mathcal{V} ; \qquad j' = \frac{(p_j - p + \rho_j u_j^2)\omega_j}{\mathcal{V}} = \frac{(p_j - p)\omega_j + m_j u_j}{\mathcal{V}} ;$$

in the same manner, if the total enthalpy of the injected flux is h_{ij}:

$$a' = \frac{mh_{ij}}{\mathcal{V}} ; \qquad q' = \frac{m_j h_{ij}}{\mathcal{V}} .$$

TRANSFORMATION OF EQUATIONS

Let us consider Equation (A3), and develop the left-hand side:

$$\frac{dh_i}{dt} = T\frac{ds}{dt} + \frac{1}{\rho}\frac{dp}{dt} + u\frac{du}{dt} .$$

Taking account of Equation (A2), Equation (A3) becomes:

$$\frac{ds}{dt} = \frac{q' - m'(h_i - u^2) - uj'}{\rho T} = \frac{q' + m'\left(\frac{u^2}{2} + C_p T\right) - uj'}{\rho T} . \qquad (A'3)$$

This relation permits us to eliminate $d\rho/dt$ from Equation (A1), as:

$$\frac{ds}{C_v} = \frac{dp}{p} - \gamma\frac{d\rho}{\rho} .$$

The system to be integrated is then written

$$\frac{1}{\gamma}\frac{1}{p}\frac{dp}{dt} + \frac{\partial u}{\partial x} = \frac{m'}{\rho}\cdot\frac{u^2}{2C_pT} - \frac{uj'}{\rho C_pT} + \frac{q'}{\rho C_pT} - \dot{\Omega}\,,$$

$$\frac{du}{dt} + \frac{1}{\rho}\frac{\partial p}{\partial x} = -\frac{m'u}{\rho} + \frac{j'}{\rho}\,,$$

$$\frac{ds}{dt} = \frac{m'}{\rho T}\left(\frac{u^2}{2} - C_pT\right) - \frac{uj'}{\rho T} + \frac{q'}{\rho T}\,.$$

It is interesting to introduce dimensionless values:

$$x^* = \frac{a}{L}; \qquad t^* = \frac{a_0 t}{L}; \qquad U = \frac{u}{a_0}; \qquad A = \frac{a}{a_0}; \qquad \mathcal{S} = \frac{s - s_0}{C_p}; \qquad Z = \log\frac{p}{p_0};$$

$$\rho^* = \frac{\rho}{\rho_0}; \qquad m'^* = \frac{m'L}{\rho_0 a_0}; \qquad j'^* = \frac{j'L}{\rho_0 a_0^2}; \qquad q'^* = \frac{q'L}{\rho_0 a_0^3};$$

$$M = \frac{u}{a} = \frac{U}{A}; \qquad \dot{\Omega}^* = \frac{d\Omega}{dt^*} = \frac{\partial\Omega}{\partial t^*} + U\frac{\partial\Omega}{\partial x^*}\,.$$

The system then becomes:

$$\frac{1}{\gamma}\frac{dZ}{dt^*} + \frac{\partial U}{\partial x^*} = P'\,,$$

$$\frac{dU}{dt^*} + \frac{A^2}{\gamma}\frac{\partial Z}{\partial x^*} = Q'\,,$$

$$\frac{d\mathcal{S}}{dt^*} = R'\,,$$

with:

$$P' = \frac{\gamma - 1}{\rho^*}\left[m'^*\frac{M^2}{2} - j'^*\frac{U}{A^2} + q'^*\frac{1}{A^2}\right] - \dot{\Omega}\,,$$

$$Q' = \frac{1}{\rho^*}\left[-m'^*U + j'^*\right],$$

$$R' = \frac{m'^*}{\rho^*}\left[\frac{\gamma - 1}{2}M^2 - 1\right] + \frac{\gamma - 1}{A^2}\left[\frac{a'^* - Uj'^*}{\rho^*}\right].$$

REMARK: In a part of the circuit with fixed geometry, we have

$$\dot{\Omega}^* = U\frac{d\Omega}{dx^*}\,.$$

The characteristics of system $(\mathcal{S}^*)$ are then obtained in a classical way; the equation in S is already in characteristic form. Thus it is sufficient to form with the other two the two combinations:

$$A(\mathcal{S}_1^*) \pm (\mathcal{S}_2^*)$$

and to set

$$\frac{\delta^+}{\delta t^*} = \frac{d}{dt^*} + A\frac{\partial}{\partial x^*} \qquad (\eta)$$

$$\frac{\delta^-}{\delta t^*} = \frac{d}{dt^*} - A\frac{\partial}{\partial x^*} \qquad (\xi)$$

to obtain the two characteristic equations

$$\frac{A}{\gamma}\frac{\delta^+}{\delta t^*}\cdot Z \pm \frac{\delta^+}{\delta t^*} U = AP' \pm Q' \quad \begin{cases} (\eta) \\ (\xi) \end{cases}$$

respectively associated with the acoustic wave directions

$$\binom{\eta}{\xi}\frac{d^{\pm}x}{dt^*} = U \pm A .$$

3. AUXILIARY FUNCTIONS FOR BOUNDARY LAYER LOSSES COMPUTATION

Let us consider a flow defined as abscissa x by a non-uniform velocity profile between ordinates $y = 0$ (wall) and $y = \delta$ (external part of the boundary layer). We assume that $\partial p/\partial y = 0$ and $\partial h_i/\partial y = 0$.

The discussion on losses is based on the use of auxiliary functions

$$Q(h) = \int_0^{h\delta} \frac{\rho u}{\rho_e u_e} dy \qquad \text{and} \qquad D(h) = \int_0^{h\delta} \frac{p + \rho u^2}{p + \rho_e u_e^2} dy$$

in which ρ_e, u_e are respectively the external flow data. From the equation of state and the assumptions:

$$p = C_{st} \qquad \text{and} \qquad h_i = \frac{u^2}{2} + C_p T = C_{st} ,$$

we immediately deduce

$$\frac{\rho}{\rho_e} = \frac{T}{T_e} = \left[1 + \frac{\gamma - 1}{2} M_e^2 \left(1 - \frac{u^2}{u_e^2}\right)\right] . \tag{1}$$

Let us assume that the velocity profile is given as a function of $\zeta = y/\delta$, in the classical form

$$\frac{u}{u_e} = \zeta^{1/n} \qquad (\zeta < 1) \tag{2}$$

and that

$$\frac{\gamma - 1}{2} M^2 \ll 1 .$$

We can then write at order $O[\frac{1}{2}(\gamma - 1)M_e^2]^2$

$$\int_0^{h\delta} \frac{\rho u}{\rho_e u_e} dy = \delta \int_0^h \left[1 - \frac{\gamma - 1}{2} M_e^2 + \frac{\gamma - 1}{2} M_e^2 \zeta^{2/n}\right] \zeta^{1/n} d\zeta ,$$

$$\int_0^{h\delta} \frac{\rho u^2}{\rho_e u_e^2} dy = \delta \int_0^h \left[1 - \frac{\gamma - 1}{2} M_e^2 + \frac{\gamma - 1}{2} M_e^2 \zeta^{2/n}\right] \zeta^{2/n} d\zeta .$$

The computation of losses and of boundary layer bleed was based on the use of non-uniformity functions defined by

$$Q(h) = 1 + \epsilon_q = \int_0^{h\delta} \frac{\rho u}{\rho_r u_r} \frac{dy}{\delta} ,$$

$$D(h) = 1 + \epsilon_d = \int_0^{h\delta} \frac{p + \rho u^2}{p + \rho_r u_r^2} \frac{dy}{\delta} ,$$

where $h\delta$ is the boundary layer function considered, and $\rho_r u_r$ the supposedly uniform flow for $y \geqslant \delta$.

We also assumed that, at abscissa x, we had

$$p = C_{st} \qquad \text{and} \qquad h_i = \frac{u^2}{2} + C_p T = C_{st} ;$$

we immediately deduce:

$$\frac{\rho}{\rho_e} = \frac{T}{T_e} = \left[1 + \frac{\gamma - 1}{2} \left(1 - \frac{u^2}{u_e^2} \right) M_e^2 \right]^{-1} .$$

In the applications considered here, we can always assume that

$$\frac{\gamma - 1}{2} M_e^2 \ll 1 ;$$

then, to the second order in $[(\gamma - 1)/2] M_e^2$, we have

$$\frac{\rho}{\rho_e} = 1 - \frac{\gamma - 1}{2} M_e^2 \left(1 - \frac{u^2}{u_e^2} \right)$$

if we assume that the velocity profile is in the form

$$\frac{u}{u_e} = \zeta^{1/n} , \qquad \text{with} \qquad \zeta = \frac{y}{\delta} ;$$

we then find

$$Q(h) = \frac{n}{n+1} h^{(n+1)/n} - \frac{\gamma - 1}{2} M_e^2 \left(\frac{n}{n+1} h^{(n+1)/n} - \frac{n}{n+3} h^{(n+3)/n} \right) ,$$

$$\left(1 + \frac{\rho_e u_e^2}{p} \right) D(h) = h + \frac{\rho_e u_e^2}{p} \left[\frac{n}{n+2} h^{(n+2)/n} - \frac{\gamma - 1}{2} M_e^2 \left(\frac{n}{n+2} h^{(n+2)/n} - \frac{n}{n+4} h^{(n+4)/n} \right) \right] .$$

REMARKS:

– If we consider the whole boundary layer ($h = 1$), we have

$$Q(1) = \frac{n}{n+1} - \frac{\gamma - 1}{2} M_e^2 \frac{2n}{(n+1)(n+3)} ,$$

$$\left(1 + \frac{\rho_e u_e^2}{p} \right) D(1) = 1 + \frac{\rho_e u_e^2}{p} \left(\frac{n}{n+2} - \frac{\gamma - 1}{2} M_e^2 \frac{2n}{(n+2)(n+4)} \right) .$$

– If we consider a height $H > 1$ of the flow, including the whole boundary layer, we have

$$Q(H) = Q(1) + (H - 1) ,$$

$$D(H) = D(1) + (H - 1) .$$

– If we consider a height $H > 1$ of the flow including only the part $(1 - h)$ of the boundary layer we have

$$Q(H) = Q(1) - Q(h) + H - 1 ,$$

$$D(H) = D(1) - D(h) + H - 1 .$$

Figure A4 represents the functions $Q(H)$ and $D(H)$ in the particular case where $M_e = 0.6$ for $n = 5$ and $n = 7$.

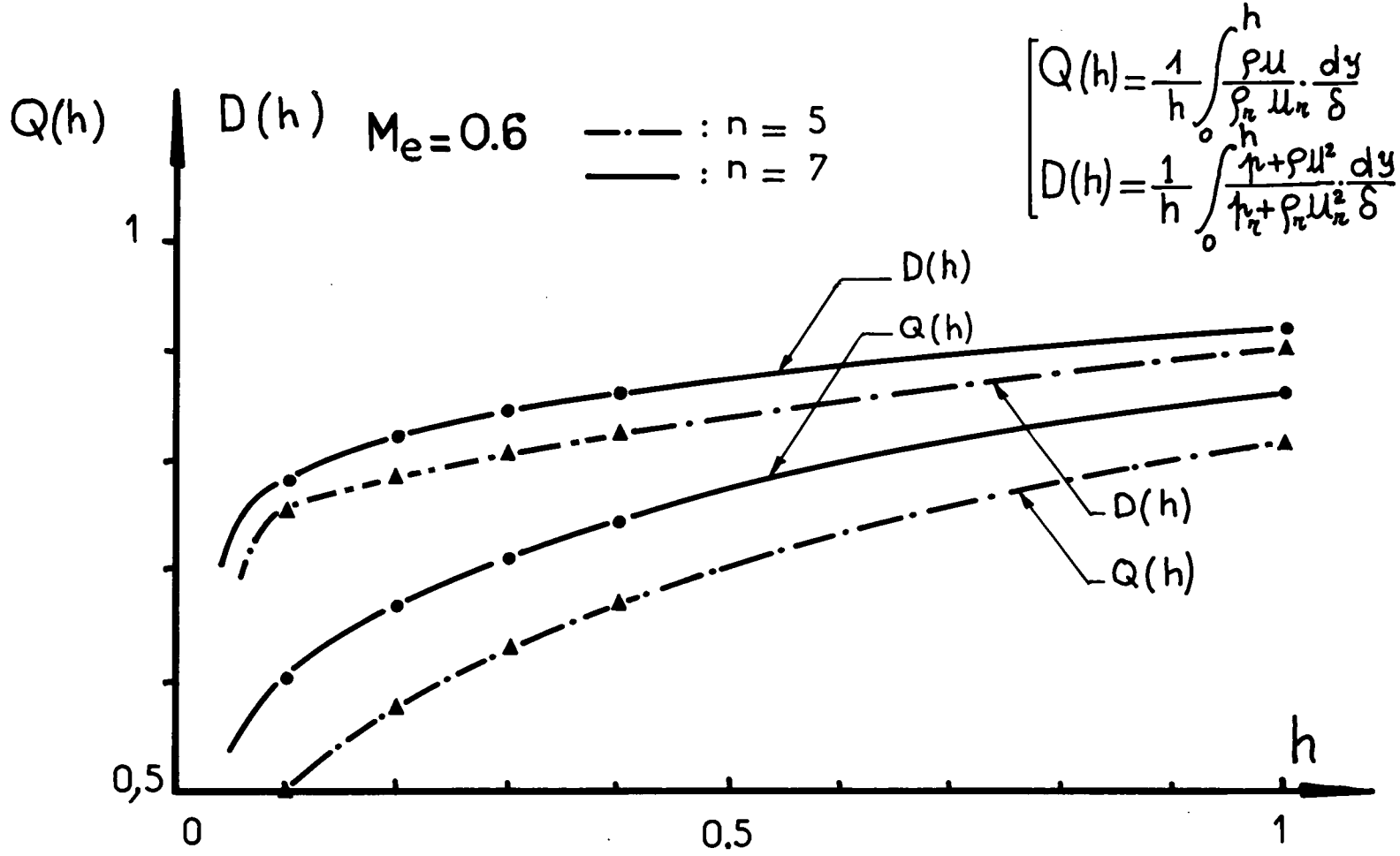

Fig.A4 DYNALPY AND MASS FLOW DEFECT IN THE TURBULENT BOUNDARY LAYER

REFERENCES

1. Roy, M. — *Tuyères, Trompes, Fusées et Projectiles.* P.S.T. Ministère de l'Air, Paris, No.203, 1947.

2. Fabri, J. et al. — *Etude Aérodynamique des Trompes Supersoniques.* Jahrb. 1953 der W.G.L. Braunschweig, pp.101-110.

3. Ginoux, J.J. (Editor) — *Supersonic Ejectors.* AGARDograph No.163, 1972.

4. Leuchter, O. — *Exemple de Calcul Numérique du Mélange Turbulent Isobare ou Non Isobare de Jets Plans Parallèles.* (To be published in Recherche Aérospatiale).

5. Holder, D.W. North, R.J. — *The 9 x 3 inch Induced Flow High Speed Wind Tunnel at NPL.* R & M No.2781, 1953.

6. Knowler, A.E. Holder, D.W. — *The Efficiency of High Speed Wind Tunnels of the Induction Type.* R & M No.2448, 1954.

7. Kogan, A. Victor, M. — *Preliminary Development of an Annular Jet Injector.* Bull. Res. Council of Israël, Vol.9c, 1961.

8. Salomon, M. et al. — *Characteristics of the 60 x 80 cm Induction Driven Close Return Transonic W.T. at the Aeronautical Research Center (Haïffa).* Israël Journ. Techn., Vol.8, No.1-2, 1970.

SOUFFLERIE A COMPRESSEUR HYDRAULIQUE

par

Maurice MENARD
Directeur de l'Institut Aérotechnique de St-Cyr
78210 - St-Cyr-L'Ecole

et

Francis CHOMETON
Maître Assistant du Conservatoire National
des Arts et Métiers
75013 - Paris

RESUME

La présente note est relative à un nouveau système moteur pour les souffleries transsoniques à grands nombres de Reynolds. Une description sommaire de l'installation permet d'en comprendre le fonctionnement. Une étude théorique du cycle thermodynamique de base donne la possibilité d'évaluer la puissance absorbée par l'installation. Pour permettre une réalisation plus économique de la soufflerie projetée, des solutions technologiques sont proposées, aussi bien pour la construction des réservoirs que pour la construction de la veine proprement dite. Un dessin d'ensemble donne une réalisation possible d'une soufflerie 5 m x 4, 20 m de section de veine.

Enfin, l'étude théorique et expérimentale de l'amorçage de la soufflerie a été effectuée sur un modèle expérimental de diamètre de veine ∅ 80 mm afin de mettre en évidence l'importance et la durée des effets instationnaires en fonction de la loi d'ouverture de la vanne de mise en fonctionnement et de la longueur de la chambre de tranquillisation.

1. INTRODUCTION

La réalisation de très grands nombres de Reynolds en soufflerie transsonique, exige des puissances motrices importantes, les différents projets en étude ont pour but de réduire la puissance absorbée, ce qui entraine une diminution du coût des essais et dans une certaine mesure le montant des investissements nécessaires à la construction.

La soufflerie continue, dont le prix de construction est trop élevé, est éliminée pour la réalisation d'installations de dimensions importantes. Seule la construction des souffleries à rafales peut être envisagée.

Parmi les différents types de souffleries à rafales les plus connus, nous retiendrons :

- Le tunnel à piston ECT
- Le tube de Ludwieg

- La soufflerie à compresseur hydraulique
- La soufflerie à induction
- La soufflerie à rafales par détente directe

Les souffleries des trois premiers types cités ci-dessus ont un système moteur "volumétrique" permettant d'obtenir des temps de rafales qui pour un nombre de Mach donné sont indépendants de la pression génératrice d'essai.

Ce système moteur est bien adapté à l'obtention de pressions génératrices élevées mais ne constitue pas l'optimum pour la réalisation de pressions génératrices modérées 2 à 3 bars par exemple.

Les souffleries à induction ou à détente directe présentent de nombreux avantages lorsqu'il s'agit d'obtenir des pressions génératrices relativement peu élevées 2 à 3 bars, mais les frais d'investissement et d'exploitation augmentent très rapidement lorsque la pression génératrice augmente.

2. DESCRIPTION DU COMPRESSEUR HYDRAULIQUE

Sous sa forme la plus schématique, le système moteur proposé se compose essentiellement de deux réservoirs R_1 et R_2 de volumes identiques disposés l'un au-dessus de l'autre (fig. 1).

Une canalisation 1 est fixée à la partie inférieure du réservoir R_2 et plonge dans le réservoir R_1.

A la partie supérieure du réservoir R_1 est connectée une canalisation 2 qui est raccordée à la soufflerie S. A l'aval de la soufflerie se trouve une vanne V puis une canalisation 3.

Sur la canalisation 3 se trouve une vanne de régulation 4 qui débouche à l'extérieur.

Une canalisation 5 fixée à la partie supérieure du réservoir R_1 permet l'introduction de gaz comprimé dans le système.

Le réservoir R_1 est rempli de liquide.

Le fonctionnement de l'installation comporte deux phases :

Phase 1
Stockage d'énergie potentielle :

On introduit par la conduite 5 un gaz comprimé au-dessus de la surface libre du liquide contenu dans le réservoir R_1, la vanne V est fermée et la vanne 4 légèrement ouverte.

Le liquide monte alors par la canalisation 1 du réservoir R_1 dans le réservoir R_2.

L'opération de remplissage du réservoir R_2 est terminée lorsque la surface libre du liquide contenu dans le réservoir R_1 atteint la partie inférieure du tube plongeur 1.

Phase 2
Transformation de l'énergie potentielle du liquide en énergie cinétique du gaz (fig. 2) :

L'admission de gaz comprimé en 5 est arrêtée.

La vanne V est progressivement ouverte pour assurer le débit gazeux nécessaire au fonctionnement de la soufflerie.

Le liquide contenu dans R_2 descend sous l'action des forces de gravité dans le réservoir R_1, la surface libre du liquide monte dans R_1 en comprimant le gaz qui passe dans la soufflerie S.

Du fait de la détente qui s'effectue dans la soufflerie, le débit volume du gaz, en aval de la tuyère subit une augmentation proportionnelle au taux de détente de la tuyère.

La vanne 4 permet à la fois d'évacuer vers l'extérieur l'excès de gaz et de maintenir constante la pression génératrice durant toute la rafale.

Pour améliorer le rendement énergétique de l'installation, la vanne 4 (fig. 3) est reliée à un réservoir R_3 dans lequel est stocké le gaz en excès.

Le fonctionnement de l'installation est le suivant :

Phase 1 :

La vanne V est fermée, la vanne 4 fermée, un compresseur C transvase en le comprimant le gaz de R_3 dans R_1, puis il transvase dans R_1 le gaz contenu dans le réservoir R_2. Ces compressions sont accompagnées d'un transfert dans le réservoir R_2 du liquide contenu dans le réservoir R_1.

Phase 2 :

L'installation utilise le cycle de fonctionnement précédemment décrit (fig. 4).

Le liquide utilisé dans le compresseur hydraulique peut être de l'eau. Pour éviter le contact entre le gaz et l'eau, on introduit dans le système un liquide de faible densité non miscible à l'eau et dont la tension de vapeur est très faible (huile par exemple). Cette huile assure une étanchéité suffisante entre l'eau et le gaz pour que la tension de vapeur de l'eau contenue dans le gaz soit très faible.

3 ETUDE THEORIQUE DU FONCTIONNEMENT DE L'INSTALLATION

3.1 Conditions initiales :

Soit Hi la dénivellation maximum exprimée en mètre entre la surface libre de l'eau du réservoir R_1 et du réservoir R_2 (fig. 5).

La pression correspondant à cette colonne d'eau est :

$$p_H = \varpi H \quad \text{pascal}$$

où ϖ = poids volumique de l'eau (9810 N/m^3).

La pression p_H exprimée en bar a pour valeur :

$$p_H = \frac{\omega H}{10^5} = \frac{9810}{10^5} \times H \cong \frac{H}{10}$$

L'état initial correspond à l'instant t après le début de la rafale, lorsque le régime peut-être considéré comme permanent.

La pression dans le réservoir R_1 est p_{1i}

La pression dans le réservoir R_2 est p_{2i}

La pression dans le réservoir R_3 est p_{3i}

La relation entre p_{1i} et p_{2i} est :

$$p_{1i} = p_{2i} + \frac{H}{10} - \Delta p \qquad (1)$$

Δp représente la perte de charge dûe à l'écoulement de l'eau dans les canalisations verticales.

3.2 Conditions finales :

Soit H_f la dénivellation minimum entre la surface libre de l'eau du réservoir R_1 et du réservoir R_2 (fig. 5). L'équation des pressions est :

$$p_{1f} = p_{2f} + \frac{H_f}{10} - \Delta p \qquad (2)$$

Comme l'on impose la constance de la pression génératrice de la soufflerie durant toute la durée de la rafale cela implique que :

$$p_{1i} = p_{1f} = p_1$$

L'air qui était contenu dans le réservoir R_1 au début de la rafale, stocké à la pression p_1 se retrouve en fin de rafale, en partie dans le réservoir R_2 à la pression p_{2_f} et en partie dans le réservoir R_3 à la pression p_{3_f}.

En fin de rafale, la vanne de régulation (4) (fig. 3) est complètement ouverte et l'on a :

$$p_{2f} = p_{3f}$$

Le rapport de pression nécessaire au fonctionnement de la soufflerie est défini par :

$$\beta = \frac{p_1}{p_{2f}} \geqslant 1{,}10 \qquad (3)$$

(on néglige les pertes par frottement de l'air le long des canalisations, la vitesse est choisie dans tout le circuit pour être comprise entre 20 et 40 m/s.).

Si l'on admet un fonctionnement isotherme de l'installation à :

$$p.\mathcal{V} = C^{te}$$

comme d'après (3) $p_{2f} < p$, ce qui entraîne : $\mathcal{V}_{2f} > \mathcal{V}_1$

Le volume de l'air après passage dans la soufflerie est plus important que le volume d'air stocké dans R_1.

Si l'on admet que les volumes des réservoirs R_1, R_2 et R_3 sont identiques, cela implique un échappement de l'air de R_1 vers R_3.

L'équation de conservation de la masse d'air contenue dans l'installation s'écrit :

$$\rho_1 \mathcal{V}_1 = \rho_{2f} \mathcal{V}_2 + \Delta M_3$$

ρ = masse volumique de l'air

$\mathcal{V}$ = volume d'un réservoir

où ΔM_3 représente la masse d'air excédentaire qui est envoyé dans R_3. Comme $\mathcal{V}_1 = \mathcal{V}_2$.

$$\Delta M_3 = \mathcal{V}_1 (\rho_1 - \rho_{2f})$$

De l'équation (2) on déduit :

$$p_1 - p_{2f} = \frac{H_f}{10} - \Delta p$$

$$p_1 \left(1 - \frac{1}{\beta}\right) = \frac{H_f}{10} - \Delta p$$

$$H_f = 10 p_1 \left(\frac{\beta - 1}{\beta}\right) + 10 \Delta p \qquad (4)$$

H_f représente la hauteur minimum entre les surfaces libres de l'eau contenue dans les réservoirs R_1 et R_2 pour que la soufflerie demeure en fonctionnement.

Si l'on écrit :

$$H_i = H_f + \Delta H = 10 p_1 \left(\frac{\beta - 1}{\beta}\right) + 10 \Delta p + \Delta H$$

où ΔH représente la variation totale des niveaux des surfaces libres dans R_1 et R_2.

L'égalité (1) peut s'écrire :

$$p_1 = p_{2i} + \frac{H_f}{10} + \frac{\Delta H}{10} - \Delta p \qquad (5)$$

De l'égalité (5) on déduit :

$$p_{2i} = p_1 - \frac{H_f}{10} - \frac{\Delta H}{10} + \Delta p \qquad (6)$$

et en remplacant H_f par sa valeur (3).

$$p_{2i} = p_1 - p_1 \left(\frac{\beta - 1}{\beta}\right) - \Delta p - \frac{\Delta H}{10} + \Delta p = \frac{p_1}{\beta} - \frac{\Delta H}{10} \qquad (7)$$

3.3 Conditions initiales (installation à l'arrêt)

La pression dans le réservoir R_1 doit être égale à p_1 et rester constante pendant la rafale. De l'égalité (1) on déduit :

$$p_{1i} = (p_{2i} - \Delta p) + \frac{H_i}{10}$$

$$p_1 = p_{2i_0} + \frac{H_i}{10} \quad \text{avec} \quad p_{2i_0} = p_{2i} - \Delta p$$

p_{2i_0} est la pression qui doit régner dans le réservoir R_2 à l'arrêt avant la rafale pour que la soufflerie puisse fonctionner normalement.

3.4 Conditions finales (installation à l'arrêt)

La vanne d'isolement de la soufflerie est fermée. L'écoulement de l'eau dans les canalisations verticales diminue progressivement de vitesse jusqu'à une valeur nulle.

Si l'on considère que le volume disponible au-dessus de la surface libre de l'eau du réservoir R_1 est petit devant les volumes des réservoirs R_1 et R_3.

De l'égalité :

$$p_{1f} = p_1 = p_{2f} + H_f - \Delta p$$

On déduit :

$$p_1 = p_{2f_o} + H_f$$

avec

$$p_{2f_o} = p_{2f} - \Delta p$$

où p_{2f_o} est la pression qui doit régner au-dessus de la surface libre de l'eau dans le réservoir R_1 lorsque la rafale est terminée et pour que la pression demeure constante dans R_1 et égale à p_1.

3.5 Définition des niveaux de pression initiale et finale dans R_3

La conservation de la masse totale de l'air contenu dans l'installation impose :

$$\rho_1 \mathcal{V}_1 = \rho_{2f} \mathcal{V}_2 + \Delta M_3 \quad \text{avec} \quad \Delta M_3 = (\rho_{3f} - \rho_{3i}) \mathcal{V}_3$$

avec l'hypothèse que les capacités des réservoirs R_1, R_2 et R_3 sont identiques on a :

$$(\rho_{3f} - \rho_{3i}) = (\rho_1 - \rho_{2f})$$

comme $p_{2f} = p_{3f}$ avec $p/\rho = C^{te}$

$$\rho_{3f} - \rho_{3i} = \rho_1 - \rho_{3f} \longrightarrow 2\rho_{3f} = \rho_{1i} - \rho_{3i}$$

ce qui entraine

$$2p_{3f} = p_1 - p_{3i}$$

$$p_{3i} = 2p_{3f} - p_1$$

comme

$$p_{3f} = p_{2f} = \frac{p_1}{\beta}$$

$$p_{3i} = p_1\left(\frac{2-\beta}{\beta}\right) \qquad (8)$$

3.6 Estimation de la puissance nécessaire au fonctionnement de l'installation

La compression isentropique de l'air nécessite une énergie par unité de masse qui est égale à :

$$\frac{E}{M} = Cp \times (\text{T finale - T initiale})$$

M = masse totale d'air à comprimer (Kg)
Cp= chaleur massique à pression constante = 1000 J/Kg°K
T = température absolue de l'air

$$\frac{E}{M} = Cp \cdot T_i \left[\left(\frac{p_i}{p_f}\right)^{\frac{\gamma-1}{\gamma}} - 1\right]$$

La puissance correspondante est égale à :

$$W_{Watt} = \frac{M}{t} \times T_i \times 1000 \left[\left(\frac{p_i}{p_f}\right)^{\frac{\gamma-1}{\gamma}} - 1\right]$$

où t est le temps pendant lequel s'effectue la compression.

3.6.1. Puissance absorbée par la compression de l'air contenu dans R_2

Pour retrouver en partant les conditions finales de pression, les conditions initiales qui permettent le fonctionnement de l'installation, il faut comprimer en la transférant dans R_1 la masse d'air M_2 contenue dans R_2.

Cette masse d'air se trouve à la pression p_{2f}, il faut l'amener au niveau de pression p_1, pendant qui s'effectuera le transfert, la pression dans R_2 passera progressivement de la pression p_{2fo} au début du transfert à la pression p_{2io} en fin de transfert.

Le rapport de compression au début du transfert sera $\frac{p_1}{p_{2fo}}$ et en fin de transfert $\frac{p_1}{p_{2i_o}}$.

La puissance moyenne correspondante sera :

$$W_{R2\,moy} = \frac{M_2}{t} \times 1000\, T_i \left[\frac{\left(\frac{p_1}{p_{2fo}}\right)^{\frac{\gamma-1}{\gamma}} + \left(\frac{p_1}{p_{2i_o}}\right)^{\frac{\gamma-1}{\gamma}}}{2} - 1\right]$$

3. 6. 2. Puissance nécessaire à la compression de l'air excédentaire contenu dans R_3

Pour aspirer la masse excédentaire d'air ΔM_3 contenue dans R_3 et la transférée en la comprimant dans R_2, la puissance nécessaire est égale à :

$$W_{R_3\,moy} = \frac{\Delta M_3}{t} \cdot 1000\,T_i \left[\frac{\left(\frac{p_1}{p_{3f}}\right)^{\frac{\gamma-1}{\gamma}} + \left(\frac{p_1}{p_{3i}}\right)^{\frac{\gamma-1}{\gamma}}}{2} - 1 \right]$$

La puissance totale nécessaire est donc : $W_t = W_{R2\,moy.} + W_{R3\,moy.}$

$$W_t = \frac{1000\,T_i}{t} \left[\left\{ M_2 \left[\frac{\left(\frac{p_1}{p_{2f_o}}\right)^{\frac{\gamma-1}{\gamma}} + \left(\frac{p_1}{p_{2i_o}}\right)^{\frac{\gamma-1}{\gamma}}}{2} - 1 \right] \right\} + \left\{ \Delta M_3 \left[\frac{\left(\frac{p_1}{p_{3f}}\right)^{\frac{\gamma-1}{\gamma}} + \left(\frac{p_1}{p_{3i}}\right)^{\frac{\gamma-1}{\gamma}}}{2} - 1 \right] \right\} \right] \quad (9)$$

Si le rendement des compresseurs est de 0, 8 :

$$W_{nec.} = \frac{W_t}{0,8}$$

3. 7 Application numérique au projet du Laws Working Group

Les grandeurs physiques caractérisant le projet du Laws Working Group. sont :

- Dimensions de veine 5 m x 4, 2 m
- Temps de rafale utile 10 secondes
- Pression génératrice de fonctionnement 6 bars
- Temps de compression 10 minutes
- Nombre de Mach maximum 1, 3
- Rapport de pression de la soufflerie β = 1, 10

Le débit volume à Mach 1 de la soufflerie est d'environ 195 $m^3/s/m^2$, ce qui implique pour un temps de fonctionnement de 11 secondes.

$$V_1 = V_2 = V_3 = 45.000\ m^3$$

Pour une vitesse de descente de l'eau dans les canalisations verticales de 7 m/s., la perte de charge est estimée à 0, 25 bar.

La variation totale de niveau dans R_1 et R_2 est arbitrairement choisie à la valeur raisonnable de :

$$\Delta H = 4,\ 5\ m$$

Pour un rapport de pression β = 1, 10 et une pression p_1 = 6 bars d'après (4) on a :

$$H_f = 10 \times 6 \left(1 - \frac{1}{1,1}\right) + 2,5 \cong 7,95\,m$$

$$H_i = H_f + \Delta H = 7,95 + 4,50 = 12,45\,m$$

d'après l'expression 6

$$p_{2i} = \frac{6}{1,1} - 0,45 \cong 5\ bar \longrightarrow p_{2i_o} = 4,75\ bar$$

$$p_{2f} = 5,45\ bar = p_{3f}$$

$$p_{2f_o} = 5,20\ bar$$

avec T_i = 288° K

$$p_{3f} = 1,225 \times 5,45 \cong 6,67\ kg/m^3$$

La pression initiale dans le réservoir R_3 donnée par (8) est égale à :

$$p_{3i} = 6\left(\frac{2-1,10}{1,10}\right) \cong 4,91 \text{ bar}$$

$$\rho_{3i} = 1,225 \times 4,91 \cong 5,98 \text{ kg/m}^3$$

Masse totale d'air contenu dans R_1

$$M_t = \rho_1 \mathcal{V}_1 = 1,225 \times 45000 = 330000 \text{ kg}$$

$$\Delta M_3 = (\rho_{3f} - \rho_{3i})\mathcal{V} = (6,67-5,98) \times 45000 \cong 31000 \text{ kg}$$

$$M_{R2} = 330000 - 31000 = 299000 \text{ kg}$$

En appliquant la formule (9) on trouve que la puissance absorbée par les compresseurs est de :

$$W_t \cong 10700 \text{ kw}$$

4 INFLUENCE DE DIFFERENTS PARAMETRES GEOMETRIQUES

4.1 Diamètre des canalisations verticales :

La pression p_{2i} qui est égale à :

$$p_{2i} = p_1\left(\frac{1}{\beta}\right) - \frac{\Delta H}{10}$$

est indépendante de la perte de charge dans les canalisations.

De même, la pression p_{3i} est indépendante de la perte de charge dans les canalisations verticales.

Par contre, la pression p_{2io}, pression qui existe dans R_2 avant la rafale et p_{2fo}, pression qui apparaît dans R_2 lorsque l'installation est arrêtée, sont fonction de cette perte de charge et l'on a :

$$p_{2io} = p_{2i} - \Delta p$$

$$p_{2fo} = p_{2f} - \Delta p$$

La puissance totale de compression est donc fonction de la vitesse de descente de l'eau dans les canalisations, en effet la formule (9) peut s'écrire :

$$W_{t_{rec.}} = \frac{1000\,T_i}{0,8t}\left\{M_2\left[\frac{\left(\frac{p_1}{\frac{p_1}{\beta}-\Delta p}\right)^{\frac{\gamma-1}{\gamma}} + \left(\frac{p_1}{p_{2i}-\Delta p}\right)^{\frac{\gamma-1}{\gamma}} - 1}{2}\right] + \Delta M_3\left[\frac{(\beta)^{\frac{\gamma-1}{\gamma}} + \left(\frac{p_1}{p_{3i}}\right)^{\frac{\gamma-1}{\gamma}} - 1}{2}\right]\right\} \qquad (10)$$

Sur la fig. 6 est représentée l'évolution de la puissance de compression en fonction de la vitesse de descente de l'eau dans les canalisations verticales pour $V_1 = V_2 = V_3 = 45.000\ m^3$.

D'autres grandeurs sont aussi fonction de la vitesse de descente de l'eau dans les canalisations verticales. En effet cette vitesse fixe aussi les hauteurs des surfaces libres de l'eau dans les réservoirs en fin de rafale, en effet :

$$H_f = 10\,p_1\left(1 - \frac{1}{\beta}\right) + 10\Delta p$$

Les courbes correspondent à différentes valeurs de p_1, β et Δp sont données fig. 7.

4.2 Influence de la variation du niveau de l'eau dans les réservoirs :

La puissance de compression exprimée par la formule (10) peut encore s'écrire avec :

$$p_{2i} = \frac{p_1}{\beta} - \frac{\Delta H}{10}$$

$$W_{t_{nec}} = \frac{1000 T_i}{0{,}8t}\left\{ M_2 \left[\frac{\left(\frac{p_1}{\frac{p_1}{\beta}-\Delta p}\right)^{\frac{\gamma-1}{\gamma}} + \left(\frac{p_1}{\frac{p_1}{\beta}-\Delta p-\frac{\Delta H}{10}}\right)^{\frac{\gamma-1}{\gamma}}}{2} - 1 \right] + \Delta M_3 \left[\frac{(\beta)^{\frac{\gamma-1}{\gamma}} + \left(\frac{p_1}{p_{3i}}\right)^{\frac{\gamma-1}{\gamma}}}{2} - 1 \right] \right\} \qquad (11)$$

La formule 11 montre que la puissance de compression est aussi fonction de la différence des niveaux de l'eau dans les réservoirs R1 et R_2.

La courbe montrant la variation de la puissance nécessaire en fonction de la différence des niveaux ΔH est donnée fig. 8.

4.3 Influence de la capacité du réservoir R_3

Lors du fonctionnement de l'installation, la conservation de la masse d'air impose :

$$\rho_1 \vartheta_1 = \rho_{2f} \vartheta_2 + \Delta M_3$$

où ΔM_3 est la variation de la masse d'air contenue dans le réservoir R_3 durant la rafale.

On a ; si $V_1 = V_2$

$$\Delta M_3 = (\rho_{3f} - \rho_{3i})\vartheta_3 = (\rho_1 - \rho_{2f})\vartheta_1$$

avec

$$\frac{p}{\rho} = C^{te} \text{ et } p_{2f} = p_{3f} \longrightarrow \rho_{2f} = \rho_{3f}$$

$$\rho_{2f}\vartheta_3 - \rho_{3i}.\vartheta_3 = \rho_1 \vartheta_1 - \rho_{2f}\vartheta_1$$

$$\rho_{3i} = \frac{\rho_{2f}(\vartheta_1 + \vartheta_3)}{\vartheta_3} - \frac{\rho_1 \vartheta_1}{\vartheta_3}$$

$$\rho_{3i} = \rho_{2f}\left(1 + \frac{\vartheta_1}{\vartheta_3}\right) - \rho_1\left(\frac{\vartheta_1}{\vartheta_3}\right) \qquad \frac{p_{3i}}{p_{2f}} = \left(1 + \frac{\vartheta_1}{\vartheta_3}\right) - \frac{p_1}{p_{2f}}\left(\frac{\vartheta_1}{\vartheta_3}\right)$$

$$\frac{\rho_{3i}}{\rho_{2f}} = \left(1 + \frac{\vartheta_1}{\vartheta_3}\right) - \frac{\rho_i}{\rho_{2f}}\left(\frac{\vartheta_1}{\vartheta_3}\right) \qquad p_{3i} = \frac{p_1}{\beta}\left(1 + \frac{\vartheta_1}{\vartheta_3}\right) - \beta\left(\frac{\vartheta_1}{\vartheta_3}\right)$$

En introduisant cette valeur de p_{3i} dans la formule (11). On montre alors que la puissance totale nécessaire à la compression de l'air est fonction du rapport des volumes.

$$W_{t_{nec}} = \frac{1000 T_i}{0{,}8t}\left\{ M_2 \left[\frac{\left(\frac{p_1}{\frac{p_1}{\beta}-\Delta p}\right)^{\frac{\gamma-1}{\gamma}} + \left(\frac{p_1}{\frac{p_1}{\beta}-\Delta p-\frac{\Delta H}{10}}\right)^{\frac{\gamma-1}{\gamma}}}{2} - 1 \right] + \Delta M_3 \left[\frac{(\beta)^{\frac{\gamma-1}{\gamma}} + \left(\frac{\beta}{\left(1+\frac{\vartheta_1}{\vartheta_3}\right)-\beta\left(\frac{\vartheta_1}{\vartheta_3}\right)}\right)^{\frac{\gamma-1}{\gamma}}}{2} - 1 \right] \right\}$$

Sur la fig. 9 est représentée l'évolution de la puissance de compression en fonction du rapport des volumes des réservoirs R_1 et R_3.

5 REGULATION DE LA PRESSION GENERATRICE DE LA SOUFFLERIE

La pression initiale dans R_2 est définie par :

$$p_{2i} = p_1 - \frac{Hf}{10} - \frac{\Delta H}{10} + \Delta p$$

La pression initiale dans R_3 est définie par :

$$p_{3i} = p_1\left(\frac{2-\beta}{\beta}\right) \quad \text{avec} \quad \vartheta_1 = \vartheta_2 = \vartheta_3$$

Le rapport de pression p_{2i}/p_{3i} est égal à :

$$\frac{p_{2i}}{p_{3i}} = \frac{p_1 - \frac{H}{10} - \frac{\Delta H}{10} + \Delta p}{p_1\left(\frac{2-\beta}{\beta}\right)}$$

et, en tenant compte de l'égalité (7)

$$\frac{p_{2i}}{p_{3i}} = \frac{p_1\left(\frac{1}{\beta}\right) - \frac{\Delta H}{10}}{p_1\left(\frac{2-\beta}{\beta}\right)} = \frac{1-\beta \cdot \frac{\Delta H}{10 p_1}}{2-\beta}$$

et finalement

$$\tau = \frac{p_{2i}}{p_{3i}} = \frac{1-\beta\,\frac{\Delta H}{10 p_1}}{2-\beta}$$

Le rapport des pressions p_{2i}/p_{3i} évoluera donc de : $\frac{1-\beta\,\frac{\Delta H}{10 p_1}}{2-\beta}$ en début de rafale à $\frac{p_{2f}}{p_{3f}} = 1$ en fin de rafale.

Sur la fig. 10 est représentée l'évolution du rapport τ pour différentes valeurs de p_1.

Remarque :

Le compresseur utilisé pour mettre l'installation complète en pression doit fonctionner avec un rapport de pression de 6 est du type compresseur à piston.

Par contre, le compresseur qui est utilisé pour le transfert de l'eau, et dont le rapport de pression max. est de 1, 4 environ peut-être du type centrifuge ou axial.

6 DESSIN DE CONSTRUCTION DE LA SOUFFLERIE

6.1 Construction en acier

Dans le but de diminuer la puissance nécessaire au transvasement de l'eau, des parois courbes sont disposées dans les réservoirs R_1 et R_2 comme le montre la fig. 5.

Ces parois courbes déterminent des cavités inférieures et supérieures qui constituent les réservoirs R_3.

Pour une même surface transversale des réservoirs, les variations des hauteurs ΔH des surfaces libres de l'eau dans les réservoirs sont plus faibles avec la solution proposée fig. 5 que pour un réservoir de section circulaire, ce qui permet d'après la courbe de la fig. 8 de réduire la puissance nécessaire au transvasement de l'eau.

Un diffuseur axi-symétrique est disposé à la partie inférieure de chaque canalisation verticale pour réduire la vitesse d'admission de l'eau dans R_1, donc les pertes de charges.

L'installation utilisant cette conception de réservoir est représentée fig. 11.

Cette installation comporte deux ensembles de 18 réservoirs, l'un disposé au niveau du sol et l'autre à environ 10 mètres au-dessus des réservoirs inférieurs.

Chaque réservoir a un diamètre de 5 mètres et une longueur de 190 mètres, la capacité totale de ces réservoirs est de 3 x 45000 m^3. Les parties supérieures des réservoirs R_1 sont reliées à deux canalisations transversales horizontales de sections évolutives. Chacune des canalisations est connectée à la chambre de tranquillisation de la soufflerie.

La soufflerie proprement dite comporte de l'amont vers l'aval :

- La chambre de tranquillisation équipée de grillages et filtre en nid d'abeilles.
- La tuyère transsonique équipée d'un col amont réglable constitué par des demi-corps fuselés se déplaçant contre les parois verticales planes et parallèles de la tuyère, dans la partie convergente de celle-ci.
- La chambre de mesure équipée de parois perforées à perméabilité longitudinale controlée. Le nombre de Mach d'essai en écoulement subsonique est réglé par un col sonique aval bidimensionnel (second col).

En aval du diffuseur subsonique se trouve une vanne plane à ouverture rapide qui permet à la fois d'assurer l'étanchéité entre les réservoirs R_1 et R_2 et de déclencher la rafale.

A l'extrémité de la soufflerie se trouve la vanne de contrôle qui assure l'écoulement de

l'air excédentaire vers R_3 et permet de maintenir la pression génératrice de la soufflerie constante durant toute la rafale.

6.2 Construction d'un réservoir unique en béton précontraint

La Société Europe Etudes a établi un projet de réservoir unique qui répond pratiquement à tous les problèmes que pose la réalisation de trois réservoirs superposés de 45.000 m^3 de capacité unitaire, par l'utilisation d'une structure en béton précontraint.

Le dessin d'un tel réservoir est représenté fig. 12. Le réservoir R_3 est situé à la partie inférieure, le réservoir R_2 à la partie supérieure, le réservoir R_1 est situé entre R_3 et R_2.

Une poutre centrale de section circulaire permet de transmettre par l'intermédiaire de voiles radiaux, les efforts qui s'exercent sur les parois extérieures du réservoir.

Le transvasement de l'eau du réservoir R_1 dans R_2 s'effectue par un canal annulaire extérieur. La vitesse de descente de l'eau durant la rafale peut être facilement abaissée à 2 m/s.

La chambre de tranquillisation de la soufflerie ainsi qu'une partie importante de la tuyère peuvent être placées entre les réservoirs R_1 et R_2, la soufflerie est alors alimentée en air par un canal annulaire. Le rapport de contraction de la veine est d'environ 6.

Le circuit de retour de la soufflerie s'effectue par deux conduites circulaires horizontales qui aboutissent à deux compartiments situés de part et d'autre de la chambre de tranquillisation. Des parois verticales permettent l'écoulement de l'air vers la partie supérieure du réservoir R_2.

Enfin, une conduite relie la vanne de réglage au réservoir R_3.

7 ETUDE THEORIQUE ET EXPERIMENTALE DE L'AMORCAGE DE LA SOUFFLERIE

7.1 But de l'étude

Une soufflerie actionnée par un compresseur hydraulique comporte à l'amont un ensemble de réservoirs situés dans deux plans horizontaux superposés. Les réservoirs situés dans le plan supérieur sont remplis d'eau, le transfert par gravité de l'eau du niveau supérieur au niveau inférieur assure la compression de l'air nécessaire au fonctionnement de la soufflerie.

En aval de la veine d'essai se trouve une vanne dont l'ouverture provoque la mise en mouvement de l'air dans la chambre d'essai.

L'ouverture plus ou moins rapide de cette vanne peut donner naissance à une onde de détente qui se propage à la vitesse du son de l'aval vers l'amont de la soufflerie.

Cette onde de détente en se réfléchissant sur les parois des réservoirs peut revenir vers l'aval puis, se réfléchissant à nouveau sur les parois aval de la soufflerie revenir vers l'amont jusqu'à amortissement complet du phénomène.

Les mouvements de ces ondes parasites peuvent entrainer des variations de pression génératrice qui nuisent au fonctionnement normal de la soufflerie.

Le but de la présente étude est de rechercher par voie théorique et expérimentale quelle est la nature des perturbations provoquées par l'ouverture de la vanne aval, d'en étudier l'amortissement et d'éventuellement rechercher des moyens propres à réduire l'intensité de ces ondes parasites. Le but des calculs, dans cette étape de l'étude, a été de préciser du point de vue de l'instationnaire l'influence des différents paramètres géométriques et physiques de l'écoulement et également de préparer le programme des essais.

7.2 Bases théoriques

L'écoulement est supposé instationnaire monodimensionnel, les sections faiblement évolutives, le fluide à propriétés physiques constantes, non visqueux et l'évolution isentropique [2] .

Dans ces conditions les équations d'évolution sont les suivantes, où ρ, p, u et A désignent respectivement la masse volumique, la pression, la vitesse et l'aire d'une section d'abscisse x, t désigne le temps :

Equation de conservation de la masse :

$$\rho_t + \rho u_x + u\rho_x + \frac{\rho u}{A}\cdot\frac{dA}{dx} = 0 \qquad (12)$$

Equation de la dynamique :

$$u_t + u u_x + \frac{1}{\rho} p_x = 0 \qquad (13)$$

Equation thermodynamique :

$$p = k\rho^{\gamma} \quad (\gamma : \text{rapport des chaleurs spécifiques}) \qquad (14)$$

Les équations (12), (13), (14) s'écrivent sous la forme ci-dessous, où a désigne la célérité locale du son, définie par $a^2 = \gamma k \rho^{\gamma-1}$

$$a u_x + \frac{2}{\gamma-1}\left(a_t + u a_x\right) + \frac{a u}{A}\cdot\frac{dA}{dx} = 0 \qquad (15)$$

$$u_t + u u_x + \frac{2a}{\gamma-1} a_x = 0 \qquad (16)$$

Le système d'équation aux dérivées partielles (15), (16) est résolu [1] par la méthode des caractéristiques : les deux directions caractéristiques sont données par :

$$\frac{dx}{dt} = u \pm a \qquad (17a)\,(17b)$$

Les équations des caractéristiques étant :

$$du \pm \frac{2}{\gamma-1} da \pm \frac{a u}{A}\cdot\frac{dA}{dx}\cdot dt = 0 \qquad (18a)\,(18b)$$

Soit f, une fonction des variables x et t, ($0 \leq t \leq T$). Nous désignerons par f_i^n l'approximation de f, à l'abscisse $x = i\Delta x$ ($i = 1, N$) et au temps $t = n.\Delta t$, ces notations étant précisées sur la figure ci-dessous, où les caractéristiques C^+ et C^- correspondent à un écoulement subsonique ($u - a < 0$).

Figure 13

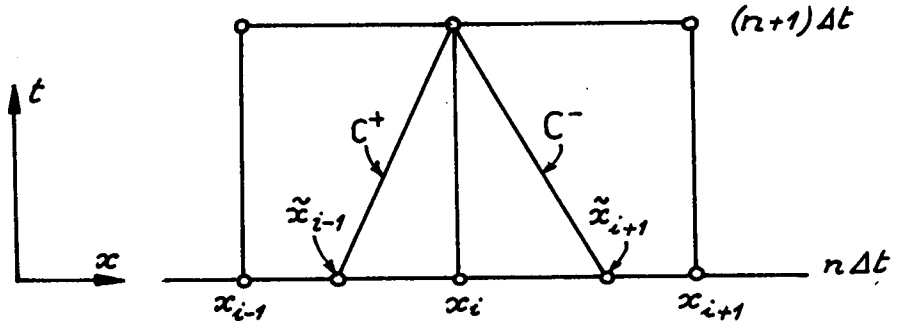

Un schéma aux différences finies du premier ordre correspondant aux deux équations (17) s'écrit :

$$(x_i - \tilde{x}_{i-1}) = \Delta t\left(u_i^n + a_i^n\right) \qquad (19a)$$

$$(x_i - \tilde{x}_{i+1}) = \Delta t\left(u_i^n - a_i^n\right) \qquad (19b)$$

Les valeurs de a et u aux abscisses $\tilde{x}_{i+1}$ et $\tilde{x}_{i-1}$ sont obtenues par interpolation linéaire à partir des valeurs en x_{i-1} , x_i et x_{i+1} :

$$\begin{cases} \tilde{a}_{i-1} = a_i^n\left[1 - \dfrac{\Delta t}{\Delta x}\left(u_i^n + a_i^n\right)\right] + a_{i-1}^n\left(u_i^n + a_i^n\right) \\ \tilde{u}_{i-1} = u_i^n\left[1 - \dfrac{\Delta t}{\Delta x}\left(u_i^n + a_i^n\right)\right] + u_{i-1}^n\left(u_i^n + a_i^n\right) \end{cases} \qquad (20a)$$

$$\begin{cases} \tilde{a}_{i+1} = a_i^n\left[1 + \dfrac{\Delta t}{\Delta x}\left(u_i^n - a_i^n\right)\right] - a_{i-1}^n\left(u_i^n - a_i^n\right) \\ \tilde{u}_{i+1} = u_i^n\left[1 + \dfrac{\Delta t}{\Delta x}\left(u_i^n - a_i^n\right)\right] - u_{i-1}^n\left(u_i^n - a_i^n\right) \end{cases} \qquad (20b)$$

Les valeurs de a et u à l'instant $t+\Delta t$ sont obtenues à partir de la résolution des équations aux différences déduites des deux équations (18), c'est-à-dire :

$$\left(u_i^{n+1} - \tilde{u}_{i-1}\right) + \frac{2}{\gamma-1}\left(a_i^{n+1} - \tilde{a}_{i-1}\right) + \frac{a_i^n u_i^n}{2A_i}\left(A_{i+1} - A_{i-1}\right)\frac{\Delta t}{\Delta x} = 0 \qquad (21a)$$

$$\left(u_i^{n+1} - \tilde{u}_{i+1}\right) - \frac{2}{\gamma-1}\left(a_i^{n+1} - \tilde{a}_{i+1}\right) - \frac{a_i^n u_i^n}{2A_i}\left(A_{i+1} - A_{i-1}\right)\frac{\Delta t}{\Delta x} = 0 \qquad (21b)$$

soit

$$a_i^{n+1} = \frac{1}{2}\left(\tilde{a}_{i+1} + \tilde{a}_{i-1}\right) + \frac{\gamma-1}{4}\left(\tilde{u}_{i-1} - \tilde{u}_{i+1}\right) - \frac{\gamma-1}{4}\cdot\frac{a_i^n u_i^n}{A_i}\left(A_{i+1} - A_{i-1}\right)\frac{\Delta t}{\Delta x}$$

$$u_i^{n+1} = \frac{1}{2}\left(\tilde{u}_{i+1} + \tilde{u}_{i-1}\right) + \frac{1}{\gamma-1}\left(\tilde{a}_{i-1} - \tilde{a}_{i+1}\right)$$

Lorsque l'écoulement est localement supersonique ($u - a > 0$), seules les relations (20 b) sont modifiées, les valeurs de $\tilde{a}_{i+1}$ et $\tilde{u}_{i+1}$ sont alors calculées à partir de a et u aux abscisses x_{i-1} et x_i

Les conditions aux limites de ce problème sont les suivantes :

- à l'abscisse x = x_1 : "entrée" de fluide à partir d'un réservoir à pression supposée constante, $p = p_i$.
- à l'abscisse x = $N.\Delta x$: "sortie" de fluide vers une enceinte à pression supposée constante p = p_e au travers d'une section évolutive en fonction du temps.

Dans les deux cas, les conditions aux limites sont traitées en faisant l'hypothèse que l'écoulement, à ces abscisses, est "quasi-stationnaire " à chaque instant.

Par exemple, à l'abscisse x = x_1, a^{n+1} et u^{n+1} sont calculés par résolution du système :

$$\left(a_i^{n+1}\right)^2 + \frac{\gamma-1}{2}\left(u_i^{n+1}\right)^2 = a_r^2$$

$$\left(u_i^{n+1} - \tilde{u}_{i+1}\right) - \frac{2}{\gamma-1}\left(a_i^{n+1} - \tilde{a}_{i+1}\right) = 0$$

Ces deux équations étant respectivement l'équation de l'énergie et l'équation (21 b) ou $dA/dx = 0$ et $a_r = \sqrt{\gamma R T_i}$, T_i étant la température du fluide dans le réservoir R_1.

8 RESULTATS DU CALCUL NUMERIQUE, COMPARAISON AVEC L'EXPERIENCE

Les résultats théoriques présentés sont relatifs aux deux configurations décrites sur la figure 14.

Dans le premier cas, la veine d'expérience est située à la distance L_1 = 2, 34 m du réservoir d'alimentation. Dans le second cas L_1 = 4, 24 m, les autres paramètres géométriques restant inchangés ainsi que la loi d'ouverture de la vanne aval.

Les conditions initiales sont dans les deux cas :

p_i = 6, 5 bars, T_i = 278°K, p_e = 1 bar

Les conditions aux limites sont :

a) p_i = cte, T_i = cte, p_e = cte

b) loi d'ouverture de la vanne de la forme :

$$\bar{A} = \left(\frac{1 - k t_o}{t_o^2}\right) t^2 + k t \qquad \text{avec :}$$

t_o = 0, 45 s. : temps d'ouverture de la vanne

$k = \left(\frac{d\bar{A}}{dt}\right)_{t=0}$ = $(0, 60)^{-1}$ sec^{-1}

et

$$\bar{A} = (A)_{t=0} / (A)_{t=t_o} \qquad (0 \leq A \leq 1)$$

Les calculs * ont été effectués pour la configuration la plus défavorable du point de vue de l'instationnaire, c'est-à-dire, L_1 et L_2 étant fixés, pour le temps t_o d'ouverture de la vanne le plus petit et en particulier pour la valeur de $k = \left(dA/dt\right)_{t=0}$ la plus grande, l'intensité de l'onde de détente au moment de l'ouverture et par conséquent la perturbation apportée à l'écoulement étant fonction de ces deux variables.

Sur les figures 15 a et 16 a sont tracées, pour les deux cas, l'évolution théorique de :

$$\frac{p-p_s}{p_i-p_s} = f(t)$$

où p désigne la pression p = p (t) dans la veine et ps la valeur stationnaire finale atteinte au même point.

Ces résultats sont à comparer aux courbes expérimentales obtenues pour les mêmes conditions physiques et géométriques, tracées figures 15 b et 16 b.

Sur les figures 17 et 18 sont tracées les évolutions théoriques de :

$$Cp = \frac{p_n - p_s}{\frac{1}{2}\rho_s V_s^2} = f(t)$$

Le coefficient Cp est négligeable ou inférieur à 1.10^{-3} à partir du temps t = 0.45 s dans le premier cas et t = 0.5 s dans le second cas.

De l'ensemble des calculs effectués on a également déduit les éléments simples suivants :

a) L'existence d'une section sonique présente l'avantage de constituer une "barrière" pour les ondes, pendant la phase instationnaire.

b) Lorsque la vitesse du son n'est pas atteinte dans cette section, les ondes provenant de l'ouverture de la vanne se réfléchissent sur l'entrée, la vanne, le convergent et le diffuseur de la soufflerie et constituent un système oscillant dont la fréquence est une fonction de L_1 et L_2.

c) Lorsque la vitesse du son est atteinte au col, la région aval n'a plus d'action sur l'écoulement dans la veine. Le système d'ondes instationnaires amorti a alors une fréquence fonction de L_1 seul de valeur

$$F \cong \frac{a_{moy}}{4 L_1}$$

où a_{moy} est la célérité du son moyenne pendant cette phase.

d) L'amortissement du phénomène instationnaire provoqué par l'ouverture de la vanne est en grande partie dû aux effets dynamiques conjugués des conditions aux limites : le convergent de la soufflerie (paroi solide), la section d'entrée de fluide au niveau du réservoir (paroi isobare) et le col sonique (non passage des ondes "à gauche" **).

9 EXPERIMENTATION

Les résultats présentés sont relatifs aux deux configurations étudiées théoriquement, l'étude portant dans ce cas sur l'influence de la loi d'ouverture de la vanne et de la longueur de la chambre de tranquillisation.

L'étude expérimentale utilise les réservoirs d'air comprimé de la soufflerie Σ4 B de l'Institut Aérotechnique de Saint-Cyr.

Les deux réservoirs R_1 et R_2 (figure 19) d'un volume unitaire de 50 m^3 sont reliés entre eux par une canalisation de ∅ 450 mm ayant la forme d'un U inversé dont les branches descendantes plongent dans les réservoirs R_1 et R_2.

Le réservoir R_2 est relié à un ensemble de réservoirs R_3 dont le volume total est de 600 m^3.

Le réservoir R_1 est relié par une canalisation de ∅ 225 mm à une tuyère convergente divergente de ∅ 80 mm.

* Calculs effectués sur UNIVAC 1108 & 1110, Faculté des Sciences d'Orsay - ORSAY (France)

** Left Travelling Wave 2

En aval de la tuyère se trouve la vanne de régulation de la soufflerie Σ4 B.

9.1 Matériel de mesure :

Il est essentiellement constitué par des capteurs de pression à circuit déposé de fréquence propre élevé (10.000 Hz) reliés à un enregistreur UV équipé de galvanomètres dont la fréquence propre est voisine de 200 Hz et par une chaîne à très court temps de réponse (capteur à quartz, amplificateur de charge et oscilloscope).

Un capteur de pression mesure la pression d'arrêt dans la conduite de ∅ 225 placée en amont de la tuyère convergente divergente, un autre capteur mesure la pression statique veine.

9.2 Programme des essais :

L'air est comprimé dans les réservoirs R_1, R_2 et R_3 jusqu'à une valeur maximum de la pression égale à 6,5 bars.

La pression dans le réservoir R_1 est ajustée de telle manière que le niveau de l'eau arrive au niveau de l'extrémité du tube en U.

Lorsque la vanne de régulation de la soufflerie Σ4 B est ouverte le transfert automatique de l'eau du réservoir R_2 dans le réservoir R_1 provoque l'écoulement de l'air dans la tuyère convergente divergente. Le nombre de Mach est maintenu constant par un col sonique fixe placé en fin de veine dans la tuyère convergente divergente.

La vanne de régulation de la soufflerie Σ4 B dont l'ouverture déclenche la rafale à une loi d'ouverture programmable par l'ordinateur CII 90-10 de la soufflerie Σ4 B.

Les positions de la vanne de régulation et les différentes pressions sont enregistrées simultanément de manière à étudier la loi de mise en régime de l'écoulement transitoire qui s'établit dans les différents éléments de la canalisation.

9.3 Résultats expérimentaux :

Configuration n° 1 (L_1 = 2,34 m) :

Sur la figure 20 est portée l'évolution en fonction du temps de la pression statique et de la pression d'arrêt dans la veine, pour un temps d'ouverture t_o = 0,50 s.

p'_i désigne la pression d'arrêt mesurée, $p'_i = p'_i(t)$

A partir du temps t = 0,25 s., l'écoulement dans la veine est parfaitement stabilisé.

Configuration n° 2 (L_1 = 4,24 m) :

Sur les figures 21 et 22 sont portées les mêmes évolutions, pour des temps d'ouverture t_o = 0,72 s. et t_o = 1,69 s. On remarquera que pour le temps d'ouverture le plus long, l'écoulement après l'amorçage de la tuyère, n'est pas perturbé.

Sur la figure 23 est représentée l'évolution de la pression statique dans la chambre de tranquillisation, à l'abscisse x = 1,40 m, pour des temps d'ouverture variables de la vanne de régulation. Ces enregistrements sont obtenus à partir de la chaîne piézoélectrique.

Oscillogramme n° 1 (temps d'ouverture t_o = 1,63 s.)

Pendant le début de l'ouverture, c'est-à-dire avant que la tuyère ne soit amorcée, $\Delta p/p$ est de l'ordre de 3.10^{-3}. Au temps t ≅ 0,9 s., $\Delta p/p$ est non décelable sur les enregistrements.

Oscillogramme n° 2 (temps d'ouverture t_o = 0,90 s.)

La première onde est plus importante que dans le cas précédent ; ($\Delta p/p \cong 6.10^{-3}$). Au temps t ≅ 0,2 s., les oscillations sont amorties puis deviennent négligeables.

Oscillogramme n° 3 (temps d'ouverture t_o = 0,75 s.)

L'onde de détente est amortie à t ≅ 0,4 s. (l'onde de compression au temps t ≅ 0,8 s. provient de la fermeture de la vanne).

10. AMORTISSEMENT DES ONDES : EXPERIENCES PRELIMINAIRES

Il a paru intéressant d'amorcer l'étude de dispositifs statiques, placés à l'entrée de la soufflerie et dont le but est de réduire le temps d'amortissement du phénomène ou même d'éviter le retour vers la veine de l'onde de détente issue de l'ouverture de la vanne ou de toute autre perturbation.

Parmi les solutions à ce problème, une, consiste à créer sur une limite, une paroi absorbante du point de vue de l'instationnaire et par exemple constituée d'éléments du type "paroi solide" et du type "paroi isobare".

Quelques résultats d'essais préliminaires sont tracés sur la figure 24 : il s'agit de l'évolution en fonction du temps de la pression en un point d'un tube à choc dont l'extrémité de la chambre basse-pression est ouverte sur l'atmosphère. Le dispositif est donc atteint par une onde de choc de faible intensité qui se réfléchit soit en détente, soit en onde de choc selon que l'extrémité est ouverte ou fermée. Les enregistrements montrent que l'on peut passer d'une manière continue de l'une à l'autre de ces conditions et donc absorber l'onde incidente.

D'autres dispositifs sont à l'étude.

REFERENCES

1 Ralston & Wilf : Mathematical methods for digital computer - John Wiley

2 The dynamics and Thermodynamics of Compressible Fluid Flow Asher H. SHAPIRO Ronald.

Fig 2

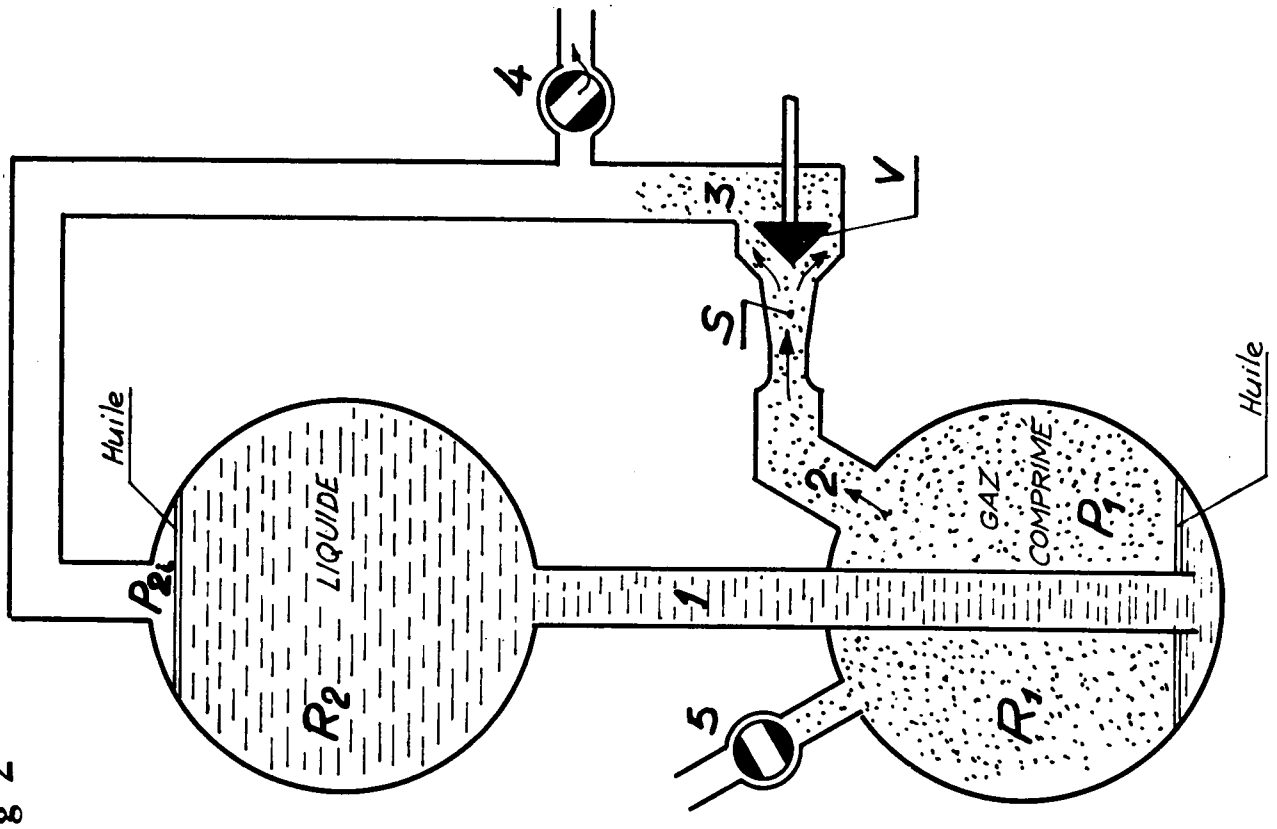

Fig 1

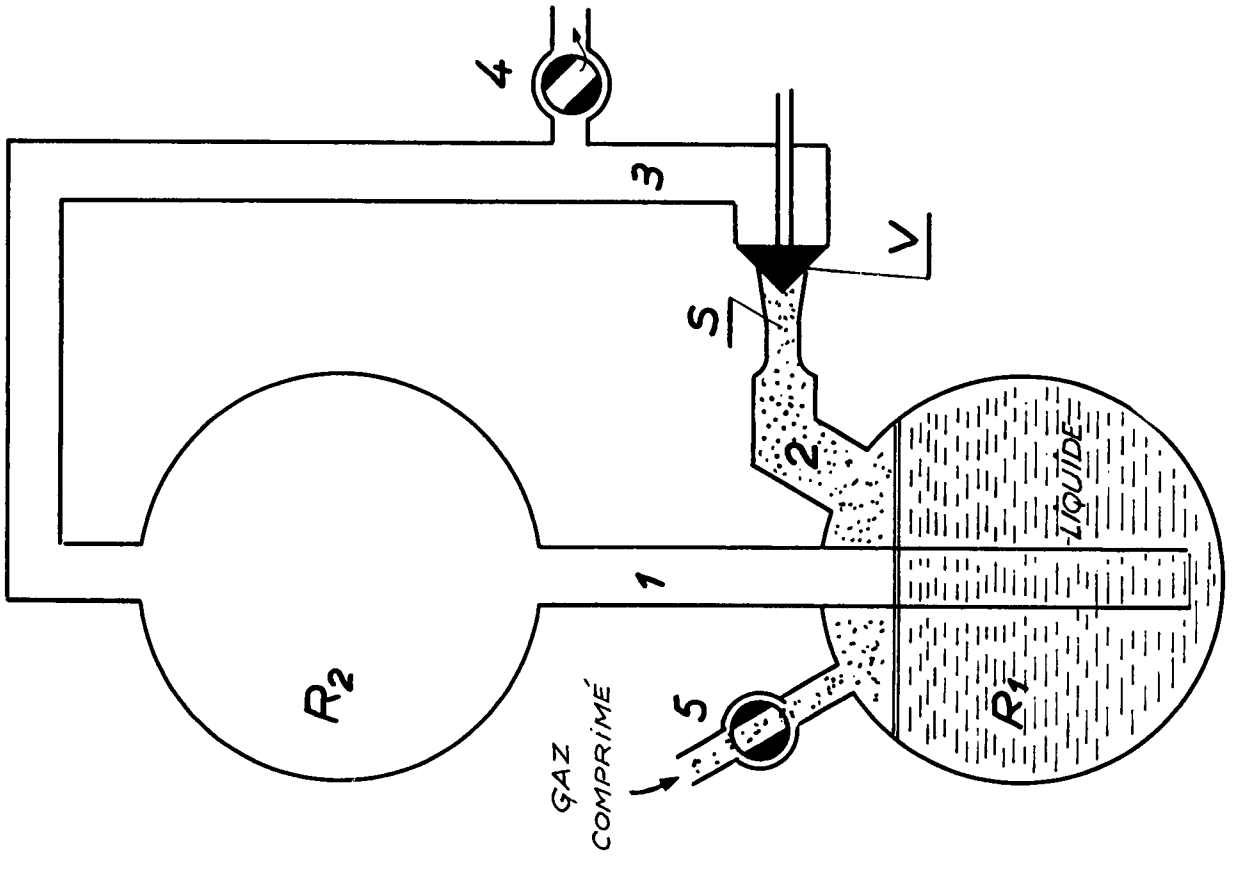

Fig 3

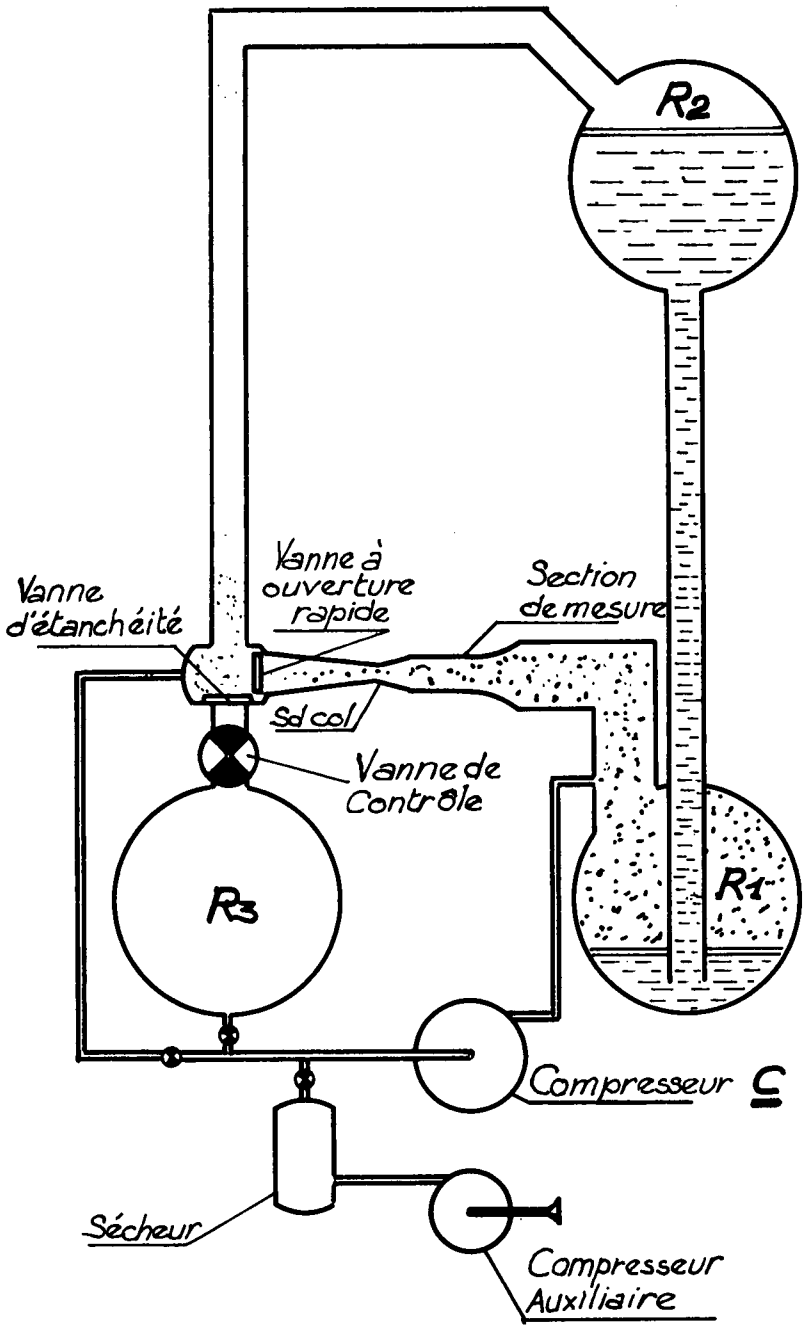

Fig 4

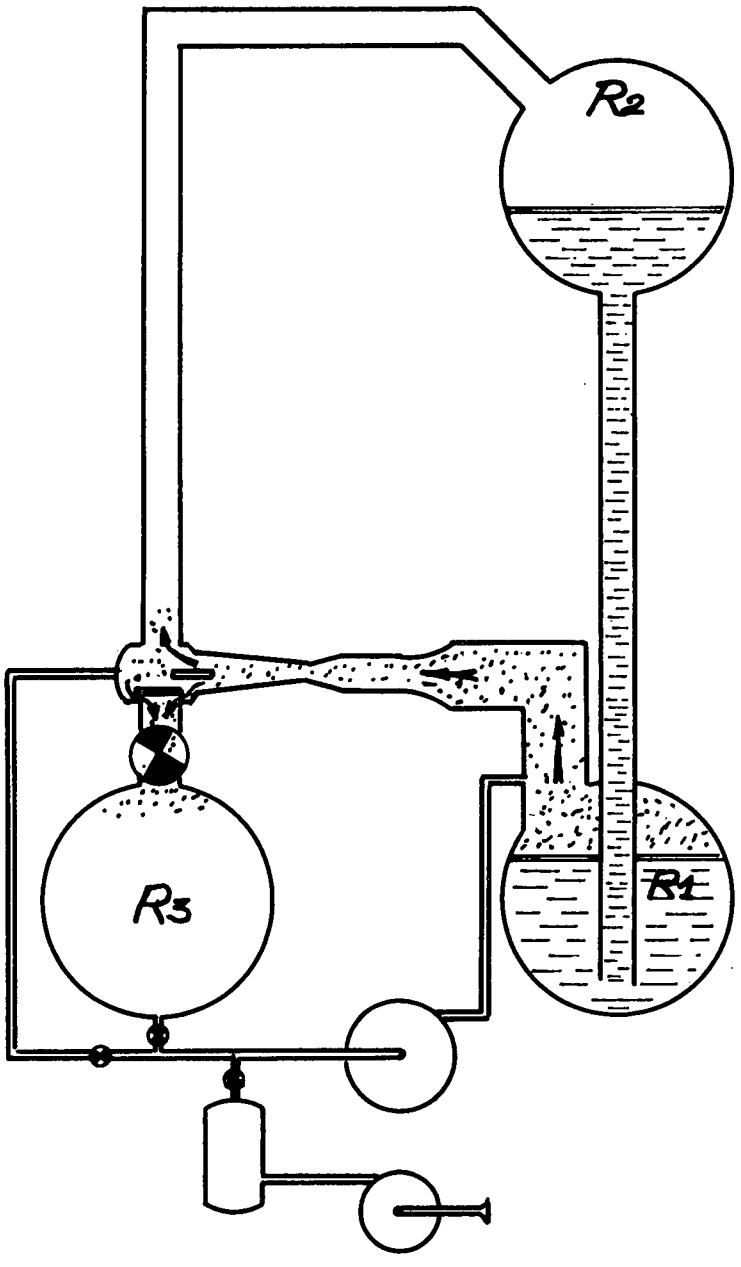

Fig 5

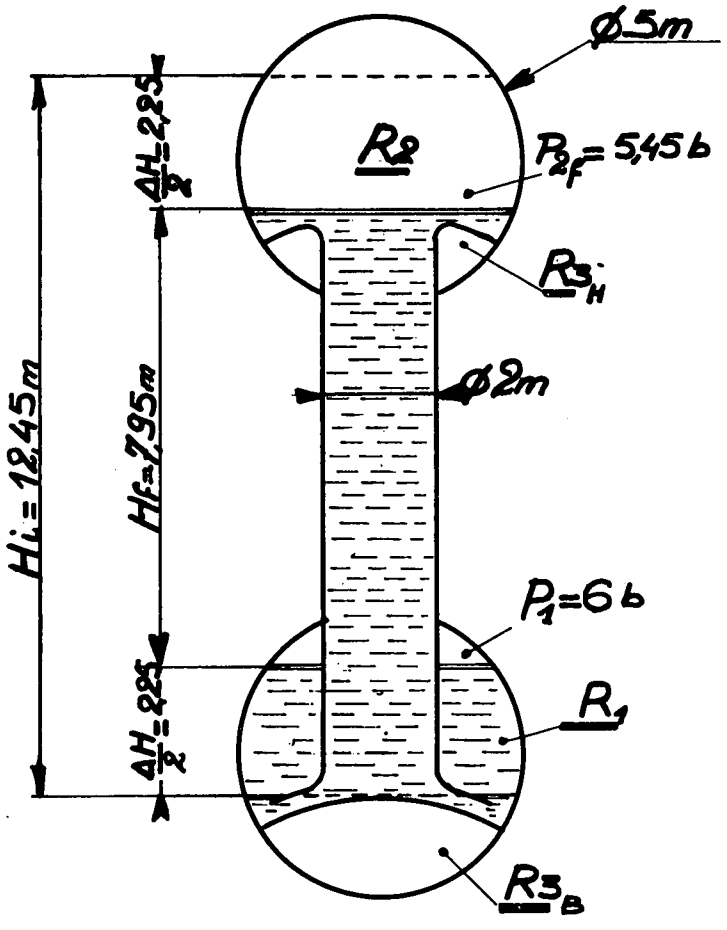

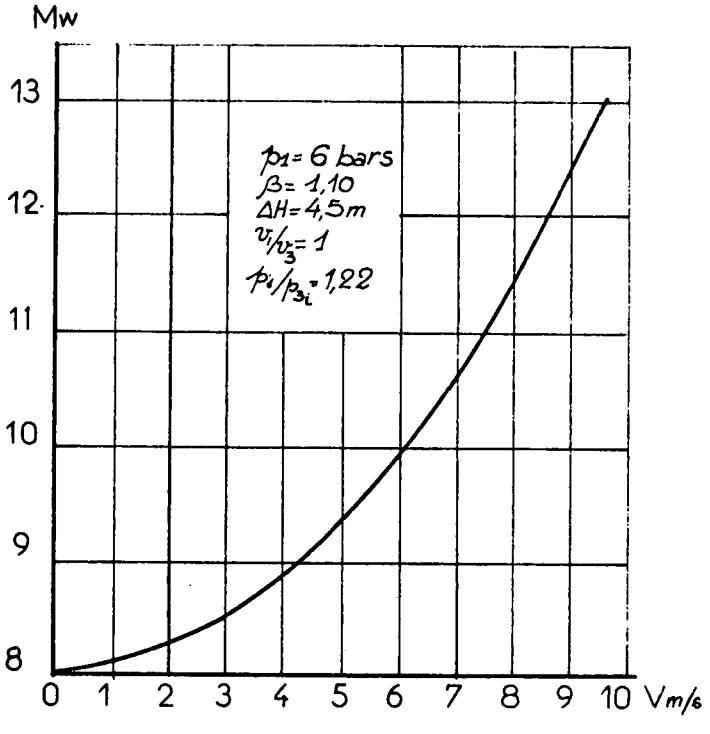

Fig6

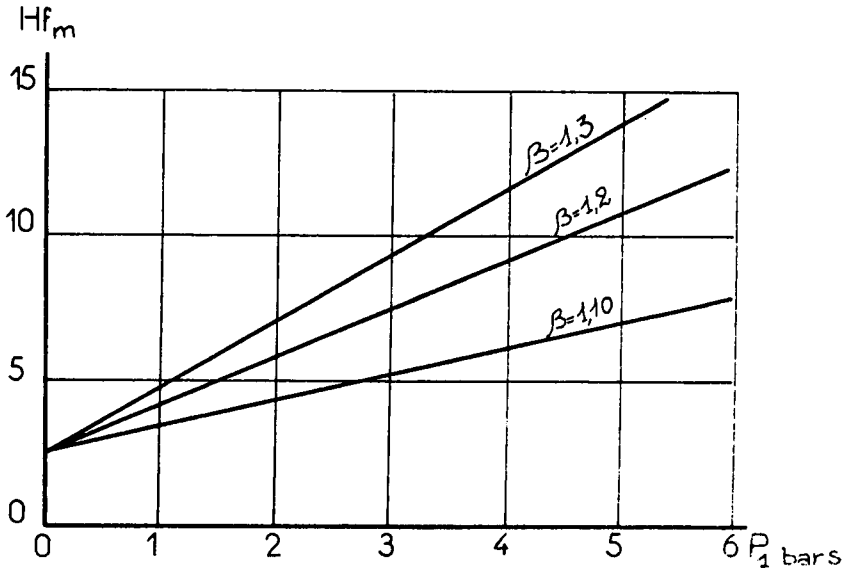

Fig 7

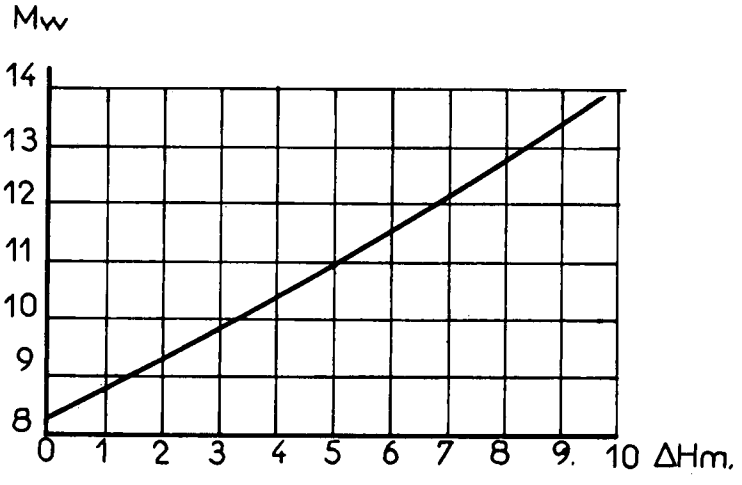

Fig 8

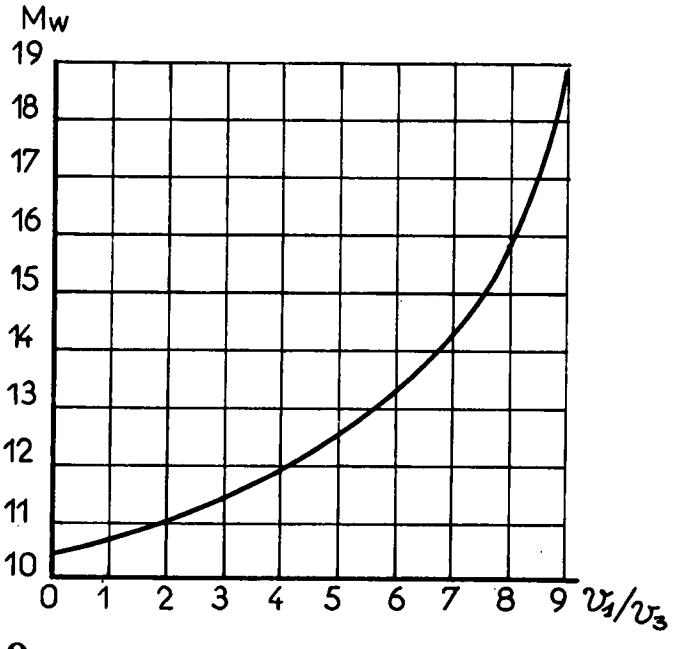

Fig 9

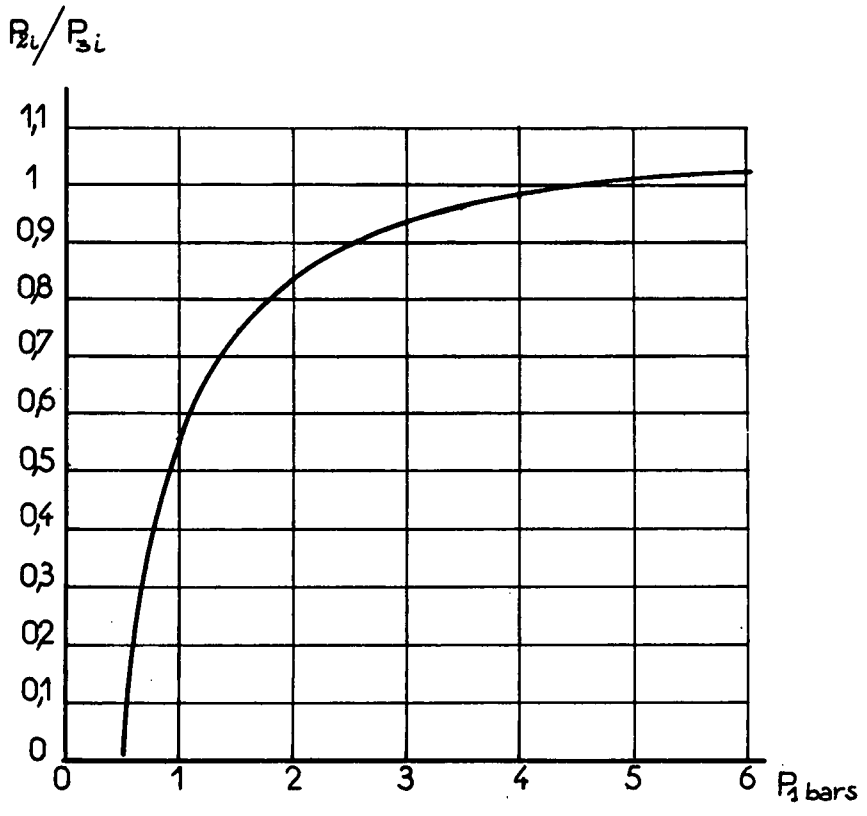

Fig 10

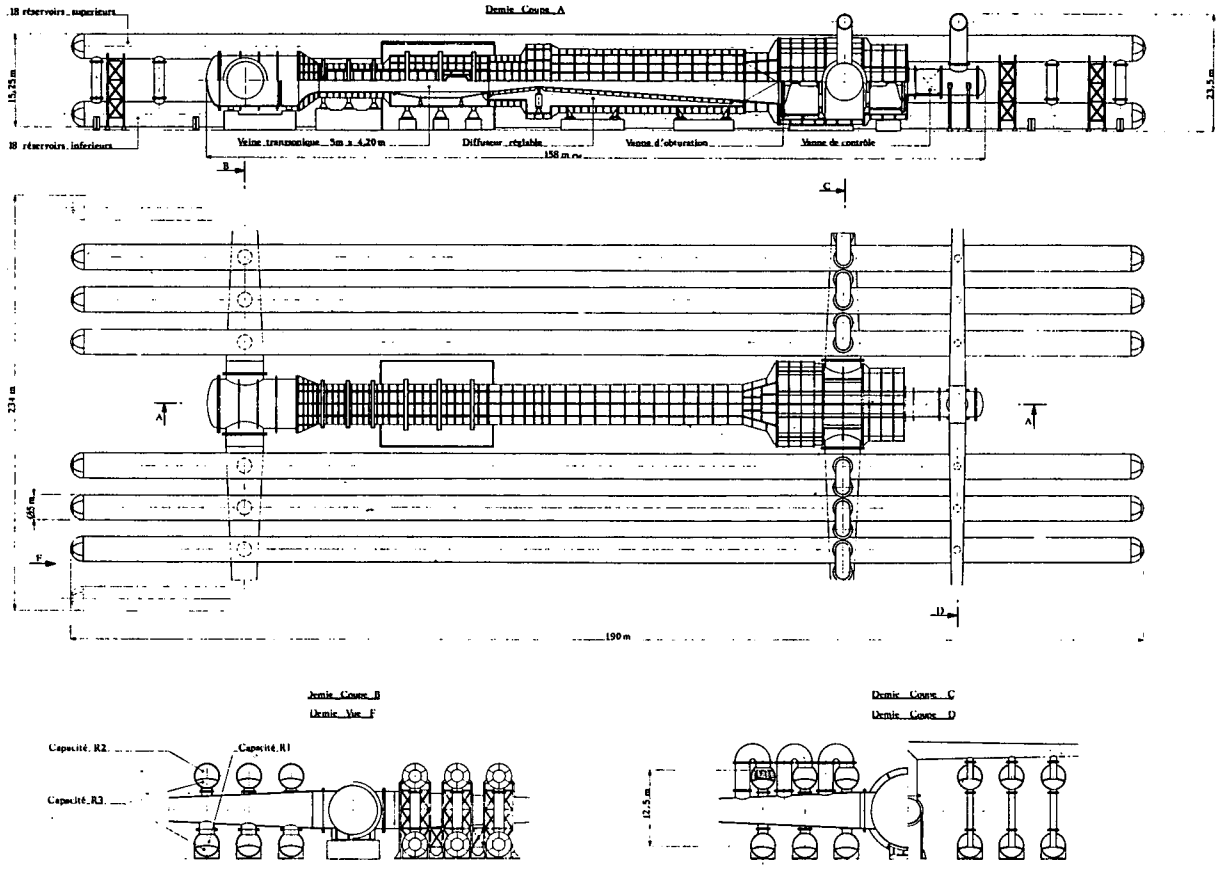

Fig 11

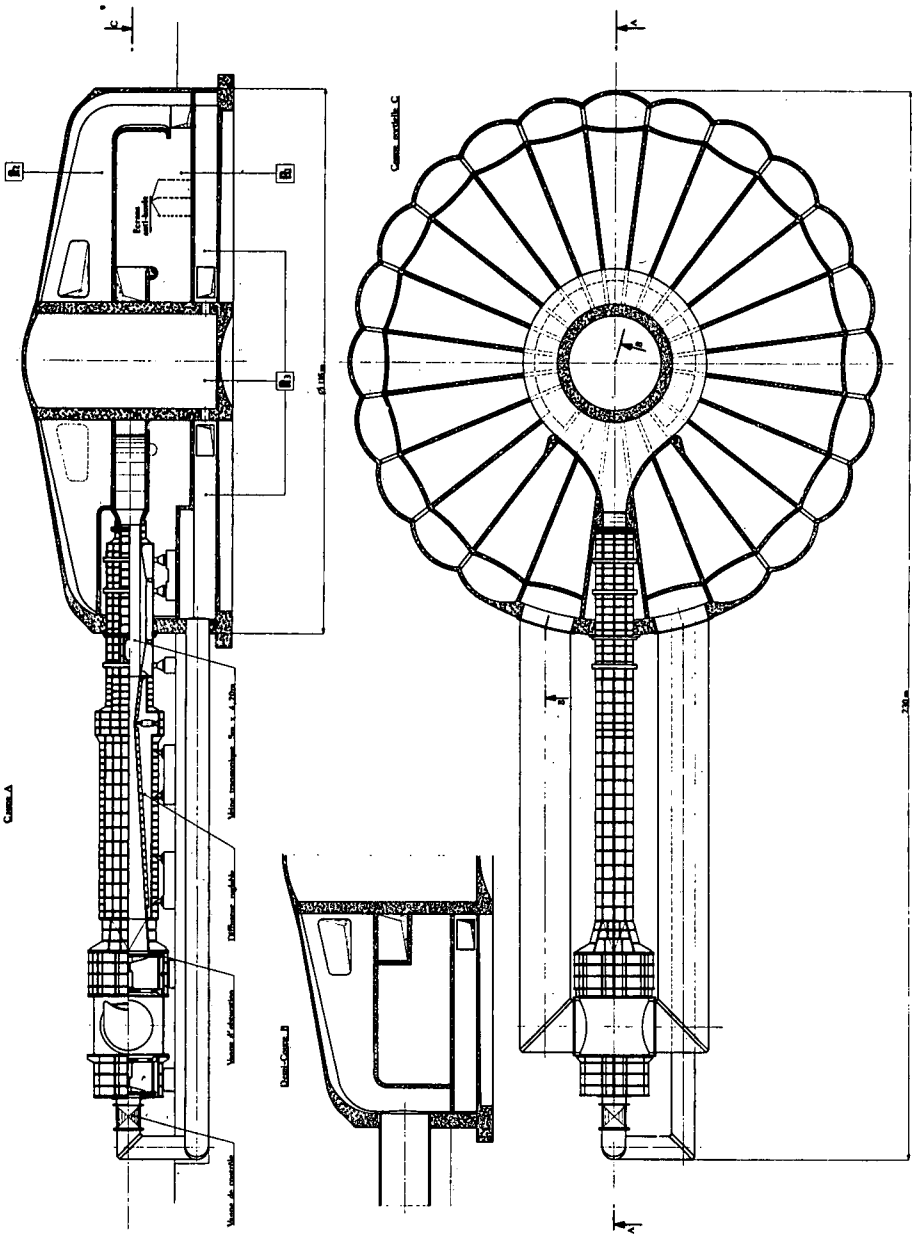

Fig 12

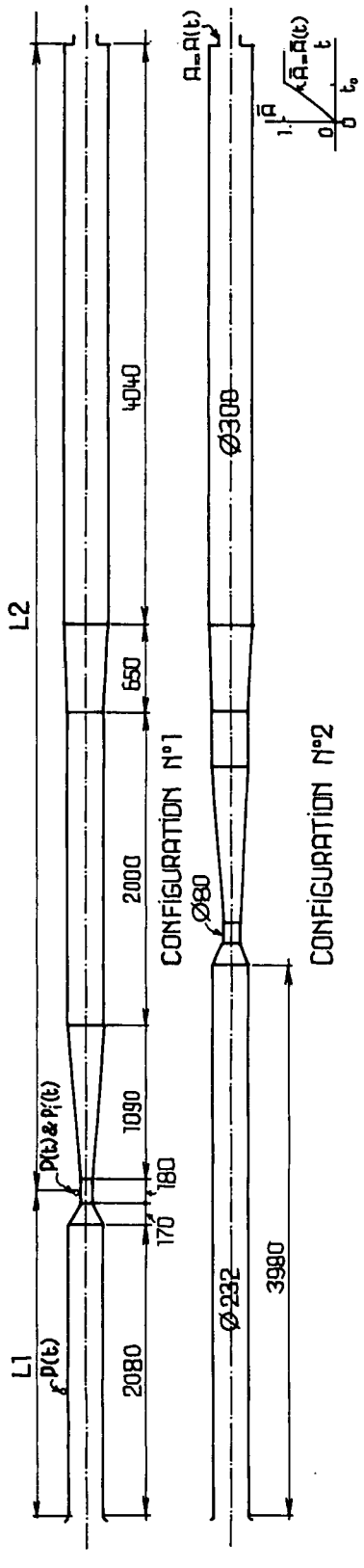

FIG. 14 MODÈLE THÉORIQUE

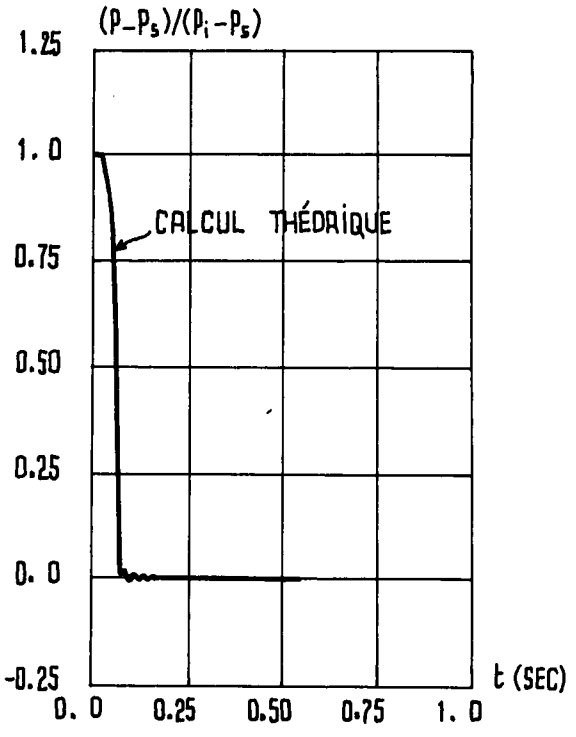

FIG. 15 a, P STATIQUE VEINE

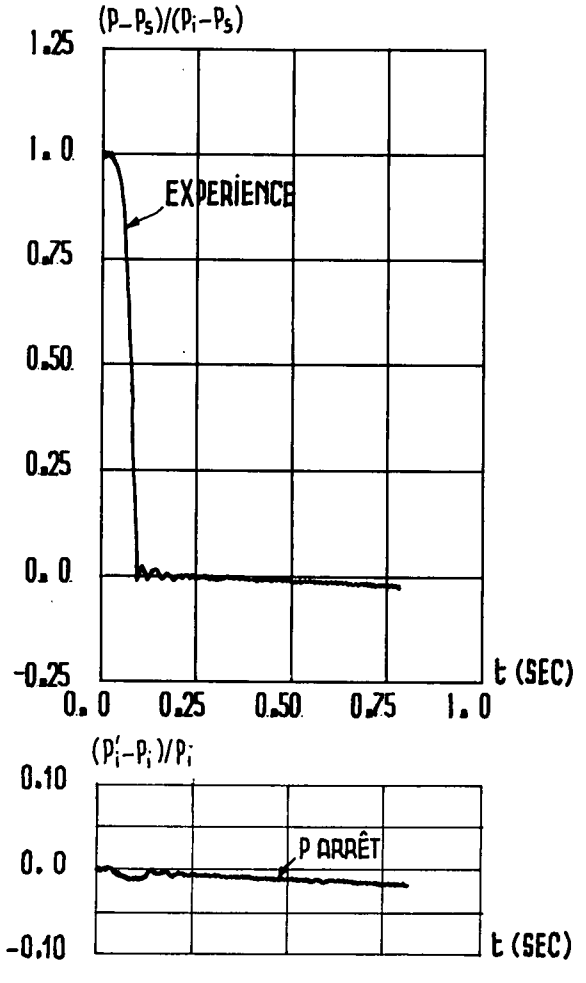

FIG. 15 b . EXPERIENCE

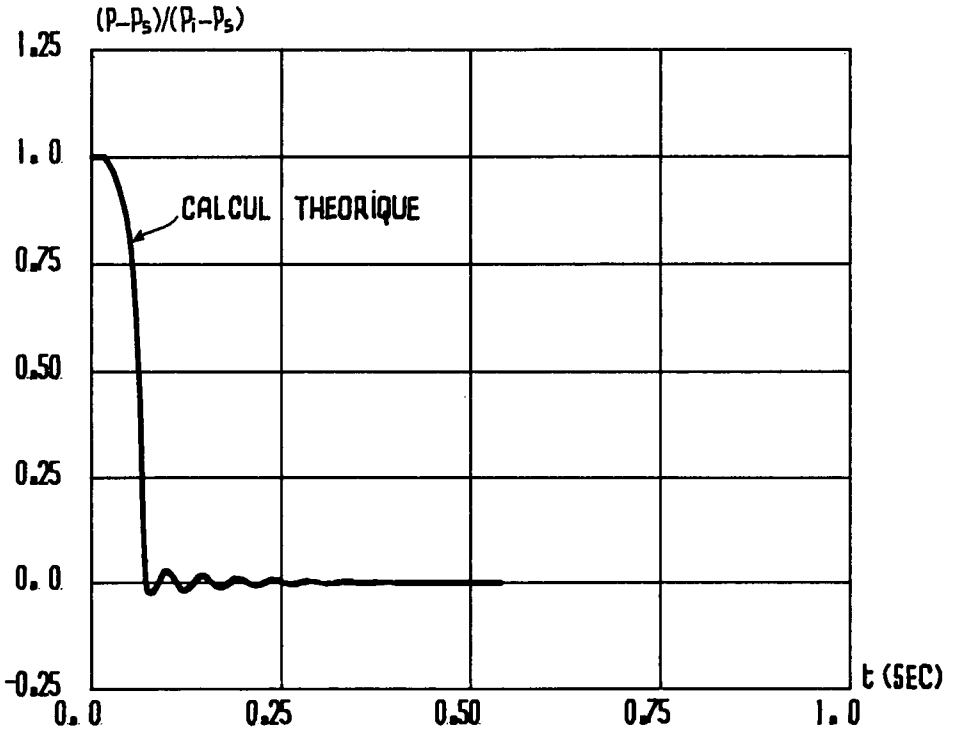

FIG. 16 a, P STATIQUE VEINE,

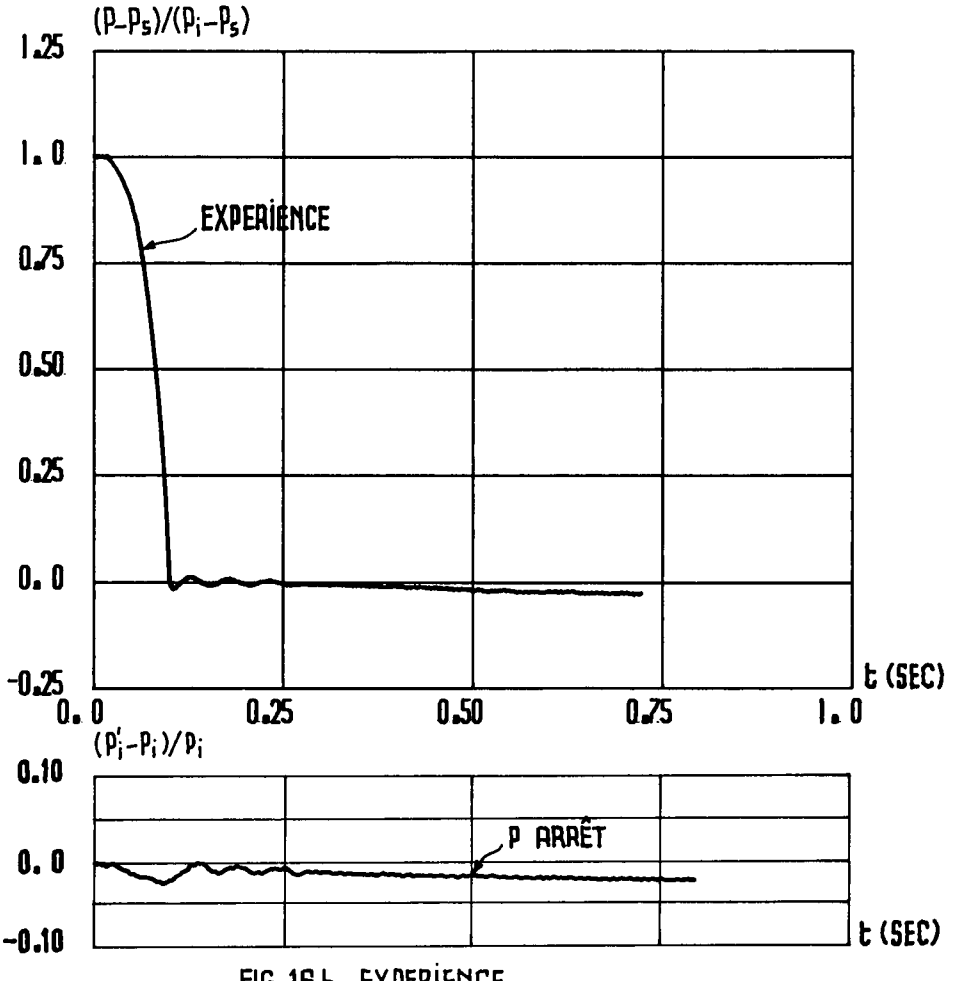

FIG. 16 b, EXPERIENCE.

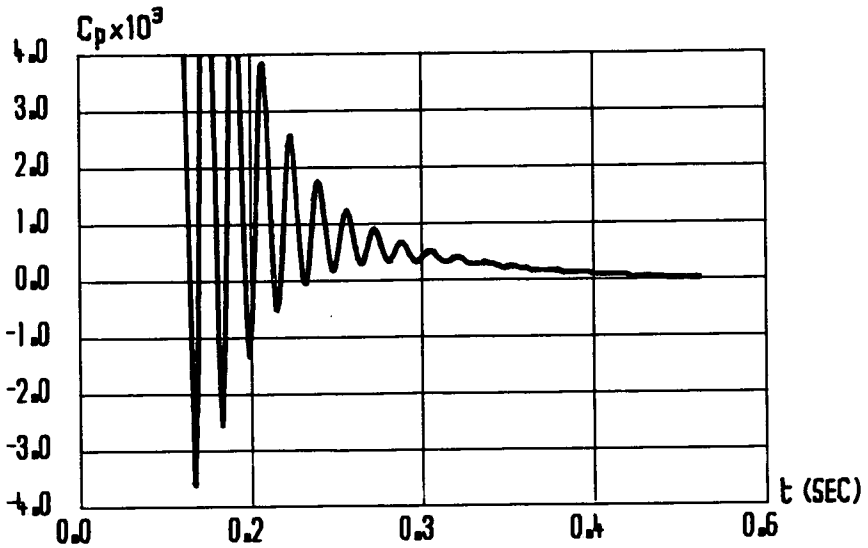

FIG. 17, C_p VEINE (CAS 1)

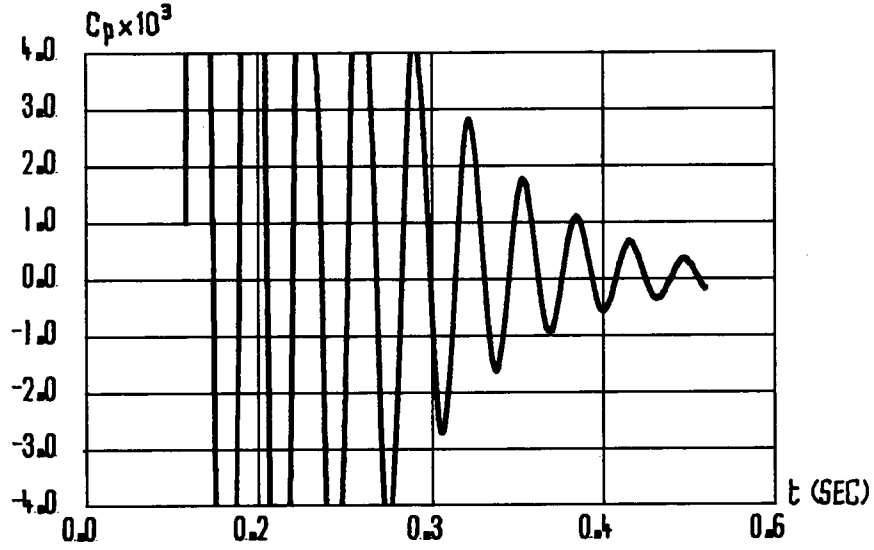

FIG. 18, C_p VEINE (CAS 2)

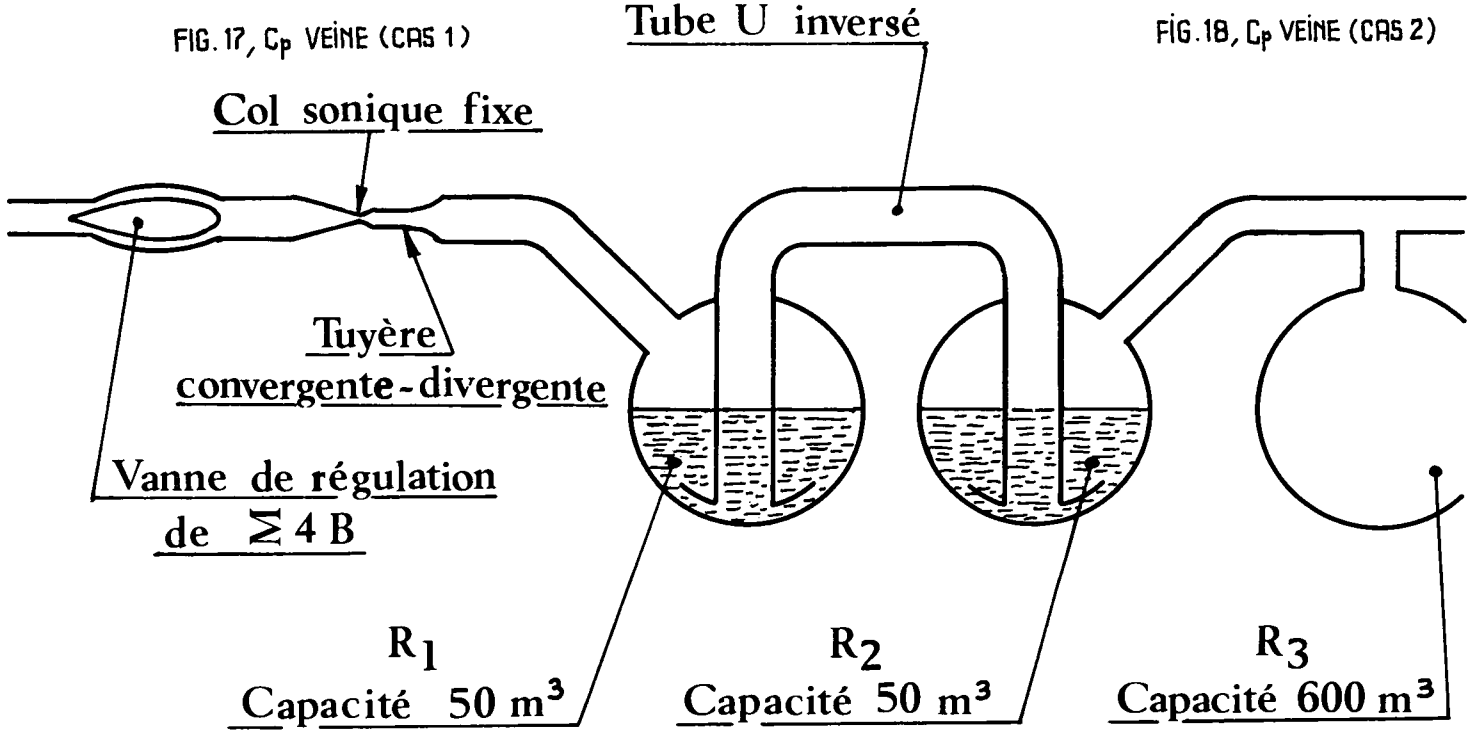

FIG. 19, MODÈLE EXPÉRIMENTAL

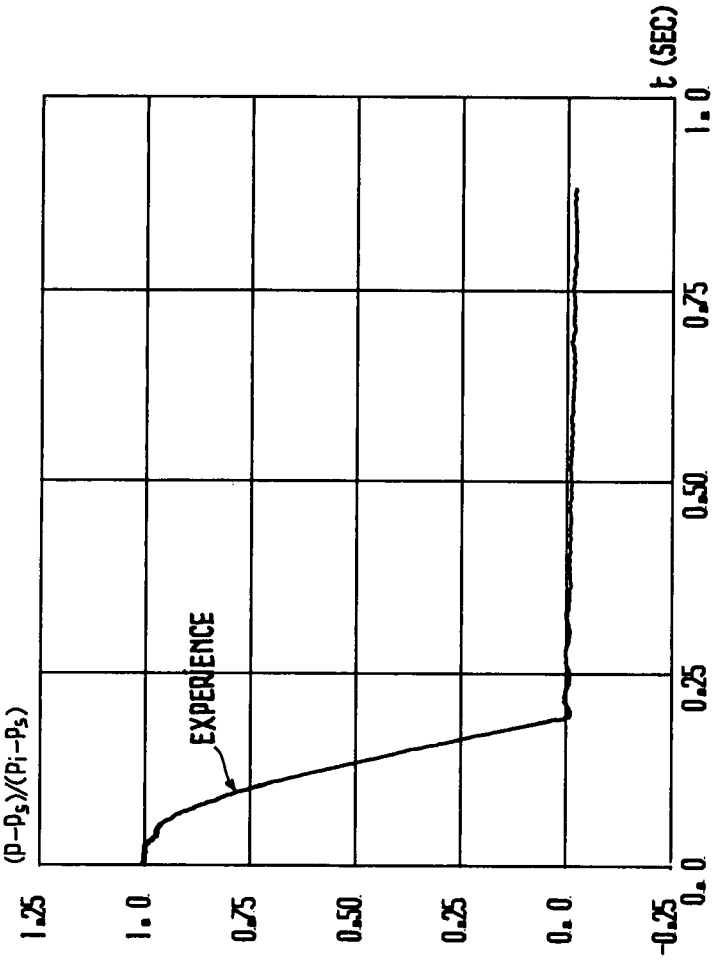

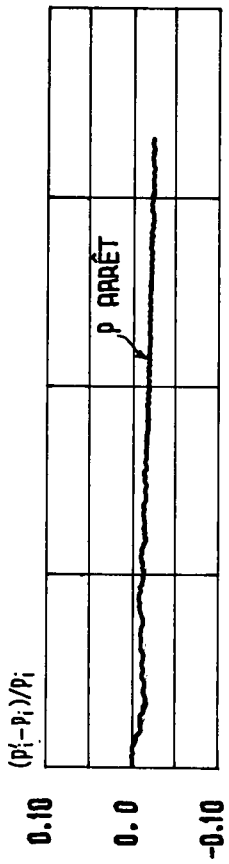

FIG.21 EXP. CAS 2
(t_o = 0,72 S)

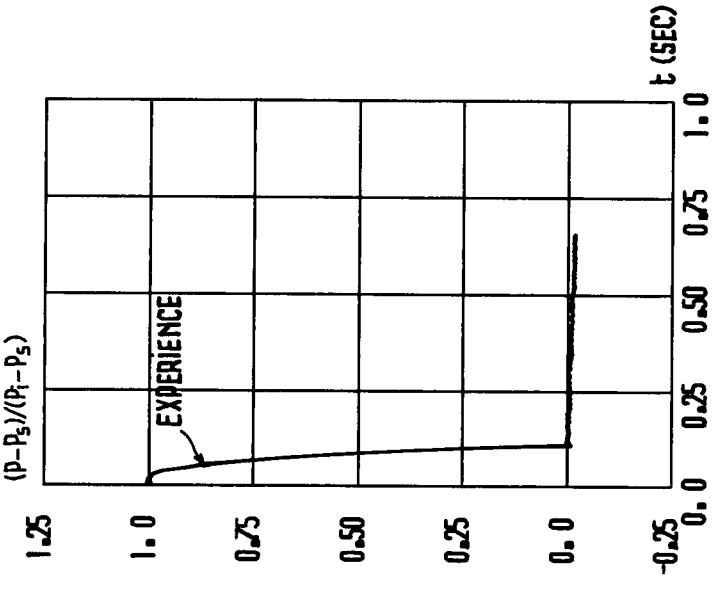

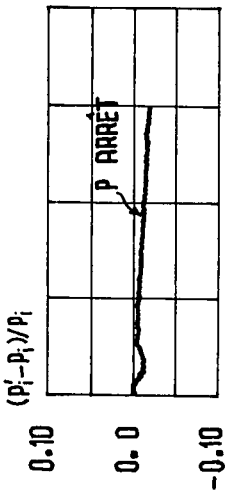

FIG.20 EXP. CAS 1.
(t_o=0,50 S)

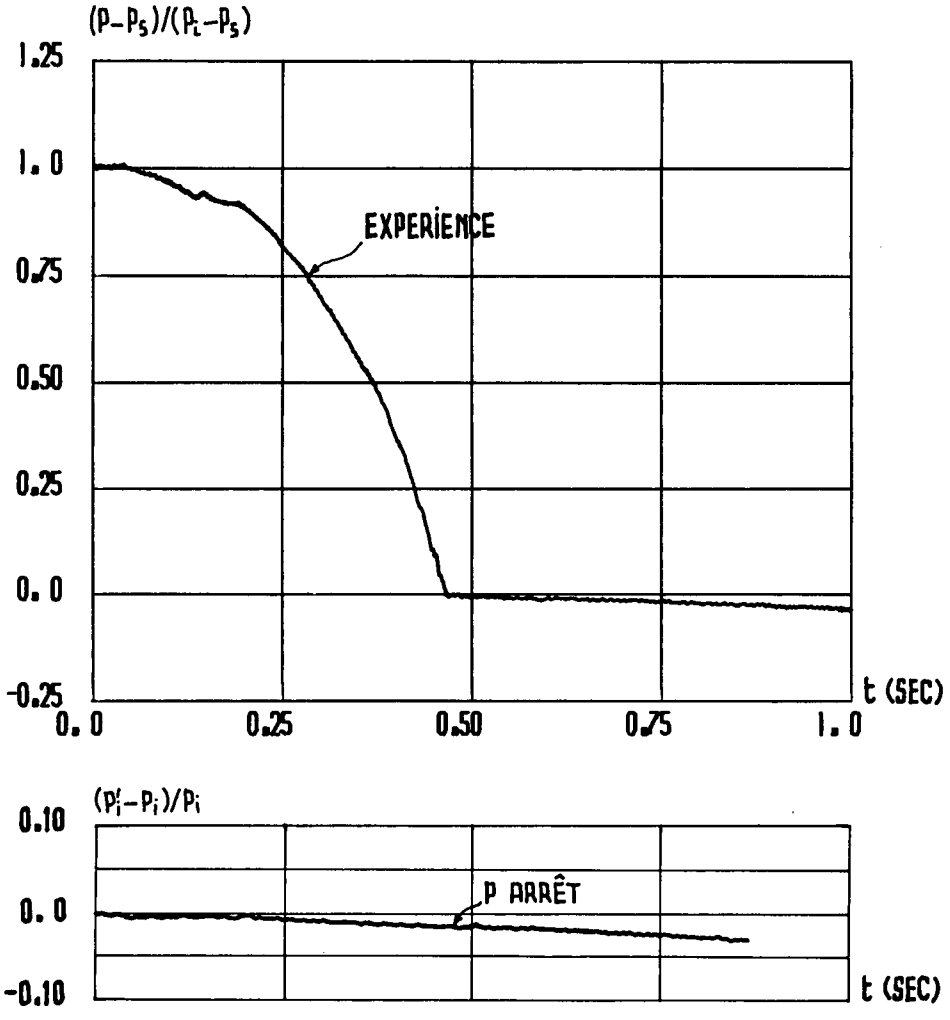

FIG.22, EXP.CAS 2 (t_o= 1,69 S)

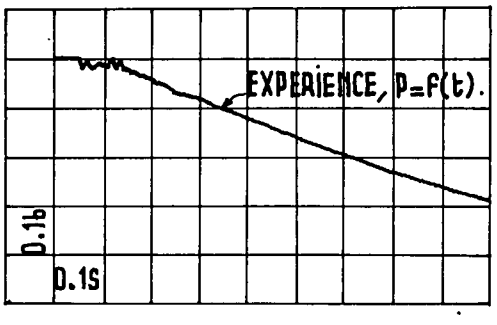

_1., t_o= 1,63 S

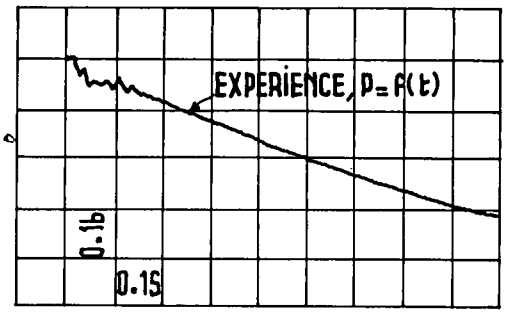

_2., t_o= 0,90 S

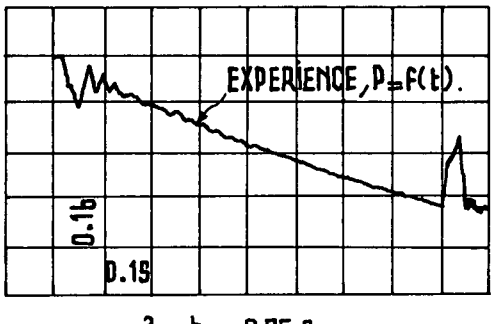

_3., t_o= 0,75 S

FIG.23, P CHAMBRE DE TRANQUILLISATION, t_o VARIABLE.

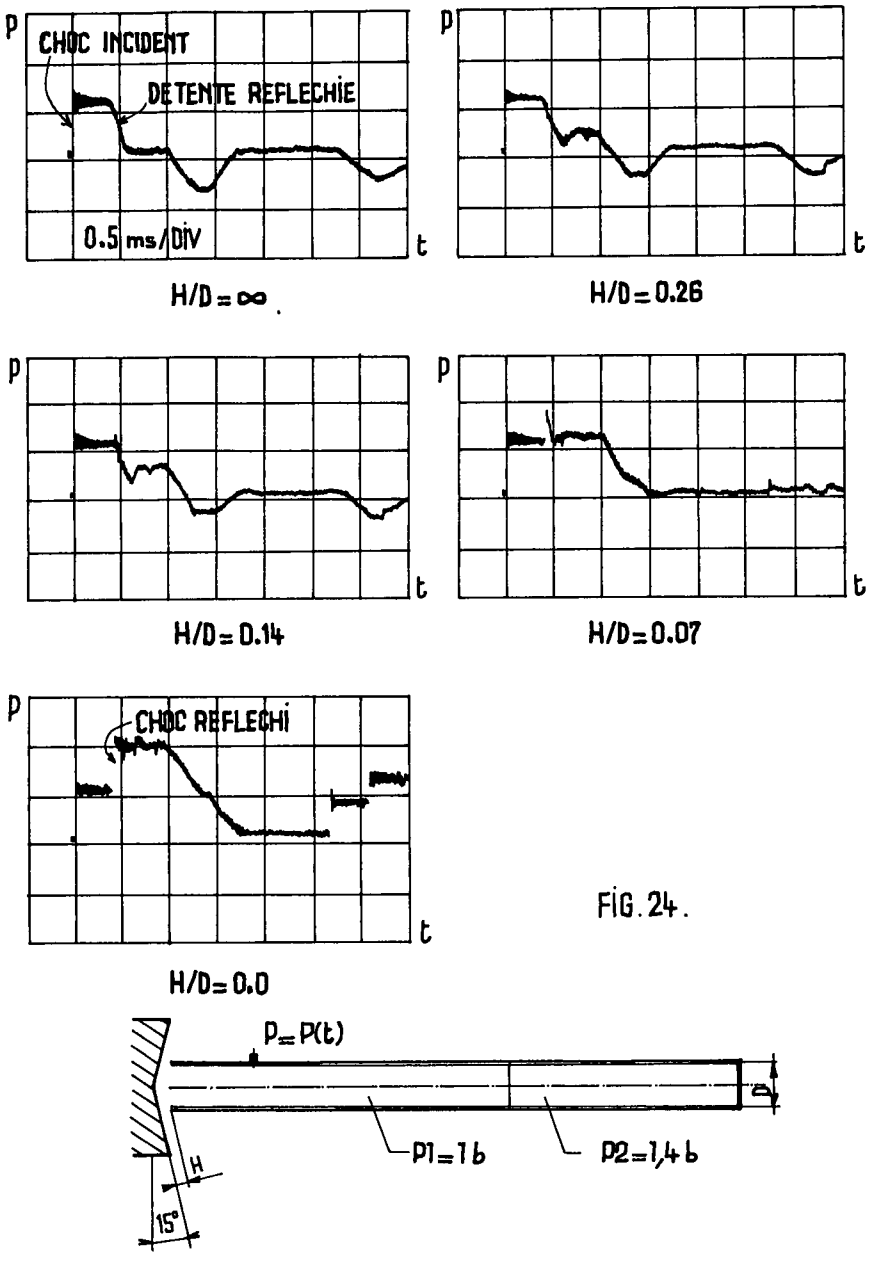

FIG. 24.

FACILITIES FOR AERODYNAMIC TESTING AT HYPERSONIC SPEEDS

by

F.Jaarsma and W.B. de Wolf
National Aerospace Laboratory, NIR
Amsterdam, the Netherlands

SUMMARY

An assessment is made of the usefulness and potential of existing European hypersonic facilities, on the basis of the planned U.S. space shuttle project and a hypothetical hypersonic transport aircraft. With respect to aerodynamic testing of space shuttle type of vehicles it is pointed out that a significant gap exists between $M = 10$ and $M = 15$.

At low-hypersonic Mach numbers the facilities in Europe will generally meet the minimum requirements for testing hypersonic transport models. European capabilities appear to be rather similar to those in the U.S. hypersonic wind tunnels, though the U.S. capabilities will be increased considerably in the near future.

It is further concluded that European facilities fall short in their performance of what is required, in the field of propulsion (including supersonic combustion tests) and also of hardware testing.

1. INTRODUCTION

This LaWs paper will be mainly concerned with the requirements for aerodynamic and propulsion testing in wind tunnel facilities for developmental work in the hypersonic speed regime i.e. on vehicles flying at Mach numbers greater than about 5. Two types of vehicles are of current interest, namely the space shuttle and the hypersonic transport aircraft (H.S.T.).

The space shuttle is to enter the development phase by mid 1972. Outside the U.S. European participation in the project has been considered (Ref. 1) but is not very likely at the moment of writing (Ref.2). The system under development will be propelled by rocket engines. In order to make regular space launches more economical, however, an airbreathing propulsion has to be used. It is generally expected that such a system will be developed after the rocket system under current development. This line of thought may eventually lead to the hypersonic transport system at the end of this century yielding less sonic boom problems at cruise as compared with the SST.

Advanced hypersonic missiles, either rocket or (sc)ramjet propelled are also to come, though little is known of the requirements.

The chances that Europe may participate with the U.S. in the development of one of these projects in the next few years are probably small. On the other hand much work of a more exploratory or fundamental nature, such as described for instance in References 3 and 4 respectively, has to be done before the development phase of a ramjet/scramjet propelled hypersonic transport can be initiated. In this field the present wind tunnel facilities in Europe with only limited performance, compared with full scale requirements are certainly of great value.

Before the development of a HST can be started the economic feasibility of the system has to be demonstrated. The payload being only a small percentage of the total weight, the aerodynamic, propulsive and structural characteristics should be known with a high degree of accuracy (Ref. 3). To accomplish this, facilities must be available where aerodynamic testing at high enough Reynolds numbers is possible and where engine-airframe integration can be studied with representative intake and exhaust jet simulation, to mention just one aerodynamic problem. Also high performance long duration facilities are needed for hardware testing of the propulsion system and of the structure of the vehicle which will be subjected to severe aerodynamic heating.

In the next discussion on hypersonic facilities the requirements will be centered on the requirements for the development work on the space shuttle and the hypersonic transport taking two typical examples.* Hence a judgement can be made on the work that can be done in the European facilities that is of fundamental and of practical interest, and in which areas of research and development European hypersonic facilities show shortcomings.

---

* In a recent article (Ref.84) military hypersonic cruise aircraft are foreseen in the late 1980's which would open a new corridor for weapons delivery. With speeds of Mach 5 – 12 at over 100,000 ft altitude it would have performances of a missile and flexibility and recallibility of an aircraft. The requirements will be comparable with those of the HST.

In the past, several European facilities have been used for military project development (i.e. tactical and ballistic missiles). This type of activities will undoubtedly remain in the future but the merits will not be discussed in the present paper, due to lack of detailed information. It can be remarked however that for such applications the usefulness and potential of present European facilities are quite satisfactory.

Typical trajectories for the various types of hypersonic vehicles are found in the altitude-velocity diagram of Figure 1, which is a compilation of data found in the literature.

1.1 Basic studies

Before being able to write down realistic specifications for hypersonic vehicles such as semi-ballistic entry vehicles (Gemini, Apollo), lifting entry vehicles (Space shuttle) and the hypersonic transport, many basic questions have to be answered first. As far as the fluid dynamic aspect is concerned, information is needed on topics such as boundary layer transition (location and occurrence), radiative heat transfer during re-entry, fuel injection in a scramjet engine, and ablation heat shield properties, mentioning only a few arbitrary examples.

Not only in the United States, which is the only Western nation that has developed manned hypersonic vehicles such as the Apollo, the X-15 and presently the space shuttle, but also in Europe a rather extensive hypersonic research program exists. An inventory of the European research and facilities can be found in References 5–7. This inventory is the result of the initiative to create Eurohyp, a more or less informal body to bring people together working in the same field, to disseminate information on the hypersonic work in Europe and to create a better co-operation. A summary of the activities of Eurohyp since 1968 can be found in the introduction of Reference 5.

It is concluded from the survey that a significant amount of work is being done in Europe and much of it will be applicable to the design of the real hypersonic vehicles that will be discussed in the subsequent sections.

1.2 The space shuttle

The proposed U.S. space shuttle will be a two-stage system, consisting of unmanned wingless solid propellant recoverable boosters and a manned orbiter. The orbiter will be a delta winged lifting vehicle with a length of 33.6 m and a span of 22.6 m. The wing load during re-entry is estimated to be somewhere between 200 and 250 kg/m^2. The landing weight will be about 75 tons. Orbiter propulsion is by three liquid rocket engines. The maximum acceleration during launch or re-entry is limited to 3 g (Ref. 1, 8 and 9). Stage separation will occur at about Mach 7 at an altitude of about 60 km.

Experimental studies in Europe have been largely devoted to lifting bodies with lift/drag ratios higher than the present U.S. design. Quite a lot of work has been done in Germany (Ref. 4, 10) not only at hypersonic speeds but also in the transonic and subsonic speed regime. In the U.K. high L/D configurations have been studied by the RAE. A good discussion on this subject may be found in Reference 11.

For the proposed U.S. space shuttle, a cross range of 1100 naut. miles (Ref. 1) will correspond with a hypersonic lift/drag ratio L/D = 1.3 (Ref. 11). The aerodynamic coefficients of such a vehicle are considered to be represented accurately enough for the calculation of the flight trajectories by the data from Reference 12.

These data give

α (deg)	C_L –	L/D –	C_N –	C_X –	*Condition*
25	0.3	1.3	0.37	0.08	Maximum L/D
55	0.7	0.6	1.36	0.10	Maximum C_L

For a wing loading W/S = 200 kg/m^2 three equilibrium re-entry glide trajectories have been calculated, defined as re-entry with constant L/D and bank angle ϕ (Ref. 13) and zero vertical acceleration. The pull-out phase which occurs at a flight altitude of about 80 km is not considered. Also viscous effects which affect the L/D ratio at high altitude have not been considered, following Reference 13. The following three conditions have been calculated.

1. $C_{L\,max}$, $\phi = 0$ which minimizes the heat transfer rates to the vehicle
2. $(L/D)_{max}$, $\phi = 0$ which gives the maximum range (zero cross range)
3. $(L/D)_{max}$, $\phi = 60°$. This bank angle gives an acceleration in the horizontal plane of about 2.3 g, which is

well below the maximum permissible value of 3. The cross range for this non-modulated trajectory has been calculated by a numerical integration in crude steps (13 steps for the complete trajectory) and was found to be about 925 naut. miles, which is not too far from the required maximum cross range. This simplified trajectory seems therefore a reasonable approximation of the real maximum cross range trajectory.

The results have been plotted in the altitude-velocity diagram of Figure 2.

Finally it should be noted that the descent trajectory of the boosters is not indicated due to lack of data. When booster recovery is required however, the aerodynamic behaviour should certainly be studied.

1.3 The hypersonic transport

For quite some years the hypersonic transport concept has been studied. A review on the subject is for instance presented in Reference 14. Early studies considered flight speeds up to Mach 15 but more recent studies by NASA are rather concentrated on the Mach 6–8 speed. range. A typical example is the vehicle, presented in Reference 15 powered with four hydrogen-fueled turboramjet engines designed to fly at a cruise Mach number of 6 at an altitude of about 30 km. The vehicle should carry a payload of about 23 tons which is about 9% of the gross take-off weight. It has a length of 76.5 m and a span of 38 m.

The hypersonic transport will typically accelerate at $q = .5$ kg/cm^2 until the cruise Mach number and will then increase its altitude towards the level of optimal cruise (Ref. 15) at close to maximal lift-over drag ratio. (Fig. 1 and 2). For a wing loading of 200 kg/m^2 (Ref. 15) the lift coefficient is then $C_L = 0.04$. The airbreathing space shuttle which might come after the rocket powered launchers and orbiters will closely follow the same ascent trajectory as the HST (Ref. 16).

At sustained hypersonic flight the vehicles will be propelled by ramjets or by scramjets (supersonic combustion ramjets), the former for low hypersonic Mach numbers ($M < 6$ to 7) and the latter for high hypersonic Mach numbers ($M > 6$ to 7). Figure 3 (Ref. 14, 16) illustrates the superiority of the scramjet operation over the subsonic burning ramjet at high Mach numbers (H_2 fuel). Dual-mode scramjets which can operate with either subsonic or supersonic burning of fixed geometry are studied in the USA by AirResearch/NASA and in Europe by ONERA (Ref. 17). ONERA has also performed an extensive wind tunnel testing program on hypersonic transport configurations (Ref. 18). The other establishments in Europe who performed detailed studies on hypersonic lifting vehicles are the RAE and the DFVLR (Ref. 4). Much work has been concerned with wave riders, based on simple flow fields such as wedge flows and cone flows. The significance of these shapes is seen not only for the hypersonic transport (Refs. 19, 20, 21) but also for the space shuttle (Ref. 11). It is advocated as a distinctly European contribution to the design of lifting propulsive bodies (Ref. 22).

1.4 Scramjets

The advantage of supersonic combustion is mainly due to the increased inlet performance relative to the subsonic burning mode (the flow remains supersonic, hence less static pressure rise and no normal shock losses), the low static temperature in the burner ($\sim$ 1000°K versus well over 2000°K and hence more sensitive heat addition due to less dissociation after combustion) and, last but not least, improved nozzle performance due to less freezing of chemical species in the expansion process (Ref. 23). In case of a subsonic burning ramjet the inlet can be tested separately from the combustor and the combustor usually does not yield much performance problems since the subsonic combustor technology is well established. The increase in flight speed will only ease the burning rate problem due to the increased temperatures; however, cooling and material problems will show up.

The technology of supersonic combustion is however still rather new and much should still be done before good performance assessment is possible, particularly if the engine has to be run both at the subsonic and supersonic burning mode during the acceleration phase. A good match must be made between the three components: inlet, combustor and nozzle.

Two main problems exist for scramjet propelled aircraft namely, the performance assessment of the isolated engine and the engine integration into the airframe. At hypersonic speed the required engine frontal area (or free stream capture area) increases strongly with respect to the supersonic speed case. For example for Concorde the total inlet area is less than 1% of the wing area whereas for a $M = 7$ airplane this ratio is of the order of 3 to 4%. This increase is mainly due to the fact that the net thrust is only a small fraction of the engine gross thrust (the same situation as with high by-pass ratio fan engines at subsonic speed). This means that inlet, supersonic combustor and nozzle performances are very critical since a 1% gross thrust loss might give a 10% increase in fuel consumption. Further, this large relative inlet area increases the engine-interference problems, both at the inlet side, but mainly at the nozzle side.

Studies (Ref. 24) have shown that deflection of the large gross thrust vector can yield significant gains in lift with little loss in available thrust. In addition the pressures of an under-expanded nozzle flow of a HST configuration could provide favourable interference effects if the exhaust flow washed a large area of the wing lower surface (Ref. 25). These engine forces will cause trimming problems of the aircraft.

Concluding: the airbreathing engines of a hypersonic vehicle form such an integral part of the aircraft that engine simulation (both inlets and exhaust) should always be performed and the installed engine performances must be carefully assessed on special test benches, which will look like hypersonic wind tunnels. The ONERA S4MA tunnel for instance is in fact a pebble bed heated wind tunnel with its test section nozzle replaced by a complete ramjet/scramjet engine (Ref. 26).

2. FLOW PARAMETERS TO BE SIMULATED IN GROUND FACILITIES

In order to obtain information on the behaviour and performance in the design and development phase of the vehicles described above, wind tunnel testing under simulated environmental conditions is indispensable. This testing includes aerodynamics, propulsion systems and hardware. These three aspects may often be treated separately but also combined studies are needed, for instance airframe-engine integration (aerodynamics plus propulsion) and engine endurance and reliability testing (propulsion plus hardware).

2.1 Aerodynamic testing

The hypersonic flow regime can be divided into three regimes with different flow parameters of primary interest:

- the low hypersonic regime from Mach 5 up to say Mach 10 or 12, where duplication of the Mach number and the Reynolds number are of primary interest
- the hypervelocity regime where the flow velocity (or enthalpy) and the flow density are most important parameters, rather than Mach number and Reynolds number and where real gas effects may play an important role
- the low density regime at altitudes above 50 to 70 km where the mean free path between the molecules becomes comparable with characteristic body dimensions. The ratio of the mean free path and the laminar boundary layer thickness is proportional to $M/\sqrt{Re}$, which is the main parameter to be simulated. The low density effects become important above about $M/\sqrt{Re} = 0.01$ (Ref. 4).

During the greater part of re-entry high temperature effects (hypervolocity regime) as well as low density effects are present. The scaling laws for these flight conditions are so different (convective versus radiative heating, non-equilibrium chemistry) that only partial simulation in ground facilities is possible (Ref. 27), when no full scale testing is done.

For the low hypersonic regime, with or without low density effects present, aerodynamic testing of scaled models is well possible.

In Figure 4 the trajectories of Figure 2 have been translated into a Mach number-Reynolds number diagram. Also the boundary of continuum flow $M/\sqrt{Re} = 0.01$ is indicated. In the next paragraphs its consequences for the flow parameters to be simulated for the space shuttle orbiter and the hypersonic transport are discussed in somewhat more detail.

2.1.1. The Space Shuttle

A good review of the aerodynamic problems related to the space shuttle vehicle is found in Reference 28. Although data on the final North American Rockwell configuration are not presented, the data for the high cross-range orbiter (Ref. 28, p. 285 e.g.) show good agreement with the simplified trajectories presented in Figure 4.

Ideally the flow conditions around the full scale vehicle should be duplicated around the model. This is done by duplicating the Mach number M, the Reynolds number Re and the wall temperature to free stream temperature ratio T_{w/T_∞} if high temperature real gas effects are excluded for the moment.

2.1.1.A Mach Number

Mach number duplication is necessary for shock shape duplication. It is known however, that at high enough Mach numbers the shock becomes very close to the under-surface of space shuttle-like bodies at representative angles of attack and is almost insensitive to further increase in flow Mach number. Also the situation at the leeward side where severe flow separations exist becomes insensitive to Mach number changes. It is therefore suggested that duplicating the flow Mach number at Mach 15 or 20 is not vital for the space shuttle (Ref. 29).

This suggestion is supported by looking at the slip flow boundary in Figure 4. In the slip flow regime where the Mach numbers are above 15 to 20, the force data can be correlated on the rarefaction parameter $M/\sqrt{Re}$. For more details see section 2.1.1.C.

2.1.1.B Reynolds Number

Reynolds number duplication and temperature ratio T_w/T_∞ duplication is required for duplication of the boundary layer thickness and the kind of boundary layer (laminar or turbulent).

For a proper design of the thermal protection system knowledge of the location of the boundary layer transtition region is essential. According to Reference 30, there is yet no definite conclusion how the transition data, found in wind tunnels, should be interpreted for the full scale vehicle.

In Reference 31 some new free flight transition data are presented and various transition criteria are discussed. For local Mach numbers above 5, the Reynolds number based on the conditions at the edge of the boundary layer and the wetted length Re_{x_t} which indicates the onset of transition was somewhere between 10^6 and 10^7 (data scatter). Below $M_e \approx 4$ values of Re_{x_t} between 10^4 and 5×10^6 are found with a data scatter of about two orders of magnitude. These lower Re_{x_t} values are obtained at high angles of attack on the lower side of the vehicle and are probably largely influenced by 3-dimensional effects. It should be remarked that Re_x is not the best correlating parameter but rather Re based on a boundary layer thickness, in combination with the local Mach number and Reynolds number per unit length (Ref. 31). In Reference 31 it was found that for a $\alpha = 40°$ re-entry onset of transition starts on the lower side of the vehicle somewhere between 70 and 80 km but Reference 32 gives about 65 km.

Comparison of these data with Figures 2 and 4 indicates that the somewhat vague boundary between continuum flow and slip flow coincides more or less with the boundary between full laminar flow and laminar plus transitional flow. Left and above this boundary in Figure 4 the Mach number and the Reynolds number are the main flow parameters.

The required Reynolds numbers for correct boundary layer transition duplication in wind tunnels seems to be an unsolved problem, considering the accuracies required for the design of an optimum thermal protection system.

In this context the parameter T_w/T_∞ should also be mentioned. This is an important parameter not only for the skin friction coefficient or the heat transfer coefficient (see for instance Reference 33), but also for the boundary layer transition point (see for instance Reference 34).

The wall temperature will depend on the method of cooling but may vary between 600 and 1700°K along the vehicle wall, which means that T_w/T_∞ will vary between about 3 and 8. For wind tunnel testing the maximum Reynolds number is attained when the free stream temperature is as low as possible, the limitation being the condensation temperature of the gas which varies between 30 and 60°K for air and nitrogen, the value increasing with stagnation pressure (Ref. 35). A wall temperature of the model equal to room temperature may be a reasonable value to simulate an average of the non-uniform wall temperature of the full scale vehicle.

In conclusion the best way to deal with the transition problem seems to duplicate the Reynolds number and if possible the temperature ratio T_w/T_∞ in the continuum regime indicated in Figure 4. The boundary layer thickness will then be properly simulated and the transition region generally will be more upstream than on the full scale vehicle (see data of Reference 31), which generally will not lead to too optimistic predictions for the thermal protection requirements. Mach number-Reynolds number duplication also eliminates the necessity for possible Reynolds number corrections for the phenomena on the leeward side of the vehicle where large regions of separated flow exist.

2.1.1.C Visuous Interactions and Low Density Effects

The space shuttle orbiter will experience peak heating and deceleration at 60–70 km altitude (Ref. 28, 36), where low density effects can certainly not be neglected. The slip flow regime which extends roughly between $M/\sqrt{Re} = 0.01$ and 0.1 is indicated in Figure 4. The low density regimes at higher altitudes such as the near free molecule and the free molecule regime are of less importance for the space shuttle re-entry from a practical point of view. From Reference 29 the following remarks are quoted.

The most significant practical effects, as far as overall performance is concerned, occur on slender, high L/D vehicles. Not only are much larger viscous interaction induced forces generated on this type of vehicle, resulting in a large reduction in L/D (see Reference 4 for instance), but the effects extend to relatively lower altitudes than the other low density effects.

In the case of the space shuttle a large percentage of the re-entry flight time is spent in manoeuvring in the high altitude regions dominated by rarefield flow effects. It has been established that rarefaction effects are likely to be significant over the whole of a slender vehicle, over localized regions such as on control surfaces, if the value of the viscous interaction parameter $M/\sqrt{Re_\infty}$, L is greater than about 0.01. For a 20m long vehicle this corresponds to about 75 km altitude over the forward surfaces if they were at 40° incidence to about 55 km over the leeward surface at about −10° incidence (end of quotation).

In order to have an indication of the viscous interaction effects on the longitudinal range, calculations have been made for the highest re-entry trajectory of Figure 2, where these effects will be most significant. For the sake of simplicity it is assumed that C_L remains unaffected. The effect on L/D is assumed to be represented by Reference 37, Figure 26: at $M/\sqrt{Re} = 0.1$ the L/D value is half the inviscid value of 0.6.

Starting from the vertical equilibrium condition at an altitude of 90 km the following longitudinal range is attained when the flight velocity has decreased to 1 km/sec: L/D = const. R = 6200 km and if L/D influenced by viscous effects R = 4600 km or about 75 percent of the inviscid value. This is the result of a rather crude calculation (numerical integration in eleven steps).

For vehicles with much higher L/D values for the samel W/SC_L the influence of viscous interaction on the range performance is even much larger. In Reference 38 calculations show for a L/D = 4 vehicle reductions in range of more than 50%. For a discussion on the relevance of such high L/D vehicles the reader is referred to References 11 and 39.

The examples mentioned show that knowledge of the aerodynamic behaviour at high altitudes is essential for the assessment of the vehicle performance. Analyses which do not take low density effects into account can give misleading results.

It is concluded from Figure 4 that aerodynamic testing of the vehicle behaviour should be done for values of $M/\sqrt{Re}$ between 0.01 and 0.1 at Mach numbers above, say 15 (see also sub *2.1.1.A*). Its significance should be considered against the background of the influence of high temperature real gas effects.

2.1.1.D High Temperature Real Gas Effects

At very high altitude, where the flow is completely free molecular and at low altitudes where the air is continuum, forces acting on a vehicle can be predicted theoretically with a good degree of certainty. Between these limits, however, the flow is a complex function of each type and most of our understanding has to be gained by experiments in wind tunnels (Ref. 29). Very unfortunately in this same area high temperature real gas effects complicate the picture considerably.

A discussion on the problems of aerodynamic testing in this hypervelocity regime where the flow velocity itself and the free stream density are the primary flow parameters can be found in Reference 27. Proper scaling is difficult and often completely impossible: radiative heat transfer for instance is proportional to the nose radius of the vehicle and convective heat transfer is proportional to the inverse of the square root of the nose radius. Also non-equilibrium effects may become important, especially at higher altitudes : relaxation lengths of the order of several meters may occur on a space shuttle (Ref. 40).

The dissociation and ionisation of the air in the stagnation region and elsewhere around the vehicle could lead to adverse effects on lift, trim and heat transfer. Prediction of these effects is still uncertain; they cannot be investigated in a wind tunnel of the usual blow down type, for the very process of expansion through a nozzle from stagnation conditions representative of high altitude re-entry causes thermodynamic non-equilibrium in the nozzle flow which is not like the flow around the vehicle in the real atmosphere.

Another reason is the incompatibility of the scaling laws for convective and radiative heat transfer and for non-equilibrium chemistry (binary and tertiary collisions of recombining molecules for instance) (Ref. 27).

What can be done in this area experimentally is providing data for theoretical predictions such as chemical reaction rates and radiative heat transfer data obtained from facilities like shock tubes, expansion tubes and plasma facilities, eventually boosted by a magneto hydrodynamic device and the development of high performance facilities where flow non-equilibrium is largely avoided (see Ref. 41).

2.1.2 The Hypersonic Transport

In Figure 2 the trajectory is given of a hypersonic transport accelerating at a constant dynamic pressure of q = 0.5 atm up to a non-specified cruise Mach number (Ref. 15). The corresponding flight conditions are plotted in the Mach number-Reynolds number diagram of Figure 4. It is seen that the Reynolds numbers based on vehicle length for a given Mach number, are one to two orders of magnitude larger for the HST than for the space shuttle during re-entry. The consequences for the aerodynamic parameters to be simulated are discussed below.

2.1.2.A Mach Number

The Mach number must be duplicated in wind tunnel tests to obtain the same shock shape as in real flight. This requirement should not be violated as was permitted for the high Mach number tests for the space shuttle. This may be illustrated by referring to the engine intake region where the position of the shock waves from the external compression surface relative to the intake lip should be duplicated accurately.

2.1.2.B Reynolds Number

From Figure 4 it follows that a hypersonic transport designed for a cruise Mach number of 6 to 8 (see Ref. 15 for a typical example) will fly at Reynolds numbers well above 10^8, based on the total vehicle length. Although the significance of the transition data obtained in wind tunnels for the full scale vehicle is still not definitely settled (Ref. 30), the Reynolds numbers at which the HST will operate are so large that the boundary layer on the vehicle will be almost completely turbulent.

In Reference 42 shock tunnel measurements are described on a HST-model over a Reynolds number range from about 0.5 million to 160 million. It is found that transitional boundary layer effects on the axial force coefficient begin to emerge at Re_L of about 2 million. These effects predominate for about a decade in Reynolds number until the turbulent boundary layer exerts the major influence at Reynolds numbers of about 20 million.

From this Figure it is concluded that a Reynolds number of about $Re_L = 20$ million is a minimum requirement for wind tunnel tests for the development of hypersonic transport aircraft where absolute performance data should be obtained. Reliable extrapolation to the much higher full scale Reynolds numbers seems feasible in that case (Ref. 42).

The value $Re_L = 20$ million is in fact still open to discussion. A value of 50 million as was presented in the first provisional version of the present paper is probably on the safe side but a value of 5 million as suggested in Reference 29 is apparently too low when the drag data of reference 42 are considered. Up to what value of Re_L testing is necessary will also depend on the required accuracy of the data which have to be extrapolated to full scale Re_L values.

When the model is tested at Reynolds numbers below say 20 million, the transition region moves too far downstream. In that case the transition might be moved upstream again by artifical trips, but at hypersonic velocities the trips must be so large that even the flow outside the boundary layer is disturbed, causing an additive interference drag (Ref. 29, 43, 44). Artificial boundary layer transition is therefore not an attractive method at hypersonic speeds.

For cases where the boundary layer itself is an important parameter such as for engine intakes preceded by a compression ramp and for shockwave-boundary layer interaction as for instance occurs near flap hinges, the consequences of testing at lower Reynolds numbers than the full scale values should be considered with great care. The turbulent boundary layer thickness being inversely proportional with the one-fifth power of the Reynolds number, testing at $Re_L = 2 \times 10^7$ gives a boundary layer thickness which is about 60% larger than testing at the real value of $Re_L = 2 \times 10^8$ at Mach 8. Isolated testing of partial models in the correct flow environment may yield usable results in these cases.

The average wall temperature/free stream temperature ratio in the wind tunnel will have a value of the same order as for the full scale vehicle when the tunnel is operated near its condensation limit and the model is at room temperature (see also *2.1.1.B.*).

2.1.2.C Low Density and Real Gas Effects

Only near the leading edges viscous interaction effects may occur. Testing at too low Reynolds numbers may lead to undue conclusions such as concerning aerodynamic heating. Partial model testing may be useful in this area. At speeds up to, say Mach 8 the high temperature real gas effects on the aerodynamic behaviour are still small. For refined measurements, however, they may be taken into account.

As an example Reference 45 gives for the lower side of a flat plate flying at 30 km altitude at Mach 8 at an angle of incidence of 20° a pressure coefficient which is about 1 percent lower than in a wind tunnel where the free stream temperature is 55°K.

High temperature real gas effects are however very important as far as the airbreathing propulsion is concerned (see section 2.2).

2.1.3 Conclusion for Aerodynamic Testing

For *space shuttle* type of vehicles the following is concluded for the flow parameters to be simulated for wind tunnel testing.

The Mach number should be duplicated up to about 15 to 20. Above this Mach number the viscous parameter $M/\sqrt{Re}$ is of primary importance for the aerodynamic behaviour, when $M/\sqrt{Re} > 0.01$. When $M/\sqrt{Re}$ is smaller than this value, the flow behaves as a continuum and for the space shuttle this coincides approximately with the onset of boundary layer transition. Interpretation of wind tunnel transition data for full scale flight behaviour still being in discussion, the best to do is testing at duplicating Mach number and Reynolds number when $M/\sqrt{Re} < 0.01$. This also gives the correct boundary layer thickness.

A model temperature equal to room temperature will provide a reasonable T_w/T_∞ value in many cases. In practice, however T_w is non-uniform.

High temperature real gas effects such as occur during a great part of the re-entry may be studied experimentally by partial simulation only.

For *hypersonic transports* development testing in wind tunnels the following conclusions are made.

Mach number duplication is essential to duplicate the shock shape. The boundary layer being predominatly turbulent, in many cases wind tunnel testing at Reynolds numbers above, say 20 million allows probably good prediction of the vehicle performance by a correction of the skin friction to the full scale Reynolds number value.

For cases where the boundary layer itself is an important parameter such as for engine intakes and shockwave-boundary layer interaction, Reynolds number duplication and/or partial model testing will be necessary.

A model temperature equal to room temperature will provide a reasonable T_w/T_∞ -value in many cases. High temperature real gas effects on the aerodynamic performance are rather small up to say Mach 8.

2.2 Propulsion Testing

Since the ramjet and scramjet do not contain devices to increase the total pressure of the internal flow (turbomachinery), the engine flow simulation at hypersonic airplane models is in principle easier to achieve than at the lower speed regimes. If the internal flow is not heated, either in a subsonic or supersonic stream, the nozzle total pressure will not be matched with the scaled nozzle geometry and the stream tube leaving the nozzle will be too small. Hence, the interference with the outer flow is wrongly matched. Two methods are available to obtain the simulated nozzle flow field and pressure distribution, namely by adding large quantities of additional gas such that $\dot{m}\sqrt{RT}$ is simulated for the nozzle, or burning a fuel within the internal flow. In the latter case it is required to use air as the tunnel fluid and the total temperature of the air should be duplicated if the same fuel is used as for the full scale flight. In that case the scaling law for the burning rate process is approximately equal to the scaling law for the Reynolds number (p.l. = constant). The high total temperature required for duplication however, is in conflict with the lowest possible stagnation temperature for maximal Reynolds number and wall-free stream temperature ratio. Until recently few tests have been performed on HST models with simulation of the engine flow (Ref. 24 and 25).

In a scramjet the heat release within the supersonic flow is either of a 2-dimensional or 3-dimensional nature. As yet a good understanding of heat release in multidimensional supersonic flows has not been attained. A very strong unknown interplay exists between the chemical kinetics, mixing, fuel jet penetration, shock waves and duct area. Local heat release in supersonic flow will cause thermal compression, however shock waves should be avoided. In supersonic combustion tests the entrance Mach number, pressure level, temperature and chemical composition are of primary importance. For propulsion testing the total engine mass flow and flow duration give additional requirements to the test facilities.

Figure 5 gives in the flight Mach number-altitude plot the required stagnation temperatures, pressure and mass flow per unit capture area of the inlet for complete environment duplication. For large hypersonic Mach numbers these conditions are hard to achieve in the laboratory as is also the case for hypersonic wind tunnels. Therefore in the next discussion emphasis will be focussed on the parameters which are of primary importance for engine and combustion tests.

2.2.A Mach Number in the Combustor

It is evident that Mach number duplication in the combustor is essential due to the strong interaction between the flow field (compression) and local heat release. In the following it will be always assumed that the Mach number is duplicated.

2.2.B Temperature

For low static temperature at the supersonic combustor entrance the overall reaction rate will be limited by the chemical kinetics, whereas at sufficient high static temperature the turbulent mixing between the fuel and air will be the rate limiting factor. Hence static temperature duplication in the combustor is of primary importance at low hypersonic Mach numbers, since if the flow is decelerated from hypersonic speed to supersonic speed in the combustor, the static temperature will be between the ambient static temperature and stagnation temperature depending upon the Mach number ratio. For various performance reasons, a rough rule of thumb is that the combustor entrance Mach number is about one-third of the flight Mach number (Ref. 23). Figure 6 gives the typical static temperatures versus Mach number for the NASA Hypersonic Research Engine (HRE) burning hydrogen (Ref. 46). Figure 7 shows the importance of the initial temperature for hydrogen as fuel. Since hydrogen is the most probable fuel for scramjets for performance and cooling reasons, the combustor entrance static temperature should be above about 1000°K. Over about 1500°K mixing will be the dominant factor. These conditions occur at

$M \gtrsim 10$ to 11. This means that for supersonic combustion tests the stagnation temperature should be duplicated up to $M = 10$ to 12, hence $T_0 = 4000°K$ to 5000°. Other fuels might also be used such as the metalized fuels (for example Trime- tylaluminium, Triëthylaluminium, Trimethylborane) or hydrocarbons (Ref. 23). The first group will yield spontaneous ignition even at atmospheric temperatures, whereas the latter group will also need preheated air for fast ignition.

2.2.C Pressure

The static pressure level in the supersonic combustion chamber depends primarily on the flight altitude, the inlet process efficiency (K_D) and inlet Mach number ratio. The actual value will be at about 1 kg/cm² (say 1/5 to 5 kg/cm²). Figure 8 gives some typical inlet values as will be encountered in flight, respectively total pressure ratio, and static pressure levels (Ref. 48). Particularly in this pressure regime and for temperatures between 1000 and 1500°K the ignition delay time for hydrogen is a strong irregular function of the pressure, making use of appropriate scaling laws for pressure unsuitable (Fig. 9). For higher temperatures the induction time is inversely proportional to the pressure level ($\tau_{i.t.}\ p = f(T)$.

Once the chemical reaction is started the characteristic reaction time for hydrogen is proportional to $p^{-1,65}$. For hydrocarbon the reaction time is proportional to $p^{-1,8}$ (sometimes also taken as p^{-2}). (See also Ref. 49).

Therefore for good understanding of the combustor phenomena the pressure level should be duplicated as well as the geometry. Scaling laws can only be used if the overall chemical kinetics behaviour can be described by simple rules and if variable induction times do not exist.

Ideally the hypersonic engine (scramjet) should be placed in the freejet of a hypersonic facility, duplicating the stagnation condition (temperature and pressure) and free stream Mach number in which the complete system can be tested (inlet, combustor and nozzle). This may be difficult to achieve in a hypersonic wind tunnel due to the high required stagnation levels, particularly if the duplicated Mach number approaches the value 8 (see section 3.2).

One means of omitting the high stagnation pressure level is to utilize a direct connection set-up at which the flow is expanded only to the required supersonic speed in the combustor (See Fig. 10 of ONERA from Ref. 50). This will reduce the required tunnel reservoir pressure by the ratio as indicated in Figure 8 (typically a factor 2 to 5, depending inlet geometry). The inlet performance and combustor extrance flow field can be determined in separate wind tunnel tests at the full scale Reynolds number (but reduced temperature) at the representative relative boundary layers thickness.

2.2.D Mass Flow

The required mass flow for propulsion testing depends primarily on the required net thrust to overcome drag, to accelerate and to climb. The first term is of primary importance and depends on the flight I/D ratio of the vehicle. For a cruise vehicle this value will be between 4 and 6. For a hypothetical 200 ton HST with four engines the net thrust should be over 10 tons. Flying for example at $M = 7$ where the thrust coefficient is about $C_T = 0.6$,

$$\left(C_T = \frac{F_N}{q\ A_{capture}}\right)$$

for a hydrogen fueled engine, the required mass flow per engine is about 200 kg/sec. This value increases for other fuels. Typically, using kerosine the required mass flow will roughly double the value using H_2 at $M = 7$. It can be computed that the HRE of NASA-Lewis consumes about 5 kg air per second at $M = 7$ and 100 000 ft altitude.

A mass flow rate of 200 kg/sec requires a combustor entrance of 0.4 m² at $M_{entrance} = 2.3$. These conditions are rather typical for medium size unheated supersonic wind tunnels, but are exhaustive for hypersonic wind tunnels, which are necessarily fitted with a heating system. Only the Tripltee tunnels at NASA Langley and at AEDC (under design) fulfil these conditions up to $M \approx 7$ (Ref. 51 and 52).

2.3 Hardware Testing

2.3.A Ablation testing

For the structure of hypersonic vehicles one of the most significant parameters is the aerodynamic heat load to which it will be subjected. The magnitude of the heat load and the exposure time are rather different for the space shuttle and for the hypersonic transport and hence the structural concepts which deal with these heat loads. The feasibility of these concepts will have to be verified by hardware testing under simulated flight conditions.

For the space shuttle the heat transfer rates are one order of magnitude larger than for the HST (Ref. 53), but the total heat transferred to the vehicle (per unit wetted surface and per flight cycle) will be much smaller than for the HST.

For the space shuttle a passive heat protection system has been considered for early versions consisting of ablative material on an aluminium substructure, which requires refurbishment after each flight (Ref. 8). At the moment of writing this paper, three different insulation systems are foreseen: a low-weight elastromer on the upper surface (up to 340°C), a new ceramic material on the lower surface (up to 1370°C) and a new oxidation-inhibited, reinforced carbon material for the wing leading edges and the nose cap where temperatures up to 1650°C are anticipated (Ref. 54).

A discussion on the testing of ablative materials which is also useful to understand the problems of testing of non-ablative protective coatings can be found in Reference 55.

For ablation studies near the nose region of a re-entry body the major requirement is to simulate the stagnation enthalpy and the pitot pressure on the model (Ref. 27). For the shuttle lower re-entry trajectory of Figure 2 the following conditions are found at the vehicle stagnation point (equilibrium flow assumed) (Ref. 56).

Altitude H (kft)	300	250	200	150
Velocity u (kft/sec)	25.8	25.0	22.6	12.1
Stagn. enthalpy $h_{s/R\ (°K)}$	10.8×10^4	10.2×10^4	8.8×10^4	2.4×10^4
Pitot pressure p_s (atm)	1.39×10^{-3}	1.97×10^{-2}	1.20×10^{-1}	2.3×10^{-1}
$\dot{q}\sqrt{r_n}\left(\frac{BTU-in}{ft^2-sec}\right)$	73	262	533	201

$\dot{q}$ is the convective heat transfer rate at the stagnation point and r_n is the nose radius in inches. For nose radii up to 1 foot the radiative heat transfer is more than one order of magnitude less than the convective heat transfer (Ref. 57).

It is found that the required values of stagnation enthalpy can be generated in arc heater facilities but for $h_{s/R} = 10^5\ °K$ the reservoir pressure should not exceed 5 atm (Ref. 58, state of the art 1961). The total pressure in a wind tunnel, required for flow duplication, is however of the order of 10^3 to 10^6 atm.

The solution is to duplicate the stagnation enthalpy and to test the model at fairly low Mach numbers, typically Mach 2–5 (Ref. 27,55).

2.3.B Structure Testing

For the hypersonic transport a rather simple passive thermal protection system as for the space shuttle will not be employed, but the walls are to be cooled by the hydrogen fuel. This cooling may be accomplished directly, using wall materials with good thermal conductivity, or indirectly by blowing pre-cooled sheets of air over the outer wall surface i.e. by slot cooling (Ref. 53). These active cooling systems are much more vulnerable to failures and extensive testing will be necessary on reliability, thermal fatigue, effect of transients, etc. The same arguments are valid for the testing of the HST propulsion system. A discussion on the development and hardware testing of airbreathing engines for large hypersonic vehicles can be found in Reference 51.

The facility requirements for development testing of full or large-scale airbreathing propulsion systems and associated airframe can be appreciated by considering the requirements as described in Section 2.2. The same requirements for complete flow duplication (p_t, T_t, M) are valid, and result in the use of large tripltee tunnels. The required running time of these tunnels will largely influence the design of the tunnel heating systems. It is generally agreed that at least a few minutes running time is required, however, aeropropulsion people quote figures as high as 15 minutes.

It should be noted that such a large facility allows also Mach number-Reynolds number duplication of the HST up to Mach 7 when the tunnel is operated at equilibrium condensation condition (see Fig. 11), $p_o L_m$ being of the order of 750 atm.m.

3 PRACTICAL AND PRINCIPAL LIMITATIONS FOR GROUND TEST FACILITIES

3.1 Hypersonic Wind Tunnels for Aerodynamic Testing

For the bulk of aerodynamic tests at hypersonic speeds in ground test facilities the primary aim is to duplicate the Mach number and the Reynolds number of the full scale flight condition (see Section 2.1). In order to achieve this with the least amount of energy the tunnel is operated at the lowest possible temperature. This temperature follows from the requirement that the static temperature in the test section flow should not be below the condensation temperature (Ref. 35). In Figure 11, which will be discussed later, the stagnation temperatures,

necessary to avoid equilibrium condensation are indicated as a function of Mach number and stagnation pressure for a perfect gas (dashed lines). For a real gas the minimum stagnation temperatures are lower than indicated in Figure 11.

Calculations for a real gas (with Refs. 35, 45 and 59) show that at Mach 18 at minimum stagnation temperature the degree of dissociation of the gas in the stagnation region of a blunt body model in the test section is about 1% for stagnation pressures between 10 and 1000 atm. It is concluded that in a wind tunnel operated at minimum stagnation temperature, high temperature real gas effects are restricted to molecular vibration only, when the test section Mach number is below Mach 18. The discussion on aerodynamic facilities in this Section 3.1 will be confined to facilities operating under conditions where molecular vibration is the only high temperature real gas effect to be taken into account. Its effect may, however, still be considerable: the pitot pressure may be 65% of the ideal gas value for instance (Ref. 45, Fig. 20).

Methods to correct the wind tunnel data for the full scale vehicle real gas effects such as dissociation and ionization will not be discussed here. They may be provided by theoretical analyses supported by experimental data of a more fundamental character such as radiative heat transfer measurements and chemical reaction rate data and partical flow simulation.

The "pure" aerodynamic phenomena are duplicated when the Mach number and Reynolds number around the vehicle are duplicated and the correct wall temperature-free stream temperature ratio T_w/T_∞ exists. For practical reasons the non-uniform wall temperature distribution along the full scale vehicle is often approximated by a uniform wall temperature of the wind tunnel model (room temperature). Non-uniform increase of the wall temperature during wind tunnel tests should not be overlooked. At flight conditions where $M/\sqrt{Re}$ is larger than about 0.01, i.e. during high altitude re-entry, the parameter $M/\sqrt{Re}$ should be duplicated, rather than M and Re separately.

In order to find the stagnation pressures needed to generate the necessary Reynolds numbers, indicated in Figure 4, calculations have been performed for a wind tunnel model with a standard length of 1 meter, operated at the equilibrium condensation temperature for air (Ref. 35). This will give the highest Reynolds number for a given stagnation pressure and Mach number. No real gas effects have been taken into account. The results have been plotted in Figure 11.

Real gas effects however, may have considerable influence as is indicated in the example below, calculated with aid of Reference 59.

real gas				*equivalent perfect gas*	
p_o	T_o	Re/m at $M_{cond.}$		p_o	T_o
atm	°K	m^{-1}	–	atm	°K
488	1500	2.2×10^6	12.77	379	1671
1072	1500	6.5×10^6	12.56	1085	1736
2308	1500	18.7×10^6	12.48	3241	1846
4920	1500	50.7×10^6	12.80	10960	2084

The real gas effects are in fact twofold, namely high pressure effects (van der Waals effects) and high temperature effects. For given free stream conditions at hypersonic Mach numbers the stagnation temperature is lower than according to the perfect gas calculations and the stagnation pressure can be either higher or lower.

In Reference 60 the combination of both effects has been considered and is presented in graphical form, two figures being reproduced as Figures 12a and 12b of the present paper, valid for nitrogen, which closely resembles air. These graphs can be used in combination with Figure 11, which is valid for a perfect gas, to calculate the real required tunnel stagnation conditions.

As was already pointed out, above $M/\sqrt{Re} = 0.01$ the viscous interaction parameter $M/\sqrt{Re}$ should be duplicated rather than Mach number and Reynolds number. From Figure 11 it follows that this procedure allows testing at lower stagnation temperatures and pressures than if Re and M both had to be duplicated along the complete re-entry trajectory of a space shuttle. This is a very important consideration from a facility engineering point of view.

It can be discussed whether M-Re duplication for the lower shuttle re-entry trajectory should be pursued up to Mach 19 where $M/\sqrt{Re} = 0.01$, because of the necessary high values for $p_o L$ and T_o (facility engineering and high-temperature real gas effects). For a model length $L_m = 1$ meter Figures 11 and 12 give as required real gas stagnation conditions about $p_o = 2600$ atm and $T_o = 2900°K$ at the point considered.

A minimum tunnel requirement may be that M-Re duplication must be possible up to such a value that interpolation to the $M/\sqrt{Re} > 0.01$ data is possible with acceptable and reasonable accuracy. This value may be different for tests where for instance boundary layer transition is important (heat transfer for example) or for force tests where M and $M/\sqrt{Re}$ are more important. In the following sections the practical and principal limitations will be discussed, which are important for validation of the performance of hypersonic facilities for aerodynamic testing.

3.1.A Stresses in the Sting Support

Due to the aerodynamic forces stresses will develop in the model and the sting which supports it. For a given model and sting support these stresses are a function of the angle of incidence and the dynamic pressure only and a weak function of the flow Mach number. The stress in the sting with diameter d_s at the model base is calculated for a static load assuming that the normal force N (perpendicular to the model axis) acts on a point at a distance $2/3\ L_m$ from the nose.

For the space shuttle a minimum sting diameter $d_s = 0.1\ L$ may be employed (about equal to the base diameter of the vehicle) and for the HST a value $d_s = 0.04\ L$ is a realistic value (Ref. 61). The bending stresses due to aerodynamic forces in the sting are then calculated from the moment

$$M = (1 - \tfrac{2}{3})\ LN = \tfrac{1}{3} L^3\ C_N q . \frac{S}{L^2}$$

where L is the model length, S the reference area for the normal force coefficient C_N and q is the dynamic pressure. For a solid circular sting follows

$$\sigma = 3.3 \left(\frac{L}{d_s}\right)^3 \frac{S}{L^2}\ C_N q$$

A value $\sigma = 5000$ kg/cm² at normal static aerodynamic load is considered as the structural limit: starting and stopping loads and a safety factor are not included. Also the strength of the model itself and the allowable elastic deformation of model and support are not considered.

When a maximum normal force coefficient C_N is assumed for the space shuttle $C_N = 1.5$ (see chapter 1.2), which is the modified Newtonion pressure coefficient for an angle of incidence of 65 degrees, and for the HST a maximum $C_N = 0.25$ corresponding with an angle of attack of 16° for a typical configuration at Mach 6 (Ref. 62) the following maximum dynamic pressures q_m are calculated for a stress in the sting $\sigma_m = 5000$ kg/cm² from

$$q_m = 0.3\ \sigma_m \left(\frac{d_s}{L}\right)^3 \frac{L^2}{S} \frac{1}{C_N}$$

This gives a maximum dynamic pressure $q_m = 1.5$ kg/cm² for the space shuttle and $q_m = 2.2$ kg/cm² for the HST, This may limit the performance for facilities with high stagnation pressure capabilities at low hypersonic Mach numbers.

For instance at Mach 8 a maximum stagnation pressure of 325 atm is allowed for space shuttle testing if q is limited to 1.5 kg/cm² and to 480 atm for HST-testing at $C_N = 0.25$. In Reference 42, however, a HST-model has been tested at a stagnation pressure of 1300 atm. In that case however, C_N was about 0.085 and the sting diameter d_s was about $0.05\ L_m$. This will give a stress in the sting of 2400 kg/cm² which is well below the limit set at 5000 kg/cm². For $d_s = 0.04\ L_m$ the stress would have been 4600 kg/cm², which indicates that the limits for q_m of 1.5 kg/cm² for the space shuttle and 2.2 kg/cm² for the HST are not exact boundaries. It will be largely dependent on model-sting geometry and safety factor which has to include starting and stopping loads which are also facility dependent and the maximum q at which the HST is to be tested.

Another criterion may be derived from the assumption that the space shuttle model should be tested at values of dynamic pressure and angle of incidence where the normal force is four times the weight of the vehicle along the full scale trajectory (3-g is maximum design acceleration) and for the HST a normal force of two times the weight of the vehicle is attained, corresponding with a 2-g turn.

For a full-scale model and flow duplication the stresses in the sting would then be calculated from

$$\sigma_f = 3.3\left(\frac{L}{d_s}\right)^3 \frac{S}{L^2} C_N\, q_f$$

where $C_N \cdot q_f = 4\frac{W}{S} = 800$ kg/m² for the space shuttle and $C_N\, q_f = 2\frac{W}{S} = 500$ kg/m² for the HST. However, due to the fact that the tunnel can operate at a much lower temperature, the Reynolds number can be increased by a factor of about 4 (was 3 in the draft version of the present paper) when M-Re duplication is employed at tunnel equilibrium condensation conditions instead of flow duplication.

Introducing a scale factor $B = L_f/L_m$, the ratio between the full scale length and the model length, one finds for M-Re duplication of the $N = 4W$ and $N = 2W$ conditions that $\sigma_m/B = \frac{1}{4}\ \sigma_f = 22$ kg/cm² for the space shuttle and 111 kg/cm² for the HST (σ is proportional with q or p_o).

For a maximum stress $\sigma = 5000$ kg/cm² the maximum scale factor B or minimum model length L_m is found as

Space shuttle	$B_{max} = 228$	$L_{m_{min}} = 0.15$ m
Hypersonic transport	$B_{max} = 45$	$L_{m_{min}} = 1.70$ m

When $Re_L = 2 \times 10^7$ is required and not full scale Re_L duplication then the model size can be decreased proportionally, keeping the stagnation conditions constant.

Both sting load criteria can be worked out and the results are found in Figure 13. The p_o = constant curves for M-Re simulation were calculated from Figure 11. The sting load limits are indicated in Figure 13 as $C_N = 1.5$ (0.25), which is equivalent with $q_m = 1.5$ (2.2) kg/cm³ and as $N = 4W$ (2W) valid for the space shuttle (HST).

Although these sting load criteria are not to be used as exact figures it follows from Figure 13 that both criteria indicate approximately the same minimum model size (within a factor 2) and that the minimum model size for M–Re duplication of the HST is one order of magnitude larger than for M-Re duplication of the space shuttle and testing of a HST-model at $Re_L = 2 \times 10^7$.

3.1.B Maximum Stagnation Pressure

In Figure 11 the stagnation pressures are presented which generate the required Reynolds numbers over a model with a standard length of 1 meter. The wind tunnel is operated at the equilibrium condensation limit. The curves are valid for a perfect gas.

The results of Figure 4 and 11 are used to calculate the required model length L_m for M-Re duplication for various stagnation pressures. The results are plotted in Figure 13. Also the minimum model lengths as determined by the tolerable sting loads as was calculated in Section 3.1.A are indicated.

From a practical point of view a value of 5000 atm should be considered as an upper limit for the stagnation pressure p_o which can be contianed in the reservoir of a blow down wind tunnel: the highest design value of present facilities is 60,000 psi or 4200 atm (Ref. 36, 63). This limit is also indicated in Figure 13.

For force testing of wind tunnel models with an internal balance, fairly small models can be used. In Reference 64 for instance force tests are reported on a space shuttle configuration in a gun tunnel with a length of 0.10 meter. For more detailed measurements, however, such as pressure and heat transfer distribution on the model surface, larger models are required. For a well instrumented model, such as used for development work, a model length of more than 0.3 to 0.5 m seems to be a sensible requirement. It also makes aerodynamic loading of the sting and the model less critical.

From Figure 11 it follows that for a HST configuration with a model length $L_m = 0.50$ m, $Re_L = 2 \times 10^7$ can be obtained up to Mach 8 with a reservoir pressure $p_o = 200$ atm. Recent HST studies do not indicate higher design Mach numbers (see also Section 13).

For M-Re duplication of the space shuttle lower trajectory conditions the requirement are more demanding than for a HST model at Mach 8 and $Re_L = 2 \times 10^7$ as can be seen from Figures 11 and 13. This is due to the fact that the Mach number range of interest is much higher than for the HST. If for instance M-Re duplication is necessary up to Mach 15, a stagnation pressure $p_o = 2000$ atm is required for a model length of 0.50 m.

It is concluded from Figure 13 that stagnation pressures larger than $p_o = 2000$ atm and models smaller than about $L_m = 0.3$ to 0.5 m are not very interesting for development testing of the space shuttle or HST-configurations when the "pure" aerodynamic phenomena along the whole trajectory should be simulated, including boundary layer transition.

For M-Re duplication of the HST up to Mach 8 only large models with $L_m \sim 2$ meter and $p_o \sim 1000$ atm can keep model and sting loads within acceptable values when testing up to $C_N = 0.25$ ($\sigma \sim 16°$) is required.

3.1.C Facility Power

It is found that already for a small hypersonic wind tunnel for development work with a test section of 0.50 m and a stagnation pressure of 1000 atm operating at the condensation limit, very large energies are contained in the flow. For example at Mach 5 the total energy flux through the test section would be about 600 MWatt and at Mach 10 about 50 MWatt. This lower figure for a higher Mach number is due to the fact that although the velocity is about 50 percent larger, the throat area is only 5% of the value at Mach 5. From these illustrative figures it is clear that only blow down facilities are to be considered. Such a facility is charged between the runs with a limited power (compressors, storage heaters, capacitor). The accumlated energy is released during the running time which is only a small fraction of the time interval between the successive runs.

The released power P can be written as

$$P = \tfrac{1}{2}\rho\, uA.u^2 = \tfrac{1}{2}\,Re_L\, M^2 a^2 \mu \frac{A}{L.}$$

For a given Mach number and Reynolds number and a given free stream temperature, which determines the local speed of sound a and viscosity μ, it is found that the released power increases proportional with a linear dimension of the facility. From this point of view a small facility, working at a high stagnation pressure is attractive. Also facility and model costs will be generally lower than for large wind tunnels working at the same Reynolds number. The minimum size will be determined by considerations, discussed elsewhere in this Chapter 3.1.

3.1.D Throat Erosion and Cooling

The feasability of a high pressure facility however, is not only limited by the strength of the pressure reservoir but also by the limit of throat melting. This becomes a problem at high Mach numbers when high reservoir temperatures are required to avoid condensation of the test gas.

The heat transfer to the wall of the nozzle throat is higher than anywhere in the facility. Its value is given as (Ref. 65, p.192):

$$Q = 0.0014\, \rho^* u^* C_p (T_o - T_w)$$

where ρ^* and u^* are the density and flow velocity in the throat. This equation can be written to:

$$Q = 0.56\, p_o\, T_o \left(1 - \frac{T_w}{T_o}\right) \frac{Watt}{cm^2}$$

where p_o is the stagnation pressure in atm and T_o the stagnation temperature in °K.

For water cooled nozzle throats limits for the tolerable heat load are given in Reference 58. A practical upper limit is 5 kW/cm². For a given p_o this determines the maximum Mach number for condensation free flow in a facility with a water cooled nozzle. It follows for a wall temperature $T_w = 600°K$ (Ref. 65).

p_o (atm):	100	500	1000	2000	5000
$T_{o_{max}}$ (°K):	9100	1225	860	720	645

When these figures are compared with Figure 11, it follows that for a wind tunnel with a water cooled nozzle throat only limited possibilities exist when M-Re duplication is to be realized.

Instead of water cooling also film or transpiration cooling of the nozzle throat may be employed such as in the NASA Ames 3.5 ft tunnel (helium cooling) (no reference known with detailed information) and the Northrop Mach 10 hypersonic facility (Ref. 66). Less than 10 percent of the tunnel weight flow is injected upstream of the throat. For a more analytical approach to the problem, see Reference 67 to 69.

Much higher heat fluxes than 5 kW/cm² can be tolerated when running times are employed which are so short that the surface temperature rise is acceptable. In Reference 41 the heat flux required to melt a tungsten throat within 1 millisecond is presented as a function of reservoir pressure and temperature (melting temperature is 3700°K) and oxygen-free nitrogen must be used as a test gas to prevent throat erosion.

The permissible pressure is inversely proportional with the square root of the running time (Ref. 70) and from Reference 41, Figure 6, the following maximum reservoir pressures are omitted for a running time of 100 milliseconds:

P_o	(atm):	100	500	1000	2000	5000
$T_{o_{max}}$	(°K):	10000	5750	4700	4000	3700

It is concluded that throat heating does not limit the M-Re duplication capabilities as required in Figure 11, when the maximum Mach number is limited to Mach 18 (see Section 3.1) and for running times shorter than 100 millisec. For longer running times and other materials the Mach number limit may be lower.

3.1.E Real Gas Effects

Almost all hypersonic facilities are based on the blow-down principle where the gas is rapidly expanded and accelerated in a converging-diverging nozzle from the stagnation or reservoir condition. This may happen so rapidly that the various degrees of freedom cannot accommodate rapidly enough and flow non-equilibrium occurs in the nozzle. A certain amount of the available enthalpy "freezes" and cannot be transformed into kinetic energy of the test section flow. Non-equilibrium effects make the flow diagnosis and definition of the test section flow conditions much more complicated and should be avoided, if possible (Ref. 71).

In Reference 41 a value for the entropy $S/_R \leqslant 32$ is selected as the criterion for equilibrium flow to be present, Reference 71 prefers $S/_R \leqslant 31$. Reference 59 gives for these entropies (real gas effects included):

P_o = 200 atm	$S/_R$ = 31	T_o =	4700°K
	32		5260°K
P_o = 1000 atm	$S/_R$ = 31		6080°K
	32		6870°K

As was pointed out in the general remarks of Section 3.1 high temperature real gas effects in the wind tunnel can be restricted to molecular vibration only, when the test section Mach number is below Mach 18 and the tunnel is operated at its equilibrium condensation temperature.

For tunnels operating at these conditions, comparison of the figures quoted above with Figure 11 would indicate that no-equilibrium nozzle flow is completely avoided. In fact however, Reference 41 sets $S/_R = 32$ as the boundary for chemical non-equilibrium. Vibrational non-equilibrium however, appears to be present at much lower entropy values than $S/_R = 31$ or 32 as is concluded from the data, presented in Reference 72.

For a throat diameter of 0.25 inch = 6.35 mm and a 5 degree half angle nozzle with a parabolic throat contour, which is a realistic case for the present discussion, it was found (Ref. 72) that for a stagnation pressure p_o = 4000 psi = 280 atm the frozen enthalpy is about 3.7% of the stagnation enthalpy for $T_o = 2000°K$ and 4.1% for $T_o = 3000°K$. These stagnation conditions correspond with entropy values $S/_R = 25.6$ and $S/_R = 27.6$ respectively.

It is concluded that vibrational non-equilibrium effects in the nozzle flow as well as around the model (Ref. 72) are in many cases not negligible. They can be minimized by using slender nozzles. For a fixed value of T_o and of $p_o L_m$ and thus also $p_o x$ throat diameter (if L_m is proportional to the test section diameter), the slenderness of the throat and the nozzle is the only parameter that affects the vibrational non-equilibrium phenomena (Ref. 72).

3.1.F Running Time

Finally, some lower limits for the running time should be considered.

Firstly, the running time must be long enough to permit steady flow to be established in the test section and around the model. For facilities with short running times, say less than 100 milliseconds, the flow is started impulsively in general by breaking a diaphragm near the nozzle throat. The starting process has been described in the literature, see for instance References 13 and 14.

A practical definition of the start time is the time during which the steady flow through the nozzle throat is not transformed into a steady flow in the test section but is rather passing through unsteady expansion waves and/or shock waves which exist in the nozzle during the starting processes. As follows from consideration of the data presented in Reference 73 and 74, this time is found by constructing the u-a characteristic for the steady-state nozzle flow in a wave diagram along the nozzle, the singularity at the throat being discussed in Reference 73 and

the particle trajectory of the steady state flow. The starting time is then equal to the ordinate in the wave diagram (or x-t diagram) in the throat where $x = 0$, of the particle trajectory which arrives at the same time in the test section as the u-a characteristic from the origin of the wave diagram (Ref. 74). This applies for an initial pressure below the free stream static pressure that will be generated when the tunnel has started. For a conical nozzle with a throat radius r_t, a nozzle half-angle tangent β and a sound speed a_o at reservoir conditions the nozzle starting times t_s have been calculated and also the time t_b between the breaking of the throat diaphragm and the establishment of steady flow in the test section.

M :	5	10	15	20
$t_s \beta \frac{a_o}{r_t}$:	1.35	2.65	4.14	5.85
$t_b \beta \frac{a_o}{r_t}$:	3.54	13.30	32.10	62.06

For instance a Mach 15 conical nozzle with a half-angle of 5 degrees at $T_o = 2000°K$ and an exit diameter of 100 cm would give $t_s = 0.5$ millisec and $t_b = 3.9$ millisec ($r_t = 0.95$ cm with high temperature real gas effects included). A contoured nozzle, which is about twice as long as a conical nozzle with the same maximum half-angle and exit diameter (without boundary layer effects) will have starting times which are roughly two times longer than the values from the table above.

For the flow establishment around the model stabilization of separated flows is the governing factor. For laminar separated flows it has been found that about 30 body lengths of flow were required for the pressure in the base region of a sphere to stabilize (body length equal to sphere diameter) and for the heat transfer a factor of two longer time was needed to reach equilibrium. For shock induced separation the flow establishment times are much shorter for the cases of interest (Ref. 75). On the leeward side of the space shuttle larger regions of laminar separated flow may occur during re-entry at large angles of incidence. The diameter of the fuselage being of the order of 0.15 of the length and assuming that 60 diameters are required for flow establishment (a somewhat arbitrary value) the flow establishment time t_e is 9 L/u, where u is the free stream velocity. For a local sonic speed of 150 m/sec (near condensation) it is found that $t_e = 60$ L/M millisec, where L is the body length in meters. This figure should be considered as an order of magnitude and will depend on the body geometry and flow conditions such as Reynolds number etc.

For a contoured nozzle with a test section diameter of 1 meter and a maximum wall angle of 5 degrees and a model length of 1 meter the following data on starting times are found

M :	5	10	15	
T_o :	500	1000	2000	°K
r_t :	10.0	2.23	0.95	cm
t_s :	6.9	2.1	1.0	millisec
t_b :	18.0	10.7	7.6	millisec
t_e :	12.0	6.0	4.0	millisec
$t_s + t_e$:	18.9	8.1	5.0	millisec

The quantity $t_s + t_e$ is to be considered as a maximum for the non-useful duration of flow from the reservoir. In practice this time will be shorter because t_s and t_e will partially overlap each other. Shock tunnels are in fact the only facilities which have been used for configuration testing which have running times that are so short that the question of flow establishment time arises. The throat size of such a facility must be compatible with the preceding shock tube diameter. A throat diameter of 20 cm as required for a Mach 5 nozzle with an exit diameter of 1 meter is certainly not realistic for present or even future high-pressure shock tunnel technology. In fact the nozzle of the Cornell shock tunnel which has been used for HST-configuration testing (Ref.42) has a 0.61 m diameter nozzle when operating between Mach 5.5 and 8.2 and a 1.22 m nozzle for Mach numbers between 10 and 17.

The running time is 2 to 13 milliseconds, the high value being for the lowest stagnation temperatures (Ref.76).

The flow establishment times being proportional with the linear dimension of the tunnel and the model it is concluded from this discussion, that possibilities of shock tunnel testing of models with a length larger than 0.5 meter are marginal at low hypersonic Mach numbers from considerations of the required running time.

Another minimum testing time criterion follows from the requirement that force measurements on complete vehicle models should be made. The consequences for the required running times are discussed in Reference 71. In impulse facilities such as shock tunnels and hot shot tunnels the force data are obtained with acceleration compensated balances. These are designed on the premise that the test model being evaluated, vibrates as a rigid

body (Ref. 71). Slender bodies and/or large models tend to generate vibrations within the model, yielding imperfect inertia compensation. When these bending resonance frequencies are high enough, they can be filtered out. For shock tunnels a minimum frequency of roughly 1000 Hz can be tolerated and this limits the model scale to something of the order of 45 cm for a model slenderness ratio of 10. For the same model geometry this frequency is inversely proportional with the model length. When a balance system, based on the premises mentioned in Reference 71 is employed, facilities with test times of the order of 50 milliseconds or more should be used for development work where model lengths of more than 0.5 meter are tested and shock tunnels fall short of this requirement.

It should be noted, however that at Cornell Aero Labs force testing was done with a HST-model with a length of 0.66 meter (Ref. 42). Interference of the vibration modes with the inertial compensation may have been avoided in this case by placing several accelerometers inside the model and then excite the model on a shaker to establish the compensation required in analogue circuits (Ref. 29).

Free flight testing techniques (Ref. 77 for instance) are probably not attractive for the development testing described in this paper because of the relatively large aerodynamic loads and the required integrity of the light weight model during flight and of the facility after impact of the model. Also the cost of complicated throw-away models should be considered.

In summary it is concluded that the running times of present shock tunnels which are of the order of 10 millisecond are marginal for development testing of models longer than, say 0.5 meter but testing is not impossible. Test times of the order of 50 milliseconds require much less attention as far as flow starting times and inertia compensation for force measurements is concerned. Also the feasibility of probe traverses (Ref. 78), scannivalves (Ref. 79) and variation of the angle of incidence during the run (Ref. 43) is greatly increased, which will increase the efficiency of each run. Also dynamic testing is facilitated when the running time is 50 milliseconds or more.

3.1.G Conclusions

The practical and principal limitations of hypersonic wind tunnel facilities for Mach number-Reynolds number duplication can be summarised as follows.

1. Acceptable sting loads require for M-Re duplication of hypersonic transport aircraft models with a length of the order of 2 meters. For testing up to Mach 8 reservoir pressures of the order of 1000 atm are then required. Whether the construction and use of such a facility is justified is open to discussion.

2. For the case of M-Re duplication of a space shuttle and for boundary layer transition close to the leading edges of a hypersonic transport ($Re_L = 2 \times 10^7$) flying not faster than Mach 10 the requirements of tunnel size/stagnation pressure are largely overlapping (Fig. 13). If one facility should do both jobs the design should lie within the following limits:

   (a) Model length $L_m > 0.3$ to 0.5 m to prevent excessive sting loads and to allow ample instrumentation

   (b) Stagnation pressure $p_o < 5000$ atm from structural considerations for the tunnel

   (c) Stagnation pressures $p_o L_m > 500$ atm.m (beter is $p_o L_m > 1000$ atm.m) in order to duplicate the Reynolds number up to large enough Mach numbers.

   (d) Up to Mach 18 at equilibrium condensation conditions high temperature real gas effects are restricted to vibrational excitation of the molecules only, and up to that Mach number the required Reynolds number can be generated without severe throat erosion problems for running times shorter than 100 milliseconds for a tungsten throat and oxygen-free nitrogen as test gas

   (e) Running times of less than 10 milliseconds are marginal for development testing on models longer than 0.5 m from the point of view of flow establishment times. A running time of more than 50 milliseconds offers more flexibility in this respect and in measurement techniques.

3.2 Facilities for Combustion and Propulsion Testing (Including Hardware Testing).

Many of the arguments which are discussed in Section 3.1 hold also for the facilities for scramjet combustion and propulsion tests. These facilities must generate the correct environment in the supersonic combustion chamber with regard to Mach number, pressure and temperature. For a given flight Mach number simulation, these facilities will run at higher stagnation temperatures and lower stagnation pressures than wind tunnels, which means that no direct limitations exist with respect to stress levels, either in the tunnel reservoir or in the combustor model. Limitations will show up with respect to tunnel power and heating system, throat cooling and erosion, running time and the composition of the air.

3.2.A Facility Power and Air Heating

For mass flows of the order of 200 kg/sec as quoted in Section 2.2 a power is required of the order of 10^3 MWatts during the run. This power is equal to a large power station and hence prohibitive in many circumstances. Therefore short running facilities with accumulation energy storage are developed. The compression heating systems (shock tunnels and gun tunnels) are the cheapest facilities in this respect. The shock tunnel might give too short running times ($<$ 10 msec), but gives almost unlimited stagnation temperature duplication (Ref. 48). Calculations show that a gun tunnel with preheated barrel may generate about 3000°K during 50 msec. with mass flows in the 10-50 kg per second range. Also hot shots (arc heating) show this performance (Ref. 48). In the gun tunnel the temperature drop due to cooling may be compensated by increasing stagnation pressure during the run (see Ref. 78 for a pressure record); in the hot shot this cooling effect is much more troublesome (see also 3.2.C).

Regeneration heating systems (such as the pebble bed) are limited by the maximal solid material temperatures attainable, typically less than 2500°K. The running times may be however several seconds to a minute or longer and therefore show good promise for hardware testing (see also 2.3).

An attractive means to increase the stagnation temperature of the supersonic burning test facility is to burn upstream of the nozzle a hydro-carbon, hydrogen or nitrogen containing fuel (NH_3, N_2H_4) and add additional oxygen (Ref. 80, 81). The air is then called vitiated air. The attainable temperature in combination with the regenerative heating system might be in the 3000°K range.

The only means to obtain higher temperatures for long periods of time, $\gtrsim$ 10 sec, is to use arc heating. However continous arc heating is limited to only moderate pressures (a few hundred atm) (Ref. 55), decreasing with increasing temperatures and hence flight Mach number, conflicting with the requrement that the tunnel stagnation pressure must increase with Mach number to allow flow duplication. The flight altitude for which arc heater facilities can provide flow duplication above say Mach 8 to 10 is therefore too far above the HST real flight altitude to allow realistic hardware testing in free jet test sections of the blow down type. However, continuous arc facilities are very useful for ablation testing, since pitot pressure and wall static pressure duplication is required rather than Mach number.

3.2.B Throat Cooling

The heat transfer equation of Section 3.1.D is used to compute the temperature-pressure limitation of continuous propulsion and hardware test facilities. This line is represented in Figure 5 (upper boundary). If the connected pipe supersonic combustion testing method is used (Fig. 10) the lower line in Figure 5 is obtained taking into account the total pressure recovery of Figure 8. These lines probably will coincide with the arc heating capacilities of the former section. Hence it can be concluded that for hardware testing (long run times) the laboratory facilities are limited to approximately free flight Mach number of 8 for free jet facilities, and to $M = 10$ for connected pipe testing for a $q = 0.5$ kg/cm^2 flight condition (Fig. 2).

3.2.C Flow Duration

The least required flow duration is of primary consideration for facility type, heating system design and throat cooling requirements. Two kinds of tests can be distinguished, namely: first, fundamental flow field and combustion tests and second, hardware tests. The first kind can be performed in short duration facilities in which the certainty of flow establishment is the main criterion apart from data collection time considerations. Reference 48 reveals that a few milliseconds seem to be sufficient, through Reference 49 indicates that tests in a hot shot tunnel, having a 200 msec runtime, yields difficulties interpreting the results, mainly due to temperature variation. Test times of at least 10 msec seem preferable. Hardware tests should be of representative duration, hence of the order of several minutes (see also Section 2.3).

3.2.D Air Contamination

From power requirements point of view the vitiated air system is very attractive, since direct heating occurs by burning. However, almost all fuels for the vitiation system contain hydrogen, so that free radicals such as OH will be present at the entrance of the combustor. These free radicals will substantially shorten the ignition delay times in the combustor, and hence will yield unrepresentative results. Furthermore the thrust as produced by the nozzle will be typically 10% less than for clean heated air (Ref. 80). Many facilities use the vitiated cycle as a topping cycle for regenerative heated air (Ref. 81). Caution must be exercised to translate results from vitiated facilities to flight conditions. For duration tests and mixing tests vitiated air systems will be useful.

3.2.E Conclusions

For long duration combustion and propulsion tests ($>$ 1 sec) complete scramjet performance assessment is limited to $M \simeq 8$, due to throat cooling capabilities. The same is true for structural testing in the real flow environment. For combustor and nozzle tests the flight Mach number duplication is limited to about 10 in the laboratory. For higher Mach number free flight testing is the only means. For scramjet hardware test a vitiated

air system gives an economical solution with respect to power requirements. For supersonic combustion and aerodynamic performance tests of scramjets short duration facilities can be used with sufficient running time. Facilities with a combination of preheating and compression heating such as gun tunnels with preheated barrel or tunnels such as the ONERA R4Ch will probably show good prospects. Also shock tunnels such as Sheffield University are very useful though the latter might be short of flow duration. For ablation studies continuous arc heaters are the best choice.

4 REMARKS ON EUROPEAN FACILITIES FOR HYPERSONIC TESTING

This section will present a brief evaluation of the performance of the major hypersonic facilities in Europe. In these facilities as well as in the smaller facilities which are located mainly at colleges and universities much work has been done of a more fundamental or exploratory character, as was mentioned in Section 1.1. (see also Ref. 5, 6 and 7). In this section, however, the usefulness of the available major facilities will be considered against the background of the requirements for testing related to the development of the space shuttle and the hypersonic transport as described in the previous sections.

4.1 Aerodynamic Testing

In Reference 7 information is presented on all hypersonic facilities existing in Europe. Their usefulness for development testing at high enough Reynolds numbers as described in the preceding chapters can be appreciated if their maximum $p_o L_m$ performance (stagnation pressure x model length) is plotted as a function of the Mach number at which the facility can be operated. Figure 11 where the required $p_o L_m$ values are plotted is then the background against which the available $p_o L_m$ can be projected.

During re-entry the space shuttle will fly at angles of attack of 25° to 60°. In order to avoid blockage of the wind tunnel flow, the model length L_m should not exceed half the core diameter (Ref. 29). For the present evaluation $L_m = 0.5\ D_m$ is assumed for the space shuttle with D_m equal to the nominal test section diameter, which is listed in Reference 7.

For the HST which is much more slender than the space shuttle and which is tested only at small angles of attack up to say 10° or 15° (Ref. 42, 62) the model length L_m can be much larger without blockage. For the present case $L_m = D_m$ is assumed for the HST.

In Reference 7 only the maximum stagnation pressure p_o of each facility is given. Having no detailed information on the dependence of p_o on the Mach number it is assumed that all facilities operate at their maximum p_o over the full Mach number range with the restriction that the maximum dynamic pressure q_m is not exceeded. This is assumed to be $q_m = 1.5$ kg/cm² for space shuttle testing and 2.2 kg/cm² for HST testing (Section 3.1.A).

This assumption on p_o can be criticized, but if the true $p_o - M$ data had been plotted in Figures 14 and 15 this had to be done for all facilities to obtain a fair basis of comparison. These data are presently not available. It is suggested that these should be included in the next edition of Reference 7.and/or it should be stated at what Mach numbers the Reynolds numbers, mentioned in Reference 7 are attained. Some remarks dealing with the p_o assumptions are given in the next sections.

From the facilities listed in Reference 7 the "major" facilities should be selected. The following criteria have been used:

Test section diameter $D_m > 0.25$ m. This means that not only facilities for models longer than say 0.3 m are included as was required for development testing (see Section 3.1.G), but also smaller facilities which are suitable for more basic or exploratory studies.

$p_o L_m > 10$ atm.m. Lower values allow adequate M-Re simulation below Mach 5, which is outside the hypersonic regime.

Running time longer than 5 milliseconds, so that most shock tunnels may also be included.

An exception is made for the few arc heater facilities and low density tunnels where no restriction is made on $p_o L_m$. The arc heater facilities can in fact be used as low density facilities, but also high temperature phenomena such as occur during re-entry can be studied.

The relevant characteristics of the remaining facilities from Reference 7, together with some additional information from Reference 4, 29 and 30 can be found in Table 1. The resulting $p_o L_m$ performance is plotted in Figure 14 and 15.

It should be remarked that most facilities operate only at specific Mach numbers rather than infinitly variable Mach numbers and the lines in Figures 14 and 15 are to be considered as facility potential performance, which can often be used by simply employing different throat blocks. Also operation at lower values of $p_o L_m$ than indicated

is of course possible. For the HST, facilities which operate only at Mach numbers above 15 and/or which have maximum Re_L-capability below 10^6 have not been plotted in Figure 15. For shock tunnels the maximum model length is assumed to be 0.5 meter to avoid too large difficulties with flow establishment times (see Section 3.1.F).

From the data on tunnel performance the following conclusions may be drawn:

4.1.A Hypersonic Testing of Space Shuttle Configurations

From Figure 14 it is concluded that the estimated performance of the large shock tunnel at TH Aachen covers the required M-Re performance for space shuttle re-entry above Mach 7.5. It is not known whether the running time is long enough, while it is given in Reference 7 as 1-10 millisec. Also the conical nozzle is a disadvantage because this entails axial pressure gradients which makes corrections necessary.

In the low hypersonic regime between Mach 5 and Mach 9 several facilities are available which have Reynolds number performance close to the lower trajectory. Some remarks are made below.

The Imperial College gun tunnel is probably still the only gun tunnel with a test section larger than 0.25 m presently available in Europe since work at Bristol and RARDE (both in the U.K.) has come to an end (Ref. 30). Although the model length is rather limited ($L_m \simeq 0.15$ m) the Reynolds numbers are rather high, which combined with a good parallel flow quality, makes the facility a useful tool in the European hypersonic tunnel inventory. In a recent note data became available of a gun tunnel at the Institute de Méchanique des Fluides at Marseille. Though this tunnel has good performances the flow in the test section is of the source type and the running time is only limited.

The ONERA S4MA blow down tunnel has an attractive Reynolds number potential capability. The facility can also be used as a combustion tunnel for ramjet/scramjet testing.

The smaller shock tunnel of TH Aachen shows no superior performance while the disadvantages are the same as for the large shock tunnel.

The blow down facilities of FFA (Sweden), ARA (U.K.) and of CEAT and the ONERA R3Ch (France) have about the same performance. Model size and tunnel costs will have to be considered.

From an economic point of view the Ludwieg tube facilities of the DFVLR and the ONERA R4Ch slow piston tunnel are attractive but their present performance is rather low.

It is doubted whether the DFVLR arc facility PK2 can work at a stagnation pressure of 100 atm down to a Mach number of 6 as indicated in Figure 14. The performance envelopes shown in Reference 4 show rather a constant maximum Re_L between $M = 5$ and 15. It is therefore supposed that the PK2 facility is not suitable for M-Re duplication and is to be used exclusively as a low density and/or high enthalpy facility.

Between about Mach 10 and 15 a gap exists where no M-Re duplication on space shuttle wind tunnel models can be realized.

Above Mach 15 the simulation of the Mach number is less urgent (see section 2.1.1.A) but several facilities for testing between Mach 15 and 20 are available in Europe namely the VKI long shot and the hot shot tunnels of ONERA. The Sud shock tunnel has the same performance as the hot shots but with a considerably shorter running time. The Reynolds number performance of the long shot duplicates Re_L at Mach 15 for the lower trajectory and is twice the hot shot tunnel Re_L performance. The model length L_m is of the order of 0.30 m for all $M > 15$ facilities. A disadvantage is the divergence of the test section flow caused by the conical nozzle except for the ONERA Arc 2 tunnel, which has a contoured nozzle.

It should be noted that testing at lower Mach numbers with the present long shot and hot shot facilities has only limited possibilities. This is because for both facility types the test gas flows out of a rather small reservoir with a constant volume, causing the stagnation pressure to drop during the run. This drop is proportional with the throat size and hence lower Mach numbers bring about a faster pressure drop (and temperature drop) during the run. This disadvantage is not present in gun tunnels and slow piston tunnels.

For low density testing several facilities are available as is shown in Table 1. It should be noted that the inviscid core diameter of the test section flow is considerably smaller than the nominal nozzle exit diameter for low density facilities due to the thick boundary layers. Therefore only the largest facilities should be considered for testing complex models. These are the DFVLR PK2 tunnel with a 60 cm nozzle diameter and the new RAE low density tunnel with a 76 cm nozzle. The PK2 facility has a uniform core diameter of 10 cm at Re/cm = 5000 at Mach 15 (?) (Ref. 4), giving a viscous interaction parameter $M/\sqrt{Re} = 0.7$ for a model length of 10 cm which is probably too small for development testing.

It is concluded that up to Mach 9 several facilities exist or are planned in Europe which offer good possibilities for space shuttle tests at duplication Reynolds numbers. A facility with a larger test section diameter of about 1 meter would offer a Re_L simulation capability covering the lower trajectory requirement as indicated in Figure 14 without being limited by the $q = 1.5$ kg/cm^2 boundary set for excessive sting loads. A model length of 0.5 m could then be accommodated, which allows more detailed measurements than presently available. Also extension of the M-Re duplication capability to higher Mach numbers to say Mach 12 is advisable to close the gap between the present Imperial College Mach 9 gun tunnel and the VKI Mach 15-20 long shot facility.

It should be noted that the lower flight altitude boundary given in this paper (Fig. 2) may shift to larger altitudes when vehicles are operated at higher lift coefficients than the present shuttle to alleviate aerodynamic heating (Ref. 11) with a corresponding decrease in maximum Reynolds number requirement. For low density research and development a facility which is large enough to accept large and complex models is presently not available in Europe. Such a tunnel should cover values of $M/\sqrt{Re}$ between 0.1 and 0.5. Provisions should be made in the tunnel pumping system for accepting not only nozzle flows but also exhaust gases from motors, reaction jets or mass injection gas (Ref. 29).

4.1.B Hypersonic Testing of HST Configuration

For testing of hypersonic configurations up to Mach 8 at $ReL = 2 \times 10^7$ European facility performance is adequate as can be concluded from Figure 15. Reynolds number duplications requires test section diameters one order of magnitude larger than presently available. The HST is a more slender configuration than the space shuttle and force measurements will be more sensitive to axial pressure gradients. Conical nozzles as employed for instance in the shock tunnels of TH Aachen are therefore unsuitable for HST tests, which require great accuracies to determine the economic feasibility of a HST system. It is questionable whether the available facilities are suitable for HST development testing where the aerodynamic behaviour of the complete airframe-engine system should be properly simulated. This requires proper engine flow simulation and a correct boundary layer thickness (at the engine intake for instance). Then higher Reynolds numbers are required which can only be realized in large facilities to avoid excessive sting loads. This requires a facility like the large Tripltee tunnels described in Section 4.2.

4.1.C Comparison with U.S. Facilities

In Reference 82 data on hypersonic facilities in the United States are presented, excluding those of the AEDC. The older AEDC facility data can be found in Reference 65. These data have been plotted in Figure 16 from which a performance envelope could be drawn. For the lower Mach numbers no dynamic pressure limits are set and only facilities with contoured nozzles have been selected. It should be noted that p_o times the test section diameter D_m is plotted rather than p_o times the model length L_m as was done in Figures 14 and 15.

In the same figure the performance envelope of the European hypersonic facilities with contoured and conical nozzles has been plotted. The S4MA facility which is presently used exclusively for propulsion testing is indicated separately.

It is found that up to about Mach 10 the M-Re duplication performance of the European facilities and the selected U.S. facilities is not very different. However, when the larger Tripltee facilities mentioned in Section 2.3, fitted with contoured nozzles are added, the picture is drastically changed. The NASA Langley 8 ft structures tunnel attains $p_o D_m = 670$ atm.m at Mach 7.5 which is close the HST Reynolds number duplication requirement and one order of magnitude larger than the performance of European facilities.

Between Mach 10 and Mach 15 there is a wide gap between U.S. and European facility Reynolds number performance, which has been widened by the new NOL 5 foot blow down facility which is to be operational by late 1972 (Ref. 63). Between Mach 15 and 29 this facility with contoured nozzles has even a higher Re_L capability than the VKI long shot.

When only facilities with contoured nozzles should be considered it should be noted that above Mach 15 no facilities are available in Europe, except for the Imperial College gun tunnel fitted with a Mach 18 nozzle and the ONERA Arc 2 tunnel.

4.1 Combustion, Propulsion and Hardware Testing

Table 2 gives a review of the facilities as used in Europe for scramjet tests and supersonic burning studies. A comparison is made with the largest facilities in the U.S. at NASA.

The main capability in Europe, the S4MA tunnel of ONERA and the main facility in the U.S. are projected in Figure 5 also. It shows that research and testing in the field of supersonic combustion and scramjets is as yet only possible at the very lower end of the practical applicability region for this propulsion means. Hence, there is a need for better facilities for this field of research and development if the hypersonic flight with the economical air breathing propulsion units is going to come.

In Europe good work of fundamental nature in the field of supersonic burning is done at the University of Sheffield in the high enthalpy shock tunnel and at the DFVLR at Porz Wahn in the pebble heated facilities.

For heat shield ablation testing the arc heated facilities of the DFVLR might be used in principle, their stagnation temperature being of the order of 5000°K (air, nitrogen) to 10000°K (argon). In order to duplicate the pitot pressure of the full scale vehicle during re-entry the facility will have to be operated at low Mach numbers, between say Mach 2 and 5 (see Section 2.3).

The PK2 facility which is the largest facility available has a power supply of 1000 KW and operates at reservoir pressures between 0.1 and 100 atm (Ref. 4). This is well within the range of the facilities for ablation testing listed in Reference 55.

On the other hand at the sixth meeting of the LaWs working group it was stated that ablation tests cannot be performed adequately in Europe. It seems therefore open to discussion whether the PK1 facility is large enough for ablation testing on a development scale.

For hardware testing connected with the hypersonic transport and its propulsion system no facility is available in Europe with sufficiently long running times, which should be more than several minutes.

However considerable effort is put in the U.S. in the design and development of Tripltee tunnels as might be concluded from the next survey.

Tripltee facilities with a test section diameter of about 1 meter are the NASA Lewis facility which recently became operational (temperature duplication up to Mach 7) and the Aerodynamic and Propulsion Test Unit (APTU), presently under construction at AEDC (Ref. 52). The NASA Lewis Hypersonic Propulsion Research Facility has a nozzle exit diameter of 1.06 meters and operates at a maximum stagnation pressure of 80 atm (Ref. 81) and a stagnation temperature of 2300°K which can be boosted to 2670°K by vitiation. The running time is 2 to 3 minutes.

In the APTU clean air flow duplication is possible up to Mach 6 (clean air) and the maximum stagnation pressure is 210 atm, which allows flow duplication at Mach 6 down to 17 km. The NASA Lewis facility was designed for testing ramjet type engines which operate at high altitudes. The APTU will provide the higher pressures and massflows needed for testing low-level and run-in missile engines (Ref. 52).

Nominally these facilities will produce the desired test flows at less than 1 m diameters. Free jet testing of missile engines can therefore be conducted only at small angles-of-attack. Succesful development of the ramjet and air-augmented rocket engines has long awaited availability of these facilities. However, these facilities are not large enough to test the small research and missile engines at high angle-of-attack conditions or any of the larger engines which will be needed for aircraft applications.

Large Tripltee facilities are the NASA Langley 8-Foot High Temperature Structures Tunnel which has been considered for testing structural test engines to be adopted for the HST (Ref. 51). In this blow-down Mach 7.5 tunnel stagnation pressures up to 280 atm and temperatures up to 2500°K can be generated (Ref. 65).

At AEDC a large Tripltee facility has been designed of the same category i.e. a nozzle with an exit diameter of 10.2 ft (3.2. meter), a stagnation pressure of 240 atm and a stagnation temperature of 2400°K. At these stagnation conditions the flow at Mach 7.7 at an altitude of about 25 km is duplicated and the running time is then about two minutes (Ref. 52). Running times of 30 minutes are possible when the flow is duplicated at Mach 7 and 43 km altitude or Mach 4 at 30 km altitude.

The performance of these U.S. Tripltee facilities corresponds with the requirements already discussed in Section 3.2.

5 CONCLUSIONS

1. During the past two decades hypersonic research has been substantial in Europe. Present activities and facilities are reflected in the Eurohyp inventory. Up to now the European facilities have been used primarily for research of a more fundamental and exploratory character. Much of this work will be applicable to the design of the space shuttle and the hypersonic transport.

2. For the space shuttle aerodynamic development testing, M-Re duplication is necessary up to about Mach 15 to include boundary layer transition effects. For the lower re-entry trajectory of the present space shuttle orbiter design this corresponds with $Re_L = 3 \times 10^7$ at Mach 6 and 6×10^6 at Mach 15.
   At high flight altitudes and velocities where the boundary layer is fully laminar, high altitude phenomena occur in the form of viscous interactions. For $M/\sqrt{Re} > 0.01$ this viscous interaction parameter should be duplicated rather than M and Re separately.
   High temperature real gas effects cannot be duplicated in sub-scale testing due to conflicting scaling laws. Partial simulation and experiments of a more basic nature should provide the required information.

3. For the hypersonic transport attention is focussed to Mach 6-8 cruise conditions. The Reynolds number Re_L for a 75 m long vehicle is then of the order of 2×10^8, giving a boundary layer which is almost completely turbulent. $Re_L = 2 \times 10^7$ is considered as a minimum requirement for HST development testing where absolute performance data should be obtained. Reliable extrapolation to the full scale Re_L seems then feasible. The boundary layer thickness at $Re_L = 2 \times 10^7$ is however 60% larger than at $Re_L = 2 \times 10^8$, the consequences of which should be considered with care.

4. For scramjet propulsion testing the Mach number in the combustor must be duplicated. For hydrogen fueled scramjets the combustor entrance static temperature should be above 1000°K and up to about 1500°K reaction rates are dominant over mixing in the combustion process. This corresponds with a flight Mach number of 10 to 12 or a stagnation temperature of 4000°K to 5000°K. Up to these temperatures T_o duplication is essential. For good understanding of the combustion phenomena the pressure level should be duplicated as well as the geometry. Scaling laws can only be used if the overall chemical kinetics behaviour can be described by simple rules and if variable induction times do not exist.

5. Hardware testing of ablative materials is generally performed in arc heated facilities where the stagnation enthalpy and the pressure on the vehicle are the primary simulation parameters. For hardware testing of the HST airframe and propulsion system large true temperature tunnels (Tripltee facilities) are required with running times of at least several minutes. Typical characteristics are $p_o = 250$ atm, $T_o = 2500$°K and a test section diameter of the order of 3 meters.

6. For aerodynamic testing of space shuttle and HST configurations the following limitations were found:

   (a) Sting loads. For space shuttle testing the dynamic pressure should not exceed about 1.5 atm when testing at maximum normal force coefficient. For HST models the dynamic pressure limit will be determined by the angle of attack range. At $C_N = 0.25$ the dynamic pressure should not exceed about 2 atm (cruise condition is $C_N \simeq 0.04$). Starting and stopping loads have not been considered.

   (b) The tunnel reservoir pressure should not exceed 5000 atm for structural reasons.

   (c) Up to Mach 18 throat heat transfer does not limit the Reynolds number capacity when the tunnel is operated at minimum temperature for condensation free flow and for running times shorter than 100 milliseconds (tungsten throat, nitrogen test gas). For longer running times and other materials the Mach number limit may be lower.

   (d) Real gas effects can be restricted to molecular vibration only, if the flow Mach number is below 18 when the tunnel is operated at equilibrium condensation conditions.

   (e) A running time of the order of 10 milliseconds as is current shock tunnel practice is marginal for testing of models longer than say 0.5 meter due to tunnel starting and flow establishing times.

7. For propulsion testing the following factors affect the facility performance. For long duration ($>$ 1 sec) test complete scramjet performance assessment, including intake performance, is limited to about Mach 8 due to throat cooling capabilities. For combustor and nozzle tests the flight Mach number is limited to about 10 in the laboratory. For scramjet hardware testing a vitiated air system gives an economical solution with respect to power requirements. For combusting and aerodynamic performance tests of scramjets short duration facilities can be used. Gun tunnels with preheated barrel or shock tunnels will show good prospects, though the latter may be short of flow duration.

8. The following conclusions are made on the European facility performance for aerodynamic development testing:

   (a) For testing of space shuttle configurations at duplicating Reynolds numbers and of HST configurations at $Re_L = 2 \times 10^7$ several facilities are available in Europe up to Mach 9. Betweeen Mach 9 and Mach 15 no facilities exist with high enough Reynolds numbers. Between Mach 15 and 20 some facilities with high enough Reynolds numbers are present but they have conical nozzles which give no parallel test section flow. Low density phenomena can be simulated up to $M/\sqrt{Re}$ values of more than 1.

   (b) The model sizes which can be accommodated are rather small and sometimes even too small for development work. Space shuttle models with a length of about 0.3 m can be accommodated and in the low density facilities the model length will be of the order of 0.1 m at high $M/\sqrt{Re}$ values. For HST configurations a model length of about 0.5 m can be accepted and this is again rather small for development work.

   (c) For HST development testing at duplicating Reynolds numbers no facility is available in Europe.

   (d) Three extensions of the present European testing capability can be considered:

      (i) A facility with a contoured nozzle with an exit diameter of about 1 meter and operating up to Mach 12 or 15 and a maximum stagnation pressure of the order of 1000 atm.

      (ii) A low density facility which can accommodate fairly large and complex models in which also jet pluming phenomena (reaction jets for instance) can be studied. The facility should cover values of $M/\sqrt{Re}$ between 0.1 and 0.5 and the inviscid core diameter should be of the order of at least 0.5 m.

(iii) A large facility with a test section diameter of about 3 m, and stagnation conditions of 250 atm operating up to Mach 7 or 8 for HST development testing.

9. On the combustion testing capability in Europe it is concluded that this is presently only possible up to corresponding flight Mach numbers of about 6 which is at the very lower end of the applicability region of scramjets. The work in the Sheffield University shock tunnel at high stagnation temperatures but rather short running times and the available longer duration facilities (> 1 sec) might be complemented by a 100 millisecond facility with a stagnation temperature capability of $2500 - 3000°K$ and mass flows between 10 and 100 kg/sec.

10. For hardware testing the following is concluded. For ablation tests on a reasonable scale the facility performance of the largest available arc heated facilities is marginal and possibly not adequate. For hardware testing connected with the hypersonic transport a large Tripltee facility with a running time of several minutes or longer is required. No such facility at present exists in Europe.

ACKNOWLEDGEMENT

The authors wish to thank Dr L.Pennelegion of RAE for his valuable comments on the draft version of the present paper.

REFERENCES

1. Ulsemer, E. — *Almost all Conditions are "Go" for the Space Shuttle.* Aerospace International, May–June 1972, pp.6-16.

2. Anon. — *European Delay Post-Apollo Meeting.* Aviation Week and Space Technology, July 17, 1972, p.19.

3. Ceresuela, R. — *Stabilité et Contrôle d'Avions Hypersoniques.* L'Aéronautique et L'Astronautique, 1971, 5, pp.33-47.

4. Koppenwallner, G. — *Wind Tunnel Testing on Real Configurations in Hypersonic Flow.* A summary of current studies at DFVLR. DLR FB 71–49.

5. Davies, L. (ed.) — *Eurohyp, European Hypersonic Research.* Part 1. List of programme items. RAE Tech Memo Aero 1345, 1971.

6. Davies, L. (ed.) — *Eurohyp, European Hypersonic Research.* Part 2. Comments on current work. RAE Tech Memo Aero 1351, 1971.

7. Rogers, E.W.E., Davies, L. (ed.) — *European Hypersonic Research: Experimental Facilities.* 2nd (revised) edition RAE Tech Memo Aero 1308, 1971.

8. Hieronymus, W.S. — *Three Shuttle Concepts Studied.* Aviation Week and Space Technology, Jan. 10, 1972, pp.46-48.

9. Anon. — *Sortie Module may cut Experiment Cost.* Aviation Week and Space Technology, Jan. 17, 1972, p.17.

10. Tolle, H. et al. — *Entwicklung der Konfiguration eines aerodynamischen Wiedereintrittsflugversuchkörpers unter besonderen Berücksichtigung der Stabilität und der Manövrierbarkeit.* Presented at 7th ICAS, 1970 and in DGLR Jahrbuch 1970, p.59-74.

11. Townend, L.H. — *Some Design Aspects of Space Shuttle Orbiters.* RAE TR 70139, 1970.

12. Mysliwetz, F., Przibila, H. — *Aerodynamische Erwärmung in Hyperschallbereich und Flugeigenschaften von Raumflugkörper.* Teil II. BMBW-FB, W71–49, 1971.

13. Tannas, L.E. — *Re-Entry Guidance through Closed-Form Equations.* AIAA J., June 1967, pp.1102-1109.

14. Eggers, A.J. et al. — *Hypersonic Aircraft Technology and Applications.* Astronautics and Aeronautics, June 1970, p.30-41.

15. Bencze, D.P., Sorensen, N.E. — *A Comparative Study of Three Axisymmetric Inlets for a Hypersonic Cruise Mission.* J. Aircraft, July 1971. p.516-522.

16. Escher, W.J.D. — *Composite (Rocket/Airbreathing) Engines Overview and Technology Assessment.* UTST-VKI Lecture Series on Technology of Space Shuttle Vehicles, November 1970.

17. Marguet, R., Huet, C. — *Recherche d'une Solution Optimale de Stato-Reacteur à Géometrie Fixe, de Mach 3 à Mach 7, avec Combustion Subsonique, puis Supersonique.* T.P. ONERA No.656.E (1968).

18. Ceresuela, R. — *Aérodynamique d'un Avion Propulsé à Mach 7.* L'Aéronautique et l'Astronautique 1969–6, pp.45-55.

19. Küchemann, D. — *Hypersonic Aircraft and their Aerodynamic Problems.* RAE Tech Memo Aero 849, 1964.

20. Seddon, J., Spence, A. — *The Use of Known Flow Fields as an Approach to the Design of High Speed Aircraft.* AGARD Conf. Proc. No.30, 1968.

21. Kipke, K. — *Experimental Investigation of Wave Riders in the Mach Number Range from 8 to 15,.* AGARD C.P.30, 1968.

22. Küchemann, D. — *A Survey of Some European Hypersonic Research.* RAE Tech Memo Areo 1239, 1970.

23. Fuhs, A.E. — *Combustion Research Problem Associated with Advanced Air Breathing Engines.* AIAA Paper 71-1. AIAA 9th Aerospace Sciences Meeting, Jan. 1971.

24. Johnson, P.J. et al. — *Studies of Engine Airframe Integration on Hypersonic Aircraft.* Journal of Aircraft, Vol.8, No.7, July 1971.

25. Cubbage, J.M., Kirkham, F.S. — *Investigation of Engine-Exhaust-Airframe Interference on a Cruise Vehicle at Mach 6.* NASA TND-6060, Jan. 1971.

26. Soulier, C. et al. — *La Soufflerie Hypersonique S4MA. Utilisation pour des Essais de Statoréacteurs à Combustion Supersonique d'Hydrogène.* L'Aéronautique et l'Astronautique. No.36, 1972–4, pp.25-36.

27. Van der Bliek, J.A. — *Aerodynamic Testing at High Velocities.* Von Kármán Institute CN 45, 1964.

28. NASA — NASA Space Shuttle Technology Conference. Volume I – *Aerothermodynamics, Configurations and Flight Mechanics.* NASA TM X-2272, 1971.

29. Pennelegion, L. — *Comments on LaWs Paper 87.* Private communication. June 1972.

30. Stollery, J.L. — *A Position Paper on Hypersonic Boundary Layer Research.* Techn Rep. ARC 33 491 HYp. 893, 1972.

31. Johnson, C.B. — *Boundary Layer Transition and Heating Criteria Applicable to Space Shuttle Configurations from Flight and Ground Tests.* NASA TM X-2272, Paper 5 (see Ref. 25).

32. McNamara, J. — *Orbiter Entry Trajectory Control.* Part I: *High Speed Entry Phase.* NASA TM X-2272, Paper 19-1 (see Ref.25).

33. Hopkins, E.J., Inouye, M. — *An Evaluation of Theories for Predicting Turbulent Skin Friction and Heat Transfer on Flat Plates at Supersonic and Hypersonic Mach Numbers.* AIAA J. June 1971, pp.993-1003.

34. Van Dries, E.R., Boison, J.C. — *Experiments on Boundary Layer Transition at Supersonic Speeds.* J. Aeron. Sciences, Dec. 1957, pp.885-899.

35. Daum, F.L., Gyarmathy, G. — *Condensation of Air and Nitrogen in Hypersonic Wind Tunnels.* AIAA Journal, March 1968, pp.458-465.

36. Anon. — *Capabilities of the Von Kármán Institute for Fluid Dynamics Relevant to the Space Shuttle Program.* Issued November 1970.

37. Wuest, W., Koppenwallner, G. — *Experimentelle und theoretische Untersuchungen verschiedener Konfigurationene von tragenden Wiedereintrittskörpern in hypersonischer Strömung geringer Dichte.* Presented at 7th ICAS, 1970 and in DGLR Jahrbuch 1970, pp.75-90.

38. Hidalgo, H., Vaglio-Laurin, R. — *High Altitude Aerodynamics and its Effects on Lifting Re-Entry performance.* Proc. of 18th Intern. Astronautical Congress, Belgrade 1967. Propulsion and Re-entry, Vol. III.

39. Süsz, A. — *Studie über die Nützlichkeit steuerbarer auftriebserzeugender Wiedereintrittskörper.* BMBW-FB W70-49, 1970.

40. Bray, K.N.C. — *Non Equilibrium Flow Problems of Space Shuttles.* ARC 32, 408 Hyp. 834, 1970.

41. Leonard, R.L., Rose, P.H. — *Feasability of a High Performance Aerodynamic Impulse Facility.* AIAA Journal, March 1969, pp.448-457.

42. Penland, J.A., Romeo, D.J. — *Advances in Hypersonic Extrapolation Capability Wind Tunnel to Flight.* AIAA Paper No. 71-132, 1971 or J. Aircraft, Nov. 1971, pp.881-884.

43. Poisson-Quinton, Ph. — *From Wind Tunnel to Flight, the Role of the Laboratory in Aerospace Design.* J. Aircraft, May–June 1968, pp.193-214.

44. Whitehead, A.J. — *Flow Field and Drag Characteristics of Several Boundary Layer Tripping Elements in Hypersonic Flow.* NASA TN D-5454, 1969.

45. Ames Research Staff — *Equations, Tables and Charts for Compressible Flow.* NACA Rep. 1135, 1953.

46. Rubert, K.F. — *Hypersonic Ramjets for Space Shuttle.* UTST-VKI Lecture Series on Technology of Space Shuttle Vehicles, Nov. 1970.

47. Just, Th., Schmelz, F. — *Measurements of Ignition Delays of Hydrogen-Air Mixtures under Simulated Conditions of Supersonic Combustion Chambers.* AGARD C.P. 34, Sept. 1968.

48. Swithenbank, J., Parsons, R.J. — *Experimental Techniques for Supersonic Combustion Research in a Shock Tunnel.* AGARD C.P.38, Sept. 1967.

49. Osgerby, I.T., Smithson, H.K. — *Operation of Hotshot Tunnel F with Air as Test Gas.* Fifth Hypervelocity Techniques Symposium, Vol.I, Univ. of Denver, March 1967.

50. ONERA — Activités 1970, p.6 and idem 1971, p.142.

51. Henry, J.R. McLellan, C.H. — *Air-Breathing Launch Vehicle for Earth-Orbit Shuttle.* New technology and development approach. J. Aircraft, May 1971, pp.381-387.

52. Anon. — AEDC hypersonic true temperature tunnel (Tripltee).

53. Becker, J.V. — *Prospects for the Actively Cooled Hypersonic Transport.* Astronautics and Aeronautics, Aug. 1971, pp.32-39.

54. Anon. — *Two Sides of the Shuttle.* Flight International, 6 July 1972, pp. 30 and 31.

55. Hurwicz, H. — Aerothermo chemistry studies in ablation. In: *Combustion and Propulsion, High Temperature Phenomena*, Fifth AGARD Colloquium held in Braunschweig, April 1962, Edited by R.P.Hagerthy et al. Pergamon Press 1963.

56. Lewis, C.H., Burgess, E.G. III — *Altitude-Velocity Table and Charts for Imperfect Air.* AEDC-TDR-64-214, 1965.

57. Kivel, B. — *Radiation from Hot Air and its Effect on Stagnation Point Heating.* J. Aerospace Sciences, Febr. 1961.

58. Cann, G.L., Buhler, R.D. — *A Survey and Prediction of the Performance Capability of Co-Axial Arc Heaters.* AGARDograph 84, Part I, pp.283-321, 1964.

59. Brahinsky, H.S., Neel, C.A. — *Tables of Equilibrium Thermodynamic Properties of Air.* Vol. III. Constant entropy. AEDC-TR-69-89, 1969.

60. Culotta, S., Richards, B.E. — *Methods for Determining Conditions in Real Nitrogen Expanding Flows.* VKI TN 58, 1970.

61. O'Lone, R.G. — *Hypersonic Transport Study Grows.* Aviation Week and Space Technology, June 22, 1970, pp.44-50.

62. Ellison, J.C. — *Investigation of the Aerodynamic Characteristics of a HST Model at Mach Numbers to 6.* NASA TN D-6191, 1971.

63. Giowacke, W.J. et al. — *The NOL Hypervelocity Wind Tunnel.* AIAA Paper No. 71-253, 1971.

64. Davies, L. et al. — *Experiments on Flat Delta Wings and Waveriders up to Angles of Incidence and Mach Numbers Suitable for Lifting Re-Entry.* Proc. of 8th Internat. Shock Tube Symposium, London 1971, Ed. J.L.Stollery et al.

65. Pope, A., Goin, K.L. — *High Speed Wind Tunnel Testing.* John Wiley, New York, 1965.

66. Wong, W.F. — *Comments on Film Cooling of the Nozzle Throat of the Northrop Aerosciences Lab. (NAL) Mach 10 Hypersonic Facility.* Private Communication Ref. 3744-70-8, 1970.

67. Librizzi, J. Cresci, R.J. — *Transpiration Cooling of a Turbulent Boundary Layer in an Axisymmetric Nozzle.* AIAA Journal, April 1964, pp.617-624.

68. Roland, H.C. et al. — *Film and Transpiration Cooling of a Nozzle Throat.* AEDC-TR-66-88, 1966.

69. Lewis, H.F., Horn, D.D. — *A Film Cooling Experiment on a Convergent-Divergent Nozzle.* AEDC-TR-66-78, 1966.

70. Cox, R.N., Winter, D.F.T. — *The Light Gas Hypersonic Gun Tunnel at ARDE.* AGARD Rep. 139, 1957.

71. Neumann, R.D. — *Special Topics in Hypersonic Flow, Section IV: Ground Test Facilities.* AGARD Lecture Series No.42, Vol. I, Lecture 7, edited 1972.

72. Stollery, J.L. et al. — *The Effects of Vibrational Relaxation on Hypersonic Nozzle Flows.* Chapter 3 of: *The High Temperature Aspects of Hypersonic Flow.* AGARDograph 68, 1964.

73. Smith, C.E. — *The Starting Process in a Hypersonic Nozzle.* J. Fluid Mechanics, Vol.24, Part 4, pp.625-640, 1966.

74. Marmey, R., Guibergia, J.P. — *Etude Expérimentale des Phénomènes Accompagnant l'amorcage d'une Tuyère Hypersonique.* Comptes Rendus, Acad. des Sciences de Paris, Tome 271, 15 juillet 1970. Série A, pp.106-109.

75. Holden, M.S. — *Establishment Time of Laminar Separated Flows.* AIAA Journal, Nov. 1971, pp.2296-2298.

76. Anon. — *Description and Capabilities of the Cornell Aeronautical Laboratory Hypersonic Shock Tunnel.* May 1969.

77. Enkenhus, K.R. et al. — *Free Flight Static Stability Measurements of Cones in Hypersonic Flow.* Von Kármán Institute VKI TN 66, 1970.

78. Perry, J.H., East, R.A. — *Experimental Measurements of Cold Wall Turbulent Hypersonic Boundary Layers.* In: *Hypersonic Boundary Layers and Flow Fields.* AGARD Conference Proc. No.30, 1968.

79. Hawkins, R., Charlton, E. — *The Use of a Gun Tunnel for Hypersonic Intake Calibration.* Bristol Rep. No. AP 5477, 1967.

80. Edelman, R.B., Spadaccini, L.J. — *Theoretical Effects of Vitiated Air Contamination on Ground Testing of Hypersonic Airbreathing Engines.* Journal of Spacecraft, Vol.6, No.12, Dec. 1969.

81. Pirrello, C.J., et al. — *An Inventory of Aeronautical Ground Research Facilities.* Vol.II *Air Breathing Engine Test Facilities.* NASA CR-1875, November 1971.

82. Pirrello, C.J., et al. — *An Inventory of Aeronautical Ground Research Facilities.* Vol. I *Wind Tunnels.* NASA CR-1874 or ARC 33485, November 1971.

83. Suttrop, F. — *Ueberschallverbrennung, Zweck und eigene Versuchseinrichtungen.* Jahrbuch 1963 der WGLR.

84. Stewart, J.T. — *Evolving Strategic Air Power and B-1.* Astronautics and Aeronautics, June 1972.

TABLE 1

Hypersonic Wind Tunnels in Europe (Ref.38)

Test section > 0.25 m diameter or height
Running time > 5 millisec
Test gas: air or nitrogen
Stagnation pressure x test section diameter ⩾ 10 atm–m

Blow Down Tunnels (running time more than 2 seconds)

Facility	*Test section/ diameter*	M	$p_{0_{max}}$	$T_{0_{max}}$	*Running time*	*Countoured nozzle*
	m		atm	°K	sec.	–
ONERA R2Ch	0.33	5, 6, 7	80	650	35	yes
ONERA R3Ch	0.33	5–10	170	1100	10–35	yes
ONERA S4MA	0.69	6	40	1850	60	
ONERA S4MA	0.7 – 0.9	7–12	150	1850	10–60	planned
CEAT Poitiers	0.63	7, 8.2	100	1000	40	yes
DFVLR Hyp H2	0.60	6–11.2	60	1400	120	
DFVLR Üs A_H	0.30 x 0.30	– 6.3	40	570	30–60	
CRA	0.35	6–8	100	800	30	
CRA	0.35	10–12	100	1400	40	
FFA Hyp 500	0.50	7.15	120	800	180	yes
RAE Bedford 3′ x 4′	0.92 x 1.22	5	12	420	cont.	yes
ARA Bedford	0.30	6, 7, 8	200	850	60	
BAC 18″	0.46 x 0.46	6	20–34	460	380	
Tube Tunnels					millisec	
DFVLR Göttingen	0.5	5–7	40	400–600	300	
	0.5	9–12	150	750–1100	300	
Slow Piston Tunnels						
ONERA R4Ch	0.325	10–15	200	1700	200	
Hot Shot Tunnels						
ONERA ARC1	0.50	15–20	2000	5000	100	
ONERA ARC2	0.70	15–20	1500	7000	100	yes
CRA Hot shot	0.60	10–20	–	8000	40–70	
Long Shot Tunnels						
VKI	0.61	15–20	4000	2600	10–40	no
Gun Tunnels						
Imperial College No.2	0.31	9	700	1500	20	yes
Imperial College No.2	0.46	18	700	1500	20	yes
I.M.F. Marseille	0.35	9–10	400	~1500	5–10	no
Shock Tunnels						
Sud C_2	1.20	18	1000	4500	12–16	
TH Aachen	0.50*	6–15	200	7000	1–10	
TH Aachen	2.00*	6–25	2000	8000	1–10	no
RAE Farnborough 15″	0.38 x 0.38	7–15	250	4500	10	yes, to be uprated
ARC Heaters						
DFVLR PK1	0.30	5–20	10	5000	cont.	
DFVLR PK2	0.60	5–20	10(100)	6000	cont.	
DFVLR Göttingen	0.25	4–10	0–4	8000	cont.	

(Continued)

* A maximum throat diameter of 5 cm – which is current shock tunnel practice (Ref.76) – has been assumed, giving a smaller test section at the lower Mach numbers. No real gas effects are taken into account for calculation of this test section diameter.

Table 1 continued

Facility	*Test section/ diameter*	M	$p_{0\,max}$	$T_{0\,max}$	*Running time*	*Contoured nozzle*
	m		atm	°K	sec.	–
Low Density Tunnels						
ONERA R5	0.35	7–10	~1	1100	50	
CNRS SR3	0.36	18, 20	4	1800	cont.	
Low Density Tunnels						
DFVLR Göttingen VK1	0.25	7, 25	3;500	3000	8 hr	
DFVLR Göttingen VK2	0.40	10, 15, 20	30	1200	cont.	
RAE LDT	0.76	6, 10	50	1400 (Air) 2300 (N_2)	cont.	yes, to be uprated

TABLE 2

Facilities in Europe for Hypersonic Engine Tests and US Tripltee Facilities

Institute, name	$T_{0\,max}$	p_0	*mass flow*	*combustion test section area*	*kind of heating*	*run time*	*Ref.*
	°K	atm	kg/sec	cm^2		sec.	
ONERA S4MA*	1850	15	5 at $T_0 = 1850$°K	~130	pebble bed	10–60	26
	1850	150	35	–	pebble bed		
R4Ch	1700	3.7 (after throttling)	2.5 at $T_0 = 1700$°K	80	slow piston compression in preheated tube	0.2	17
Univ. of Sheffield	2000–6000	500		80	shock tunnel	0.004	48
DFVLR P.W.	1800		0.15	25	pebble bed		83
P.W.?	1800	60	1		pebble bed		83
NASA Langley 8 ft HTST	2500	280		47000 (free jet)			65
NASA Lewis TTT	2300(2670)	80	100	8000 (free jet)	inductive heating (with vitiation)	120–180	81
AEDC APTU	1700	210			pebble bed		52
AEDC TTT (design)	2400	240	2300	80000	pebble bed	30–3600	52

* Condition for a particular case

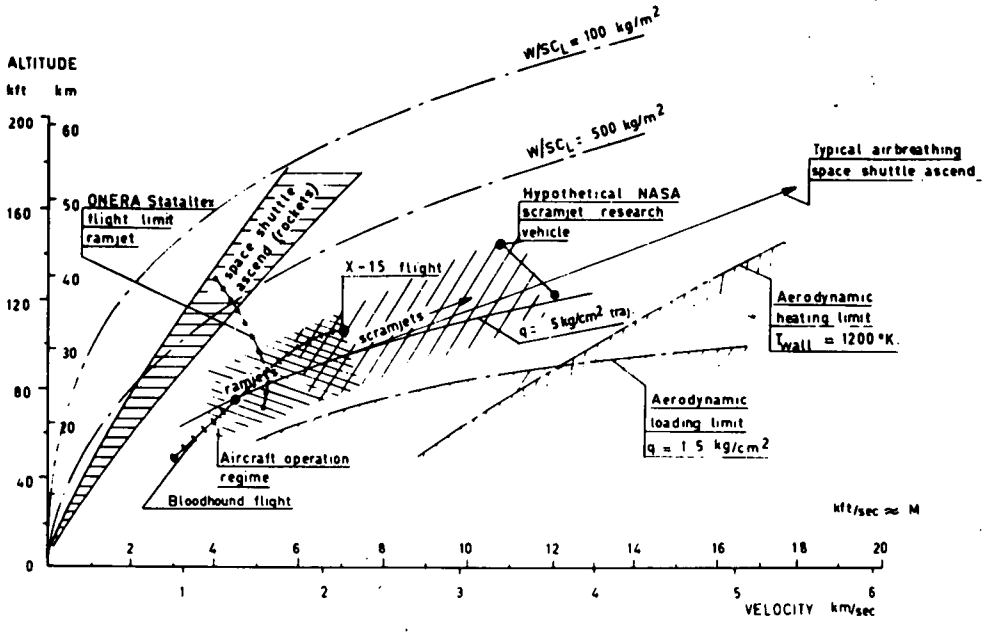

FIG. 1 TRAJECTORIES OF VARIOUS FLYING AND HYPOTHETICAL VEHICLES WITH AIRBREATHING ENGINES.

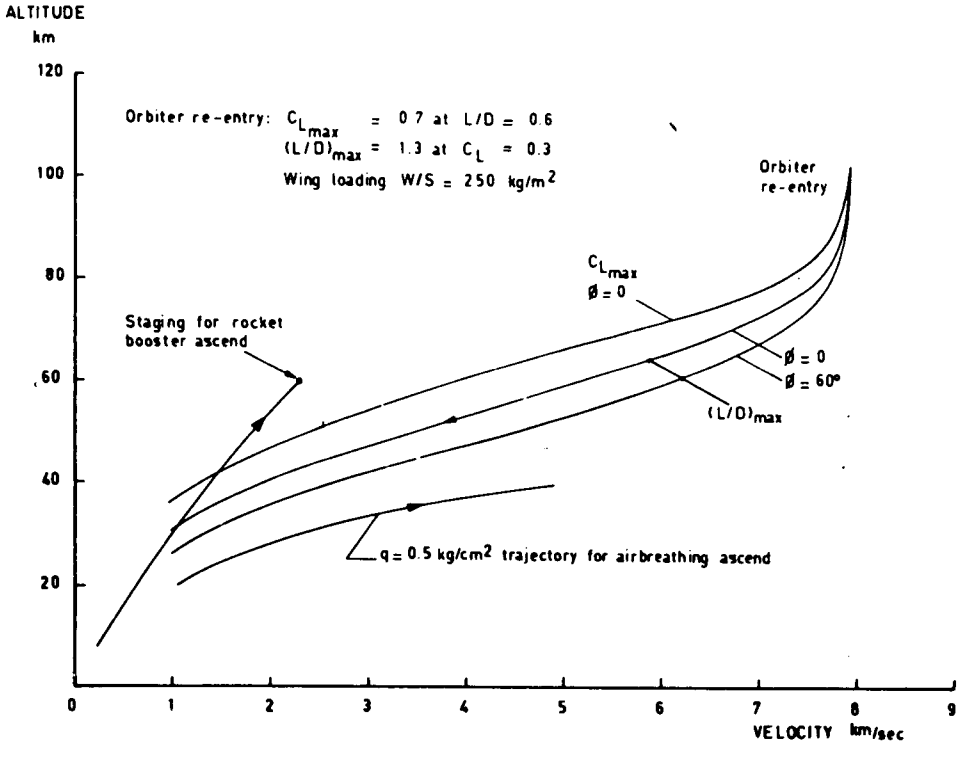

FIG. 2 SPACE SHUTTLE TRAJECTORIES FOR ASCEND AND DESCEND.

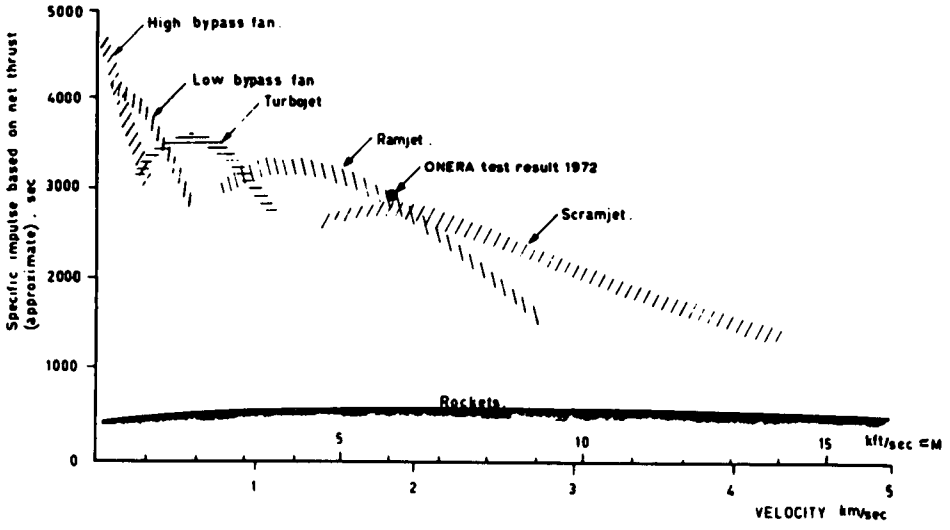

FIG. 3 SPECIFIC IMPULSE VS. FLIGHT SPEED FOR VARIOUS ENGINES.

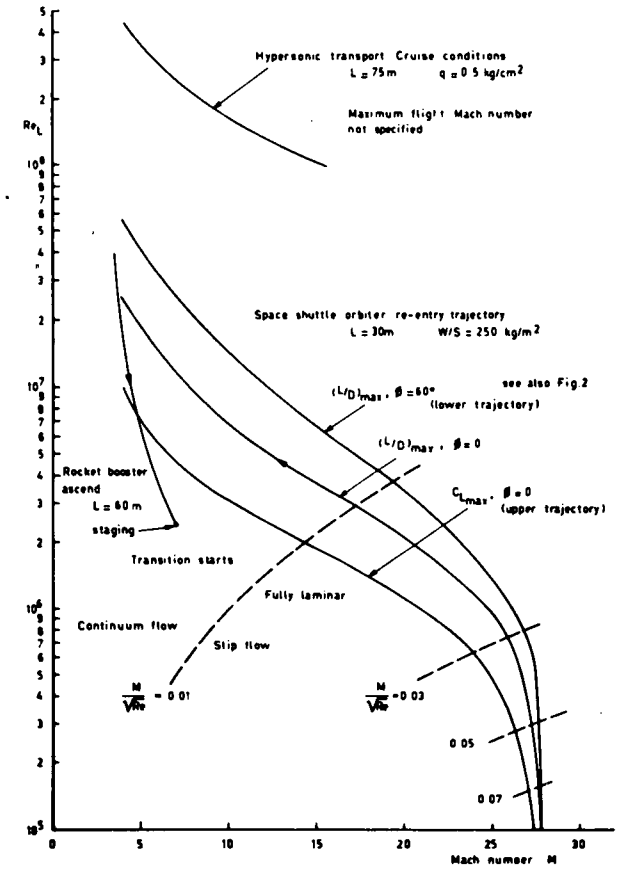

FIG. 4 REYNOLDS NUMBER – MACH NUMBER CHART FOR THE SPACE SHUTTLE AND A HYPERSONIC TRANSPORT.

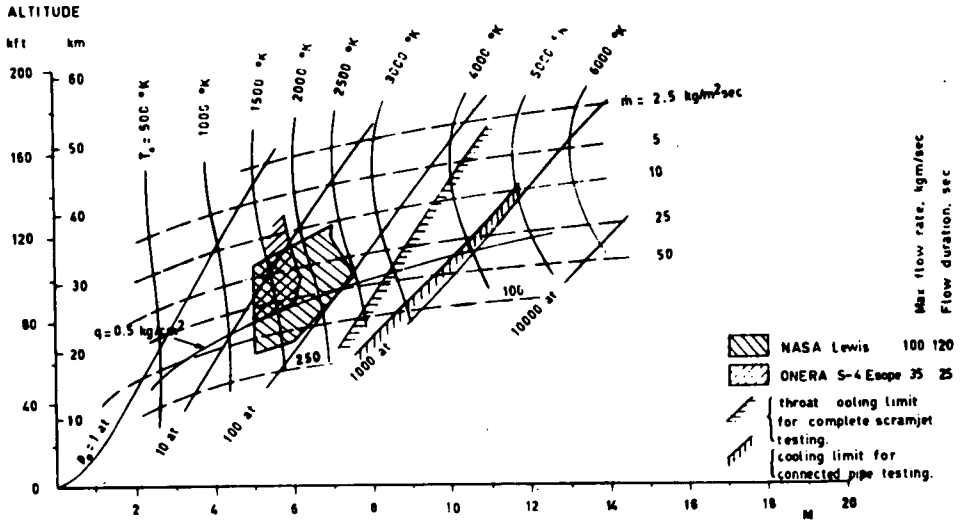

FIG. 5 STAGNATION CONDITIONS FOR FLOW DUPLICATION AND REQUIRED MASS FLOW PER UNIT CAPTURE AREA FOR GROUND TEST PROPULSION FACILITIES.

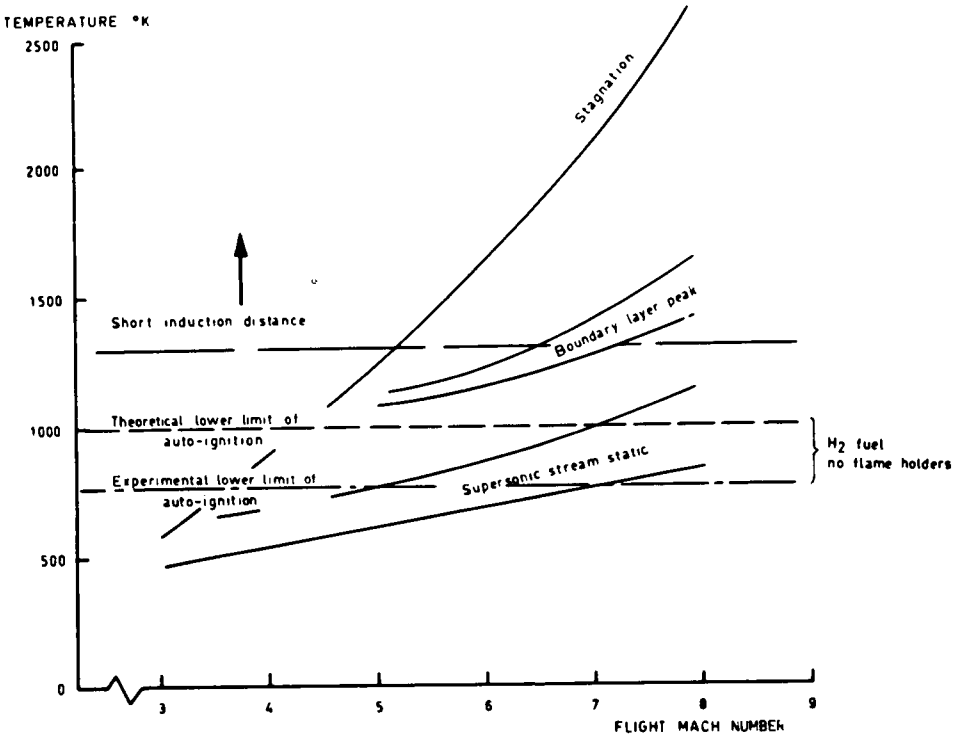

FIG. 6 COMBUSTOR ENTRANCE TEMPERATURE FOR A RANGE OF FLIGHT MACH NUMBER.

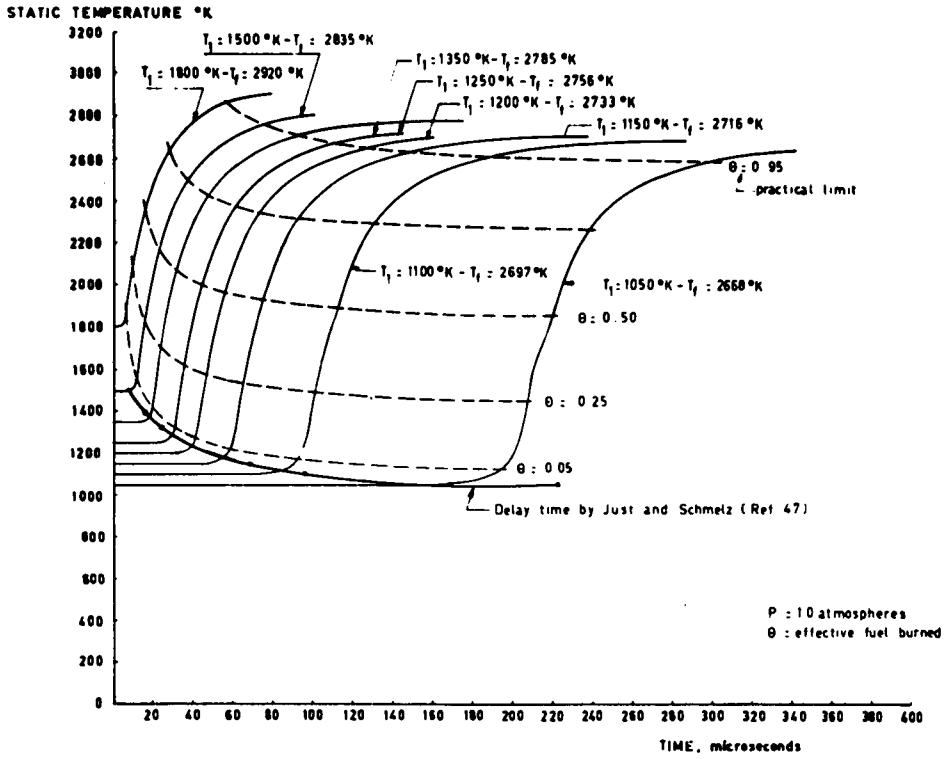

FIG. 7 COMBUSTION TEMPERATURE VARIATION WITH TIME FOR PREMIXED STOICHIOMETRIC HYDROGEN.

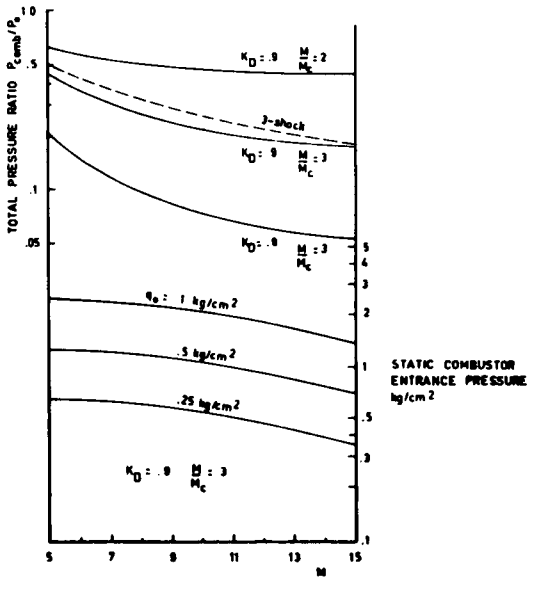

FIG. 8 TYPICAL TOTAL PRESSURE RECOVERIES FOR SCRAMJET INLETS AND CHAMBER STATIC PRESSURE LEVEL VERSUS FLIGHT MACH NUMBER (REF. 44).

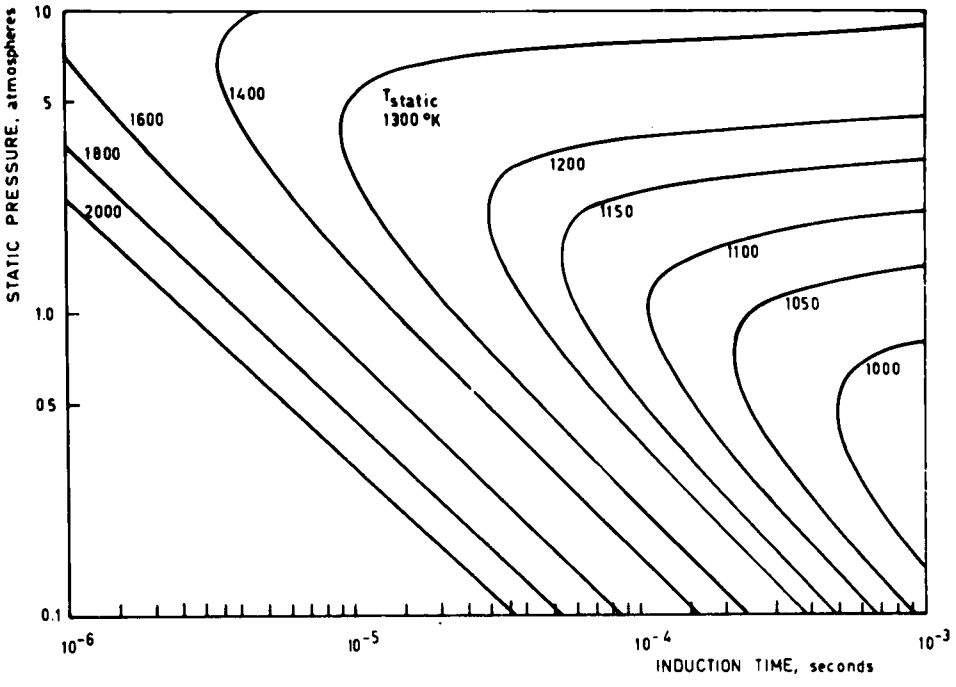

FIG. 9 STOICHIOMETRIC HYDROGEN–AIR INDUCTION TIME VERSUS STATIC PRESSURE AND TEMPERATURE. OH CONCENTRATION AT 10^{-5} MOLES/LITER.

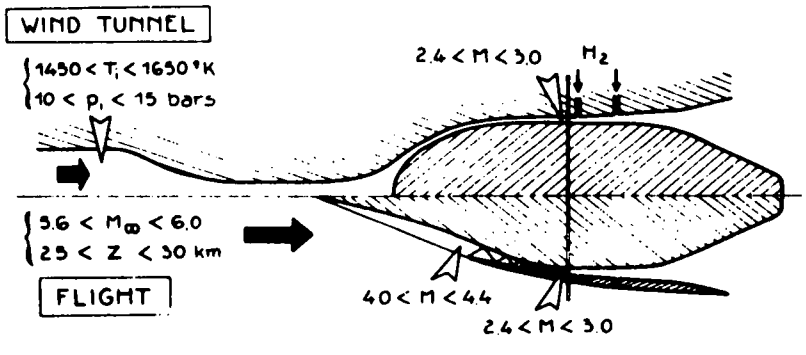

FIG. 10 SCRAMJET SIMULATION WITH CONNECTED PIPE (ONERA – ESOPE).

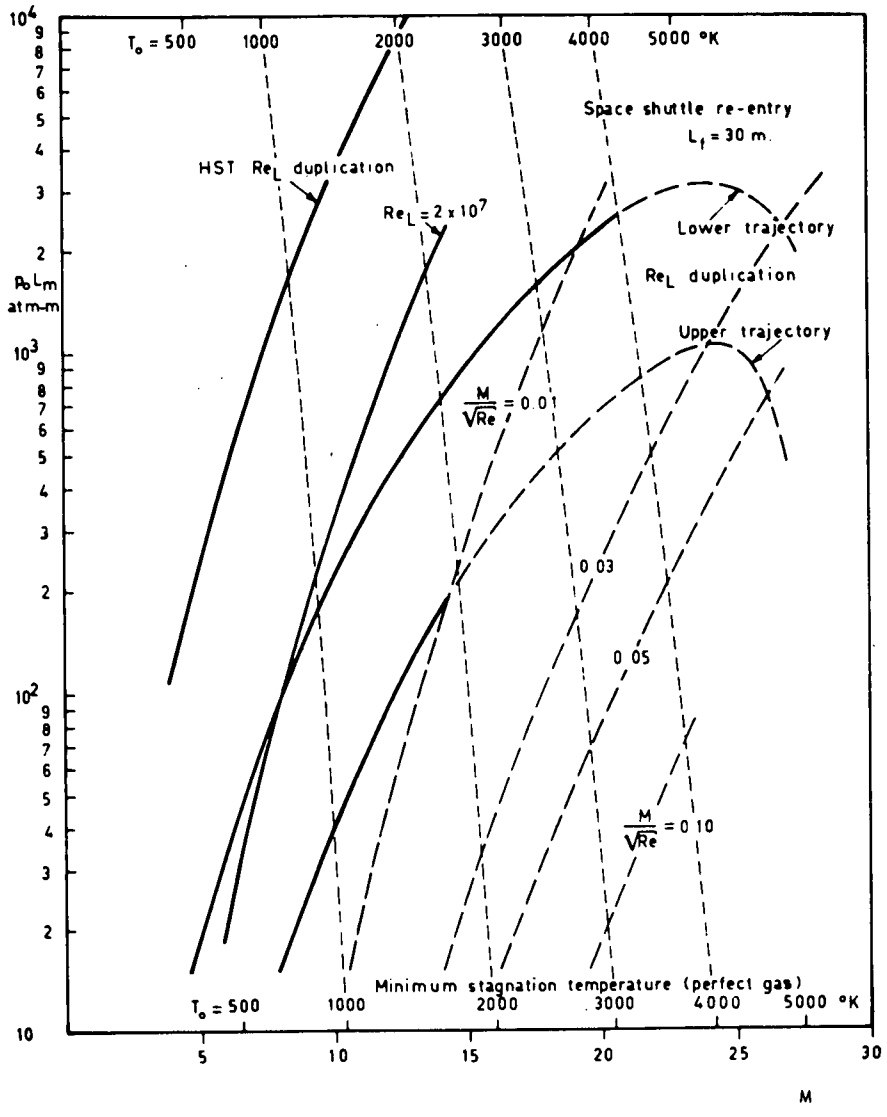

PERFECT GAS
EQUILIBRIUM CONDENSATION LIMIT
MODEL LENGTH L_m = 1 METER
SEE ALSO FIG. 4

FIG. 11 WIND TUNNEL STAGNATION PRESSURE TIMES MODEL LENGTH, REQUIRED FOR REYNOLDS NUMBER DUPLICATION.

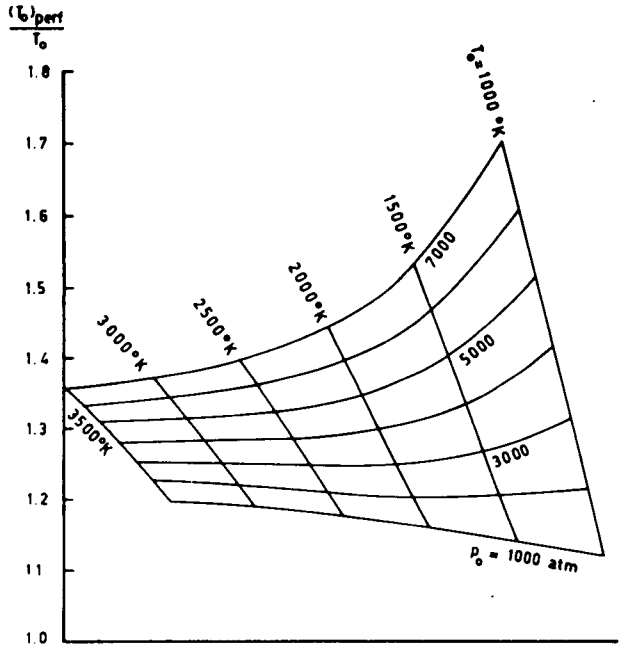

FIG. 12a EQUIVALENT PERFECT CORRECTION FACTORS FROM MEASURED SUPPLY CONDITIONS (FROM REF. 60).

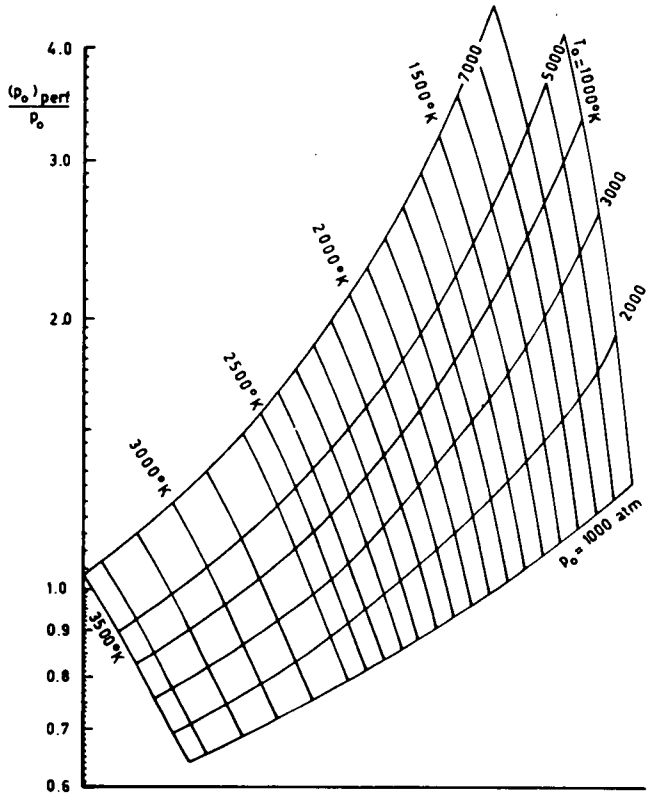

FIG. 12b EQUIVALENT PERFECT CORRECTION FACTORS FROM MEASURED SUPPLY CONDITIONS (FROM REF. 60).

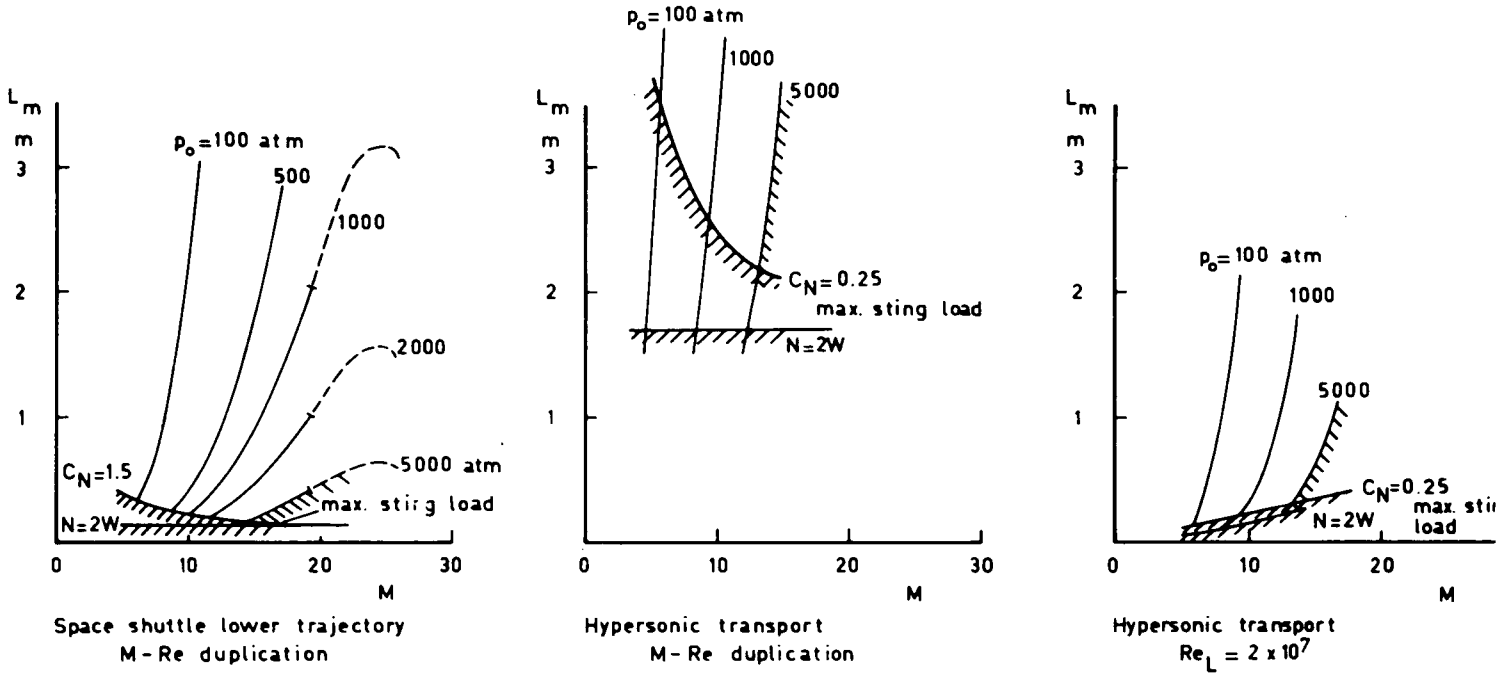

FIG. 13 MODEL LENGTH L_m REQUIRED FOR MACH NUMBER – REYNOLDS NUMBER DUPLICATION, CALCULATED FOR A PERFECT GAS (SEE FIG. 11).

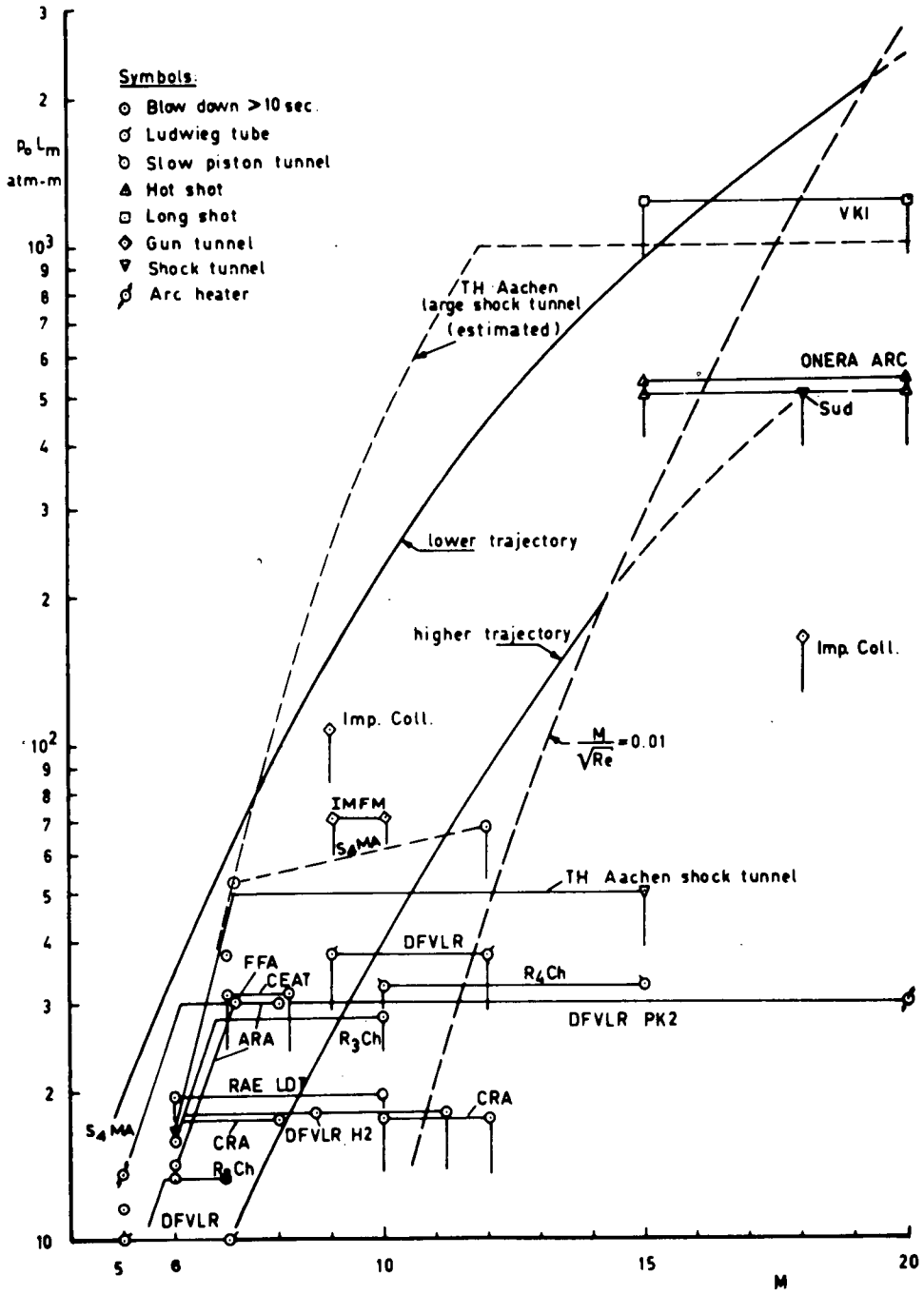

MODEL LENGTH $L_m \leq \frac{1}{2}$ TEST SECTION DIAMETER D_m.
DYNAMIC PRESSURE $q \leq 1.5\ kg/cm^2$. TRAJECTORY DATA FROM FIG. 11

FIG. 14 MACH NUMBER – REYNOLDS NUMBER SIMULATION CAPABILITY OF EUROPEAN WIND TUNNELS – SPACE SHUTTLE TESTING.

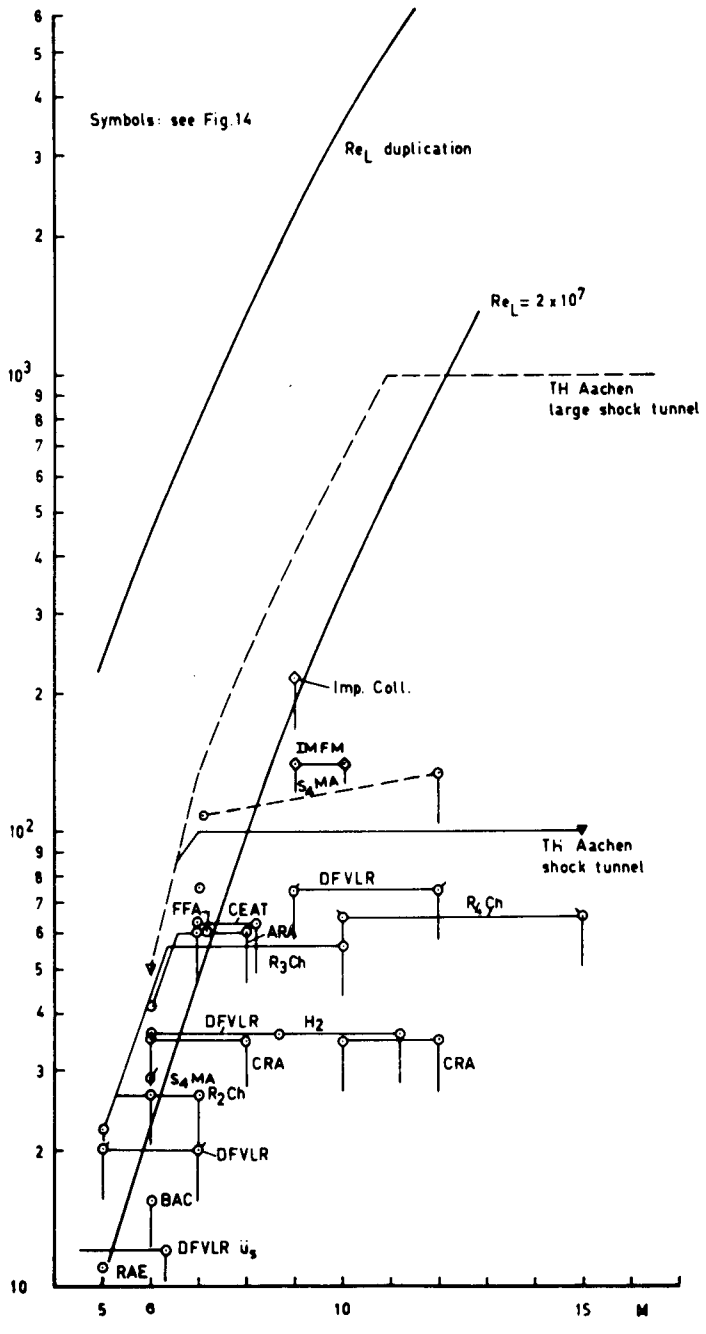

MODEL LENGTH L_m = TEST SECTION DIAMETER D_m.
DYNAMIC PRESSURE $q \leq 2.2\ kg/cm^2$.
TRAJECTORY DATA FROM FIG. 11.

FIG. 15 MACH NUMBER – REYNOLDS NUMBER SIMULATION CAPABILITY OF EUROPEAN WIND TUNNELS – HYPERSONIC TRANSPORT TESTING.

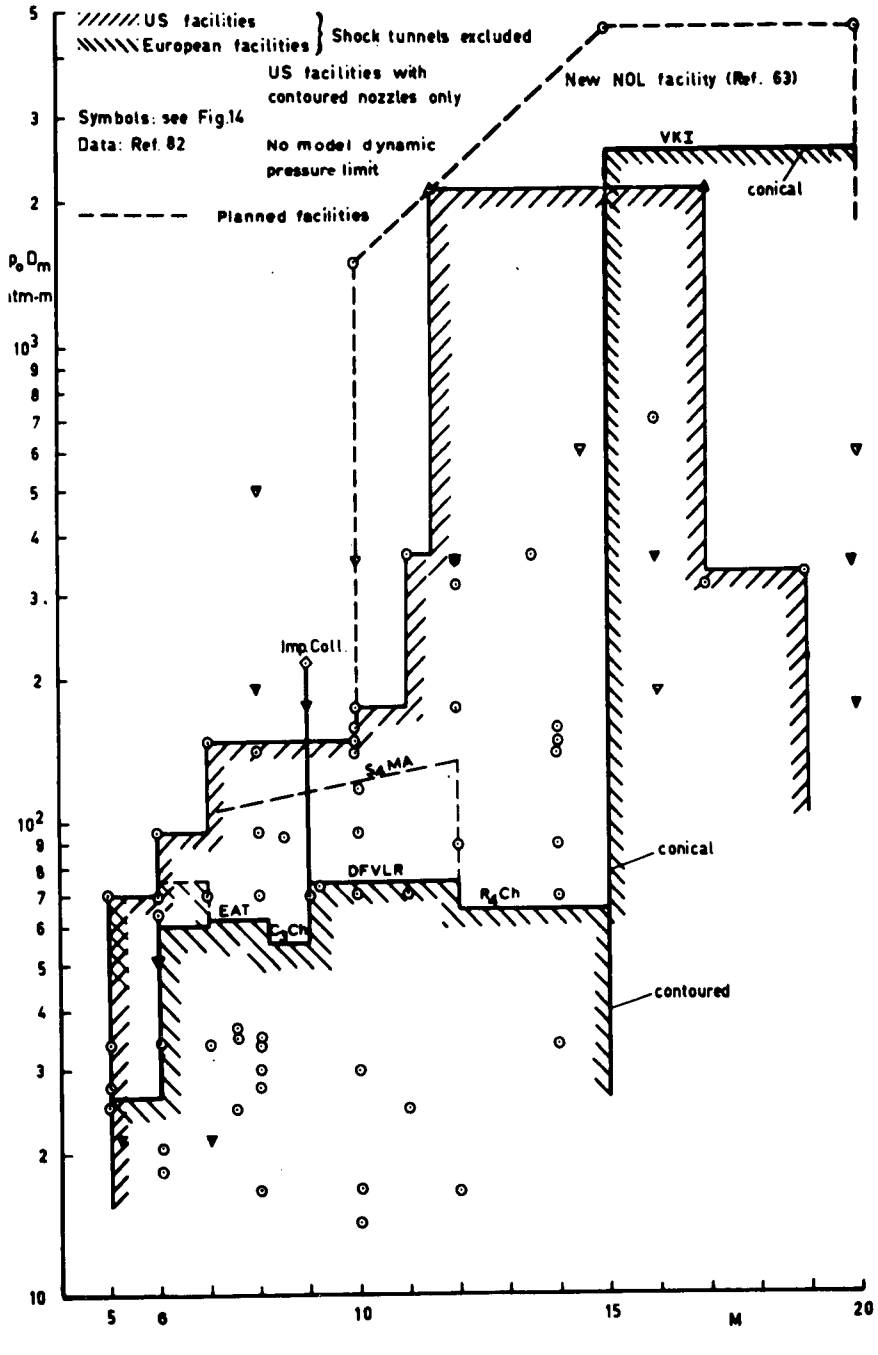

FIG. 16 PERFORMANCE OF US HYPERSONIC FACILITIES.

APPENDIX I

This Report is one of four issued as documents complementary to Advisory Report 60 of the Large Wind Tunnels Working Group of the AGARD Fluid Dynamics Panel. The other reports in the series are as follows:

AGARD REPORT No.598

EXPERIMENTS ON MANAGEMENT OF FREE-STREAM TURBULENCE: by R.I.Loerke and H.N.Nagib

AGARD REPORT No.601

PROBLEMS IN WIND TUNNEL TESTING TECHNIQUES

Review of some problems related to the design and operation of low-speed wind tunnels for V/STOL testing: by M.Carbonaro.

Survey of methods for correcting wall constraints in transonic wind tunnels: by J.C.Vayssaire.

Interference effects of model support systems: by E.C.Carter.

Minimum required measuring times to perform instationary measurements in transonic wind tunnels: by J.W.G.van Nunen, G.Coupry and H.Försching.

Some considerations of tests under dynamic conditions in low-speed wind tunnels: by D.N.Foster.

Use of model engines (V/S/CTOL): by E.Melzer and R.Wulf.

Wind tunnel requirements for helicopers: by I.A.Simons and H.Derschmidt.

Acoustic considerations for noise experiments at model scale in subsonic wind tunnels: by T.A.Holbeche. and J.Williams.

AGARD REPORT No.602

FLUID MOTION PROBLEMS IN WIND TUNNEL DESIGN

The influence of the free-stream Reynolds Number on transition in the boundary layer on an infinite swept wing: by E.H.Hirschel.

Some examples of the application of methods for the prediction of boundary-layer transition on sheared wings: by D.A.Treadgold and J.A.Beasley.

The need for High-Reynolds-Number Transonic Tunnels: by C.R.Taylor.

The influence of free-stream turbulence on a turbulent boundary layer, as it relates to wind tunnel testing at subsonic speeds: by J.E.Green.

Effects of turbulence and noise on wind tunnel measurements at transonic speeds: by A.Timme.

Design of ventilated walls, with special emphasis on the aspect of noise generation: by R.N.Cox and M.M.Freestone.

AGARD Report No.600
Advisory Group for Aerospace Research and Development, NATO
PROBLEMS OF WIND TUNNEL DESIGN AND TESTING
Published December 1973
180 pages

This Report, together with R598, R601 and R602 is issued as a complementary document to Advisory Report 60 of the Large Wind Tunnels Working Group. It contains six papers prepared for the Working Group, dealing with European needs for low-speed wind-tunnels, project studies for transonic tunnels using Ludwieg tube, ECT, induction and hydraulic systems, and testing at hypersonic speeds.

AGARD-R-600
533.6.071

Wind tunnels
Design
Test facilities
Subsonic wind tunnels
Transonic wind tunnels
Hypervelocity wind tunnels
Hydraulic equipment

AGARD Report No.600
Advisory Group for Aerospace Research and Development, NATO
PROBLEMS OF WIND TUNNEL DESIGN AND TESTING
Published December 1973
180 pages

This Report, together with R598, R601 and R602 is issued as a complementary document to Advisory Report 60 of the Large Wind Tunnels Working Group. It contains six papers prepared for the Working Group, dealing with European needs for low-speed wind-tunnels, project studies for transonic tunnels using Ludwieg tube, ECT, induction and hydraulic systems, and testing at hypersonic speeds.

AGARD-R-600
533.6.071

Wind tunnels
Design
Test facilities
Subsonic wind tunnels
Transonic wind tunnels
Hypervelocity wind tunnels
Hydraulic equipment

AGARD Report No.600
Advisory Group for Aerospace Research and Development, NATO
PROBLEMS OF WIND TUNNEL DESIGN AND TESTING
Published December 1973
180 pages

This Report, together with R598, R601 and R602 is issued as a complementary document to Advisory Report 60 of the Large Wind Tunnels Working Group. It contains six papers prepared for the Working Group, dealing with European needs for low-speed wind-tunnels, project studies for transonic tunnels using Ludwieg tube, ECT, induction and hydraulic systems, and testing at hypersonic speeds.

AGARD-R-600
533.6.071

Wind tunnels
Design
Test facilities
Subsonic wind tunnels
Transonic wind tunnels
Hypervelocity wind tunnels
Hydraulic equipment

NATIONAL DISTRIBUTION CENTRES FOR UNCLASSIFIED AGARD PUBLICATIONS

Unclassified AGARD publications are distributed to NATO Member Nations through the unclassified National Distribution Centres listed below

BELGIUM
Coordonnateur AGARD – VSL
Etat-Major de la Force Aérienne
Caserne Prince Baudouin
Place Dailly, 1030 Bruxelles

CANADA
Director of Scientific Information Services
Defence Research Board
Department of National Defence – 'A' Building
Ottawa, Ontario

DENMARK
Danish Defence Research Board
Østerbrogades Kaserne
Copenhagen Ø

FRANCE
O.N.E.R.A. (Direction)
29, Avenue de la Division Leclerc
92, Châtillon-sous-Bagneux

GERMANY
Zentralstelle für Luftfahrtdokumentation
und Information
Maria-Theresia Str. 21
8 München 27

GREECE
Hellenic Armed Forces Command
D Branch, Athens

ICELAND
Director of Aviation
c/o Flugrad
Reykjavik

ITALY
Aeronautica Militare
Ufficio del Delegato Nazionale all'AGARD
3, Piazzale Adenauer
Roma/EUR

LUXEMBOURG
Obtainable through BELGIUM

NETHERLANDS
Netherlands Delegation to AGARD
National Aerospace Laboratory, NLR
P.O. Box 126
Delft

NORWAY
Norwegian Defense Research Establishment
Main Library,
P.O. Box 25
N-2007 Kjeller

PORTUGAL
Direccao do Servico de Material
da Forca Aerea
Rua de Escola Politecnica 42
Lisboa
Attn of AGARD National Delegate

TURKEY
Turkish General Staff (ARGE)
Ankara

UNITED KINGDOM
Defence Research Information Centre
Station Square House
St. Mary Cray
Orpington, Kent BR5 3RE

UNITED STATES
National Aeronautics and Space Administration (NASA)
Langley Field, Virginia 23365
Attn: Report Distribution and Storage Unit

* * *

If copies of the original publication are not available at these centres, the following may be purchased from:

Microfiche or Photocopy

National Technical
Information Service (NTIS)
5285 Port Royal Road
Springfield
Virginia 22151, USA

Microfiche

ESRO/ELDO Space
Documentation Service
European Space
Research Organization
114, Avenue Charles de Gaulle
92200, Neuilly sur Seine, France

Microfiche

Technology Reports
Centre (DTI)
Station Square House
St. Mary Cray
Orpington, Kent BR5 3RE
England

The request for microfiche or photocopy of an AGARD document should include the AGARD serial number, title, author or editor, and publication date. Requests to NTIS should include the NASA accession report number.

Full bibliographical references and abstracts of the newly issued AGARD publications are given in the following bi-monthly abstract journals with indexes:

Scientific and Technical Aerospace Reports (STAR)
published by NASA,
Scientific and Technical Information Facility,
P.O. Box 33, College Park,
Maryland 20740, USA

Government Reports Announcements (GRA),
published by the National Technical
Information Services, Springfield,
Virginia 22151, USA.

Printed by Technical Editing and Reproduction Ltd
Harford House, 7-9 Charlotte St, London. W1P 1HD